ABSTRACT

KOLLITZ, ERIN MATTSON. Functional Diversification of the Vitamin D Receptor (VDR) with Increasing Genome Complexity in Vertebrates. (Under the direction of Dr. Seth W. Kullman.)

The vertebrate genome is a result of two rapid and successive rounds of genome duplication (1R and 2R). Teleost fish maintain a greater number of nuclear receptors (NRs) compared to other vertebrates due to a third genome duplication specific to their lineage (3R). The retention of multiple nuclear receptor pairs in teleosts provides a unique opportunity to gain insight into how receptor paralogs evolve through specific evolutionary processes. This dissertation examines the functional diversification of the vitamin D receptor (VDR) with increasing genome complexity within teleost and vertebrate evolution. VDR function is assessed in response to 1α, 25-dihydroxyvitamin D_3 (1, $25D_3$) and lithocholic acid (LCA), a toxic secondary bile acid.

Chapter 1 examines the hypothesis that teleost VDRα and VDRβ paralogs are derived from the 3R event, and that retention of duplicate VDRs is likely due to sub- or neofunctionalization. VDR paralogs were cloned from the Japanese medaka (*Oryzias latipes)* and the zebrafish (*Danio rerio)*. We demonstrate that high affinity binding to 1, $25D_3$ has been conserved between paralogs, however transactivational efficacy varies significantly. Subsequent studies demonstrate that VDRα paralogs exhibit preferential DNA binding compared to the VDRβ paralogs, and demonstrate differential protein-protein interactions between paralogs and essential co-regulators including RXR and the SRC family of nuclear receptor co-activators. We speculate that the observed functional differences are due to subtle conformational differences between paralogs.

Chapter 2 examines the hypothesis that the receptor-ligand partnership between VDR and 1, $25D_3$ is ancient and traceable to basal extant vertebrate species. Basal VDRs were cloned from the sea lamprey (*Petromyzon marinus*) a jawless fish; the little skate (*Leucoraja erinacea*), a cartilaginous fish; and the Senegal bichir (*Polypterus senegalus*), a primitive 2R ray-finned fish. Similar to the teleost VDR paralogs, we demonstrate that basal VDR orthologs maintain high affinity for 1, $25D_3$, maintain similar DNA binding characteristics, and that this ligand serves as a potent transactivational agonist with these receptors. However, transactivational efficacy varies significantly between VDR orthologs. Subsequent studies indicate protein-protein interactions between basal VDRs and essential co-regulators exhibit significant differences between VDR orthologs. Results from a cluster analysis support the notion that the observed functional differences are predominantly driven through differential interactions between receptors and their coregulators. Results from the cluster analysis suggest that the basal VDRs function similar to the VDRβ paralogs, while the VDRα paralogs function more similar to human VDR. Our results provide further evidence a functional divergence between the teleost VDR paralogs, and support the hypothesis that the 1, $25D_3$ – VDR partnership is ancient.

Chapter 3 examines the hypothesis that that the ligand-receptor partnership between VDR and LCA is a result of exaptation. It has been speculated that the VDR-lithocholic acid partnership in mammals resulted from an adaptive process associated with the synthesis and detoxification of the bile acid in higher vertebrates. However, the evolutionary history of this partnership is not well understood due to the lack of data from non-mammalian vertebrates. We demonstrate that LCA and 3-Keto both function as full agonists only with human VDR and the teleost VDRα paralogs. Interaction between the bile acids and VDRβ paralogs did not

facilitate transactivation or RXR heterodimerization, and display attenuated coactivator recruitment. Similarly, VDR from basal vertebrates were not able to mediate any response to LCA or 3-Keto beyond ligand binding. Bioinformatics analysis suggests that functional differences between VDRs are driven though differential interactions between VDRs and essential coactivators. Our results suggest that the ability of LCA to function as a VDR ligand evolved before the bile acid itself, most likely though a process of exaptation followed by co-option once the need to detoxify LCA arose in higher vertebrates.

© Copyright 2014 Erin Mattson Kollitz

All Rights Reserved

Functional Diversification of the Vitamin D Receptor (VDR) with Increasing Genome Complexity in Vertebrates

by
Erin Mattson Kollitz

A dissertation submitted to the Graduate Faculty of
North Carolina State University
in partial fulfillment of the
requirements for the degree of
Doctor of Philosophy

Toxicology

Raleigh, North Carolina

2014

APPROVED BY:

_____	_____
Dr. Seth W. Kullman Committee Chair	Dr. Gerald A. LeBlanc
_____	_____
Dr. John Godwin	Dr. Mary Beth Hawkins

DEDICATION

I would like to dedicate my dissertation to my amazing family: my parents Jim and Gayle, my sister Katie, and my brother-in-law Mith. Honestly, this dissertation would never have happened without their unwavering love, support, and encouragement. There were times where I lost faith in myself, but my family never did. I would never have made it this far without them, and I am so thankful for them every single day.

BIOGRAPHY

Erin Mattson Kollitz was born on July 8, 1981 in San Diego, California. Erin and her family moved to St. Paul, Minnesota in 1984, where she lived until she graduated from high school in 2000. Following graduation, Erin attended Bard College in Annandale-on-Hudson, New York from 2000 to 2004. After graduating from Bard College with a Biology degree in December 2004, Erin was unsure of her future career direction, and decided to apply for an internship to gain experience in fields that interested her.

Erin moved to Sarasota, Florida, where she worked at Mote Marine Laboratory to begin an internship with the chemical fate and effects program within the Center for Ecotoxicology studying the fate and effects of brevetoxins from Florida red tide. Following her first internship, she accepted a second internship with the elasmobranch physiology and environmental biology program at the Center for Shark Research studying the effects of environmental estrogens on local shark populations. Her second internship with the CSR cemented her desire to pursue a career in toxicology with a focus on endocrine disruption and nuclear receptors. Following the completion of this internship, Erin worked as an unpaid volunteer with her mentor at the CSR, and worked nights at a local coffee and wine bar in order to pay the bills. Erin later accepted a position with the phytoplankton ecology program within the Center for Ecotoxicology where she worked as a biologist until 2008.

Her experiences at Mote motivated Erin to return to school to pursue a doctoral degree in toxicology. In 2008 she moved to Raleigh, North Carolina to begin her first year of graduate school in the Department of Environmental and Molecular Toxicology at North Carolina State University. She joined the laboratory of Dr. Seth Kullman in January 2009 where she

began her doctoral research on the vitamin D receptor in non-mammalian vertebrates.

ACKNOWLEDGMENTS

While I may be listed as the only author, a dissertation is never truly the work of only one individual. Therefore, I would like to acknowledge and thank the following people for their contributions to this work, my graduate career, and in some cases, helping me to maintain my sanity.

First I would like to acknowledge and thank my mentor, Dr. Seth Kullman, and the past and present members of the Kullman Lab: Dr. Erin Yost, Crystal Lee Pow, Atlee Watson, Dr. Debabrata Mahapatra, Dr. Arnaud van Wettere, Hong Li, Gwijon Kwon, Dr. Melanie Fraites, Dr. Wu Dong, Dr. Sheran Law, and Dr. Deanna Howarth. They were instrumental in the success of this project, and were also quite a lot of fun to work with.

This dissertation would not have been possible without the guidance and support of my committee: Dr. Seth Kullman, my committee chair and mentor, Dr. Gerald LeBlanc, Dr. John Godwin, and Dr. Mary Beth Hawkins. I would additionally like to acknowledge Dr. Andrew Wallace, a former committee member who left NC State in pursuit of a new career path.

I would also like to thank the laboratories of Dr. James Bonner and Dr. Scott McCulloch. The radiation lab I had been working in was shut down in the middle of my project, and they quickly opened their doors to me so I could finish my work. In particular, I would also like to thank Lexie Taylor and Shannon Tofton, the technicians of the Bonner and McCulloch labs, who were both instrumental in helping me get set up in their respective labs.

I would like to thank Dr. Kerr Whitfield and Dr. Mary Beth Hawkins for their extensive assistance with the radioligand binding assays.

While the following people may not have participated in the science part of this dissertation, their contributions were vital to the success of this project:

First, my wonderful and amazing family: my parents Jim and Gayle, my sister Katie, and my brother-in-law Mith. You guys are the best possible family a person could ask for. I would never have made it this far without you. I love you more than words can express.

A huge, heartfelt THANK YOU to my amazing friends. From providing emotional support, to editing my drafts, and even cleaning my kitchen, you all have been phenomenal. I thank you from the bottom of my heart.

Without the support of numerous funding sources, this dissertation would not have been possible. Before I joined the Kullman lab, my tuition and stipend funding were provided through the National Institute of Environmental Health Sciences training grant (T32-E2007046), which was awarded to me through the Department of Environmental and Molecular Toxicology at North Carolina State University. My primary source of funding was though a grant awarded to Dr. Kullman from the National Science Foundation (IOS0818799). Dr. Kullman, Dr. Yost, and I spent July of 2010 at Mount Desert Island Biological Laboratory (MDIBL) in Salisbury Cove, Maine. My expenses for this trip were partially covered by the Stan and July Fellowship awarded to me by MDIBL.

In addition, six months of tuition, fees, health insurance, and my stipend were covered through the Dissertation Completion Grant (DCG) awarded to me by the Graduate School of North Carolina State University from July to December 2013. The purpose of this grant was to provide necessary financial support to allow me to completely focus on writing my dissertation. I met weekly with my writing coach and other grant recipients to discuss our

current drafts. In addition, the grant recipients and I met in a weekly support group, as a way for the Graduate School to provide emotional support to the recipients. This opportunity was invaluable to me. I would like to thank the Graduate School of North Carolina State University for awarding me this grant. This was an amazing (and much needed) opportunity to focus on learning how to write in science. In particular, I would like to thank my writing mentors Dr. Mike Carter and Dr. Meghan Kittle Autry for their dedication and support, and their extremely helpful coaching. I would also like to thank my fellow graduate students who took part in this opportunity with me: Alice Broadhead, Amanda Traud, Carlos Ortiz, Heidi Hess von Ludewig, Iris Wagstaff, Kristin Williams, and Tim Ellis. I learned so much from all of you, and I had a fantastic time working with you. I would also like to thank Dr. Sipho Mbuqe for his unwavering support.

And finally, to my dog Cole: I love you buddy, and I promise we'll start hiking again once I'm finished!

TABLE OF CONTENTS

LIST OF TABLES

LIST OF FIGURES

GENERAL DISCUSSION

APPENDIX C

APPENDIX D

APPENDIX E

APPENDIX G

APPENDIX H

APPENDIX I

LIST OF ABBREVIATIONS

1, 25D_3	1α, 25-dihydroxyvitamin D_3
1R, 2R, or 3R	Refers to first, second, or third WGD
3-keto LCA	3-keto lithocholic acid
AF2	Activation function 2
ACTR	Activator of thyroid and retinoid receptors (SRC family)
CAR	Constitutive androstane receptor
DBD	DNA binding domain
DR3	Direct repeat-3
EMSA	Electrophoretic mobility shift assay
GRIP1	Glucocorticoid receptor interacting protein-1 (SRC family)
H#	Refers to helices (1-12) in the LBD
LBD	Ligand binding domain
LBP	Ligand binding pocket
LCA	Lithocholic acid
M2H	Mammalian 2-hybrid
NR	Nuclear receptor
NR1I1	Nuclear receptor subfamily 1, group I, number 1
PXR	Pregnane X receptor
RXR	Retinoid X receptor
SRC-1	Steroid receptor coactivator-1 (SRC family)
TT	Transient transactivation
VDR	Vitamin D receptor
VDRα	Vitamin D receptor, alpha paralog
VDRβ	Vitamin D receptor, beta paralog
VDRE	Vitamin D response element
WGD	Whole genome duplication
XREM	Xenobiotic response element modulator

GENERAL INTRODUCTION

Overview

Teleost fish (class Actinopterygii) comprise approximately 27,000 extant species, and are among the most diverse and successful group of vertebrates (1). These organisms represent an extensive array of phenotypic characteristics and maintain considerable genetic diversity. It appears that much of the complexity of the teleost genome is a result of successive rounds of whole genome duplications (WGDs). Two rounds of WGD are hypothesized to have occurred early in vertebrate evolution, while a third WGD occurred within Actinopterygii, and is specific to teleost fish (2-7). The presence of multiple gene copies is believed to have had a large impact on the evolution of teleosts and vertebrates in general, as larger genomes are thought to facilitate functional diversification and increase gene family size (8,9). The duplication of the entire genome provides an abundant source of genetic material for evolutionary forces to act upon, resulting in the evolution of more complex gene interactions and gene networks. This increase in genomic complexity may lead to increased morphological variation, physiological plasticity, and functional innovation (10-12). In numerous instances, teleost fish have two or more copies of single-copy mammalian genes. While there are multiple mechanisms of small-scale duplication, WGD appears to be the most practical explanation for the large number of paralogous genes (13).

Two Rounds of Whole Genome Duplication in Vertebrate Evolution

Current evolutionary theory hypothesizes that vertebrate species are derived from two successive rounds (2R) of whole genome duplication over the course of vertebrate

evolution (2) (Fig. 1). The 2R hypothesis predicates that vertebrates may have up to four copies for each single-copy ortholog found in other chordates. Preliminary evidence in support of the 2R hypothesis comes from studies examining the evolution of *Hox* gene clusters. *Hox* genes encode transcription factors that control embryonic patterning and morphology along the anterior-posterior axis in vertebrate embryogenesis. *Hox* genes typically occur in one or more clusters of genes, and the number of *Hox* gene clusters has been correlated with the number of WGD in a lineage. For example, the primitive cephalochorate *Amphioxius* has a single *Hox* cluster. The sea lamprey (*Petromyzon marinus)* is a member of the class Agnatha, the most basal vertebrate lineage that diverged after the first WGD. The ancestral Agnathan speculated to have maintained two *Hox* clusters following the 1R duplication, although the sea lamprey maintains four due to a lamprey-specific duplication event (14). Vertebrates that diverged after the 2R event, such as sharks, birds, and mammals, all maintain four *Hox* clusters (15,16). The observation that the number of *Hox* gene clusters doubles in animals that diverged after each WGD is consistent with the 1R and 2R hypothesis. Observations further supporting the 2R hypothesis include the fact that clusters of duplicate genes are found on different chromosomes, yet they tend to remain linked, often in the same order, and maintain synteny between species over large evolutionary distances (4). This degree of synteny would not be maintained through numerous small-scale gene duplications.

Evidence for a third WGD specific to teleost fish

The Actinopterygii are the largest, most successful, and most diverse group of vertebrates. Of the roughly 27,000 species that comprise the class Actinopterygii, only ~55 are not teleost fish (1). This handful of species comprise the four basal lineages of Actinopterygii (*Polypteriformes*, *Acipenseriformes*, *Lepisosteiformes*, and *Amiiformes*) that are collectively referred to as "ancient fish" as they are considered to be living fossils due to the fact that their morphology has remained unchanged over long periods of time, and their lineages are relatively species poor (1,3). In contrast to their more ancient cousins, teleost fish display a far greater degree of morphologic variation and species diversity, supporting the argument that increased genome content can result in increased species diversification and phenotypic complexity (4). Evidence has mounted that teleosts went through a third whole genome duplication (3R) roughly 350 million years ago, after the divergence of more basal actinopterygians (3,6,17) (Fig. 1). The 3R event has been hypothesized to have facilitated the diversification of teleosts by providing the raw genetic material necessary for the evolution of new genes with novel functions, leading to increased species diversity, phenotypic plasticity, and evolutionary innovations. Unlike their older relatives, teleosts display a remarkable assortment of morphologic and phenotypic species diversity, and have adapted to living in even the most hostile environments such as the deep seas, mountain streams, volcanic hot springs, and Antarctic oceans (1).

As discussed above, examination of *Hox* clusters provides a mechanistic window in which gene duplication events can be evaluated and quantified. Studies examining *Hox* clusters in teleosts yielded surprising results: teleosts have roughly twice as many *Hox*

clusters as other vertebrates. While most 2R vertebrates have four clusters, seven clusters have been identified in teleosts, including the zebrafish (*Danio rerio*) (18), the pufferfish *Takifugu rupripes* (19), the Japanese medaka (*Oryzias latipes*) (20) and *Astatotilapia burtoni*, a cichlid fish (21). Furthermore, studies examining non-*Hox* genes in teleosts have found a similar trend in additional gene families, including nuclear receptors (22-24), transcription factors (25,26), repressor proteins (27), and proteases (28). The presence of multiple paralogous genes in teleosts gave rise to the theory that a third whole genome duplication event (3R) had taken place in the ray-finned fish in the stem lineage of teleosts. Additional observations supporting the 3R hypothesis include 1) many paralogous genes in teleosts appear to have originated at the same time, 2) teleost fish share many of the same gene duplicates with each other, and 3) paralogous regions of differing chromosomes maintain conserved synteny (4,17,29).

The fate of duplicate genes

The Classic Model – Nonfunctionalization and Neofunctionalization

Whole genome duplication initially creates two gene copies that are functionally redundant. This redundancy results in relaxed selective pressures, as mutations in one copy are considered to be neutral, as they have no effect on the phenotype due to the presence of a second functional copy (30-32). The relaxation of selective constraints also results in an increased rate in the accumulation of mutations that would normally be eliminated, eventually turning one copy into a non-functional pseudogene. With time, a pseudogene may further deteriorate until it can no longer be recognized in the genome (10). The loss of one

copy is referred to as nonfunctionalization, and this process is predicted to be the fate of 50-90% of gene pairs.

Although nonfunctionalization inactivates a gene, this process still plays an important role in increasing species diversity through the creation of reproductive barriers. The loss of different copies of a gene in two populations can lead to reproductive isolation, due to the fact that gametes produced by hybrid offspring may completely lack functional genes for a duplicate pair (33). Reproductive incompatibility due to reciprocal gene loss in separate populations after a whole genome duplication event could ultimately lead to speciation (32). Reciprocal gene loss at only 20-30 loci pairs that encode essential genes is sufficient to result in reproductive isolation. A study conducted by Sémon and Wolfe estimated that about 1,700 loci have undergone reciprocal gene loss in the spotted green pufferfish (*Tetraodon nigroviridis*) and zebrafish (*Danio rerio*), and hypothesize that the reciprocal gene loss between these two species influenced their speciation (34).

While the vast majority of mutations are deleterious (35), the classic model originally proposed by Dr. Susumo Ohno (8), hypothesizes that in rare instances one paralog will received a beneficial mutation that confers a novel function, while the second copy maintains the original function (8). Thus the functions of both paralogs are no longer redundant, and both are maintained in the genome. This process is referred to as neofunctionalization (Figure 2). An example of neofunctionalization in teleosts is an antifreeze glycoprotein (AFGP) found in the GI tract of teleosts in the order *Nototheniodei.* The AFGP gene evolved from a duplicated pancreatic trypsinogen gene, as an adaptive mechanism to inhibit ice crystal formation in the intestinal tract in these Antarctic fish (36). This example describes a

neofunctionalization event that occurred within the protein-coding region of a gene. Neofunctionalization may also occur in regulatory regions, resulting in novel spatio-temporal expression patterns. For example, a gene may be expressed in a new tissue, or in a new developmental period.

The Duplication-Degeneration-Complementation model (Subfunctionalization)

The Duplication-Degeneration-Complementation (DDC) model is an alternative theory to Ohno's classic model regarding the fate of gene duplicates that was proposed by Force et al in their 1999 paper (26). According to the DDC model, after a duplication event (duplication), both duplicates receive degenerative mutations (degeneration) that result in the complementary loss of function (complementation). The loss of complementary subfunctions between paralogs necessitates the retention of both copies in the genome in order for the organism to maintain the ancestral function (26). This is referred to as subfunctionalization (Fig. 2). In the DDC model, mutations that lead to subfunctionalization can occur in the regulatory region and/or within the protein-coding region of the gene.

Subfunctionalization can be spatial, quantitative or temporal. Spatial subfunctionalization occurs when both duplicates exhibit differential tissue expression patterns, and thus both are needed to maintain the expression pattern of the original gene. Quantitative subfunctionalization occurs when the amount of protein product produced by both genes decreases, so the combined expression of both is necessary to maintain ancestral levels. In temporal subfunctionalization, both paralogs are expressed in the same tissues but at different times and under different regulatory elements (37). For example, one copy may be expressed during embryogenesis while the second may be expressed during adult life.

Unlike a nonfunctionalization event, the deleterious mutations in both loci result in the retention of both duplicates. It has also be suggested that the retention of duplicates through subfunctionalization extends the time period in which these genes are exposed to natural selection, enhancing the chance that a rare beneficial mutation will occur in at least one loci, leading to a neofunctionalization event (31). Subfunctionalization can lead to speciation when the paralogs of two populations develop lineage-specific subfunctionalization patterns, resulting in reproductive isolation between populations (12,37).

Gene retention is not a random process

Comparative genomic studies have revealed that gene retention following a WGD is not a neutral or random process. Regulatory genes, such a genes involved in signal transduction, transcription regulation, and developmental signaling, have been preferentially retained in duplicate following a WGD (38,39). Regulatory genes tend to operate as part of a macromolecular complex that interact with additional proteins to control essential processes such as gene transcription, and are dependent on the stoichiometric balance of their subunits to maintain normal function. The imbalance of a complex due to under- or overexpression of a subunit may impact the assembly of the complex as a whole, with detrimental effects on downstream function (40-42) (Fig. 3). Selective forces act to maintain proper balance in regulatory pathways in order to maintain normal function. Therefore regulatory genes are usually lost in order to maintain pathway balance during small scale duplication. As the entire pathway is duplicated following a WGD all of the genes involved in that pathway are protected against their loss in order to maintain balance and normal function (41).

The production of a duplicate, redundant regulatory pathway by WGD is hypothesized to be a factor of evolutionary innovation and increasing complexity in vertebrate evolution by facilitating innovation at the pathway level (11,12,41). However, in order for a pathway to evolve a new function it must first escape the strong selective constraints maintaining it. Alterations to the pathway may include novel protein-protein interactions with new co-activators or co-repressors, the recruitment of additional transcription factors to the replication complex, the recognition of new target genes, and novel expression patterns (41,43). It has been suggested that the duplication, retention, and divergence of entire regulatory pathways have made a significant contribution to vertebrate diversity and complexity. Novel regulatory pathways and gene expression networks can lead to increased diversification, morphological complexity, and speciation (9,12). It is evident that the duplication of an entire regulatory pathway allows for increased evolutionary plasticity compared to the duplication of a single gene.

Teleost nuclear receptor paralogs and an overview of nuclear receptor biology

One group of regulatory genes that has been significantly retained in duplicate following the 3R duplication is the nuclear receptor (NR) superfamily (22-24). Nuclear receptors form a large family of ligand-activated transcription factors that enable cells to fine-tune their response to an external ligand. Ligands are small lipophilic compounds that can cross the cell membrane, and are derived from both endogenous sources (bile acids, hormones) and exogenous sources (vitamins, fatty acids, xenobiotics, and pharmaceuticals). Upon ligand binding, nuclear receptors regulate gene transcription by binding to specific

response elements upstream of target genes, and work in concert with coactivators and corepressors to regulate expression. NRs regulate a diverse array of functions essential to vertebrate life, including reproduction, development, homeostasis, and detoxification.

Nuclear receptors share a common protein structure made up of several highly conserved functional domains. The basic structure of a nuclear receptor is shown in figure 4 (also see Appendices D and E), which uses the vitamin D receptor as an example. The N-terminal A/B domain, containing the AF-1 region, is highly variable in both length and sequence, and is not well conserved between receptors (44). The C domain contains the DNA binding domain (DBD) and is the most highly conserved domain of NRs. The DBD is composed of two α-helices that each form a zinc finger DNA-binding motif that is responsible for directly binding DNA response elements with high specificity and affinity. Specific amino acid motifs at the base of each zinc finger confer additional specificity in DNA recognition (P-box) and dimerization (D-box) (45). The DBD and the ligand-binding domain (LBD) are separated by the hinge region (D), a variable domain thought to serve a spacer function between the LBD and DBD and confer flexibility for protein folding. Further studies have identified a region within the hinge referred to as the c-terminal extension (CTE) that maintains two functional subdomains that confer additional receptor specificity. The A-box of the CTE has been demonstrated to contribute additional response element specificity, while the T-box interacts with the DBD of the NR dimer partner (46). The E domain contains the ligand-binding domain (LBD), a multifunctional region with essential roles in ligand binding, heterodimerization, coactivator (CoA) recruitment, and transactivation. The LBD consists of 12 α-helices containing amino acid residues that are responsible for direct ligand-

receptor interaction. Ligand binding induces a dramatic conformational change in the receptor, where H12 rotates 180º to pack tightly over H3, H4, and H5, creating a hydrophobic ligand-binding pocket (47,48). The positioning of H12 creates a "charge clamp" between the negatively charged glutamate residue (E420 in human VDR) of the AF2 region of H12, and positively charged lysine residue (K246 in human VDR) of H3. The charge clamp is responsible for coactivator interaction by directly binding with the LXXLL motifs within the NR box of coactivators (49). The c-terminal F domain is highly variable, and its function is not well understood.

To date, true nuclear receptors have only been identified in metazoans (50). In teleosts, orthologs for all mammalian NR sub classes have been identified, including those for steroid hormones and orphan receptors (22-24). In fact, teleosts maintain a larger complement of nuclear receptors than mammals. For example, humans have 48 receptors (51), while 68 have been identified in *Takifugu rubripes* (22), 71 in *Tetraodon nigroviridis* (23), 71 in the Japanese medaka (*Oryzias latipes*) (52), and 70 in zebrafish (*Danio rerio*) (24). This is likely due to global retention of regulatory genes within the teleost genomes subsequent to the 3R event (9,41,53). In contrast to teleosts and other vertebrates, invertebrates have far fewer NRs: 17 have been identified in the urochordate *Ciona intestinalis* (54), 21 in *Drosophila* (55), 25 in *Daphnia pulex* (56)and 17 in *Nematostella vectensis*, a cnidarian (57). *Amphimedon queenslandica,* a member of the phylum *Porifera,* the most ancient metazoan phylum, only has two NRs (58). As NRs are important transcription factors for numerous endocrine-mediated processes, NR duplication and divergence may contribute to signal diversification and development of more complex gene

networks, leading to speciation and development of evolutionary novelties. However, the functional role of duplicate NRs remains unresolved in teleosts.

The Vitamin D Receptor

The vitamin D receptor (VDR, NR1I1) is a member of the NR1I subfamily of nuclear receptors, which also includes the pregnane X receptor (PXR, NR1I2) and the constitutive androstane receptor (CAR, NR1I3) (59). Within Chordates, true VDRs have only been identified in vertebrates. Mining of the cephalochordate genome has not identified any NR1I receptors, although a proto-NR1I receptor that maintains moderate homology to both VDR and PXR has been identified in the urochordate *Ciona intestinalis* (54,60). Urochodates are the sister group to vertebrates, however this proto-VDR/PXR appears to be insensitive to both VDR and PXR ligands (61,62).

An abundance of literature is available describing the canonical role of mammalian VDR in regulating calcium homeostasis and skeletal maintenance in vertebrates. Subsequent studies in mammals have identified VDR expression in over thirty-six tissues, indicating VDR signaling plays an active role in numerous biological processes beyond calcium homeostasis (63) (Fig. 5). In fact, recent investigations of VDR function using knockout mouse models have revealed that VDR signaling maintains additional non-calcemic functions, including roles in cell proliferation and differentiation, immune system function, detoxification and embryonic development (64,65). In addition the loss or perturbation of VDR function is associated with the etiologies of a variety of diseases, such as cancer, diabetes, autoimmune diseases, and developmental abnormalities (64,66,67).

VDR maintains the canonical protein structure of NRs described in section 1.5, and the mechanism of VDR activation is analogous to that of other nuclear receptors (Figure 4A and B). The biological effects of VDR are mediated through the binding of 1, 25α-dihydroxyvitamin D_3 (1, $25D_3$), the hormonally active metabolite of vitamin D_3 (Fig. 6). In the absence of a ligand, the receptor protein maintains significant conformational mobility that is stabilized upon ligand binding (68) . The most c-terminal α-helix (H12) containing the AF2 region projects away from the rest of the LBD, and is the most mobile region of the receptor (69). Ligand-binding induces a dramatic conformational change in the receptor, where H12 rotates 180º to a "closed" position over the ligand-binding pocket (LBP), positioning the AF2 region as a platform for coactivator interaction. H12 is stabilized in this position by two ligand contacts with 1, $25D_3$ and several hydrophobic and polar contacts with H3, H4, H5, and H11 (47). Ligand binding induces heterodimerization between VDR and RXR, the obligate dimer partner of VDR. Heterodimerization is accomplished through the interactions of H9 and H10 of both receptors. The VDR:RXR heterodimer is non-permissive, meaning that only the cognate ligand for VDR, not RXR, can activate transcription. Work by Bettoun et al has demonstrated that VDR is able to allosterically modify unliganded RXR to the active conformation so that the AF2 region of RXR is positioned for coactivator interaction (70). The AF2 regions of H12 of both receptors are essential for VDR-mediated transcription, and the removal of the AF2 from either receptor abolishes VDR activation (71). The heterodimer then translocates to the nucleus and binds to vitamin D response element (VDRE) motifs upstream of target genes. DNA binding is followed by the recruitment of coactivators and other essential proteins to the transcription complex.

Coactivators have an essential role in VDR-mediated transcription through both chromatin remodeling and bridging the heterodimer to the transcriptional machinery (72). How well a ligand stabilizes a receptor in the active conformation directly impacts the efficiency of these downstream processes.

Prior to the identification of functional VDRs in aquatic vertebrates, the conventional theory speculated that the vitamin D endocrine system originated in terrestrial animals (73). However, VDR and the vitamin D endocrine system has an ancient origin, as functional VDRs have been cloned from the sea lamprey (*Petromyzon marinus*), the little skate (*Leucoraja erinacea*) and numerous fish (59,74). Homology comparisons of vertebrate VDR protein sequences demonstrate VDR maintains a high degree of conservation across species, suggesting that the vitamin D endocrine axis may be highly conserved throughout vertebrate evolution (61). Supporting this theory is the fact that many non-mammalian vertebrates maintain high concentrations of circulating vitamin D_3, and enzymes necessary for vitamin D synthesis and transport have been identified in many species (75). However, increasing evidence suggests that calcium homeostasis may not have been a critical function of ancestral VDR. The fact that aquatic vertebrates live in an environment that serves as an abundant calcium source, and functional VDRs have been identified in animals with and without calcified skeletons indicates that VDR may have evolved long before the need for strict hormonal control of calcium. VDR is known to be vital to embryogenesis, and VDR is expressed prior to bone development in both *Xenopus* and zebrafish (73,76). Additionally, VDR shares number of transcriptional targets thought to play a role in detoxification with the other members of the NR1I family that are well known for their detoxification roles.

In agreement with the 3R duplication event, two distinct VDR genes have been identified in multiple 3R teleosts including the Japanese medaka (*Oryzias latipes*), zebrafish (*Danio rerio*), the two pufferfishes *Tetraodon nigroviridis* and *Takifugu rubripes*, and flounder (*Paralichthys olivaceus*) (22-24,77,78). Evidence indicating that the duplicates are indeed paralogs, and not isoforms, include the observation that the VDRα and VDRβ paralogs are shared with multiple species across large evolutionary distances, they appear to have originated at the same time, and is further substantiated by the observation that the paralogs are found within distinct chromosomal loci yet maintain conserved synteny (3,4). Homology comparisons have revealed that the paralogs maintain a high degree of sequence identity to tetrapod VDRs, although are most similar to paralogs from other teleosts (77,78). However, additional studies have revealed that functional conservation cannot be assumed based on sequence similarities (79,80). Tissue expression studies revealed both VDR paralogs are expressed in a wide variety of tissues, similar to results with mammalian VDRs, however VDRα and VDRβ exhibited differential spatial or quantitative tissue expression in each species (22,52,76). While VDR paralogs are highly conserved, functional studies have identified differential paralog functions, including differences in ligand sensitivities and target genes, which suggests a divergence of VDR function at the molecular level (76,77). Despite the sharp contrast between strong sequence conservation yet stark functional differences, little has been done to characterize crucial molecular functions of the VDRα and VDRβ paralogs. The identification of divergent NR functions between both the VDR paralogs, and ancestral vs. derived vertebrates may reveal important clues driving VDR evolution.

Research Objectives

While the molecular biology and roles of mammalian VDR have been extensively studied, large data gaps exist in our knowledge of non-mammalian VDRs beyond homology comparisons and transactivation in response to 1, $25D_3$. Teleost fish are of particular interest as they have undergone a whole genome duplication event specific to their lineage, and as a result maintain two paralogous VDRs while other vertebrates maintain a single ortholog. The presence of paralogous nuclear receptors in teleost fish provides a unique opportunity to study the evolution and functional divergence of duplicate NRs following a WGD. The purpose of this dissertation is to examine the functional diversification of the vitamin D receptor (VDR) with increasing genome complexity within teleosts and vertebrate evolution. In Chapter 1, I investigate the hypothesis that teleost VDR paralogs have undergone a functional divergence due to sub and/or neofunctionalization. However, the ability to evaluate derived and ancestral functions of teleost VDR paralogs is limited due to the lack of data on ancestral VDR function. Therefore in Chapter 2, I examine critical NR molecular functions of basal vertebrate VDRs, and hypothesize that the VDR-$1,25D_3$ partnership is ancient. Lastly, in Chapter 3 I examine the hypothesis that the evolution of lithocholic acid as a functional VDR ligand is a result of exaptation, rather than an adaptation specific to higher vertebrates. Finally, functional data from these chapters will be combined into a bioinformatics analysis in an attempt to determine possible drivers of the observed functional differences.

REFERENCES

1. Nelson JS. *Fishes of the World.* 4th Edition ed. New York: J. Wiley; 2006.

2. Dehal P, Boore J. Two rounds of whole genome duplication in the ancestral vertebrate. *Plos Biol.* 2005;3(10):1700-1708.

3. Hoegg S, Brinkmann H, Taylor J, Meyer A. Phylogenetic timing of the fish-specific genome duplication correlates with the diversification of teleost fish. *J Mol Evol.* 2004;59(2):190-203.

4. Volff JN. Genome evolution and biodiversity in teleost fish. *Heredity (Edinb).* 2005;94(3):280-294.

5. Crow K, Stadler P, Lynch V, Amemiya C, Wagner G. The "fish-specific" Hox cluster duplication is coincident with the origin of teleosts. *Mol Biol Evol.* 2006;23(1):121-136.

6. Taylor J, Van de Peer Y, Braasch I, Meyer A. Comparative genomics provides evidence for an ancient genome duplication event in fish. *Philos T Roy Soc B.* 2001;356(1414):1661-1679.

7. Taylor J, Van de Peer Y, Meyer A. Revisiting recent challenges to the ancient fish-specific genome duplication hypothesis. *Curr Biol.* 2001;11(24):R1005-R1007.

8. Ohno S. *Evolution by gene duplication.* New York: Springer-Verlag; 1970.

9. Crow K, Wagner G. What is the role of genome duplication in the evolution of complexity and diversity? *Mol Biol Evol.* 2006;23(5):887-892.

10. Zhang J. Evolution by gene duplication: an update. *TRENDs in Ecology and Evolution.* 2003;18(6):292 - 298.

11. Freeling M, Thomas BC. Gene-balanced duplications, like tetraploidy, provide predictable drive to increase morphological complexity. *Genome research.* 2006;16(7):805-814.

12. Van de Peer Y, Maere S, Meyer A. OPINION The evolutionary significance of ancient genome duplications. *Nat Rev Genet.* 2009;10(10):725-732.

13. Postlethwait JH. The zebrafish genome in context: ohnologs gone missing. *J Exp Zool B Mol Dev Evol.* 2007;308(5):563-577.

14. Force A, Amores A, Postlethwait JH. Hox cluster organization in the jawless vertebrate Petromyzon marinus. *J Exp Zool.* 2002;294(1):30-46.

15. Kuraku S, Meyer A. The evolution and maintenance of Hox gene clusters in vertebrates and the teleost-specific genome duplication. *Int J Dev Biol.* 2009;53(5-6):765-773.

16. Lemons D, McGinnis W. Genomic evolution of Hox gene clusters. *Science.* 2006;313(5795):1918-1922.

17. Meyer A, Van de Peer Y. From 2R to 3R: evidence for a fish-specific genome duplication (FSGD). *Bioessays.* 2005;27(9):937-945.

18. Amores A, Force A, Yan Y, Joly L, Amemiya C, Fritz A, Ho R, Langeland J, Prince V, Wang Y, Westerfield M, Ekker M, Postlethwait J. Zebrafish hox clusters and vertebrate genome evolution. *Science.* 1998;282(5394):1711-1714.

19. Amores A, Suzuki T, Yan Y, Pomeroy J, Singer A, Amemiya C, Postlethwait J. Developmental roles of pufferfish Hox clusters and genome evolution in ray-fin fish. *Genome Res.* 2004;14(1):1-10.

20. Naruse K, Fukamachi S, Mitani H, Kondo M, Matsuoka T, Kondo S, Hanamura N, Morita Y, Hasegawa K, Nishigaki R, Shimada A, Wada H, Kusakabe T, Suzuki N, Kinoshita M, Kanamori A, Terado T, Kimura H, Nonaka M, Shima A. A detailed linkage map of medaka, Oryzias latipes: comparative genomics and genome evolution. *Genetics.* 2000;154(4):1773-1784.

21. Hoegg S, Boore JL, Kuehl JV, Meyer A. Comparative phylogenomic analyses of teleost fish Hox gene clusters: lessons from the cichlid fish Astatotilapia burtoni. *BMC Genomics.* 2007;8:317.

22. Maglich J, Caravella J, Lambert M, Willson T, Moore J, Ramamurthy L. The first completed genome sequence from a teleost fish (Fugu rubripes) adds significant diversity to the nuclear receptor superfamily. *Nucleic Acids Res.* 2003;31(14):4051-4058.

23. Metpally RPR, Vigneshwar R, Sowdhamini R. Genome inventory and analysis of nuclear hormone receptors in Tetraodon nigroviridis. *J Biosciences.* 2007;32(1):43-50.

24. Bertrand S, Thisse B, Tavares R, Sachs L, Chaumot A, Bardet PL, Escriva H, Duffraisse M, Marchand O, Safi R, Thisse C, Laudet V. Unexpected novel relational links uncovered by extensive developmental profiling of nuclear receptor expression. *PLoS genetics.* 2007;3(11):e188.

25. Cresko WA, Yan YL, Baltrus DA, Amores A, Singer A, Rodriguez-Mari A, Postlethwait JH. Genome duplication, subfunction partitioning, and lineage divergence: Sox9 in stickleback and zebrafish. *Developmental dynamics : an official publication of the American Association of Anatomists.* 2003;228(3):480-489.

26. Force A, Lynch M, Pickett F, Amores A, Yan Y, Postlethwait J. Preservation of duplicate genes by complementary, degenerative mutations. *Genetics.* 1999;151(4):1531-1545.

27. Jenny MJ, Karchner SI, Franks DG, Woodin BR, Stegeman JJ, Hahn ME. Distinct Roles of Two Zebrafish AHR Repressors (AHRRa and AHRRb) in Embryonic Development and Regulating the Response to 2,3,7,8-Tetrachlorodibenzo-p-dioxin. *Toxicological Sciences.* 2009;110(2):426-441.

28. Cheng C, Chen L. Evolution of an antifreeze glycoprotein. *Nature.* 1999;401(6752):443-444.

29. Naruse K, Tanaka M, Mita K, Shima A, Postlethwait J, Mitani H. A medaka gene map: the trace of ancestral vertebrate proto-chromosomes revealed by comparative gene mapping. *Genome research.* 2004;14(5):820-828.

30. Hahn MW. Distinguishing Among Evolutionary Models for the Maintenance of Gene Duplicates. *Journal of Heredity.* 2009;100(5):605-617.

31. Roth C, Rastogi S, Arvestad L, Dittmar K, Light S, Ekman D, Liberles DA. Evolution after gene duplication: Models, mechanisms, sequences, systems, and organisms. *J Exp Zool Part B.* 2007;308B(1):58-73.

32. Lynch M, Conery J. The evolutionary fate and consequences of duplicate genes. *Science.* 2000;290(5494):1151-1155.

33. Lynch M, Force A. The origin of interspecific genomic incompatibility via gene duplication. *Am Nat.* 2000;156(6):590-605.

34. Semon M, Wolfe KH. Reciprocal gene loss between Tetraodon and zebrafish after whole genome duplication in their ancestor. *Trends in genetics : TIG.* 2007;23(3):108-112.

35. Lynch M, Walsh J. *Genetics and Analysis of Quantitative Traits.* Sunderland, MA: Sinauer Associates; 1998.

36. Chen L, DeVries AL, Cheng CH. Evolution of antifreeze glycoprotein gene from a trypsinogen gene in Antarctic notothenioid fish. *Proceedings of the National Academy of Sciences of the United States of America.* 1997;94(8):3811-3816.

37. Postlethwait J, Amores A, Cresko W, Singer A, Yan Y. Subfunction partitioning, the teleost radiation and the annotation of the human genome. *Trends Genet.* 2004;20(10):481-490.

38. Blomme T, Vandepoele K, De Bodt S, Simillion C, Maere S, Van de Peer Y. The gain and loss of genes during 600 million years of vertebrate evolution. *Genome Biol.* 2006;7(5):R43.

39. Kassahn KS, Dang VT, Wilkins SJ, Perkins AC, Ragan MA. Evolution of gene function and regulatory control after whole-genome duplication: comparative analyses in vertebrates. *Genome research.* 2009;19(8):1404-1418.

40. Veitia RA, Bottani S, Birchler JA. Cellular reactions to gene dosage imbalance: genomic, transcriptomic and proteomic effects. *Trends Genet.* 2008;24(8):390-397.

41. Edger PP, Pires JC. Gene and genome duplications: the impact of dosage-sensitivity on the fate of nuclear genes. *Chromosome Res.* 2009;17(5):699-717.

42. Birchler JA, Yao H, Chudalayandi S. Biological consequences of dosage dependent gene regulatory systems. *Biochim Biophys Acta.* 2007;1769(5-6):422-428.

43. Lynch VJ, Wagner GP. Resurrecting the role of transcription factor change in developmental evolution. *Evolution; international journal of organic evolution.* 2008;62(9):2131-2154.

44. Aranda A, Pascual A. Nuclear hormone receptors and gene expression. *Physiol Rev.* 2001;81(3):1269-1304.

45. Shaffer P, Gewirth D. Vitamin D receptor-DNA interactions. *Vitam Horm.* 2004;68:257-273.

46. Hsieh JC, Whitfield GK, Oza AK, Dang HT, Price JN, Galligan MA, Jurutka PW, Thompson PD, Haussler CA, Haussler MR. Characterization of unique DNA-binding and transcriptional-activation functions in the carboxyl-terminal extension of the zinc finger region in the human vitamin D receptor. *Biochemistry.* 1999;38(49):16347-16358.

47. Rochel N, Wurtz J, Mitschler A, Klaholz B, Moras D. The crystal structure of the nuclear receptor for vitamin D bound to its natural ligand. *Mol Cell.* 2000;5(1):173-179.

48. Ciesielski F, Rochel N, Mitschler A, Kouzmenko A, Moras D. Structural investigation of the ligand binding domain of the zebrafish VDR in complexes with 1 alpha,25(OH)(2)D-3 and Gemini: purification, crystallization and preliminary X-ray diffraction analysis. *J Steroid Biochem.* 2004;89-90(1-5):55-59.

49. Savkur RS, Bramlett KS, Clawson D, Burris TP. Pharmacology of Nuclear Receptor-Coregulator Recognition. In: Litwack G, ed. *Nuclear Receptor Coregulators.* Vol 68. San Diego: Elsevier Academic Press; 2004:145-183.

50. Bertrand S, Brunet FG, Escriva H, Parmentier G, Laudet V, Robinson-Rechavi M. Evolutionary genomics of nuclear receptors: from twenty-five ancestral genes to

derived endocrine systems. *Molecular biology and evolution.* 2004;21(10):1923-1937.

51. Robinson-Rechavi M, Carpentier AS, Duffraisse M, Laudet V. How many nuclear hormone receptors are there in the human genome? *Trends in genetics : TIG.* 2001;17(10):554-556.

52. Howarth DL. *Characterization of FXR alpha in medaka and its involvement in hepatobiliary injury* [Dissertation]. Durham: Integrated Toxicology and Environmental Health Program, Duke University; 2009.

53. Taylor J, Raes J. Duplication and divergence: The evolution of new genes and old ideas. *Annu Rev Genet.* 2004;38:615-643.

54. Dehal P, Satou Y, Campbell RK, Chapman J, Degnan B, De Tomaso A, Davidson B, Di Gregorio A, Gelpke M, Goodstein DM, Harafuji N, Hastings KE, Ho I, Hotta K, Huang W, Kawashima T, Lemaire P, Martinez D, Meinertzhagen IA, Necula S, Nonaka M, Putnam N, Rash S, Saiga H, Satake M, Terry A, Yamada L, Wang HG, Awazu S, Azumi K, Boore J, Branno M, Chin-Bow S, DeSantis R, Doyle S, Francino P, Keys DN, Haga S, Hayashi H, Hino K, Imai KS, Inaba K, Kano S, Kobayashi K, Kobayashi M, Lee BI, Makabe KW, Manohar C, Matassi G, Medina M, Mochizuki Y, Mount S, Morishita T, Miura S, Nakayama A, Nishizaka S, Nomoto H, Ohta F, Oishi K, Rigoutsos I, Sano M, Sasaki A, Sasakura Y, Shoguchi E, Shin-i T, Spagnuolo A, Stainier D, Suzuki MM, Tassy O, Takatori N, Tokuoka M, Yagi K, Yoshizaki F, Wada S, Zhang C, Hyatt PD, Larimer F, Detter C, Doggett N, Glavina T, Hawkins T, Richardson P, Lucas S, Kohara Y, Levine M, Satoh N, Rokhsar DS. The draft genome of Ciona intestinalis: insights into chordate and vertebrate origins. *Science.* 2002;298(5601):2157-2167.

55. Adams MD, Celniker SE, Holt RA, Evans CA, Gocayne JD, Amanatides PG, Scherer SE, Li PW, Hoskins RA, Galle RF, George RA, Lewis SE, Richards S, Ashburner M, Henderson SN, Sutton GG, Wortman JR, Yandell MD, Zhang Q, Chen LX, Brandon RC, Rogers YH, Blazej RG, Champe M, Pfeiffer BD, Wan KH, Doyle C, Baxter EG, Helt G, Nelson CR, Gabor GL, Abril JF, Agbayani A, An HJ, Andrews-Pfannkoch C, Baldwin D, Ballew RM, Basu A, Baxendale J, Bayraktaroglu L, Beasley EM, Beeson KY, Benos PV, Berman BP, Bhandari D, Bolshakov S, Borkova D, Botchan MR, Bouck J, Brokstein P, Brottier P, Burtis KC, Busam DA, Butler H, Cadieu E, Center A, Chandra I, Cherry JM, Cawley S, Dahlke C, Davenport LB, Davies P, de Pablos B, Delcher A, Deng Z, Mays AD, Dew I, Dietz SM, Dodson K, Doup LE, Downes M, Dugan-Rocha S, Dunkov BC, Dunn P, Durbin KJ, Evangelista CC, Ferraz C,

Ferriera S, Fleischmann W, Fosler C, Gabrielian AE, Garg NS, Gelbart WM, Glasser K, Glodek A, Gong F, Gorrell JH, Gu Z, Guan P, Harris M, Harris NL, Harvey D, Heiman TJ, Hernandez JR, Houck J, Hostin D, Houston KA, Howland TJ, Wei MH, Ibegwam C, Jalali M, Kalush F, Karpen GH, Ke Z, Kennison JA, Ketchum KA, Kimmel BE, Kodira CD, Kraft C, Kravitz S, Kulp D, Lai Z, Lasko P, Lei Y, Levitsky AA, Li J, Li Z, Liang Y, Lin X, Liu X, Mattei B, McIntosh TC, McLeod MP, McPherson D, Merkulov G, Milshina NV, Mobarry C, Morris J, Moshrefi A, Mount SM, Moy M, Murphy B, Murphy L, Muzny DM, Nelson DL, Nelson DR, Nelson KA, Nixon K, Nusskern DR, Pacleb JM, Palazzolo M, Pittman GS, Pan S, Pollard J, Puri V, Reese MG, Reinert K, Remington K, Saunders RD, Scheeler F, Shen H, Shue BC, Siden-Kiamos I, Simpson M, Skupski MP, Smith T, Spier E, Spradling AC, Stapleton M, Strong R, Sun E, Svirskas R, Tector C, Turner R, Venter E, Wang AH, Wang X, Wang ZY, Wassarman DA, Weinstock GM, Weissenbach J, Williams SM, WoodageT, Worley KC, Wu D, Yang S, Yao QA, Ye J, Yeh RF, Zaveri JS, Zhan M, Zhang G, Zhao Q, Zheng L, Zheng XH, Zhong FN, Zhong W, Zhou X, Zhu S, Zhu X, Smith HO, Gibbs RA, Myers EW, Rubin GM, Venter JC. The genome sequence of Drosophila melanogaster. *Science.* 2000;287(5461):2185-2195.

56. Thomson SA, Baldwin WS, Wang YH, Kwon G, Leblanc GA. Annotation, phylogenetics, and expression of the nuclear receptors in Daphnia pulex. *BMC Genomics.* 2009;10:500.

57. Reitzel AM, Tarrant AM. Nuclear receptor complement of the cnidarian Nematostella vectensis: phylogenetic relationships and developmental expression patterns. *BMC evolutionary biology.* 2009;9:230.

58. Bridgham JT, Eick GN, Larroux C, Deshpande K, Harms MJ, Gauthier ME, Ortlund EA, Degnan BM, Thornton JW. Protein evolution by molecular tinkering: diversification of the nuclear receptor superfamily from a ligand-dependent ancestor. *PLoS biology.* 2010;8(10).

59. Reschly EJ, Krasowski MD. Evolution and function of the NR1I nuclear hormone receptor subfamily (VDR, PXR, and CAR) with respect to metabolism of xenobiotics and endogenous compounds. *Curr Drug Metab.* 2006;7(4):349-365.

60. Schubert M, Brunet F, Paris M, Bertrand S, Benoit G, Laudet V. Nuclear hormone receptor signaling in amphioxus. *Dev Genes Evol.* 2008;218(11-12):651-665.

61. Reschly EJ, Bainy ACD, Mattos JJ, Hagey LR, Bahary N, Mada SR, Ou J, Venkataramanan R, Krasowski MD. Functional evolution of the vitamin D and pregnane X receptors. *BMC Evol Biol.* 2007;7:222.

62. Ekins S, Reschly EJ, Hagey LR, Krasowski MD. Evolution of pharmacologic specificity in the pregnane X receptor. *BMC evolutionary biology.* 2008;8:103.

63. Norman AW. From vitamin D to hormone D: fundamentals of the vitamin D endocrine system essential for good health. *Am J Clin Nutr.* 2008;88(2):491S-499S.

64. Nagpal S, Na S, Rathnachalam R. Noncalcemic actions of vitamin D receptor ligands. *Endocr Rev.* 2005;26(5):662-687.

65. Bouillon R, Carmeliet G, Verlinden L, Van Etten E, Verstuyf A, Luderer HF, Lieben L, Mathieu C, Demay M. Vitamin D and Human Health: Lessons from Vitamin D Receptor Null Mice. *Endocrine Reviews.* 2008;29(6):726-776.

66. Holick M. Vitamin D: importance in the prevention of cancers, type 1 diabetes, heart disease, and osteoporosis. *Am J Clin Nutr.* 2004;79(3):362-371.

67. Holick MF, Chen TC. Vitamin D deficiency: a worldwide problem with health consequences. *Am J Clin Nutr.* 2008;87(4):1080S-1086S.

68. Nagy L, Schwabe J. Mechanism of the nuclear receptor molecular switch. *Trends Biochem Sci.* 2004;29(6):317-324.

69. Kallenberger BC, Love JD, Chatterjee VK, Schwabe JW. A dynamic mechanism of nuclear receptor activation and its perturbation in a human disease. *Nat Struct Biol.* 2003;10(2):136-140.

70. Bettoun D, Burris T, Houck K, Buck D, Stayrook K, Khalifa B, Lu J, Chin W, Nagpal S. Retinoid X receptor is a nonsilent major contributor to vitamin D receptor-mediated transcriptional activation. *Mol Endocrinol.* 2003;17(11):2320-2328.

71. Thompson PD, Remus LS, Hsieh JC, Jurutka PW, Whitfield GK, Galligan MA, Encinas Dominguez C, Haussler CA, Haussler MR. Distinct retinoid X receptor

activation function-2 residues mediate transactivation in homodimeric and vitamin D receptor heterodimeric contexts. *Journal of molecular endocrinology.* 2001;27(2):211-227.

72. Carlberg C. Ligand-mediated conformational changes of the VDR are required for gene transactivation. *The Journal of steroid biochemistry and molecular biology.* 2004;89-90(1-5):227-232.

73. Li YC. Cloning and Characterization of the Vitamin D Receptor from Xenopus laevis. *Endocrinology.* 1997;138(6):2347-2353.

74. Whitfield GK, Dang HT, Schluter SF, Bernstein RM, Bunag T, Manzon LA, Hsieh G, Dominguez CE, Youson JH, Haussler MR, Marchalonis JJ. Cloning of a functional vitamin D receptor from the lamprey (Petromyzon marinus), an ancient vertebrate lacking a calcified skeleton and teeth. *Endocrinology.* 2003;144(6):2704-2716.

75. Lock E-J, Waagbo R, Bonga SW, Flik G. The significance of vitamin D for fish: a review. *Aquacult Nutr.* 2010;16(1):100-116.

76. Lin CH, Su CH, Tseng DY, Ding FC, Hwang PP. Action of vitamin D and the receptor, VDRa, in calcium handling in zebrafish (Danio rerio). *Plos One.* 2012;7(9):e45650.

77. Howarth DL, Law SHW, Barnes B, Hall JM, Hinton DE, Moore L, Maglich JM, Moore JT, Kullman SW. Paralogous vitamin D receptors in teleosts: Transition of nuclear receptor function. *Endocrinology.* 2008;149(5):2411-2422.

78. Suzuki T, Suzuki N, Srivastava A, Kurokawa T. Identification of cDNAs encoding two subtypes of vitamin D receptor in flounder, Paralichthys olivaceus. *Biochem Bioph Res Co.* 2000;270(1):40-45.

79. Peleg S, Liu YY, Reddy S, Horst RL, White MC, Posner GH. A 20-epi side chain restores growth-regulatory and transcriptional activities of an A ring-modified hybrid analog of 1 alpha, 25-dihydroxyvitamin D3 without increasing its affinity to the vitamin D receptor. *Journal of cellular biochemistry.* 1996;63(2):149-161.

80. Bury N, Sturm A, Le Rouzic P, Lethimonier C, Ducouret B, Guiguen Y, Robinson-Rechavi M, Laudet V, Rafestin-Oblin M, Prunet P. Evidence for two distinct functional glucocorticoid receptors in teleost fish. *J Mol Endocrinol.* 2003;31(1):141-156.

FIGURES

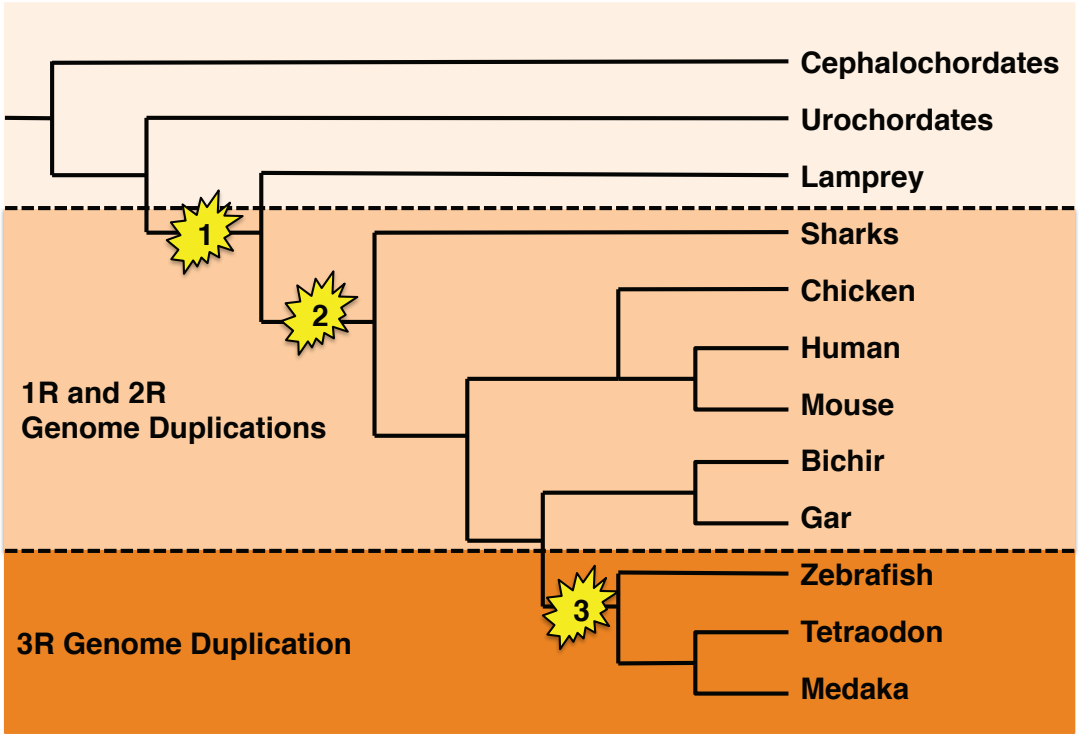

Figure 1. Whole genome duplications in vertebrate evolution. Two whole genome duplication events (1R and 2R) are speculated to have occurred early in vertebrate evolution, roughly 500-600 million years ago. The first (1R) took place in the stem lineage of vertebrates, and the second (2R) occurred after the divergence of jawless fish but before the divergence on cartilaginous fish. A third WGD (3R) is though to have occurred roughly 350 million years ago within Actinopterygii, in the stem lineage of teleost fish. Teleosts maintain paralogous copies of many single copy tetrapod genes.

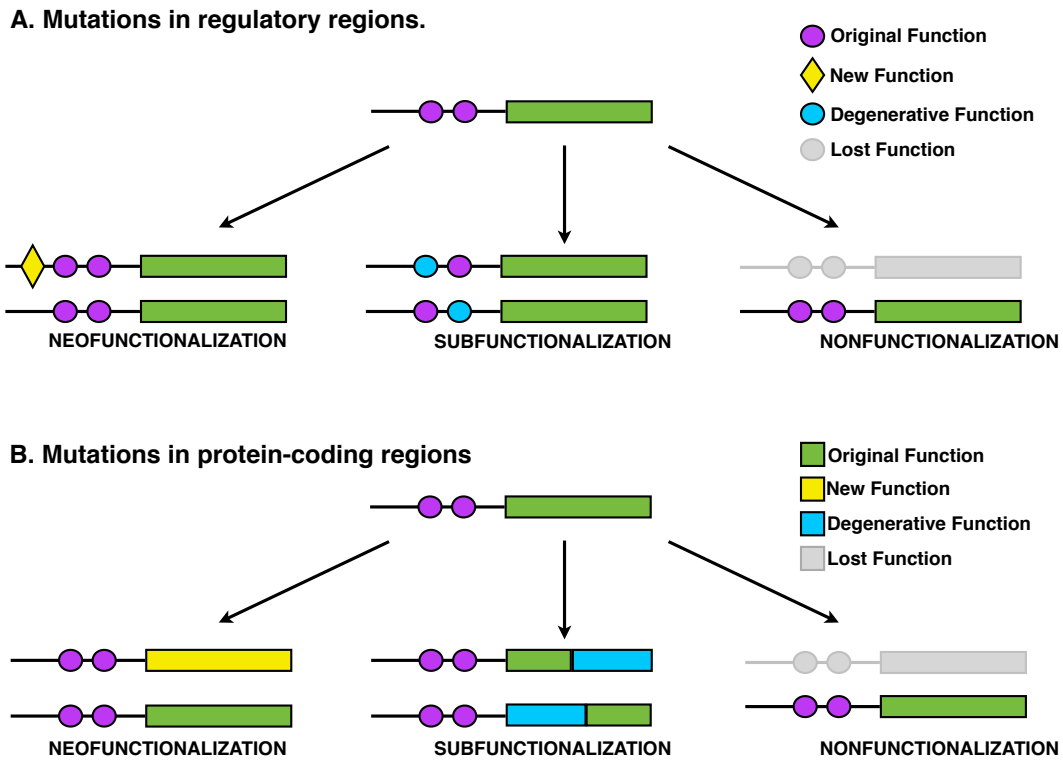

Figure 2. Evolution of gene paralogs following a WGD. Depicts changes in either (**A)** *cis*-regulatory regions or (**B)** protein coding regions of a gene. 1. One copy may gain a beneficial mutation conferring a novel function, necessitating the retention of both copies to maintain both the original and novel function (Neofunctionalization). 2. Both copies gain degenerative but complementary mutations, and thus both copies necessary to maintain the ancestral function (Subfunctionalization). 3. An estimated 50-90% of duplicates are lost through accumulated mutations and become nonfunctional, and only one copy is maintained (Nonfunctionalization).

Adapted from:
Hahn MW. Distinguishing Among Evolutionary Models for the Maintenance of Gene Duplicates. *Journal of Heredity.* 2009;100(5):605-617.

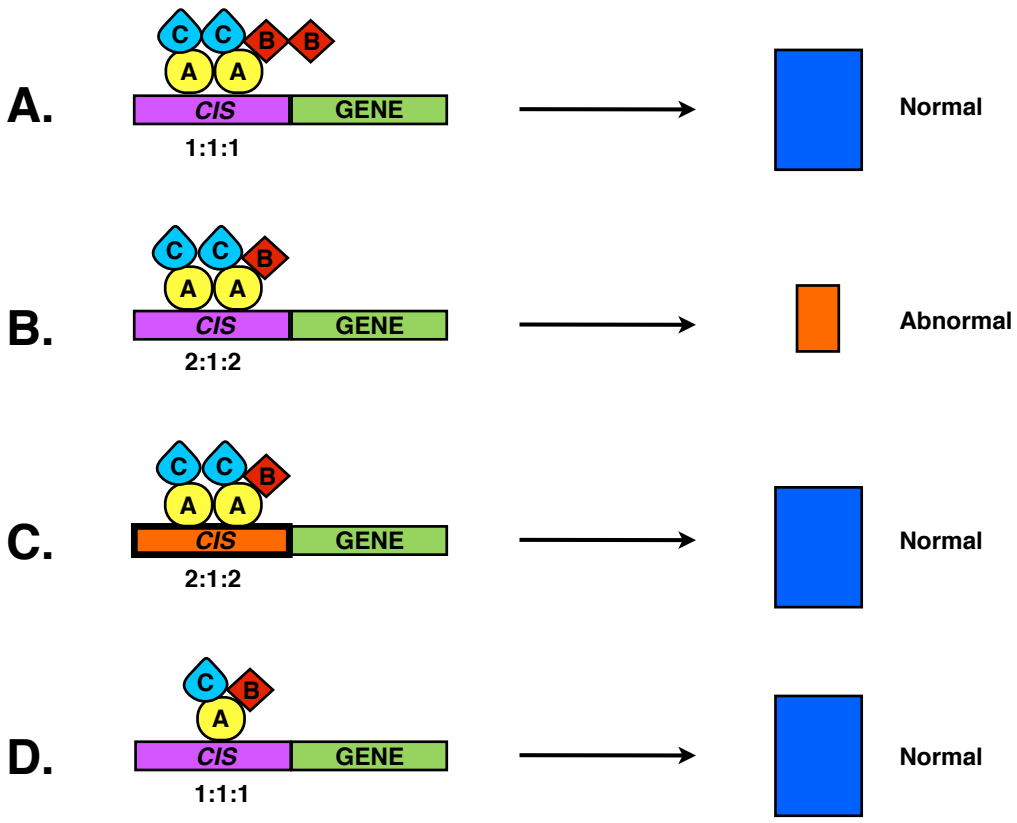

Figure 3. Stoichiometric effects on transcription complex function and resulting phenotypic consequences. **(A)** A stoichiometrically balanced (1:1:1) transcription complex is able to properly recognize response elements in target genes and activate transcription, resulting in a normal phenotype (depicted by the blue rectangle). (**B)** The loss of one subunit (B) leaves transcription complex unbalanced (2:1:2), and the complex is unable to interact with response elements in a normal fashion, resulting in an abnormal phenotype (depicted by the smaller, orange rectangle). C and D demonstrate two possible compensatory mechanisms: (**C)** depicts modification of the response element so that the unbalanced transcription complex (2:1:2) is tolerated, and a normal phenotype is produced. (**D)** co-adaptation of the

transcription complex over time to a new balanced state (1:1:1) is achieved that produces a normal phenotype.

Adapted from:
Birchler JA, Yao H, Chudalayandi S. Biological consequences of dosage dependent gene regulatory systems. *Biochim Biophys Acta.* 2007;1769(5-6):422-428.

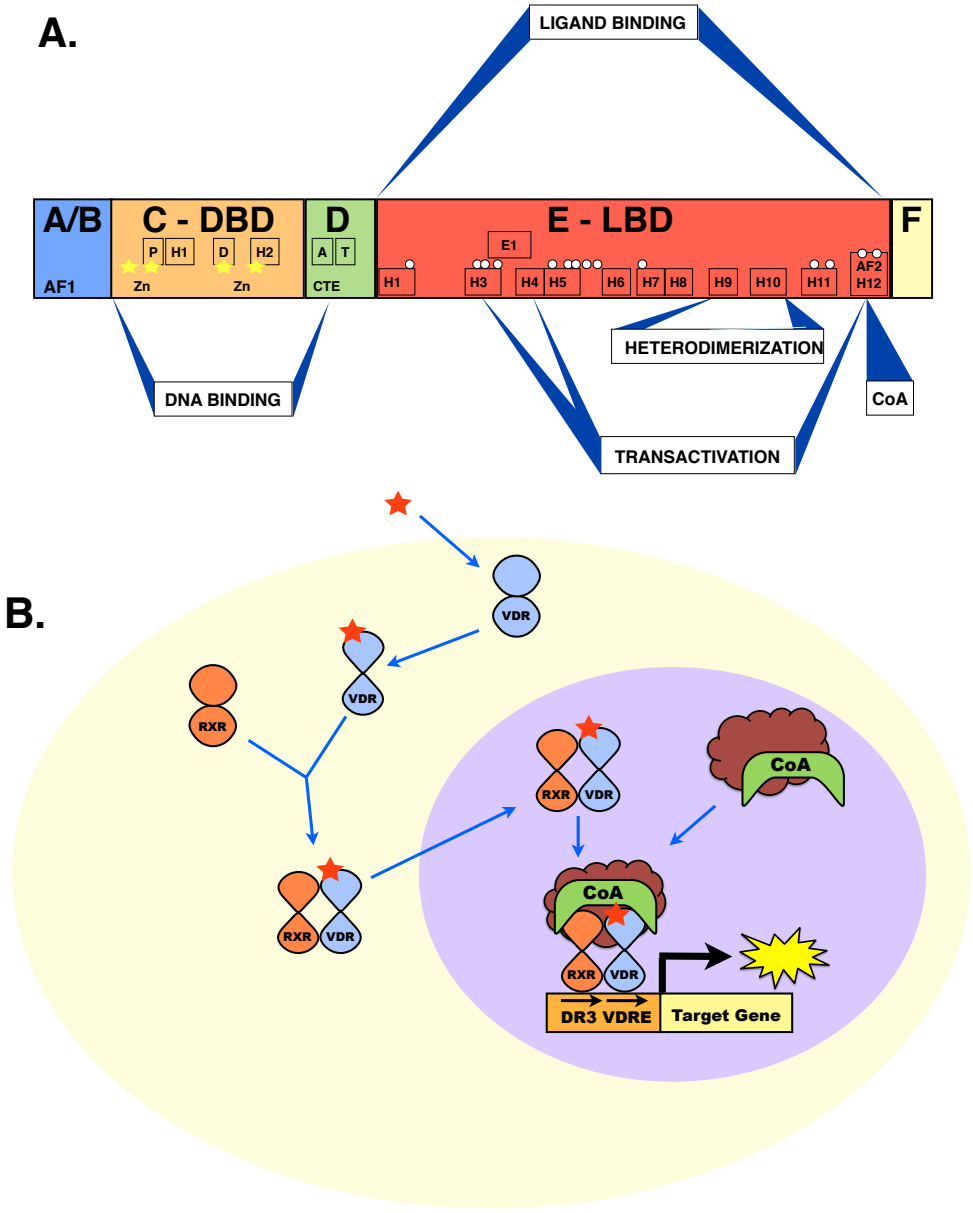

Figure 4. (A) Nuclear receptor domain structure using the vitamin D receptor (VDR) as a model. Nuclear receptors share a modular domain structure with each region corresponding to different functional domains. The N-terminal A/B region is highly variable both in size

and sequence and contains the activation function-1 (AF1) domain that participates in ligand-independent activation of the receptor. The C region contains the DNA binding domain (DBD), which is the most highly conserved NR domain. The role of the DBD is to recognize and bind to specific target sequences within the response elements of target genes. The DBD consists of two zinc finger motifs, each consisting of an α-helix (H1 and H2) with four conserved cysteine residues (yellow stars) that bind a zinc ion. The P box and D box are located at the base of each finger, and are required for specific sequences recognition and dimerization with the DBD of the heterodimer partner. H1, also known as the recognition helix binds to specific bases in the major groove. The hinge region (D) contains the c-terminal extension (CTE) that confers additional DNA specificity, and plays a "spacer" role between the DBD and LBD. The E region, or ligand binding domain (LBD) is a multifunctional region with essential roles in ligand binding, heterodimerization, coactivator (CoA) recruitment, and transactivation. The LBD consists of 12 α-helices containing amino acid residues that directly bind to the ligand (white circles). The conformational change induced in a receptor upon ligand binding positions H9 and H10 for heterodimerization with identical helices in the LBD of RXR. In addition, the ligand-induced conformational change stabilizes and positions H12 for coactivator recruitment. H12 contains the activation function-2 domain (AF2), which directly interacts with coactivators and is ligand-dependent. The c-terminal F domain is highly variable between receptors and its function is not well understood**. (B)** Steps in nuclear receptor activation using VDR as a model. Vitamin D binds to the vitamin D receptor (VDR), inducing a dramatic conformational change in the receptor to the active state. Ligand-activated VDR then heterodimerizes with RXR, and the

heterodimer translocates to the nucleus. The heterodimer recognizes and binds to vitamin D responses elements (VDREs) upstream from target genes and initiates transcription complex formation by recruiting coactivators. Gene transcription is induced once the transcription complex formation is complete.

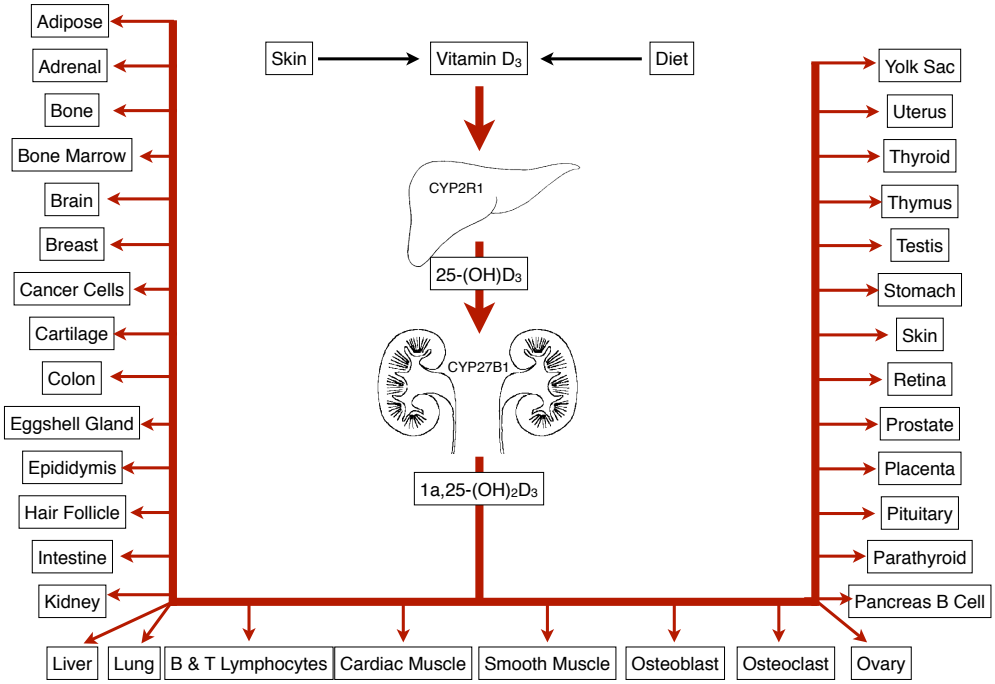

Figure 5. Organs and tissues that are targets of the vitamin D endocrine system. To date, thirty-six tissues have been demonstrated to express VDR, and are thus capable of eliciting a biological response to 1α, 25-dihydroxyvitamin D_3 (1, $25D_3$). Organs including the kidney, intestine, bone, and parathyroid are well known members of the vitamin D endocrine system and are vital to maintaining calcium homeostasis. However, more recent studies have revealed numerous non-calcemic effects of VDR and vitamin D, including control of cancer cell proliferation and differentiation, regulation of hair growth, immune cell function, insulin secretion, and central nervous system development.

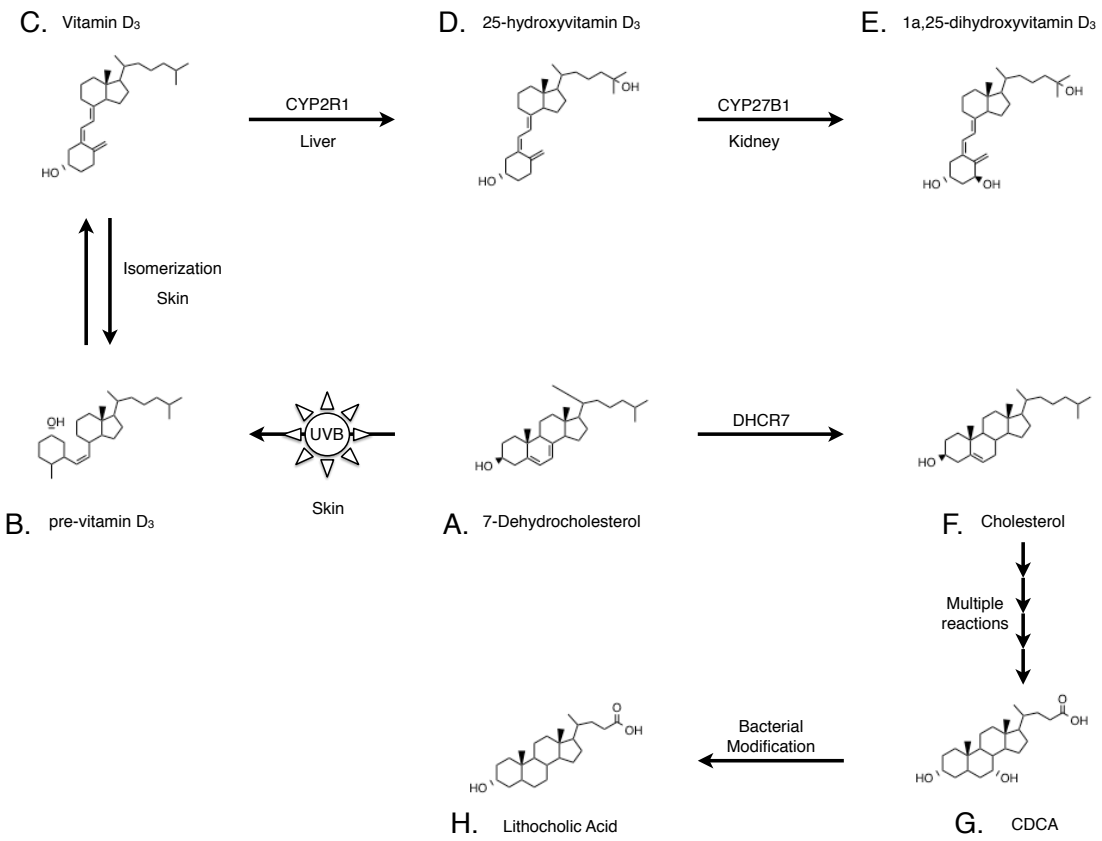

Figure 6. Synthesis pathway of 1α, 25-dihydroxyvitmain D_3 (1, $25D_3$) and lithocholic acid (LCA) from 7-dehydrocholesterol. 7-dehydrocholesterol is a cholesterol precursor found in epidermis of higher animals. **(A)** Exposure of 7-dehydrocholesterol to UV light produces pre-vitamin D_3 **(B)** after the bond between C9 and C10 is broken. Pre-vitamin D_3 is unstable, and rapidly isomerizes to vitamin D_3 **(C)**. Vitamin D_3 can also be obtained through diet, which is the major vitamin D_3 source for fish. Vitamin D_3 itself has no intrinsic activity, and must be metabolically activated via two hydroxylation reactions. Vitamin D_3 is transported in the bloodstream from the skin to the liver bound to vitamin D binding protein (VDBP), where it

undergoes the first hydroxylation reaction mediated by 25-hydroxylase (CYP2R1) **(D)**. 25-hydroxyvitamin D_3 is next transported to the kidney for the second hydroxylation by 1α-hydroxylase (CYP27B1), forming 1α, 25-dihydroxyvitamin D_3, the active metabolite of vitamin D_3 and the classic ligand of VDR **(E)**. 1α, 25-dihydroxyvitamin D_3 is transported in the blood to target tissues. An additional, more recently discovered VDR ligand is also a product of 7-dehydrocholesterol. 7-dehydrocholesterol **(A)** is a parent compound of cholesterol **(F)**, which has multiple functions essential to vertebrate life. 7-dehydrocholesterol is reduced to cholesterol via 7-dehydrocholestrol reductase (DHCR7). Through numerous reactions and multiple enzymes, cholesterol can be metabolized to CDCA **(G)**, an ampiphatic primary bile acid necessary for lipid digestion. CDCA is susceptible to bacterial modification in the gut. The removal of the C7-OH produces lithocholic acid (LCA), a toxic secondary bile acid **(H)**. As a VDR ligand, LCA induces the expression of CYP3A4, an essential enzyme in LCA detoxification. Thus VDR has a role in both mediating the endocrine effects of 1α, 25-dihydroxyvitamin D_3, and controlling the toxic levels of LCA.

CHAPTER ONE

Functional Diversification of Vitamin D Receptor Paralogs in Teleost Fish Following a Whole Genome Duplication Event

Erin M. Kollitz[1], G. Kerr Whitfied[2], Mary Beth Hawkins[3], and Seth W. Kullman[1]

[1] Environmental and Molecular Toxicology, Department of Biology, North Carolina State University, Raleigh, NC

[2] Department of Basic Medical Sciences, The University of Arizona College of Medicine, Phoenix, AZ

[3] Department of Biology, North Carolina State University, Raleigh, NC

ABSTRACT

Teleost fish comprise ~27,000 extant species and are the most diverse and successful groups of vertebrates. Much of the complexity of the teleost genome is a result of successive rounds of whole genome duplications (WGD). The retention of multiple gene pairs in teleosts provides a unique opportunity to gain insight into how genes evolve through specific evolutionary processes. This study examines whether paralogous vitamin D receptor genes (VDRs) have acquired novel function(s) and/or partitioned ancestral sub-functions subsequent to successive duplication events. VDRα and VDRβ paralogs were cloned from the Japanese medaka (*Oryzias latipes)* and the zebrafish (*Danio rerio)*, two distantly related teleosts. Saturation binding analysis demonstrates that the VDR paralogs maintain a high binding affinity for 1α, 25-dihydroxyvitamin D_3 (1, $25D_3$) that is similar to mammalian VDR. Concentration-response curves of VDR transactivation with 1, $25D_3$ suggest that while the ligand potency is highly similar, maximal transactivation efficacy is significantly different between the two VDR forms. In addition, both VDRα paralogs demonstrate preferential DNA binding compared to the VDRβ paralogs in response to 1, $25D_3$. Protein-protein interactions were investigated using co-transfection and mammalian two-hybrid, and mutation of co-regulator activation domains. Our results suggest that functional differences between VDR paralogs are driven through differential interactions between receptors and their co-regulators, including RXR and the SRC family of nuclear receptor coactivators. We speculate that the observed functional differences are due to subtle conformational differences between the two paralogs.

INTRODUCTION

The serial "2R" genome duplication hypothesis suggests that the vertebrate genome is a result of two rapid and successive rounds of genome duplication (1R and 2R) near the divergence of jawless and jawed vertebrates, approximately 500 million years ago (1). Whole genome duplication (WGD) events are proposed to be a significant force driving vertebrate evolution (2-4). These events provide a novel source of raw genetic material that can be subjected to evolutionary forces. The evolution and divergence of new genes as a result of a WGD may result in larger gene families, and permit the evolution of more complex interactions and gene networks (3,5,6). The resulting functional divergence of duplicate genes may lead to evolutionary innovations, speciation, increased vigour and adaptibility (3,4,7). Within ray-finned fishes (Actinopterygii), a third (3R) WGD occurred in the stem lineage of the teleostean fishes (8,9). It has been proposed that the 3R event has enabled significant diversification in teleosts (8,10). Support for this theory is provided in part by the fact that teleost orders that evolved after the 3R event contain almost 28,000 species, while only five families of roughly 44 species are found in more basal Actinopterygians (11).

An estimated 50-90% of redundant duplicates become nonfunctional following a WGD; however, gene retention is not random (7,12). It has been found that genes involved in signaling and regulatory pathways, such as transcription factors, have been preferentially retained in duplicate following a whole genome duplication event in order to maintain pathway integrity. These dosage-sensitive genes are sensitive to stoichiometric imbalance, and thus pathway disruption caused by the over or underexpression of network proteins could have negative pleiotropic effects, resulting in decreased fitness of the organism or lethality

(13,14). The retention of entire regulatory pathways may be a driving force of evolution, as an entire redundant network becomes free to diverge and evolve separately from the original pathway (3,6). Pathway divergence may lead to a more specialized control of regulatory functions and gene expression, facilitating species diversification and increasing morphological complexity (3,6).

One particular class of regulatory genes that exhibit preferential retention in teleosts is the nuclear receptor (NR) superfamily. NRs are ligand-dependent transcription factors that bind to lipophilic signaling molecules, resulting in systematic control and expression of target genes. Such control facilitates cellular responses to endogenous and exogenous signals through coordination of complex transcriptional processes (15,16). NRs play an essential role in many physiological and endocrine processes, including metabolism, reproduction, embryonic development, and control of cellular proliferation and differentiation (16). In teleosts, orthologs for all mammalian NR subclasses have been identified, including steroid hormone receptors and orphan receptors (17,18). In fact, teleosts maintain a larger complement of NRs than mammals. For example, while humans have 48 members of the NR family (19), while 68 have been identified in *Takifugu rubripes* (17), 71 in *Tetraodon nigroviridis* (18), 70 in *Danio rerio* (20), and 71 in the Japanese medaka (*Oryzias latipes*) (21). This is likely due to global retention of NRs subsequent to the 3R event. As NRs are important transcription factors for numerous endocrine-mediated processes, NR duplication and divergence may contribute to the evolutionary success of teleost through increased signal diversification, speciation, and development of evolutionary novelties. However, the functional role of duplicate NRs remains unresolved in these species.

The vitamin D receptor (VDR, NR1I1) was one of the first NRs identified, and its role as a high affinity receptor for mediating physiological actions of the hormonally active metabolite of vitamin D_3 (1α, 25-dihydroxyvitamin D_3 or 1, 25D_3) was quickly established (22-24). VDR has been cloned from a number of aquatic vertebrates with calcified endoskeletons. Additionally, a functional VDR has also recently been cloned from the sea lamprey (*Petromyzon marinus*) (25) and the little skate (*Leucoraja erinacea*) (Chapter 2 of this dissertation), which are both phylogenetically basal vertebrates lacking calcified endoskeletons. The presence of a functional VDR in aquatic and basal vertebrates suggests that the receptor appeared early in vertebrate evolution, before the water to land transition. This suggests that the endocrine control of calcium homeostasis may not have been a critical function of early VDRs, given that aquatic vertebrates live in environments that serve as a rich calcium source (26). However, the role of VDR and vitamin D in aquatic species remains relatively unexplored.

In this study, we build upon an initial observation that Japanese medaka (*Oryzias latipes*) VDRα and VDRβ paralogs exhibit differential sensitivities to the cognate VDR ligand despite highly homologous nucleic acid sequences (27). To further ascertain the functional basis for these transactivational differences, we examined molecular functions critical to VDR activation including: ligand affinities of 1, 25D_3 for each VDR paralog, DNA binding activities with canonical and divergent VDREs, heterodimerization with RXR, coactivator recruitment between VDR and the SRC/p160 family of nuclear receptor coactivators, and VDR transactivation with 1, 25D_3 as the primary ligand, both in the presence and absence of coactivators. We additionally extend our analysis to include

zebrafish VDRα and VDRβ paralogs to demonstrate conservation of functional differences across distantly related teleost phyla.

MATERIALS AND METHODS

Medaka and zebrafish VDRα and VDRβ cloning

Japanese medaka (*Oryzias latipes*) and zebrafish (*Danio rerio*) VDRα and VDRβ sequences were identified within the Ensembl genome database (URL: http://www.ensembl.org/index.html). Full-length transcripts were subsequently determined by identifying transcriptional start and stop codons for each gene. cDNAs containing a complete open reading frame (ORF) for each gene were produced by high fidelity polymerase chain reaction (PCR), using primer sets that spanned the entire nucleic acid sequence for each gene paralog (see Appendix A). PCR primers were flanked by restriction sites for incorporation and transfer between appropriate cloning and expression vectors. All cDNAs were amplified from extracts of medaka/zebrafish liver total RNA. Livers were homogenized with 1 ml RNA Bee (Tel Test Inc, Friendswood, TX) using a stainless steel Polytron homogenizer (Kinematica, Switzerland) followed by cleanup and on-column DNase treatment using an RNeasy Mini Kit (QIAGEN, Valencia, CA). RNA was eluted with 30 µl RNase-free water. RNA quantity and quality were verified using an Agilent 2100 Bioanalyzer and NanoDrop® ND-1000 spectrophotometer (Thermo Fisher Scientific, Waltham, MA). First strand cDNA was made from total RNA (1-3 µg) and diluted with RNase-free water to a final volume of 10 µl, and 1 µl oligo$(dT)_{15}$ (500 µg/ml; Promega, Madison, WI) and 1 µl 10 mM dNTPs were mixed with diluted RNA to yield a final volume of 20 µl. The mix was heated to 65ºC for 5 minutes and chilled on ice for 2 minutes. Following centrifugation, 4 µl 5X first-strand buffer (Life Technologies, Grand Island, NY), 2 µl of 0.1 M DDT, and 1 µl RNase OUT Inhibitor (40 U/µl; Life Technologies, Grand

Island, NY) were added to each reaction and heated to 37ºC. Following a 2 minute incubation, 1 µl Superscript Reverse Transcriptase (200 U/µl; Life Technologies, Grand Island, NY) was added to each reaction and mRNA reverse transcribed at 37ºC for 1 hour. All RT reactions were inactivated by incubation at 70ºC for 15 minutes and cDNAs were stored at -20ºC. For each 25-µl PCR reaction, first-strand cDNAs were amplified using 2 µl (100-300 ng) first-strand cDNA, 9 µl RNase-free water, 0.75 µl 10 µM forward primer (0.3 µM), 0.75 µl 10 µM reverse primer (0.3 µM), and 12.5 µl 2X Advantage Taq PCR Master Mix (Clontech Laboratories, Mountain View, CA). PCR reaction conditions were: 95ºC for 1.5 minutes followed by 35 cycles of 94ºC for 15 seconds, 55ºC for 30 seconds, and 72ºC for 2 minutes. PCR products for the VDRs were cloned into the pGEM-T Easy Vector (Promega Corporation, Madison, WI) as per manufacturer's suggestions. Full-length cDNAs for VDRα and VDRβ were sub-cloned into the pSG5 (Agilent Technologies, Santa Clara, CA) expression vector for transient transactivation, pVP16 (Clontech Laboratories, Mountain View, CA) containing the Herpes Simplex Virus VP16 activation domain up-steam of each VDR AF1 domain for mammalian two hybrid analysis or pET32a (EMD Millipore, Billerica, MA) for bacterial recombinant protein production. All constructs were restriction mapped and sequenced to ensure integrity and orientation of each VDR within defined vectors. All constructs consisted of the complete VDR ORF including internal start and stop codons, except for pET32a, where VDR stop codons were removed for inclusion of 3' His tags.

Coregulator constructs and luciferase reporters

All co-regulator expression constructs (human pSG5-SRC-1, pSG5-GRIP, pSG5-ATCR, pCDNA-RXR_{WT}, pCDNA-RXR_{AF2}) and bait constructs for mammalian two hybrid studies (human pM-SRC-1, pM-GRIP, pM-ATCR, pM-RXR_{WT}, pM-RXR_{AF2}) were a gift from Dr. Donald McDonnell (Duke University, Durham, NC). The luciferase reporters XREM-Luc, 5XGal4-TATA-Luc, and *Renilla* were obtained as previously reported (27).

VDR Transient Transactivation Assays

Cell culture media and other necessary reagents were obtained from Mediatech (Manassas, VA). HepG2 cells (ATCC #HB-8065) were cultured in T75 flasks with vented caps (BD Biosciences, San Jose, CA) using Minimum Essential Medium (MEM) containing heat-inactivated fetal bovine serum (10%), 1mM sodium pyruvate, and 1X MEM non-essential amino acids. The cells were maintained following standard protocols in a 37°C-5% CO_2 incubator and split approximately every 4-5 days when cells reached 90% confluence.

HepG2 cells were seeded in 96-well plates at 2.5 x 10^4 cells/well 24 hours prior to transfection and were transfected at 90-95% confluence overnight. Cells were transfected using Lipofectamine 2000 (Life Technologies, Grand Island, NY) with DNA diluted in Opti-MEM as per the manufacture's recommendations. For functional comparisons, 89.7 ng of medaka and zebrafish full-length pSG5-VDRα and pSG5-VDRβ were transiently transfected into HepG2 cells with 19.2 ng human XREM-Luc reporter construct consisting of both proximal DR3 and distal ER6 response elements found in the XREM region of the CYP3A4 promoter (28), and 4.5 ng of *Renilla* as an internal luciferase control. Co-regulator studies

included 18.3 ng of an expression vector containing the complete ORF of the coregulator of interest (pCDNA-RXR_{WT} or RXR_{AF2}, pSG5-SRC1, GRIP1, or ACTR). For single-dose assays, media was replaced the following day with complete MEM containing 120 nM 1α, 25-dihydroxyvitamin D_3 (1, $25D_3$) (EMD Millipore, Billerica, MA) in ethanol (<0.1% total solution). For concentration-response curves, media was replaced using a range 1, $25D_3$ concentrations between 0 - 120 nM. Twenty-four hours post-exposure the cells were tested for luciferase activity using the Dual-Glo Luciferase Assay System (Promega Corporation, Madison, WI) following the manufacturer's protocols. Luciferase readings were normalized by co-transfection with *Renilla* luciferase, and VDR response was normalized to an empty vector control. To compare VDR transactivation in the presence and absence of coregulators, VDR+coregulator response was normalized to VDR in the absence of coregulators. Experiments were repeated at least twice, and as groups of 4 replicate wells. Single-dose assays were analyzed using one-way ANOVAs followed by Tukey's HSD post hoc test. The half-maximal effective concentration (EC_{50}), 95% confidence interval (95% CI), and the maximal efficacy (E_{MAX}) of the concentration-response curves were determined via linear regression analysis using a sigmoidal dose-response calculation with variable slope. All statistics were run in GraphPad Prism 4 (GraphPad Inc, San Deigo, CA).

Protein Interaction: Mammalian 2-Hybrid Assays

Protein-protein interactions between VDR and its heterodimer partner RXR and members of SRC/p160 family of nuclear receptor coactivators were assessed using a mammalian 2-hybrid system (Clontech, Mountain View, CA). HepG2 cells were seeded into

96-well plates twenty-four hours prior to transfection as described above. Cells were transfected using Lipofectamine 2000 as per manufacturer's protocol. To determine protein-protein interactions, each well was transfected with 33.6 ng pVP16-VDR, 33.6 ng co-regulator as a fusion protein containing the yeast Gal4 DNA-binding domain fused to either full-length RXR (pM-RXR_{WT}, pM-RXR_{AF2}) or the defined NR box of the SRC coactivators (29): pM-$SRC1_{241-386}$, pM-$GRIP_{479-767}$, or pM-$ACTR_{392-1005}$. Luciferase reporters included 126.6 ng 5XGal4-TATA-Luc containing response elements for the yeast Gal4 DNA-binding domain, and 3 ng *Renilla* as an internal control. Controls consisted of transfections containing empty pM, pVP16 or both empty pM and pVP16 expression vectors or ethanol as a vehicle control. Media was replaced the following day with complete MEM containing 120 nM 1, $25D_3$ in ethanol. The cells were tested for luciferase activity twenty-four hours post-exposure using the Dual-Glo Luciferase Assay System described previously. Luciferase response was normalized to the internal *Renilla* control, and VDR-coregulator interaction was normalized to VDR in the absence of a coregulator construct. Experiments were repeated at least twice and performed in replicates of four wells. Results were analyzed via one-way ANOVAs followed by Tukey's HSD post doc test in GraphPad Prism version 4 for Mac OS X (GraphPad Software, La Jolla, CA).

Electrophoretic Mobility Shift Assays

Recombinant VDR and RXR_{WT} protein for electrophoretic mobility shift assays (EMSAs) were expressed and purified as follows. The protein expression constructs pET32a-VDR or pET32a-RXR_{WT} were transformed into the BL21-CodonPlus(DE3)-RIPL strain of

E.coli bacteria following manufacturer's protocol (Agilent Technologies, Santa Clara, CA). 10 mL of LB/amp was inoculated with a single colony and incubated overnight at 37˚C with shaking. Overnight starter cultures were used to inoculate 250 mL of LB/amp and grown at 37˚C with shaking until OD_{600} = 0.6. Protein expression was induced by the addition of 1 mM IPTG and 20 μM $ZnCl_2$. Cultures were incubated at 25˚C for three hours with shaking at 200 rpm. Following incubation, cultures were centrifuged at 4,000 *x g* for 20 minutes at 4ºC. The supernatant was discarded, and the pellets were stored at -20˚C overnight. The QIAexpress Ni-NTA Fast Start kit (QIAGEN, Valencia, CA) was used to lyse the bacteria and purify the recombinant 6xHis-tagged VDR and RXR under native kit conditions following the manufacturer's protocol. Purified protein concentrations were determined using the average of three A280 measurements using a NanoDrop® ND-1000 spectrophotometer (Thermo Fisher Scientific, Waltham, MA). Proteins were visualized via western blot using antibodies to the 6xHis-tags (QIAGEN, Valencia, CA).

Electrophoretic mobility shift assays (EMSAs) were carried out in a total volume of 20 μl containing 100 ng of recombinant VDR protein and 100 ng recombinant RXR where indicated. DNA–protein binding reactions were carried out using either the canonical VDRE (30) (5' – AGC TTC AGG TCA AGG AGG TCA GAG AGC – 3'), a mutant form of the canonical sequence (5' – AGC TTC AG*A A*CA AGG AG*A A*CA GAG AGC – 3'), or a VDRE containing the DR3 found within the distal promoter region of the CYP3A4-XREM reporter used in transient transfection studies (5' – GCT GAA TGA ACT TGC TGA CCC TCT GCT – 3') (28). Single stranded 5'-Cy5-labeled and unlabeled oligos were purchased from Integrated DNA Technologies (Coralville, IA). Oligos were resuspended to a final

concentration of 250 μM and annealed by heating equal concentrations of the sense and antisense strands in annealing buffer (10 mM Tris, 50 mM NaCl, 1 mM EDTA). Annealing reactions were heated to 95˚C for two minutes and allowed to cool to room temperature. Double stranded oligos were further diluted to a final concentration of 1 pmol/μL. For the DNA-binding reactions, receptors were incubated at 25˚ C for 45 minutes in binding buffer (100 mM KCl, 10 mM HEPES, 1 mM EDTA, 0.1 mg/ml BSA, 4 μg/mL sonicated salmon sperm, 1.0 mM DTT, 1% glycerol, 20 mM $MgCl_2$) and 100 nM 1, $25D_3$ or ethanol as a vehicle control. After 45 minutes, 1 pmol Cy5-labeled double-stranded oligo was added to each reaction, and incubated for an additional 30 minutes. Competition experiments were performed in the presence of a 100-fold molar excess of unlabeled wild type or mutant oligos. Supershift assays were conducted with untagged RXR and S-tagged VDR, with the addition of a monoclonal antibody to the S-tag (Novagen, San Diego, CA). Negative controls include expressed affinity tags isolated from empty pET32a vector stocks, binding reactions run with either VDR or RXR individually, and ethanol as a vehicle control. Protein–DNA complexes were resolved on a 6% non-denaturing acrylamide gel in ice-cold 0.5X TBE buffer (45 mM Tris base, 45 mM boric acid, 1 mM EDTA, pH 8.0) at 100 volts for 90 minutes. Gels were visualized on a Storm 865 using the red fluorescence mode (GE Healthcare Life Sciences, Pittsburgh, PA). Densitometry was measured using ImageQuaint TL 7.0 (GE Healthcare Life Sciences, Pittsburgh, PA).

Saturation Binding Analysis

Radiolabeled 1, 25D_3 (1, 25-$(OH)_2$-26, 27 [^{3}H]dimethyl-vitamin D_3, referred to as [^{3}H]-1, 25D_3) was purchased from Perkin Elmer (Waltham, MA). The protease inhibitor cocktail was purchased from EMD Millipore (Billerica, MA). Cos7 cells (ATCC #CRL-1561) were maintained in complete DMEM medium supplemented with 10% fetal bovine serum, and passaged every 4-5 days according to established protocols. To prepare lysates for saturation binding analysis, Cos7 cells were seeded at 3.0 x 10^6 cells/150 mm dish and transfected with 4 μg pSG5-VDR and 4 μg pSG5-RXR_{WT}, along with 16 μg of empty pBSII vector as carrier DNA, using Lipofectamine 2000 as described above. Media was replaced 24 hour post transfection, and 48 hour post-transfection, cells were washed twice with 10 mL DPBS and harvested by trypsinization. Cells were centrifuged for 5 minutes at 1000 x g at 4˚C, and resuspended twice in 2 mL ice-cold DPBS. After the second wash, cells were resuspended in 1 mL of ice-cold KETZD + 5 buffer (0.15 M KCl, 1 mM EDTA, 10 mM Tris HCl, 0.3 mM $ZnCl_2$, 200x dilution protease inhibitor cocktail (EMD Millipore, Billerica, MA), 5 mM DTT) and sonicated (12 1-second bursts at 25% power). After sonication, cells were centrifuged at 100,000 *x g* for 30 minutes at 4˚C. The supernatant containing the lysate was divided into 150 μL aliquots and stored at -80˚C. The pellet was discarded.

The affinity of 1, 25D_3 for the teleost VDRs was assessed as follows: lysate was diluted 1/20 in ice-cold KETZD+5 buffer. [^{3}H]-1, 25D_3 (original specific activity 157 Ci/mmol) was diluted to 25 Ci/mmol with unlabeled 1 μM 1, 25D_3 and further diluted with ethanol to obtain the desired concentrations (0 – 1.0 nM). 10 μL of the appropriate dilution was added to 200 μL lysate, shaken, and incubated overnight at 4˚C. Unbound ligand was

removed with the addition of 80 μL of a 0.5% dextran-2.5% charcoal suspension in GP Buffer (0.15 M NaCl, 0.015 M NaN_3, 0.1 M anhydrous Na_2HPO_4, 0.039 M $NaH_2PO_4 \bullet H_2O$, 10% gelatin) incubated on ice for 15 minutes with brief shaking every 5 minutes. Samples were centrifuged at 5000 x *g* for 5 minutes at 4˚C and 200 μL of the supernatant containing the bound ligand was removed for scintillation counting. All assays were repeated at least twice with duplicate tubes for each concentration. Total binding was determined by using lysate transfected with pSG5-VDR, and nonspecific binding was determined by using lysate transfected with the empty pSG5 vector. Specific binding was obtained by subtracting the nonspecific binding values from the total binding. Hyperbolic one-site binding curves were fit using GraphPad Prism. Reported dissociation constant values (K_D) are the average of three separate curves ± SEM. The K_D represents the ligand concentration where half of the receptors are occupied. Significant variation between average K_Ds was tested via a one-way ANOVA followed by Tukey's HSD post hoc test in GraphPad Prism.

RESULTS

VDR transactivation in response to 1, 25D_3

To analyze differential ligand sensitivities of VDRα and VDRβ paralogs from medaka and zebrafish, full-length VDR constructs were tested in transient transactivation assays with 1, 25D_3 as the primary ligand. As demonstrated in figure 1, each VDR construct exhibited a significant transactivational response to 120 nM 1, 25D_3 in HepG2 cells. However, a differential response was observed between the VDRα paralogs of both species exhibited a strong response to 120 nM 1, 25D_3, resulting in a 47.7-fold and 49.0-fold increase in transactivation over background for medaka and zebrafish VDRα. Comparatively, transactivation of medaka VDRβ and zebrafish VDRβ was significantly attenuated compared to their respective VDRα paralogs, with maximal transactivation of 28.4-fold for medaka VDRβ and 4.5-fold for zebrafish VDRβ.

Concentration-response curves

To analyze differential ligand potency and efficacy, concentration-response curves (using receptor transactivation as an endpoint) were also conducted with a range of 1, 25D_3 concentrations between 0 - 120 nM, and the concentration that elicited 50% of the maximal effect (EC_{50}) was determined for each VDR (Fig. 1B). Results demonstrate that EC_{50} values were all in the low nanomolar range: 2.6 nM and 3.1 nM for mVDRα and mVDRβ, 2.6 nM and 2.5 nM for zfVDRα and zfVDRβ (Fig. 1C). The concentration-response data suggests that differential ligand potencies are not driving the observed transactivational differences.

As with the single-dose assays, significant variation was observed in the maximum transactivational efficacy between VDRα and VDRβ paralogs, with medaka and zebrafish VDRβ exhibiting significant attenuation in response compared to their corresponding VDRα paralogs (Fig. 1B). The maximum efficacy for medaka VDRα and VDRβ was 52.8-fold and 30.0-fold, and 46.3-fold and 4.7-fold for zebrafish VDRα and VDRβ. Our data indicates that while the 1, $25D_3$ maintains a consistent potency (EC_{50}) for paralogous VDRs, maximum transactivational efficacy differs significantly between the VDRα and VDRβ paralogs across phylogenetically distant teleosts.

Saturation binding analysis

Innate ligand binding kinetics for each VDR form was determined using saturation bind analysis with radiolabeled [^{3}H]-1, $25D_3$ (Fig. 2A, B). Dissociation constants (K_Ds) obtained for each VDR were within the sub-nanomolar (10^{-10} M) range: 0.36 ± 0.07 nM for medaka VDRα, 0.38 ± 0.09 nM for medaka VDRβ, 0.29 ± 0.04 nM for zebrafish VDRα, and 0.44 ± 0.13 nM for zebrafish VDRβ, demonstrating high affinity binding between 1, $25D_3$ and all VDR paralogs. These values are within the range previously reported for mammalian VDR (25,31). No significant difference in binding affinities was detected between paralogs or between species, indicating a conservation of high affinity binding between VDR and 1, $25D_3$ in these species.

DNA binding

Electrophoretic mobility shift assays were conducted to test the ability of teleost VDR paralogs to bind to well-defined vitamin D response elements (VDREs), including the canonical VDRE sequences and a divergent VDRE representing the VDRE of the XREM region of CYP3A4, and is identical to the VDRE used in the XREM-Luc reporter. For medaka and zebrafish VDRα and VDRβ, protein-DNA binding between receptor and the canonical and divergent VDREs was observed only in presence of RXR_{WT} (Fig. 3A, odd lanes vs. even lanes). No binding complex was observed when VDR or RXR_{WT} was used singularly, indicating a dependence on VDR:RXR heterodimerization for DNA binding, and a definitive lack of VDR or RXR_{WT} binding to the VDREs as putative homodimers. To ensure specificity of the reaction, all EMSAs were repeated in the presence of excess unlabeled wild-type or mutant VDREs (Fig. 3B for canonical VDRE and Fig. 3C for XREM VDRE). Competition assays using unlabeled probes were effectively able to outcompete the VDR-RXR_{WT} binding with the canonical VDRE (Fig. 3B, lane 1 vs. 3, and lane 4 vs. 6). Competition assays using an unlabeled mutant probe had no effect on VDR binding to the wild type VDREs (Fig. 3B, lane 1 vs. 2 and lane 4 vs. 5). Competition assays using an unlabeled XREM probe also outcompeted VDR-RXR binding to the labeled VDRE (Fig. 3C, Lanes 3 vs. 4 and 7 vs. 8). To further confirm VDR protein-DNA interaction, supershift assays were conducted with full-length recombinant RXR with the tags removed, S-tagged full-length VDRs, and an antibody to the S-tag. As demonstrated in figure 3D, this reaction resulted in a significant “shift” in the VDR-DNA-antibody complex indicating specificity of the VDR-DNA reaction (Odd lanes vs. even lanes).

Protein-DNA interaction with both canonical VDRE and the XREM VDRE exhibited partial dependence upon the presence of 1, 25D_3. Partial VDR binding was observed with both VDREs in the absence of 1, 25D_3 (Fig. 3A, lanes 2 and 6). Binding significantly increased however with addition of 1, 25D_3 to the binding reaction (Fig. 3A, lanes 2 vs. 4 and lanes 6 vs. 8). Additionally, medaka and the zebrafish VDRα paralogs exhibited greater protein-DNA interactions compared to the VDRβ paralogs with both the canonical VDRE and distal XREM VDRE (Fig. 3B, C). This observation was consistent across a range (0-1000 nM) of 1,25D_3 concentrations with maximal protein-DNA interaction occurring at 10nM 1, 25 D_3 (data not shown).

Coregulator interaction: heterodimerization with RXR

A series of studies were conducted to determine if VDR transactivation is significantly enhanced by the presence of supplemented RXR. In co-transfection studies, addition of full-length RXR_{WT} resulted an increase in transactivation of all VDRs compared to the activity of VDR alone (Fig. 4A). Medaka and zebrafish VDRβ exhibited a greater increase in transactivation compared to their VDRα paralogs. VDRβ transactivation increased 5.4-fold for medaka and 4.0-fold for zebrafish, while medaka and zebrafish VDRα increased 2.6-fold and 3.3-fold over VDR alone. In each instance where the RXR_{AF2} mutant was substituted for RXR_{WT}, luciferase activity was significantly attenuated as expected compared to studies with RXR_{WT}.

Heterodimerization between RXR and teleost VDR paralogs was further confirmed through mammalian 2-hybrid assays. Identical assays were conducted using an AF2 mutant

RXR. Data from these studies demonstrate a direct interaction between all teleost VDRs and pM-RXR_{WT} in the presence of 1, $25D_3$ (Fig. 4B). No protein-protein interaction was observed in the absence of ligand and VDR-RXR interaction was significantly attenuated with substitution of pM-RXR_{WT} with pM-RXR_{AF2}, highlighting the necessity of the RXR AF2 domain for VDR transactivation.

Coregulator interaction: SRC family of nuclear receptor coactivators

Protein interaction studies were expanded to include the SRC/p160 family of nuclear receptor coactivators. This family includes SRC-1, GRIP1, and ACTR. These coactivators interact with nuclear receptors in a ligand-dependent manner, and enhance NR-mediated transcriptional activation through chromatin remodeling and recruitment of additional cofactors to the transcription complex.

Cotransfection of the SRC coactivators had varying effects on the VDR paralogs. SRC-1 significantly increased VDR activation in all paralogs (Fig. 5A-D). GRIP1 only enhanced zebrafish VDRα and VDRβ activation, but not the medaka paralogs. ACTR did not effect VDR activation for any of the VDRs tested.

Cotransfection of both RXR_{WT} and the SRC coactivators significantly increased the activation of all VDR paralogs. In particular, the level of transactivation achieved for both medaka and zebrafish VDRα and VDRβ was greater with the combination RXR_{WT} and SRC-1, compared to either coactivator used individually (indicated by the presence of an "R" above each bar in Fig. 5A-D). In zebrafish, but not in medaka, this increase in activation was additionally observable following cotransfection of RXR with GRIP1 and ACTR. The

combination of RXR_{WT} and the SRC proteins appeared to have a greater effect on VDRβ activation compared to VDRα for both medaka and zebrafish.

In order to determine whether the VDR paralogs are able to directly recruit the SRC coactivators, or if the observed transactivational increases are a result of indirect effects of the coactivators, mammalian 2-hybrid (M2H) assays were conducted to assess protein-protein interaction between VDR and the SRC coativators (Fig. 6A-D). As the cotransfection of both RXR_{WT} and SRC coactivators significantly enhanced VDR activation, M2H assays were conducted both with and without RXR_{WT} to determine if the heterodimer partner had an impact on VDR-coactivator interaction. All VDRs demonstrated a strong and significant interaction with SRC-1, indicating that each of the VDRs were able to directly recruit SRC-1 in response to 1, $25D_3$ (Fig. 6A-D). Of note, only the VDRα paralogs demonstrated a significant interaction with GRIP1, while the VDRβ paralogs did not interact with GRIP1 unless RXR_{WT} was present (Fig. 6A, C vs. B, D). No recruitment was observed for ACTR with any of the paralogs.

The addition of RXR_{WT} to the SRC M2H assays had contrasting effects on SRC recruitment. RXR_{WT} significantly enhanced VDR-SRC interaction with the VDRβ paralogs, but the interaction was attenuated in both VDRα paralogs (Fig. 5A, C vs. B, D). Protein-protein interactions play an essential role in NR-mediated transcription, and altered coactivator recruitment may have significant effects on VDR-mediated transcription.

DISCUSSION

The duplication and divergence of transcriptional regulators is thought to have played an essential role in the evolution of vertebrate complexity and diversity. Mining of teleost genomes has shown that a minimum of 15-20% of protein coding loci have been retained in duplicate after the teleost 3R duplication event (32,33). In the case of VDR, identification of VDRβ, which is paralogous to and separate from VDRα, suggests that this receptor represents a novel subfamily of ligand-activated transcription factors within the vertebrate NR1I family (17,27,34). To date, however, molecular function and physiological significance of duplicate teleost NRs is based predominately on structural similarities and orthology to their mammalian counterparts.

Using transient transactivation assays, we first confirmed that VDRα and VDRβ from medaka and zebrafish are capable of transactivation by the endogenous VDR ligand, 1, $25D_3$. By titrating the concentration of 1, $25D_3$, we also established an EC_{50} value for each VDR. EC_{50} values ranged from 2.5 – 3.0 nM and were highly similar between all VDRs, indicating that 1, $25D_3$ is a highly potent ligand both between species and paralogs. This data is consistent with that observed from other teleost VDR studies which employed Gal4-VDR-LBD chimeras to assess VDR transactivation across phylogenetically diverse taxa (27,35). All VDRs examined to date exhibit at least a modest transactivation and comparable EC_{50}s with 1, $25D_3$, including the sea lamprey, a primitive vertebrate (25). This suggests that the association between VDR and 1, $25D_3$ occurred early in vertebrate evolution and has been highly conserved.

Conversely, examination of maximal transactivational efficacy between the VDR

paralogs of both species revealed significant transactivational differences. We thus sought to further establish the functional basis for these transactivational differences through examining core NR functions between VDRα and VDRβ in the two teleost species. As ligand binding is the initiating event of NR transactivational function, we began our studies by asking if transactivational differences observed between VDRα and VDRβ paralogs were associated with differential binding affinity for 1, $25D_3$. VDRα and VDRβ paralogs from both species exhibited high affinity binding (10^{-10} M) with 1, $25D_3$, which is similar to previous reported values for mammalian high affinity VDR proteins. However, statistically significant differences in binding affinities were not observed between paralogs or species, indicating that differential ligand affinities are not the cause of the observed transactivational disparities between VDRα and VDRβ. In fact, it is well known that the ligand affinity and transactivation efficacy of specific NR ligands are not proportional (36). This phenomenon is likely due to the ability of ligands to induce subtle conformational alterations within receptors that elicit different biological responses such as DNA binding, coactivator recruitment and transactivation. High affinity binding but low transactivational efficacy of VDR has been observed previously in other aquatic vertebrates. For example, the sea lamprey (*Petromyzon marinus*) is an ancient vertebrate lacking a calcified skeleton, yet it maintains a functional vitamin D receptor that shares a 59-62% sequence similarity other vertebrate VDRs. While lamprey VDR exhibits high affinity binding with 1, $25D_3$ (K_D = 0.7 nM), lamprey VDR activation increased less than 4-fold over background in the presence of ligand (25).

As the observed transactivation differences did not seem to be driven by differential

ligand binding affinity, we then sought to examine whether differences in VDRα and VDRβ activation were due to modified NR functions that occur subsequent to ligand binding. We began by assessing the ability of the VDRs to bind to well-characterized VDREs. VDREs are comprised of a direct-repeat of two hexameric half elements separated by a spacer of three nucleotides (DR3). In this study, EMSAs were conducted to test the ability of the VDR paralogs to bind to VDREs consisting of both canonical and non-canonical DR3s. Results demonstrate that distinct differences in DNA binding occur between the VDRα and VDRβ paralogs, with VDRα exhibiting preferential binding compared to the VDRβ. Binding differences were conserved between species and occurred with both canonical and non-canonical VDREs.

Sequence similarities suggest that the observed DNA binding differences between VDRα and VDRβ are likely not related to sequence divergence in the DNA binding domain (DBD). The DBD consists of a core of 66 amino acids containing two zinc finger α-helices that are responsible for major groove contacts and response element specificity. The DBD sequences of the medaka and zebrafish VDRα and VDRβ are highly homologous, sharing 95-96% amino acid sequence similarity. All eight cysteine residues essential for the zinc finger structure and the recognition helix are identical between VDRα and VDRβ and human VDR (37-39). Additionally, studies have demonstrated the importance of residues in the C-terminal extension (CTE) for sufficient DNA binding and transactivation (40). These residues likely increase affinity of VDR-DNA interaction by aiding in nonspecific interaction within the minor grove of the DNA backbone and impart additional RXR dimerization and sequence specificity to the conserved DBD core region (41,42). Although more sequence

variation is observed in the CTE region between VDRα and VDRβ, the basic residues implicated in DNA binding are conserved across all paralogs (30).

Mutation studies have demonstrated that modifications within the LBD may also impact VDR affinity for VDRE binding through alterations in RXR heterodimerization (43,44). Our DNA binding studies with medaka and zebrafish VDRs demonstrate a stringent requirement for RXR. We also demonstrate that DNA binding is significantly enhanced with addition of 1, $25D_3$ suggesting that the presence of ligand may favorably alter the conformation of the LBD, enhance VDR:RXR interactions and facilitate interaction with the VDRE (45-47).

Because RXR heterodimerization and coactivator recruitment are indispensable to VDR function, the differential effects of these proteins on VDRα and VDRβ transactivation was also of great interest in this study. To test the impact of RXR on VDR transactivation efficacy, either wild-type RXR (RXR_{WT}) or a truncated RXR mutant (RXR_{AF2}) lacking the c-terminal ligand-dependent activation function 2 (AF2) region was co-transfected with VDR in transient transfection studies. Previous studies have shown that the VDR:RXR heterodimer is significantly more stable than VDR homodimer, and facilitates interaction with defined vitamin D response elements in target genes (48,49). Supporting this hypothesis are studies that demonstrate RXR is an obligate heterodimerization partner for VDR, although VDR homodimers have been observed (47,49,50). In this study, we consistently observed an increase in transactivational efficacy for each VDR tested in the presence of RXR_{WT}. The use of the RXR mutant (RXR_{AF2}) attenuated VDR transactivation, and significantly attenuated protein-protein interaction between VDR and the RXR in mammalian 2-hybrid studies. The

AF2 regions of both VDR and RXR are required for vitamin D-dependent gene transcription (51,52). We speculate that lack of response with the mutant RXR is likely due to an inability to recruit necessary coactivators, or modulation of corepressor interactions on sites previously shielded by the RXR AF2 (53). In conjunction with DNA binding data, these results support obligate interactions between VDR:RXR for essential VDR functions in both medaka and zebrafish paralogs.

In addition to RXR, we also studied the effects of the SRC family of nuclear receptor coactivators on VDR transactivation. The SRC family of nuclear receptor co-activators are defined by their ligand-dependent ability to directly interact with nuclear receptors and enhance transcription of target genes by both chromatin modification and the recruitment of additional proteins to the transcription complex (29). The SRC family members all contain a centrally located NR box comprised of three highly conserved LXXLL amino acid motifs (L = Leucine, X = any amino acid) which forms an amphipatic α-helix that interacts with the AF2 region of helix 12 of the receptor (29).

While the partnership between VDR and RXR appears to be well conserved, dramatic functional differences between VDRα and VDRβ paralogs were observed with the cotransfection of both RXR and the SRC coactivators in transient transactivation assays. Specifically, we observed preferential transactivation of VDRβ paralogs in the presence both coregulators in both species. This transactivational increase was significantly greater than the individual effects of either coregulator used singularly. In addition, results from our mammalian 2-hybrid assays further support the notion of preferential effects of RXR and SRC1 on VDRβ transactivation. Transfection of an expression vector for full length SRC-1

in the VDR-RXR mammalian 2-hybrid assay significantly enhances the interaction between VDRβ and RXR, but only has a minor effect on the interaction between RXR and VDRα. In the VDR-SRC1 mammalian 2-hybrid assays, cotransfection of an expression vector for full length RXR selectively enhances the interaction between VDRβ and SRC-1, however the interaction with VDRα and SRC-1 is significantly attenuated.

To elucidate the cause of these functional differences, we first examined protein sequences. Comparisons of VDRα and VDRβ protein sequences reveal that the differential coregulator interactions are likely not due to overall sequences divergence. VDRα and VDRβ paralogs are approximately 85% identical. Examination of key regions within VDR known for protein-protein interaction with RXR and the SRC coactivators, including H9 and H10, the AF2 and E1 region, and the T box of the CTE, all demonstrate a high degree of conservation between VDRα and VDRβ paralogs. This degree of conservation suggests that sequence differences in key functional regions are not associated with the observed functional differences. Second, the fact that each paralog binds 1, $25D_3$ with equal affinity indicates that differential ligand affinities are not driving differences in protein interactions between paralogs. Rather, we speculate that VDR transactivation by 1, $25D_3$ may result in different molecular conformations between VDRα and VDRβ that can differentially influence downstream protein–protein interactions.

It is well known that mammalian VDR bound to 1, $25D_3$ produces a significant conformational change in the receptor to the active state i.e. from the apo to the holo form (54). This conformational change appears to be consistent across all mammalian species tested thus far (55,56). In addition, crystal studies with a zebrafish VDRα complexed with

both 1, 25D_3 and Gemini, a synthetic VDR agonist, revealed a highly similar active conformation compared to human VDR (57). The fact that both human VDR and zebrafish VDRα maintain almost identical active conformation supports our data indicating a high degree of functional similarity between the two species. The crystal structures of both VDR paralogs with 1, 25D_3 may provide invaluable structural comparisons, as the differences observed between the two paralogs may be related to structural differences.

It has additionally been demonstrated that VDR conformation is ligand-specific. Jurutka et al (58) have suggested that lithocholic acid induces an alternative active conformation when bound to VDR compared to 1, 25D_3, and these conformational differences result in differential interaction with RXR and coregulator proteins. Jurutka et al further demonstrate that ligand-induced conformational differences may lead to functional differences. For example, transactivation assays with LCA demonstrate significantly attenuated VDR activation in comparisons to 1, 25D_3, and mammalian 2-hybrid assays suggest LCA-bound VDR maintains a decreased affinity for RXR and coactivators. It's speculated that the LCA-induced VDR conformation is unable to stabilize H12 for SRC interaction, and results in suboptimal positioning of H9 and H10 which attenuates heterodimerization with RXR (58,59). These diminished protein-protein interactions ultimately result in significantly reduced VDR transactivation. Differential ligand-induced active conformation between 1, 25D_3 and LCA was later verified with LCA-VDR crystal structures (59). Although 1, 25D_3 was used in as the sole ligand in this study, we speculate that subtle conformational differences between VDR paralogs may lead to the altered coregulator interactions described above. Specifically, the active conformation induced by 1,

$25D_3$ in VDRβ may be less stable compared to VDRα, resulting in attenuated affinity for RXR and the SRC coactivators under non-saturating coactivator conditions. However, enhanced activity in cotransfection studies and enhanced protein interactions observed with VDRβ may be due to compensatory effect of overexpressed coregulators. Analogous to our observations, compensatory effects of overexpressed coregulators on transactivation and protein-protein interactions has been observed with a VDR mutant associated with a form of hereditary vitamin D resistant rickets (HVDDR). In this mutant, the arginine of residue 391 in H10 is replaced with a cysteine (R391C). This mutation has been demonstrated to significantly attenuate VDR heterodimerization with RXR (45,52). However, transient transactivation assays incorporating overexpressed RXR_{WT} with the VDR_{R391C} mutant are demonstrated to restore transactivation to normal levels. As wild type VDR is able to mediate a maximum response, the overexpression of RXR has less of an enhancing effect on wild type VDR compared to the VDR mutant (45,52). Similar to these studies, we observe a preferential transactivation increase in the presence of overexpressed RXR_{WT} and SRC-1with the less effective receptor, VDRβ, compared to VDRα.

Two possible models may explain the compensatory mechanism of overexpressed RXR and SRC-1 on VDR transactivation. One possible mechanism, proposed in Thompson et al (52) involves the AF2 regions of both VDR and RXR interacting with different LXXLL motifs of the same SRC coactivator. A study with VDR and DRIP1, another VDR coactivator, found that both LXXLL motifs of DRIP1 were used by the VDR-RXR heterodimer, suggesting that DRIP1 interacted with the AF2 regions of both receptors (60). This "bridging" effect of a coactivator may help stabilize a less optimal heterodimer. The

pattern of one coactivator per heterodimer has been previous observed with other NRs. For example, ligand activation of the RXR-RAR heterodimer induces the AF2 region of both to interact with separate LXXLL motifs within the same SRC-1 molecule, helping to stabilize the complex (61).

Alternatively, a second model suggests that each heterodimer partner interacts with a distinct and separate coactivator within its LXXLL domain. A study by Yang et al (62) found that coactivator recruitment to the permissive PPARγ-RXR heterodimer is highly ligand-specific. For instance, the presence of LG268, an RXR specific ligand, resulted in protein-protein interaction only between SRC-1 and RXR and not with PPARγ. Conversely, PPARγ ligands exclusively recruited DRIP1 but not SRC coactivators to PPARγ. Differential coactivator recruitment has been demonstrated within the VDR-RXR heterodimer with regard to TIF1 and SUG1. TIF1 can interact with both RXR and VDR, while SUG1 exclusively interacts with VDR (63). Differential coactivator recruitment between heterodimer partners may potentially explain our mammalian 2-hybrid data with VDRα. The fact that the addition of RXR appears to attenuate VDR-SRC-1 interactions in mammalian 2-hybrid assays suggests that RXR may be sequestering the SRC-1 proteins, and they are in effect no longer stoichiometrically proportional for the assay.

REFERENCES

1. Dehal P, Boore J. Two rounds of whole genome duplication in the ancestral vertebrate. *Plos Biol.* 2005;3(10):1700-1708.

2. Crow K, Wagner G. What is the role of genome duplication in the evolution of complexity and diversity? *Mol Biol Evol.* 2006;23(5):887-892.

3. Freeling M, Thomas BC. Gene-balanced duplications, like tetraploidy, provide predictable drive to increase morphological complexity. *Genome research.* 2006;16(7):805-814.

4. Van de Peer Y, Maere S, Meyer A. OPINION The evolutionary significance of ancient genome duplications. *Nat Rev Genet.* 2009;10(10):725-732.

5. Taylor J, Raes J. Duplication and divergence: The evolution of new genes and old ideas. *Annu Rev Genet.* 2004;38:615-643.

6. Edger PP, Pires JC. Gene and genome duplications: the impact of dosage-sensitivity on the fate of nuclear genes. *Chromosome Res.* 2009;17(5):699-717.

7. Blomme T, Vandepoele K, De Bodt S, Simillion C, Maere S, Van de Peer Y. The gain and loss of genes during 600 million years of vertebrate evolution. *Genome Biol.* 2006;7(5):R43.

8. Hoegg S, Brinkmann H, Taylor J, Meyer A. Phylogenetic timing of the fish-specific genome duplication correlates with the diversification of teleost fish. *J Mol Evol.* 2004;59(2):190-203.

9. Crow K, Stadler P, Lynch V, Amemiya C, Wagner G. The "fish-specific" Hox cluster duplication is coincident with the origin of teleosts. *Mol Biol Evol.* 2006;23(1):121-136.

10. Meyer A, Van de Peer Y. From 2R to 3R: evidence for a fish-specific genome duplication (FSGD). *Bioessays.* 2005;27(9):937-945.

11. Nelson JS. *Fishes of the World.* 4th Edition ed. New York: J. Wiley; 2006.

12. Postlethwait J, Amores A, Cresko W, Singer A, Yan Y. Subfunction partitioning, the teleost radiation and the annotation of the human genome. *Trends Genet.* 2004;20(10):481-490.

13. Birchler JA, Yao H, Chudalayandi S. Biological consequences of dosage dependent gene regulatory systems. *Biochim Biophys Acta.* 2007;1769(5-6):422-428.

14. Veitia RA, Bottani S, Birchler JA. Cellular reactions to gene dosage imbalance: genomic, transcriptomic and proteomic effects. *Trends Genet.* 2008;24(8):390-397.

15. Gronemeyer H, Gustafsson J, Laudet V. Principles for modulation of the nuclear receptor superfamily. *Nat Rev Drug Discov.* 2004;3(11):950-964.

16. Aranda A, Pascual A. Nuclear hormone receptors and gene expression. *Physiol Rev.* 2001;81(3):1269-1304.

17. Maglich J, Caravella J, Lambert M, Willson T, Moore J, Ramamurthy L. The first completed genome sequence from a teleost fish (Fugu rubripes) adds significant diversity to the nuclear receptor superfamily. *Nucleic Acids Res.* 2003;31(14):4051-4058.

18. Metpally RPR, Vigneshwar R, Sowdhamini R. Genome inventory and analysis of nuclear hormone receptors in Tetraodon nigroviridis. *J Biosciences.* 2007;32(1):43-50.

19. Robinson-Rechavi M, Carpentier AS, Duffraisse M, Laudet V. How many nuclear hormone receptors are there in the human genome? *Trends in genetics : TIG.* 2001;17(10):554-556.

20. Bertrand S, Thisse B, Tavares R, Sachs L, Chaumot A, Bardet PL, Escriva H, Duffraisse M, Marchand O, Safi R, Thisse C, Laudet V. Unexpected novel relational links uncovered by extensive developmental profiling of nuclear receptor expression. *PLoS genetics.* 2007;3(11):e188.

21. Howarth DL. *Characterization of FXR alpha in medaka and its involvement in hepatobiliary injury* [Dissertation]. Durham: Integrated Toxicology and Environmental Health Program, Duke University; 2009.

22. Burmester JK, Maeda N, DeLuca HF. Isolation and expression of rat 1,25-dihydroxyvitamin D3 receptor cDNA. *Proceedings of the National Academy of Sciences of the United States of America.* 1988;85(4):1005-1009.

23. Burmester JK, Wiese RJ, Maeda N, DeLuca HF. Structure and regulation of the rat 1,25-dihydroxyvitamin D3 receptor. *Proceedings of the National Academy of Sciences of the United States of America.* 1988;85(24):9499-9502.

24. McDonnell DP, Mangelsdorf DJ, Pike JW, Haussler MR, O'Malley BW. Molecular cloning of complementary DNA encoding the avian receptor for vitamin D. *Science.* 1987;235(4793):1214-1217.

25. Whitfield G, Dang H, Schluter S, Bernstein R, Bunag T, Manzon L, Hsieh G, Dominguez C, Youson J, Haussler M, Marchalonis J. Cloning of a functional vitamin D receptor from the lamprey (Petromyzon marinus), an ancient vertebrate lacking a calcified skeleton and teeth. *Endocrinology.* 2003;144(6):2704-2716.

26. Lock E-J, Waagbo R, Bonga SW, Flik G. The significance of vitamin D for fish: a review. *Aquacult Nutr.* 2010;16(1):100-116.

27. Howarth DL, Law SHW, Barnes B, Hall JM, Hinton DE, Moore L, Maglich JM, Moore JT, Kullman SW. Paralogous vitamin D receptors in teleosts: Transition of nuclear receptor function. *Endocrinology.* 2008;149(5):2411-2422.

28. Drocourt L, Pascussi J, Assenat E, Fabre J, Maurel P, Vilarem M. Calcium channel modulators of the dihydropyridine family are human pregnane X receptor activators and inducers of CYP3A, CYP2B, and CYP2C in human hepatocytes. *Drug Metab Dispos.* 2001;29(10):1325-1331.

29. Leo C, Chen J. The SRC family of nuclear receptor coactivators. *Gene.* 2000;245(1):1-11.

30. Shaffer P, Gewirth D. Vitamin D receptor-DNA interactions. *Vitam Horm.* 2004;68:257-273.

31. Dusso A, Brown A, Slatopolsky E. Vitamin D. *Am J Physiol-Renal.* 2005;289(1):F8-F28.

32. Brunet FG, Roest Crollius H, Paris M, Aury JM, Gibert P, Jaillon O, Laudet V, Robinson-Rechavi M. Gene loss and evolutionary rates following whole-genome duplication in teleost fishes. *Molecular biology and evolution.* 2006;23(9):1808-1816.

33. Postlethwait JH, Woods IG, Ngo-Hazelett P, Yan YL, Kelly PD, Chu F, Huang H, Hill-Force A, Talbot WS. Zebrafish comparative genomics and the origins of vertebrate chromosomes. *Genome research.* 2000;10(12):1890-1902.

34. Suzuki T, Suzuki N, Srivastava A, Kurokawa T. Identification of cDNAs encoding two subtypes of vitamin D receptor in flounder, Paralichthys olivaceus. *Biochem Bioph Res Co.* 2000;270(1):40-45.

35. Reschly EJ, Bainy ACD, Mattos JJ, Hagey LR, Bahary N, Mada SR, Ou J, Venkataramanan R, Krasowski MD. Functional evolution of the vitamin D and pregnane X receptors. *BMC Evol Biol.* 2007;7:222.

36. Peleg S, Liu YY, Reddy S, Horst RL, White MC, Posner GH. A 20-epi side chain restores growth-regulatory and transcriptional activities of an A ring-modified hybrid analog of 1 alpha, 25-dihydroxyvitamin D3 without increasing its affinity to the vitamin D receptor. *Journal of cellular biochemistry.* 1996;63(2):149-161.

37. Freedman LP, Towers TL. DNA binding properties of the vitamin D3 receptor zinc finger region. *Molecular endocrinology.* 1991;5(12):1815-1826.

38. Liao J, Ozono K, Sone T, McDonnell DP, Pike JW. Vitamin D receptor interaction with specific DNA requires a nuclear protein and 1,25-dihydroxyvitamin D3. *Proceedings of the National Academy of Sciences of the United States of America.* 1990;87(24):9751-9755.

39. Towers TL, Luisi BF, Asianov A, Freedman LP. DNA target selectivity by the vitamin D3 receptor: mechanism of dimer binding to an asymmetric repeat element.

Proceedings of the National Academy of Sciences of the United States of America. 1993;90(13):6310-6314.

40. Hsieh JC, Whitfield GK, Oza AK, Dang HT, Price JN, Galligan MA, Jurutka PW, Thompson PD, Haussler CA, Haussler MR. Characterization of unique DNA-binding and transcriptional-activation functions in the carboxyl-terminal extension of the zinc finger region in the human vitamin D receptor. *Biochemistry.* 1999;38(49):16347-16358.

41. Khorasanizadeh S, Rastinejad F. Nuclear-receptor interactions on DNA-response elements. *Trends in biochemical sciences.* 2001;26(6):384-390.

42. Rastinejad F, Perlmann T, Evans RM, Sigler PB. Structural determinants of nuclear receptor assembly on DNA direct repeats. *Nature.* 1995;375(6528):203-211.

43. Jin CH, Kerner SA, Hong MH, Pike JW. Transcriptional activation and dimerization functions in the human vitamin D receptor. *Molecular endocrinology.* 1996;10(8):945-957.

44. Nakajima S, Hsieh JC, MacDonald PN, Galligan MA, Haussler CA, Whitfield GK, Haussler MR. The C-terminal region of the vitamin D receptor is essential to form a complex with a receptor auxiliary factor required for high affinity binding to the vitamin D-responsive element. *Molecular endocrinology.* 1994;8(2):159-172.

45. Whitfield GK, Selznick SH, Haussler CA, Hsieh JC, Galligan MA, Jurutka PW, Thompson PD, Lee SM, Zerwekh JE, Haussler MR. Vitamin D receptors from patients with resistance to 1,25-dihydroxyvitamin D3: point mutations confer reduced transactivation in response to ligand and impaired interaction with the retinoid X receptor heterodimeric partner. *Molecular endocrinology.* 1996;10(12):1617-1631.

46. MacDonald PN, Dowd DR, Nakajima S, Galligan MA, Reeder MC, Haussler CA, Ozato K, Haussler MR. Retinoid X receptors stimulate and 9-cis retinoic acid inhibits 1,25-dihydroxyvitamin D3-activated expression of the rat osteocalcin gene. *Molecular and cellular biology.* 1993;13(9):5907-5917.

47. Thompson PD, Jurutka PW, Haussler CA, Whitfield GK, Haussler MR. Heterodimeric DNA binding by the vitamin D receptor and retinoid X receptors is

enhanced by 1,25-dihydroxyvitamin D3 and inhibited by 9-cis-retinoic acid. Evidence for allosteric receptor interactions. *The Journal of biological chemistry.* 1998;273(14):8483-8491.

48. Zhang J, Chalmers MJ, Stayrook KR, Burris LL, Garcia-Ordonez RD, Pascal BD, Burris TP, Dodge JA, Griffin PR. Hydrogen/deuterium exchange reveals distinct agonist/partial agonist receptor dynamics within vitamin D receptor/retinoid X receptor heterodimer. *Structure.* 2010;18(10):1332-1341.

49. Zhang J, Chalmers MJ, Stayrook KR, Burris LL, Wang Y, Busby SA, Pascal BD, Garcia-Ordonez RD, Bruning JB, Istrate MA, Kojetin DJ, Dodge JA, Burris TP, Griffin PR. DNA binding alters coactivator interaction surfaces of the intact VDR-RXR complex. *Nat Struct Mol Biol.* 2011;18(5):556-563.

50. Choi M, Yamada S, Makishima M. Dynamic and ligand-selective interactions of vitamin D receptor with retinoid X receptor and cofactors in living cells. *Molecular pharmacology.* 2011;80(6):1147-1155.

51. Bettoun D, Burris T, Houck K, Buck D, Stayrook K, Khalifa B, Lu J, Chin W, Nagpal S. Retinoid X receptor is a nonsilent major contributor to vitamin D receptor-mediated transcriptional activation. *Mol Endocrinol.* 2003;17(11):2320-2328.

52. Thompson PD, Remus LS, Hsieh JC, Jurutka PW, Whitfield GK, Galligan MA, Encinas Dominguez C, Haussler CA, Haussler MR. Distinct retinoid X receptor activation function-2 residues mediate transactivation in homodimeric and vitamin D receptor heterodimeric contexts. *Journal of molecular endocrinology.* 2001;27(2):211-227.

53. Schulman IG, Juguilon H, Evans RM. Activation and repression by nuclear hormone receptors: hormone modulates an equilibrium between active and repressive states. *Molecular and cellular biology.* 1996;16(7):3807-3813.

54. Rochel N, Wurtz J, Mitschler A, Klaholz B, Moras D. The crystal structure of the nuclear receptor for vitamin D bound to its natural ligand. *Mol Cell.* 2000;5(1):173-179.

55. Vanhooke JL, Benning MM, Bauer CB, Pike JW, DeLuca HF. Molecular structure of the rat vitamin D receptor ligand binding domain complexed with 2-carbon-substituted vitamin D3 hormone analogues and a LXXLL-containing coactivator peptide. *Biochemistry.* 2004;43(14):4101-4110.

56. Rochel N, Moras D. Ligand binding domain of vitamin D receptors. *Curr Top Med Chem.* 2006;6(12):1229-1241.

57. Ciesielski F, Rochel N, Mitschler A, Kouzmenko A, Moras D. Structural investigation of the ligand binding domain of the zebrafish VDR in complexes with 1 alpha,25(OH)(2)D-3 and Gemini: purification, crystallization and preliminary X-ray diffraction analysis. *J Steroid Biochem.* 2004;89-90(1-5):55-59.

58. Jurutka PW, Thompson PD, Whitfield GK, Eichhorst KR, Hall N, Dominguez CE, Hsieh J-C, Haussler CA, Haussler MR. Molecular and functional comparison of 1,25-dihydroxyvitamin D(3) and the novel vitamin D receptor ligand, lithocholic acid, in activating transcription of cytochrome P450 3A4. *J Cell Biochem.* 2005;94(5):917-943.

59. Masuno H, Ikura T, Morizono D, Orita I, Yamada S, Shimizu M, Ito N. Crystal structures of complexes of vitamin D receptor ligand-binding domain with lithocholic acid derivatives. *Journal of lipid research.* 2013;54(8):2206-2213.

60. Rachez C, Gamble M, Chang CP, Atkins GB, Lazar MA, Freedman LP. The DRIP complex and SRC-1/p160 coactivators share similar nuclear receptor binding determinants but constitute functionally distinct complexes. *Molecular and cellular biology.* 2000;20(8):2718-2726.

61. Westin S, Kurokawa R, Nolte RT, Wisely GB, McInerney EM, Rose DW, Milburn MV, Rosenfeld MG, Glass CK. Interactions controlling the assembly of nuclear-receptor heterodimers and co-activators. *Nature.* 1998;395(6698):199-202.

62. Yang W, Rachez C, Freedman LP. Discrete roles for peroxisome proliferator-activated receptor gamma and retinoid X receptor in recruiting nuclear receptor coactivators. *Molecular and cellular biology.* 2000;20(21):8008-8017.

63. vom Baur E, Zechel C, Heery D, Heine MJ, Garnier JM, Vivat V, Le Douarin B, Gronemeyer H, Chambon P, Losson R. Differential ligand-dependent interactions between the AF-2 activating domain of nuclear receptors and the putative transcriptional intermediary factors mSUG1 and TIF1. *Embo J.* 1996;15(1):110-124.

FIGURES

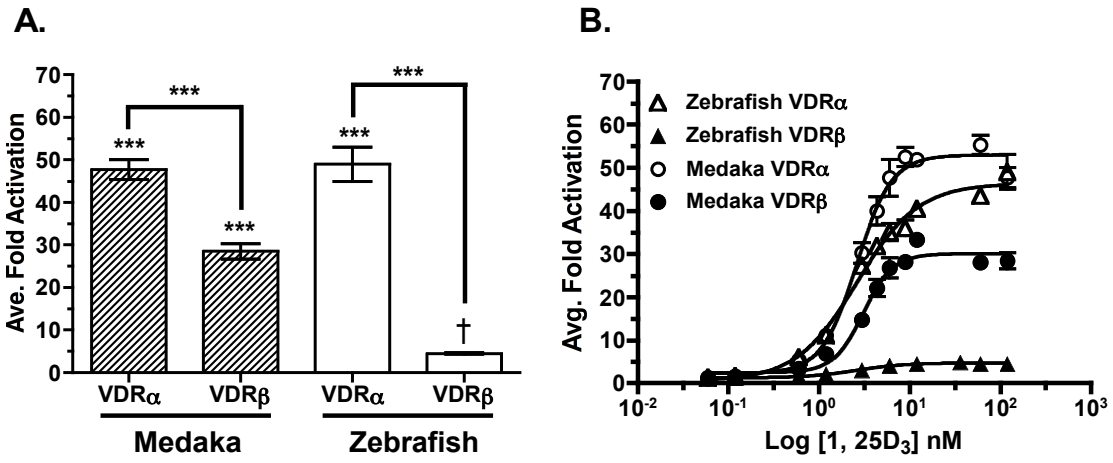

C.

Species	EC_{50}	95% C.I.	E_{MAX}
Medaka VDRα	2.6 nM	2.2 – 3.0 nM	52.9
Medaka VDRβ	3.1 nM	2.6 – 3.6 nM	30.1
Zebrafish VDRα	2.6 nM	2.1 – 3.2 nM	46.3
Zebrafish VDRβ	2.5 nM	2.0 – 3.2 nM	4.7

Figure 1. (**A**) Transactivation of medaka and zebrafish VDRα and VDRβ by 120 nM 1, $25D_3$, and (**B**) Concentration-response curves for transactivation of medaka and zebrafish VDRα and VDRβ by 0 – 120 nM 1, $25D_3$. HepG2 cells were transiently transfected with pSG5-VDR, XREM-Luc, and *Renilla* as described previously in *Materials and Methods*. Cells were treated with either (**A**) 120 nM 1, 25_2D_3 or (**B**) 0 - 120 nM 1, $25D_3$ in media for 24 hours. VDR response was measured via dual-luciferase assays. Data are represented as the

average fold activation normalized to the ethanol control ± SEM (n = 4). For (**A**), asterisks indicate significance: *** = $p < 0.001$, ** = $p < 0.01$, * = $p < 0.05$. Although the increase in VDR transactivation observed for zebrafish VDRβ was not great enough to be considered significant compared to the other VDRs in the one-way ANOVA, it was determined to be significantly different (†) from the ethanol control using an unpaired t-test ($t_6 = 24.68$, $p < 0.001$). For (**B**) and **(C),** the half-maximal effective concentration (EC_{50}), 95% confidence interval (95% C.I.), and maximum efficacy (E_{MAX}) values for each VDR was determined using nonlinear regression analysis using a sigmoidal dose-response calculation with variable slope in Prism 4.

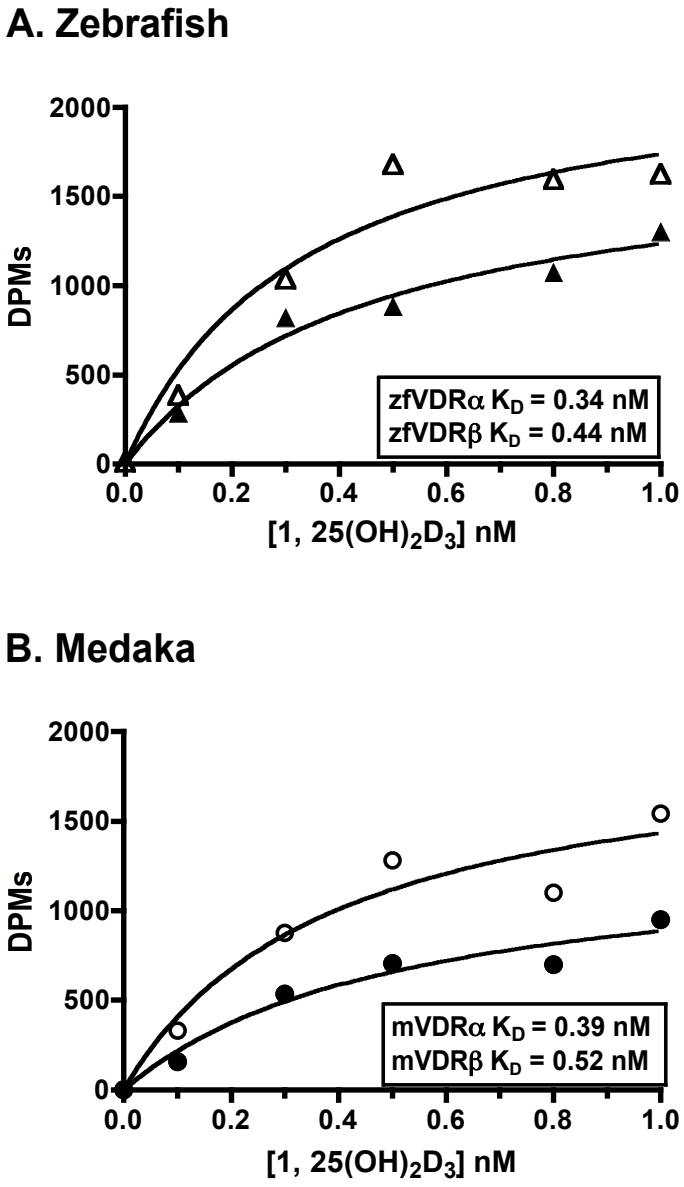

Figure 2. Saturation binding analysis of [^{3}H]-1, 25D_3 to (**A**) zebrafish VDRα (*open triangles*) and VDRβ (*solid triangles*), and (**B**) medaka VDRα (*open circles*) and VDRβ (*solid circles*). The X-axis depicts the concentration of 1, 25D_3, and the Y-axis depicts the

disintegrations per minute (DPM). Lysates were prepared from transfected Cos7 cells as described in *Materials and Methods*. Lysates were incubated with 0 – 1.0 nM [^{3}H]-1, 25D$_3$ for 18 hours at 4˚C. Unbound ligand was removed as described. Specific binding values were calculated by subtracting the average non-specific binding counts from the total binding counts. Hyperbolic one-site binding curves were fit to determine the dissociation constant (K_D). The K_D represents the ligand concentration where half of the receptors are occupied by ligand. The reported K_D in the manuscript for each VDR is the average of three separate experiments ± SEM. Shown here is data from a representative experiment.

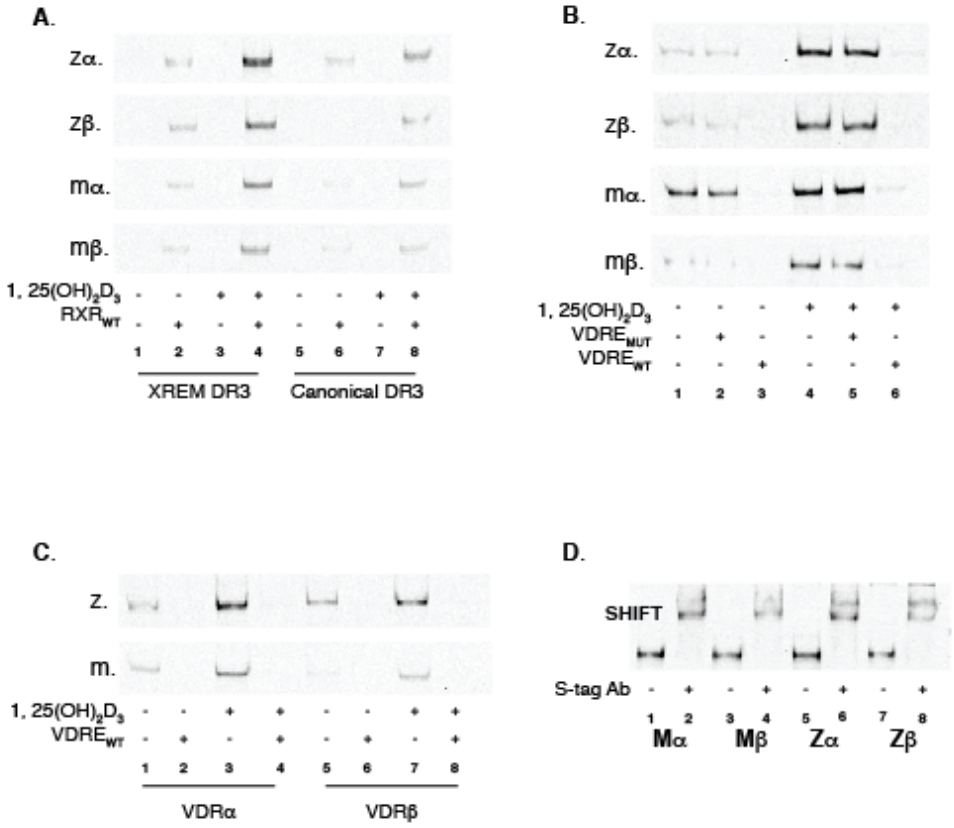

E. Canonical VDRE: AGGTCAxxxAGGTCA
F. Canonical VDR mutant: AG*AA*CAxxxAG*AA*CA
G. XREM VDRE: TGAACTxxxTGACCC

Figure 3. Electrophoretic mobility shift analysis of recombinant zebrafish (z) and medaka (m) VDRα and VDRβ binding to a canonical VDRE, a mutant form of the canonical, and a divergent VDRE from the XREM region of CYP3A4 (see E – G for sequences). **(A)** Receptors were analyzed for their ability to form DNA binding complexes on both canonical (*lanes 5 – 8*) and divergent (XREM) (*lanes 1 – 4*) VDREs in both the absence and presence of RXR_{WT} and 100 nM 1, $25D_3$ as described in *Materials and Methods*. Binding complexes were only observed in the presence of VDR and RXR_{WT} (*lanes 2, 4, 6, 8*) and DNA binding

was visibly enhanced with the addition of 1, $25D_3$ versus the ethanol control (*lane 2 vs. 4 and 6 vs. 8*). **(B)** Competition assays with the canonical VDRE using both an unlabeled mutant **(F)** and wild-type competitor **(E)**. Strong DNA binding was observed in the absence of either competitor (*lanes 1 and 4*). The addition of 100-fold unlabeled mutant competitor VDRE did not inhibit DNA binding of any VDR paralog tested (*lanes 2 and 5*). The addition of 100-fold access wild-type competitor effectively out-competed any binding to the labeled canonical VDRE (*lanes 3 and 6*). Addition of 1, $25D_3$ enhanced DNA binding, but did not alter the effects of the competitors. **(C)** Competition assays with the divergent XREM VDRE from CYP3A4. Strong binding was observed in with 1, $25D_3$ in the absence of competitor (*lanes 3 and 7*). The addition of 100-fold unlabeled XREM VDRE **(G)** effectively outcompeted VDR binding to the labeled probe (*lanes 2, 4* for VDRα; *lanes 6, 8* for VDRβ). **(D)** Supershift assay with untagged RXR_{WT} and S-tagged VDR in the presence and absence of 1 μg S-tag antibody. In all assays, enhanced binding complex formation was observed in response to 1, $25D_3$, and both VDRα paralogs demonstrated a visibly greater degree of binding in comparison to their respective VDRβ paralogs.

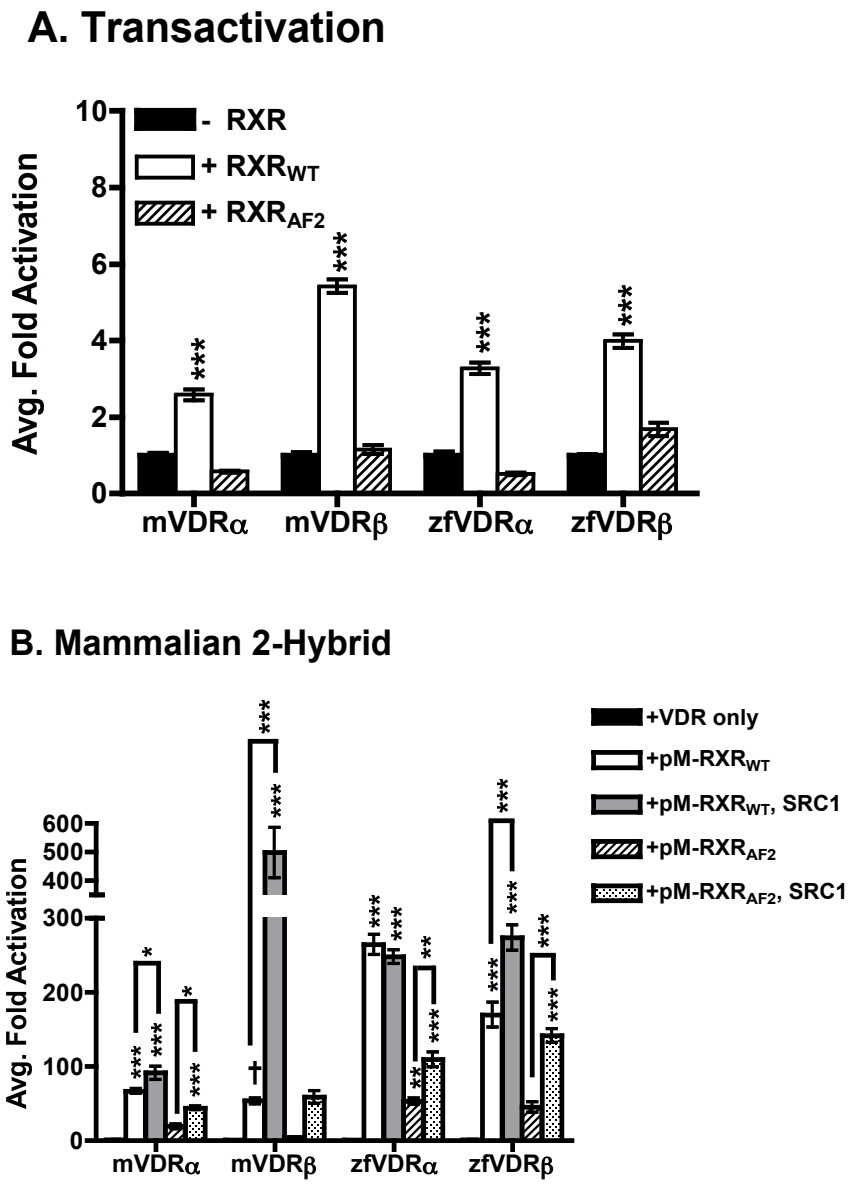

Figure 4. (A) Analysis of overexpressed RXR on VDR transactivation and **(B)** VDR-RXR heterodimerization in response to 1, 25D_3. **(A)** HepG2 cells were transiently transfected with pSG5-VDR, XREM-Luc, and Renilla as described previously in *Materials and Methods*. Select assays were cotransfection with pCDNA-RXR_{WT} or pCDNA-RXR_{AF2} where indicated.

Cells were treated with 120 nM 1, 25_2D_3 for 24 hours. VDR response was measured via dual-luciferase assays. Data are represented as the average fold activation normalized to VDR alone (no RXR) ± SEM (n=4). Asterisks represent a significant difference in transactivation compared to the VDR control: *** = $p < 0.001$, ** = $p < 0.01$, * = $p < 0.05$. **(B)** Mammalian two-hybrid assays were conducted to study VDR-RXR heterodimerization in response to 1, $25D_3$. HepG2 cells were transiently transfected with pVP16-VDR as prey and pM-RXR_{WT} or pM-RXR_{AF2} as bait, along with 5XGal4-TATA-Luc and *Renilla*. Select assays included pSG5-SRC1 where indicated. Cells were exposed to 120 nM 1, $25D_3$ in media for 24 hours. Protein-protein interaction was measured via dual-luciferase assays as described in the Materials and Methods. Data are represented as the mean fold activation ± SEM (n = 4). Data are normalized to VDR + empty pM vector (no RXR). Asterisks represent a significant interaction between VDR and RXR: *** = $p < 0.001$, ** = $p < 0.01$, * = $p < 0.05$. The interaction between medaka VDRβ and RXR was tested with an unpaired t-test: $t_6 = 13.71$, $p < 0.0001$ (†).

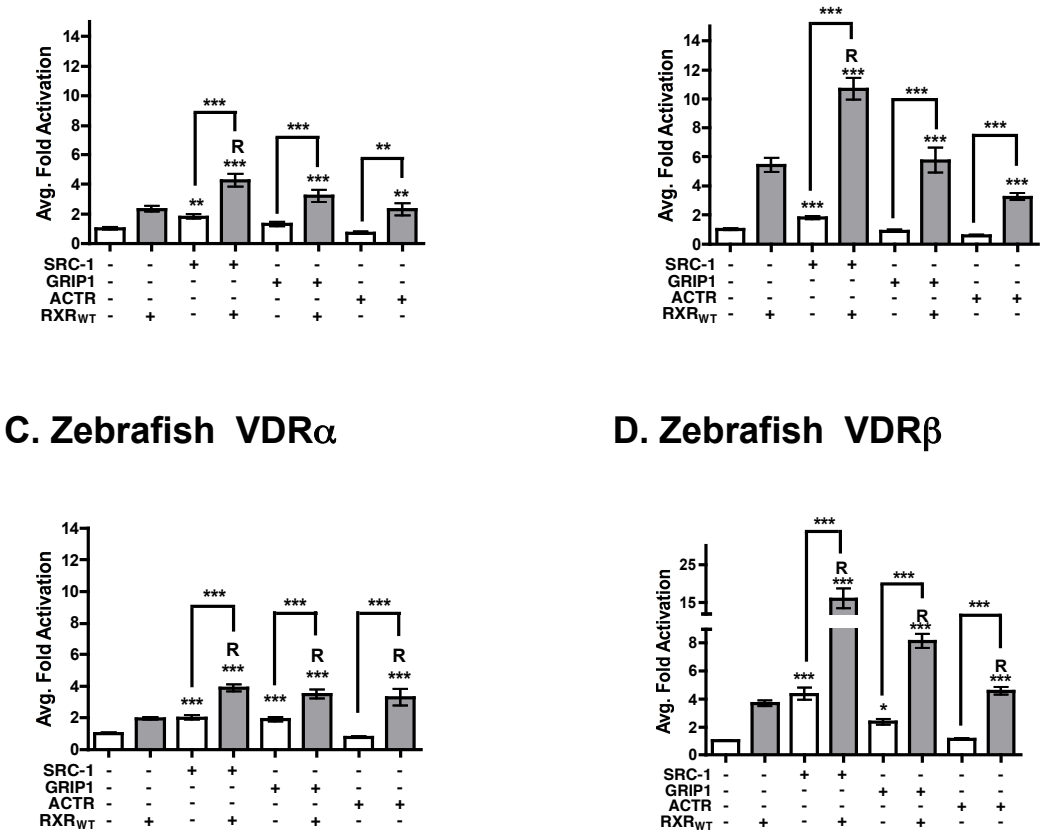

Figure 5. Analysis of overexpressed SRC-1, GRIP1, and ACTR on VDR transactivation in the presence and absence of RXR_{WT} in response to 1, $25D_3$ for **(A)** medaka VDRα, **(B)** medaka VDRβ, **(C)** zebrafish VDRα, and **(D)** zebrafish VDRβ. HepG2 cells were transiently transfected with pSG5-VDR, XREM-Luc, and Renilla as described previously in *Materials and Methods*. Select assays were cotransfected with pSG5-SRC-1, pSG5-GRIP1, pSG5-ACTR where indicated. Assays were conducted both with (*grey bars*), and without (*white bars*) cotransfected pCDNA-RXR_{WT}. Cells were treated with 120 nM 1, 25_2D_3 for 24 h.

VDR response was measured via dual-luciferase assays. Data are represented as the average fold activation normalized to VDR alone ± SEM (n=4). Asterisks above bars represent a significant difference in transactivation compared to the VDR only control: *** = $p < 0.001$, ** = $p < 0.01$, * = $p < 0.05$. Asterisks above brackets indicate a significant difference in transactivation between the presence and absence of RXR_{WT}. The letter R indicates cotransfection with both SRC and RXR_{WT} had a greater effect on VDR transactivation compared to VDR + RXR in the absence of SRC. Data are represented as the average fold activation normalized to VDR alone ± SEM (n=4).

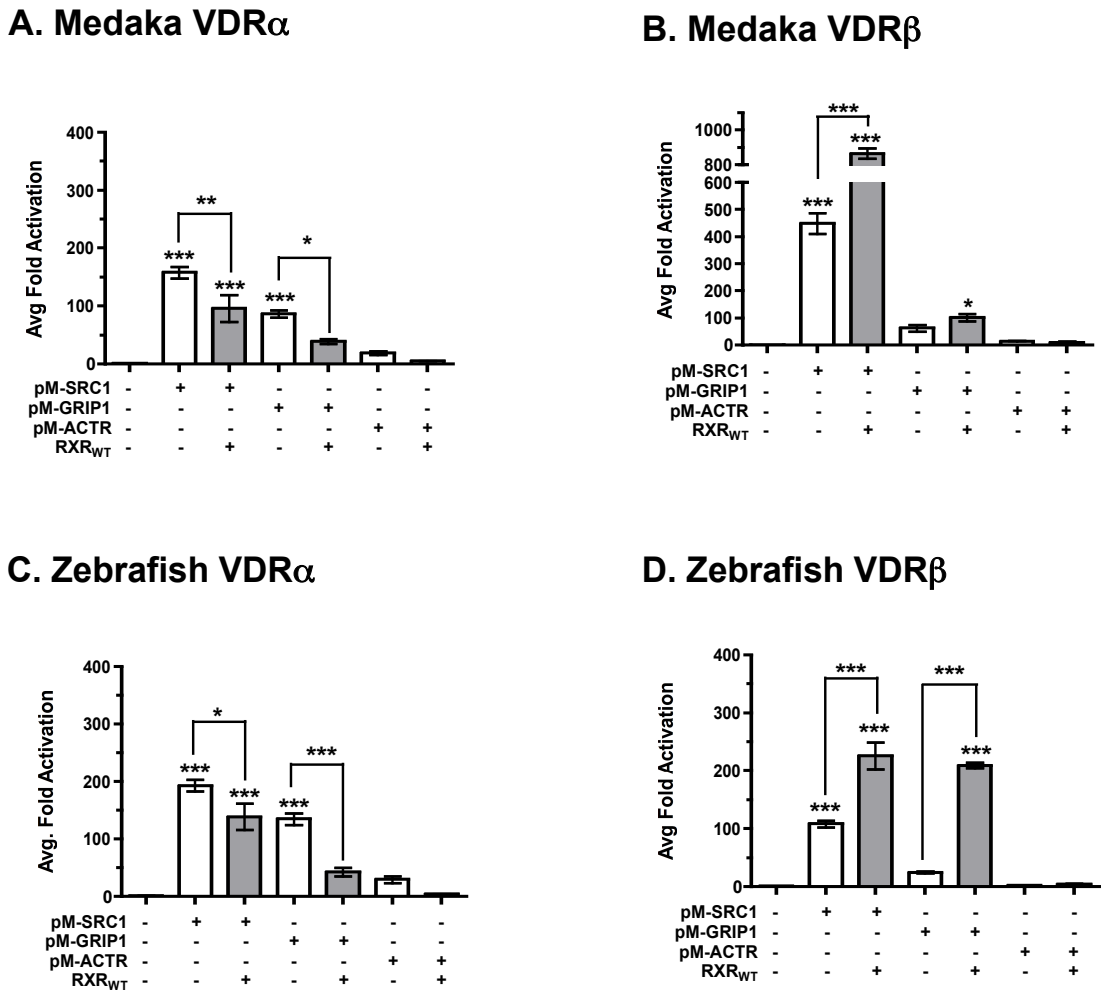

Figure 6. Mammalian 2-Hybrid analysis of VDR recruitment of members of the SRC family of nuclear receptor coactivators in response to 120 nM 1, 25D$_3$ for **(A)** medaka VDRα, **(B)** medaka VDRβ, **(C)** zebrafish VDRα, and **(D)** zebrafish VDRβ. Assays were conducted both with (*grey bars*), and without (*white bars*) cotransfected pCDNA-RXR$_{WT}$. HepG2 cells were transiently transfected with pVP16-VDR as prey, and pM-SRC-1, pM-GRIP1, or pM-ACTR as bait, along with 5XGal4-TATA-Luc and *Renilla*. Cells were exposed to 120 nM 1, 25D$_3$ in

media for 24 hours. Protein-protein interaction was measured via dual-luciferase assays as described in the *Materials and Methods*. Data are represented as the mean fold activation ± SEM (n = 4). Data are normalized to VDR + empty pM vector (no coactivators). Asterisks represent a significant interaction: *** = $p < 0.001$, ** = $p < 0.01$, * = $p < 0.05$.

CHAPTER TWO

Functional Assessment of Vitamin D Receptors Cloned from Basal Vertebrates

Erin M Kollitz[1], Guozhu Zhang[2], G. Kerr Whitfield[3], Mary Beth Hawkins[4], David M. Reif[5] and Seth W Kullman[1]

[1] Environmental and Molecular Toxicology, Department of Biological Sciences, North Carolina State University, Raleigh, NC

[2] Bioinformatics Research Center, North Carolina State University, Raleigh, NC

[4] Department of Basic Medical Sciences, The University of Arizona College of Medicine, Phoenix, AZ

[4] Department of Biology, North Carolina State University, Raleigh, NC

[5] Bioinformatics Research Center, Department of Biological Sciences, North Carolina State University

ABSTRACT

The vertebrate genome is a result of two rapid and successive rounds of genome duplication (1R and 2R). Teleost fish maintain a greater number of nuclear receptors (NRs) compared to other vertebrates due to a third whole genome duplication specific to their lineage (3R). The retention of multiple gene pairs in teleosts provides a unique opportunity to gain insight into how genes evolve through specific evolutionary processes. In this study we compare molecular activities of vitamin D receptors (VDR) from basal species that diverged at key points in vertebrate evolution to infer derived and ancestral functions of teleost paralogs. Species include the sea lamprey (*Petromyzon marinus*), a 1R jawless fish; the little skate (*Leucoraja erinacea*), a cartilaginous fish that diverged after the 2R event; and the Senegal bichir (*Polypterus senegalus*), a primitive 2R ray-finned fish that diverged before the teleost 3R event. Saturation binding assays and gel mobility shift assays demonstrate high affinity ligand binding and classic DNA binding characteristics of VDR has been conserved across evolution. Concentration response curves in transient transfection assays reveal similar EC_{50}s, however maximum transactivational efficacy varies. Protein-Protein interactions were investigated using co-transfection and mammalian 2-hybrid assays, and mutations of coregulator activation domains. Our results suggest that 1, $25D_3$ acts as a partial agonist in basal species. We combined these results with our previous study of VDR paralogs from 3R teleosts into a bioinformatics analysis. Our results suggest that functional differences between VDR are influenced by differential interactions with essential co-regulators. We speculate that we may be observing a change in the pharmacodynamic

relationships between VDR and 1, $25D_3$ throughout vertebrate evolution that may have been driven by changes in protein-protein interactions between VDR and essential coregulators.

INTRODUCTION

Teleost fishes comprise ~27,000 extant species and are among the most diverse and successful groups of vertebrates (1). These organisms represent an extensive array of phenotypic characteristics and maintain considerable genetic diversity. It appears that much of the complexity of the teleost genome is a result of successive rounds of gene and/or genome duplications. Current theory suggests that teleost complexity and diversity is likely a result of a whole genome duplication (WGD) that occurred early in their lineage. The serial "2R" genome duplication hypothesis suggests that the vertebrate genome is a result of two rapid and successive rounds of genome duplication (1R and 2R) near the divergence of jawless and jawed vertebrates, approximately 500 million years ago (2). Within ray-finned fishes (Actinopterygii), a third (3R) whole genome duplication (WGD) occurred in the stem lineage of the teleostean fishes (3,4). Whole genome duplications (WGDs) are proposed to be a considerable force in vertebrate evolution by providing a source of raw genetic material for evolutionary forces to act upon, resulting in the functional divergence of new genes with novel functions (5). The evolution and divergence of duplicate genes may result in larger gene families and permit more complex interactions and gene networks to evolve, leading to increased morphological complexity and speciation (5,6). This is consistent with the notion that larger genomes facilitate functional diversification and enable complex gene interactions. These processes in turn may facilitate morphological variation and physiological plasticity (7).

Duplicate genes have several possible fates. The classic model predicts that one copy in the majority of duplicates is usually lost, due to functional redundancy and accumulated

mutations as a result of relaxed selection. However, occasionally one copy will obtain a beneficial mutation that confers a new function while the other copy maintains the original function, referred to as neofunctionalization (8). A model hypothesized by Force et al (9) predicts that instead of one copy being lost, both copies may obtain complementary yet degenerative mutations, resulting in the partitioning of the ancestral function between the two copies, and the preservation of both copies to maintain the original function.

However, gene retention is not a random process. Highly connected genes involved in signaling and regulatory pathways, such as nuclear receptors, have been preferentially retained in duplicate following a whole genome duplication event in order to maintain pathway integrity (10-12). Pathway disruption caused by an imbalance of associated subunits may have negative effects on embryonic development, resulting in decreased fitness of the organism. Thus retention of entire regulatory pathways following a WGD is believed to be a driving force of evolution (12,13). Duplicate pathways that are able to escape selective pressure are free to evolve novel regulatory functions, leading to more specialized control of gene expression and developmental novelty.

One class of regulatory genes that have demonstrated preferential retention post-WGD is the nuclear receptor superfamily. Nuclear receptors (NRs) are ligand-dependent transcription factors that bind to lipophilic signaling molecules, resulting in systematic control and expression or silencing of target genes (14). Such control facilitates cellular responses to endogenous and exogenous signals through coordination of complex transcriptional processes. NRs play an essential role in many physiological processes including metabolism, homeostasis, reproduction, embryonic development, and control of

cellular proliferation and differentiation (14,15). In teleosts, orthologs for all mammalian NR sub classes have been identified, including those for steroid hormones receptors and orphan receptors (16-19). In fact, teleosts maintain a larger complement of NRs than mammals. For example, while humans have 48 NRs (20), 70 NRs have been identified in zebrafish (*Danio rerio*) (18), 71 NRs have been identified in the Japanese medaka (*Oryzias latipes*) (19), and 68 and 71 NRs have been identified in *Takifugu rubripes* and *Tetraodon nigroviridis*, two species of pufferfish (16,17). This is likely due to global retention of NRs and other regulatory genes within the teleost genomes subsequent to the 3R event (5,6,12). As NRs are important transcription factors for numerous endocrine-mediated processes, NR duplication and divergence may contribute to signal diversification, speciation, and emergence of evolutionary novelties in teleosts. However, the functional role of duplicate NRs remains unresolved in these species.

As the teleost-specific 3R event is in evolutionary terms "more recent", these organisms are attractive models for the study of gene evolution and functional divergence post WGD. Previous studies of teleost NR paralogs have found evidence of functional divergence fundamental NR functions, including in ligand binding (21-23), and protein interactions (Chapter 1). However, the ability to infer derived and ancestral properties of these receptors is limited by the lack of data regarding NR functions of basal vertebrates.

In previous studies our group has identified evidence of functional divergence between teleost vitamin D receptor (VDR, NR1I1) paralogs with regards to essential NR functions, including coactivator recruitment and DNA binding affinities. However, the lack of data on ancestral VDRs limited our ability to speculate on ancestral and derived functions

of the VDRα and VDRβ paralogs. In order to elucidate the evolutionary history and ancestral molecular functions of VDR, we have determined VDR function from basal vertebrates from key lineages that diverged early in vertebrate evolution. Species include the sea lamprey (*Petromyzon marinus*), considered to be one of the most basal extant vertebrates and a member of the class Agnatha, which diverged after the 1R event and before jawed vertebrates (24). The little skate (*Leucoraja erinacea*), a member of the class Chondrichthyes, the first lineage to diverge after the 2R duplication (25). In order to gain a better understanding of derived and ancestral VDR functions of the VDR paralogs, we have included the Senegal bichir (*Polypterus senegalus*), a primitive ray-finned fish that diverged before the teleost 3R event, and thus maintains only a single VDR ortholog (25,26). We have also included human as a well-studied tetropod for comparative purposes. We hypothesize that comparison of VDR function across the deep ancestry of Agnatha, Chondrichthyes and basal Actinopterygii will help facilitate a conceptual framework of mechanisms underlying nuclear receptor innovation and comparative endocrine physiology.

MATERIALS AND METHODS

DNA constructs

The pSG5-Lamprey VDR construct was a gift from the Dr. Kerr Whitfield (University of Arizona, Tuscan, AZ). The pSG5-Human VDR construct was a gift from Dr. John Moore (GlaxoSmithKline, Research Triangle Park, NC). All co-regulator expression and mammalian 2-hybrid constructs were a gift from Dr. Donald McDonnell (Duke University, Durham, NC). All luciferase reporters were obtained as described previously (23).

Skate VDR cloning

Little skate embryonic cDNA and an EST sequence representing a complete ORF for the skate VDR nucleic acid sequence were gifts from Dr. Randall Dahn at Mount Desert Island Biological Laboratory (Salisbury Cove, ME). The skate VDR cDNA sequence was amplified using a nested PCR protocol. All primers pairs were designed using the skate EST sequence and Primer 3 software (27) (see Appendix A). The first PCR reaction was conducted with 1 µL embryonic skate cDNA, 1 µL each of 10 µM forward outer primer and 10 µM reverse outer primer, 1 µL 50x dNTPs, 1 µL 50x Advantage taq (Clontech Laboratories, Mountain View, CA), 5 µL 10x Advantage Buffer, and 41 µL PCR grade water. PCR reactions were heated to 95˚C for 2 minutes followed by 40 cycles of 95˚C for 30 seconds, 55.1 ˚C for 30 seconds, 72˚C for 1.5 minutes, and a final step of 72˚C for 15 minutes. A single amplified PCR product was excised from a 1.5% agarose gel and purified. A 1 µL aliquot of the purified product from the first PCR reaction was used as the DNA template for the second PCR reaction with the internal primer sets (1 µL each of 10 µM

forward and reverse primers). Internal primers were designed with incorporated restriction sites to aid in ligation into pSG5, pVP16, and pET32a vectors (see Appendix A). The thermocycle settings were identical to those used for the outer primers, with the exception that the annealing temperature was adjusted to match each primer set. PCR products were gel purified and ligated into the pGEM-T easy vector according to the manufacturer's protocol (Promega Corporation, Madison, WI). The ligation product was transformed into GC10 *E.coli* bacteria (Genesee Scientific, San Diego, CA). Positive clones were identified via a blue/white screen. Positive clones were grown and plasmid DNA isolated using the QIAGEN High-speed miniprep kit (QIAGEN) and sequenced to confirm gene identity and construct orientation. Skate VDR cDNA was subcloned using the following restriction sites: pSG5 – BamHI/BglII (Agilent Technologies, Santa Clara, CA), pVP16 - BamHI/HindIII (Clontech Laboratories, Mountain View, CA), and pET32a – SalI/NotI (EMD Millepore, Billerica, MA). Skate VDR was subcloned by excising the skate VDR cDNA from pGEM-T via restriction digest, gel purification, and ligation into selected vectors using T4 DNA ligase (Promega Corporation, Madison, WI). Constructs were subsequently transformed into GC10 *E.coli* bacteria. All constructs were restriction mapped and sequenced to ensure identification, integrity and orientation of each VDR.

Bichir VDR cloning

Senegal bichir liver tissue was a gift from Dr. Kenneth Poss at Mount Desert Island Biological Laboratory (Salisbury Cove, ME). Liver tissue was homogenized in 1 mL of RNA Bee (Tel Test Inc, Friendswood, TX) using a Bullet Blender (Next Advance, Averill Park,

NY). Following homogenization, total RNA was isolated following the manufacturer's protocol. RNA quantity and 260/280 ratios were determined using a NanoDrop ND-1000 spectrophotometer (Thermo Fisher Scientific, Waltham, MA). First strand cDNA was synthesized using the 2 μg total RNA and the High Capacity cDNA Reverse Transcription kit (Life Technologies, Grand Island, NY) following manufacturers instructions. PCR primers were designed using Primer 3 (27) based on an identified EST from the *Polypterus senegalus* sequence project spear headed by Dr. Ben King at Mount Desert Island Biological Laboratory. During PCR amplification, select restriction sites were incorporated into primers sets for subcloning into pSG5, pVP16, and pET32a (see Appendix A). For each 50 μL PCR reaction, full length bichir VDR was amplified using 1 μL bichir cDNA, 1 μL 10 μM forward primer, 1 μL 10 μM reverse primer, 1 μL 50x dNTPs, 1 μL 50x Advantage taq (Clontech Laboratories, Mountain View, CA), 5 μL 10x Advantage Buffer, and 41 μL PCR grade water. PCR reactions were heated to 95˚C for 2 minutes followed by 30 cycles of 95˚C for 30 seconds, 61.4 ˚C for 30 seconds, 72˚C for 2 minutes, and a final step of 72˚C for 15 minutes. PCR products were resolved and excised from a 1.5% agarose gel, purified, and subcloned into the pGEM-T Easy Vector. Positive clones were identified by a blue/white screen, and sequenced for validation and orientation. Bichir VDR was subcloned into the pSG5 (EcoRI/BamHI), pVP16 (EcoRI/BamHI) and pET32a (SalI/NotI) vectors via restriction digest and ligation as described for skate VDR.

VDR transient transactivation assays

Cell culture media and other necessary reagents were obtained from Mediatech (Manassas, VA). HepG2 cells were cultured in T75 flasks with vented caps (BD Biosciences, San Jose, CA) using Minimum Essential Medium (MEM) containing 10% heat-inactivated fetal bovine serum,1 mM sodium pyruvate, and 1X non-essential amino acids. Cells were maintained following standard protocols in a 37°C/5% CO_2 incubator and split when ~70-80% confluent.

To analyze the differential transactivational activity of lamprey, skate, bichir, and human VDRs, full-length VDR constructs were tested in transient transactivation assays with 1α, 25-dihydroxyvitamin D_3 (1, $25D_3$) (EMD Millipore, Billerica, MA) as the primary ligand. Experiments were conducted using pSG5 expression vectors containing complete ORFs for each VDR in the presence of a luciferase reporter construct containing the XREM region of human CYP3A4 (XREM-Luc) that contains two imperfect DR3/ER6 vitamin D response elements (VDREs) (28). HepG2 cells were seeded in 96-well plates at 2.5 x 10^4 cells per well 24 hours prior to transfection. Cells were transfected at 90-95% confluency using Lipofectamine 2000 (Life Technologies, Grand Island, NY) with DNA diluted in Opti-MEM I Reduced Serum Medium as per the manufacture's recommendations. For functional comparisons, 89.7 ng of each pSG5-VDR construct was transiently transfected into HepG2 cells with 19.2 ng human XREM-Luc reporter and 4.5 ng of *Renilla* luciferase, which serves as an internal luciferase control (Promega Corporation, Madison, WI). Coregulator studies included the addition of 18.3 ng of either pCDNA-RXR_{WT}, pCDNA-RXR_{AF2}, pSG5-SRC-1, pSG5-GRIP-1or pSG5-ACTR where indicated. The medium was replaced twenty-four hours

post-transfection with complete MEM containing 120 nM 1, $25D_3$ for single dose assays, or a range of concentrations from 0 – 1200 nM $1,25D_3$ for concentration-response assays. Twenty-four hours post-exposure the Dual-Glo Luciferase Assay System (Promega Corporation, Madison, WI) was used to passively lyse the cells and test for luciferase activity following the manufacturer's protocols. Luciferase activities were measured using a Wallac MicroBet TriLuc Luminometer (Perkin Elmer Life Sciences, Waltham, MA). Control reactions included empty pSG5 vector and ethanol as a vehicle control. Luciferase readings were normalized to the internal *Renilla* control, and VDR response was normalized to an empty vector control. VDR + co-regulator response was normalized to VDR in the absence of co-regulators. All experiments were replicated at least twice in groups of 4 technical replicate wells. One-way ANOVAs followed by Tukey's HSD post hoc tests were run in GraphPad Prism version 4 for Mac OS X (GraphPad Software, La Jolla, CA). Nonlinear regression analysis using a sigmoidal dose-response calculation with variable slope was utilized for the concentration response curves to determine the half-maximal effective concentration (EC_{50}), 95% confidence interval (95% CI), and maximum efficacy (E_{MAX}) in GraphPad Prism 4.

Protein interaction: mammalian 2-hybrid assays

Protein-protein interactions between VDR and its heterodimer partner RXR and members of SRC/p160 family of nuclear receptor coactivators were assessed using a mammalian 2-hybrid system (Clontech, Mountain View, CA). Assays were conducted with chimeric VDRs containing the herpes simplex VP16 activation domain fused to full length

VDRs as prey (pVP16-VDR). NR co-regulators were used as bait for each reaction, and consisted of fusion proteins containing full length wild type or mutant RXR (pM-RXR_{WT}, pM-RXR_{AF2}), or the NR Box consisting of three "LXXLL" motifs of each member of the SRC family (pM-$SRC1_{241-386}$, pM-$GRIP1_{479-767}$, or pM-$ACTR_{392-1005}$) fused to the yeast Gal4 DNA-binding domain. Assays were conducted in HepG2 cells seeded into 96 well plates twenty-four hours pre-transfection as described above. Cells were transfected with 33.6 ng pVP16-VDR, 33.6 ng pM-coregulator, 126.6 ng 5XGal4-TATA-Luc reporter (containing response elements for the yeast Gal4 DNA binding domain), and 3 ng *Renilla* using Lipofectamine 2000 as described above. Controls consisted of transfections containing empty pM, pVP16 or both empty pM and pVP16 vectors. Cells were treated with either an ethanol vehicle control or 120 nM 1, $25D_3$ twenty-four hours post-transfection. Twenty-four hours post-dosing, Luciferase activity was measured using the Dual-Glo Luciferase Assay System described above. Luciferase response first was normalized to *Renilla,* and than normalized to pVP16-VDR in the absence of a coregulator bait construct. Data was analyzed using one-way ANOVAs followed by Tukey's HSD post hoc tests in GraphPad Prism version 4 for Mac OS X (GraphPad Software, La Jolla, CA).

Electrophoretic mobility shift assays

Recombinant VDR and human RXR_{WT} protein was obtained as follows. The pET32a-VDR and pET32a-RXR_{WT} protein expression constructs for each species were transformed into the BL21(DE3)pLysS strain of *E.coli* (Genesee Scientific, San Diego, CA). Positive colonies were identified through PCR screens and restriction mapping. A starter culture

consisting of 10 mL LB/amp inoculated with a single positive colony was grown overnight at 37˚C with shaking at 200 rpm. Overnight starter cultures were used to inoculate 250 mL of LB/amp and grown at 37˚C with shaking until OD_{600} = 0.6. Protein expression was induced by the addition of 1 mM IPTG and 20 μM $ZnCl_2$, and cultures were incubated at 25˚C for three hours with shaking at 200 rpm. Following incubation, cultures were centrifuged at 4,000 x g for 20 minutes at 4ºC. The supernatant was discarded, and the pellets were frozen at -20˚C overnight. The QIAexpress Ni-NTA Fast Start kit (QIAGEN, Valencia, CA) was used under native kit conditions to lyse the bacteria pellets and purify 6xHis-tagged VDR and RXR proteins from the soluble fraction. Purified protein concentrations were determined by averaging three A280 measurements using a NanoDrop® ND-1000 spectrophotometer (Thermo Fisher Scientific, Waltham, MA). Proteins were visually confirmed via Western Blot using antibodies to the 6xHis tags (QIAGEN, Valencia, CA).

Electrophoretic mobility shift assays (EMSAs) were carried out in a total volume of 20 μl containing 100 ng of recombinant VDR protein and 100 ng recombinant RXR where indicated. DNA–protein binding reactions were carried out using either a canonical VDRE (29) (5’ – AGC TTC AGG TCA AGG AGG TCA GAG AGC – 3’), a mutant form of the canonical sequence (5’ – AGC TTC AG*A A*CA AGG AG*A A*CA GAG AGC – 3’), or a VDRE located within the distal promoter region of the CYP3A4-XREM reporter used in transient transfection studies (5’ – GCT GAA TGA ACT TGC TGA CCC TCT GCT – 3’) (28). Single stranded Cy5-labeled and unlabeled oligos were purchased from Integrated DNA Technologies (Coralville, IA). Oligos were resuspended to a final concentration of 250 μM, and annealed by incubating equal concentrations of the sense and antisense strands in binding

buffer (10 mM Tris, 50 mM NaCl, 1 mM EDTA). Oligos were heated to 95˚C for two minutes and allowed to cool to room temperature. The annealed oligos were further diluted to a final concentration of 1 pmol/μL. For the DNA-binding reactions, receptors were incubated at 25˚ C in binding buffer (100 mM KCl, 10 mM HEPES, 1 mM EDTA, 0.1 mg/ml BSA, 4 μg/mL sonicated salmon sperm, 1.0 mM DTT, 1% glycerol, 20 mM MgCl2) and 100 nM 1, $25D_3$ or ethanol control. After a 45-minute incubation, 1 pmol Cy5-labeled double-stranded oligo was added and incubated for an additional 30 minutes. Competition experiments were performed in the presence of a 100-fold molar excess of unlabeled wild type or mutant oligos. Negative controls include affinity tags expressed and isolated from empty pET32a vector stocks, and ethanol vehicle control. Protein–DNA complexes were resolved on a 6% non-denaturing acrylamide gel in ice-cold 0.5X TBE buffer (45 mM Tris base, 45 mM boric acid, 1 mM EDTA, pH 8.0) at 100 V for 90 minutes. Gels were visualized on a Storm 865 using the red fluorescence mode (GE Healthcare Life Sciences, Pittsburgh, PA). Densitometry was measured using ImageQuaint TL 7.0 (GE Healthcare Life Sciences, Pittsburgh, PA).

Saturation binding analysis

Radiolabeled 1, $25D_3$ (1, 25-$(OH)_2$-26, 27 [^{3}H]dimethyl-vitamin D_3) was purchased from Perkin Elmer (Waltham, MA). The protease inhibitor cocktail was purchased from EMD Millipore (Billerica, MA). Cos7 cells (ATCC #CRL-1561) were maintained in complete DMEM medium supplemented with 10% FBS, and passaged every 4-5 days according to established protocols. To prepare lysates for saturation binding analysis, Cos7 cells (3.0×10^6 cells/150 mm dish) were transfected with 4 μg pSG5-VDR and 4 μg pSG5-

RXR_{WT}, along with 16 μg pBSII as carrier DNA, as described above using Lipofectamine 2000. Hormone-free complete DMEM media was replaced after twenty-four hours post-transfection. At forty-eight hours post-transfection, cells were harvested by trypsinization. Cells were centrifuged (1000 x g/5 minutes) and resuspended twice in 2 mL cold Dulbecco's PBS (Mediatech, Manassas, VA). After the second wash, cells were resuspended in 1 mL KETZD + 5 buffer (0.15 M KCl, 1 mM EDTA, 10 mM Tris HCl, 0.3 mM $ZnCl_2$, 200x dilution protease inhibitor cocktail, 5 mM DTT, pH 7.6). Cells were lysed by sonication (12 1-second bursts at 25% power) and centrifuged at 100,000 x g for 30 minutes at 4˚C. The supernatant containing the lysate was divided into 150 μL aliquots and stored at -80˚C until needed. The pellet was discarded.

The affinity of 1, 25-D_3 for each VDR was assessed as follows. Lysate was diluted 1/20 in ice-cold KETZD+5 buffer. 1, 25-$(OH)_2$-26, 27 [^{3}H]dimethyl-vitamin D_3 (original specific activity 157 Ci/mmol) was diluted to 20 Ci/mmol with unlabeled 1, 25D_3 (1 μM) and further diluted with ethanol to obtain the desired concentrations (0 – 1.6 nM). 10 μL ligand was added to 200 μL diluted lysate, shaken, and incubated overnight at 4˚C. Eighteen hours later unbound ligand was removed by incubation with 80 μL of a 0.5% Dextran-2.5% activated charcoal solution in GP Buffer (0.15 M NaCl, 0.015 M NaN_3, 0.1 M anhydrous Na_2HPO_4, 0.039 M NaH_2PO_4•H_2O, 10% gelatin, pH 7.0) at 4˚C for 15 minutes. Samples were centrifuged at 5000 x g for 5 minutes at 4˚C and 200 μL of supernantant was removed for scintillation counting. All assays were repeated at least twice with duplicate tubes for each concentration. Total binding was determined by using lysate transfected with pSG5-VDR, and nonspecific binding was determined by using lysate transfected with the empty

pSG5 vector. Specific binding was obtained by subtracting the nonspecific binding values from the total binding. Hyperbolic one-site binding curves were fit using Prism 4. Reported dissociation constant values (K_D) are the average of three separate curves ± SEM. Significant variation between average K_Ds was tested via a one-way ANOVA followed by Tukey's HSD post hoc test in Prism 4.

Bioinformatic summary analysis

In order to put these functional data in a broader context, the mammalian 2-hybrid (M2H) and transient transactivation (TT) data for lamprey, bichir, skate, medaka (VDRα and VDRβ), zebrafish (VDRα and VDRβ) and human were integrated into a summary cluster analysis. For this analysis, we have included previously published functional data for medaka and zebrafish (Chapter 1). The data for each assay (Figure 7: rows) was normalized across all eight VDR species (Figure 7: columns) to account for interspecies differences in absolute assay readout. The entire data matrix (visualized as a two-color heatmap) was then subjected to unsupervised, hierarchical clustering using Manhattan distance and complete linkage. The Pickett Plot to the right of the heatmap indicates the presence/absence of co-regulators within each assay, as described earlier in *Methods*. Data were visualized using the R package *Heatplus* (30).

Next, to identify particular functional assays that were drivers of both the overall cluster pattern and species subclusters, a bootstrap permutation was implemented using custom R code (31). For each of 10,000 bootstrap samples of assays, we counted the number of times the overall cluster pattern and subclusters (Lamprey, Bichir), (Medaka β, Skate,

Zebrafish β), and (Zebrafish α, Medaka α, Human) were recapitulated. Across all permutations, assays having a large effect on cluster membership (e.g. permuting $Assay_A$ significantly reduced the co-occurrence of species in $Cluster_C$) were inferred to be important drivers of VDR functional similarity.

RESULTS

VDR transactivation in response to 1, 25D_3

Full-length VDR constructs were tested in transient transactivation assays to determine if the cognate VDR ligand 1, 25D_3 would be a sufficient ligand to initiate transactivation of VDRs cloned from ancestral species. As demonstrated in figure 1A, significant transactivation is observed with all VDRs tested. However, the degree of response varies between VDR orthologs. Transactivation of lamprey VDR (1.6-fold) was weak, but still significant over background levels. Skate and bichir displayed moderate transactivation (11.4-fold and 15.5-fold, respectively). The greatest level of transactivation was observed with human (29.4-fold).

Concentration-response curves

Using receptor transactivation as an endpoint, concentration-response curves were conducted with a range of 1, 25D_3 concentrations between 0 - 120 nM, and the concentration that elicited 50% of the maximal effect (EC_{50}) was determined for each VDR (Fig. 1B, C). Observed EC_{50} values for lamprey (2.6 nM), skate (7.9 nM) and human (5.3 nM) were within the low nM range previously reported for both teleost VDR paralogs and human VDR (Chapter 1, (32)). Conversely, EC_{50} value for bichir was much greater, at 98.9 nM, suggesting that 1, 25D_3 may be a less potent agonist for this receptor.

Significant variation was additionally observed with the maximum efficacy values between VDRs (Fig. 1B, C). Similar to the initial transactivation studies, the maximum transactivational efficacy for lamprey was low (2.6-fold). Skate exhibited a maximum

efficacy of 24.6-fold, whereas bichir and human VDR exhibited similar maximum transactivational efficacies of 42.9-fold and 51.3-fold respectively. These results suggest that 1, 25D_3 functions as either a partial agonist (lamprey), or a full agonist for more derived members of Actinopterygii and Sarcopterygii tested in this study.

Saturation binding analysis

Innate ligand binding kinetics for each VDR form was determined using saturation bind analysis with radiolabeled 1, 25D_3 (Fig. 2). Dissociation constants (K_Ds) obtained for each VDR were within the sub-nanomolar range previously reported for human VDR (33,34), indicating that 1, 25D_3 is a high affinity ligand for each VDR protein tested. Nonlinear regression analysis gave K_D values of 0.53 ± 0.06 nM for lamprey, 0.72 ± 09 nM for skate, 0.34 ± 0.04 nM for bichir, and 0.30 ± 0.10 nM for human VDR. Although K_D value for lamprey is significantly greater than bichir, such a small difference in affinity is not suspected to have a large impact on transactivation. No other statistical difference between VDRs was detected. All VDRs tested bound 1, 25D_3 at a sub-nanomolar level, and thus demonstrated the characteristic high affinity binding of VDR. Differential ligand affinities are not driving the observed transactivational differences.

DNA binding

Electrophoretic mobility shift assays (EMSAs) were conducted to investigate VDR-RXR heterodimer association with both canonical and non-canonical vitamin D response elements (VDREs) in response to 1, 25-D_3 (Fig. 3A). With the canonical VDRE, VDR

binding was only observed in the presence of supplemented RXR_{WT} (Fig. 3A, lanes 2 and 6). Binding did not occur when VDR or RXR_{WT} was used singularly (Fig. 3A, lanes 1, 5 vs. 2, 6; RXR data not shown), indicating the necessity for obligate VDR: RXR_{WT} heterodimerization. However the formation of functional VDR or RXR homodimers was not examined. Competition assays using wild-type unlabeled VDRE probes were effectively able to outcompete the VDR-RXR binding with labeled canonical VDRE (Fig. 3A, lane 3 and 7). Competition assays using an unlabeled mutant VDRE probe had no effect on VDR binding to the labeled canonical VDRE (Fig. 3A, lanes 4 and 8). 1, 25-D_3 enhanced heterodimer binding to the canonical VDRE (Fig. 3A, lane 2 vs. 6).

To support transient transfection data, EMSAs were additionally conducted using an probe representing a divergent DR3 VDRE that is present within the XREM of CYP3A4 and the XREM-Luc reporter (Fig. 3B). This VDRE has previously been shown to facilitate expression of CYP3A4 and VDR transactivation of the XREM reporter (23). As with the canonical DR3, all EMSAs with the XREM VDRE probe exhibited an obligate dependence on RXR heterodimerization facilitating VDR-DNA interactions (Fig. 3B, lanes 1 vs. 2, 4 vs. 5). Competition assays using unlabeled probes were effectively able to outcompete the VDR-RXR_{WT} binding with the XREM VDRE (Fig. 3B, lanes 2 vs. 3, 5 vs. 6). Addition of 100 nM 1, 25D_3 enhanced heterodimer binding to the XREM VDRE tested in comparison to the ethanol control (Fig. 3B, lane 2 vs. 5) as determined via densitometry.

Coregulator interaction: heterodimerization with RXR

To analyze the effects of RXR on VDR transactivation, additiona transactivation studies were conducted utilizing VDR cotransfected with either full-length RXR (pCDNA-RXR_{WT}) or a truncated RXR mutant lacking the c-terminal AF2 region. (pCDNA-RXR_{AF2}). Results in figure 4A illustrate that cotransfection with RXR_{WT} significantly increased VDR transactivation compared to VDR alone. Skate, bichir, and human VDR transactivation increased 2.1 – 2.6-fold over background, whereas lamprey VDR increased almost 13-fold. In each instance where the RXR_{AF2} mutant was substituted for RXR_{WT}, luciferase activity was significantly attenuated to background levels, emphasizing the necessity of the AF2 region of RXR for VDR-mediated transactivation.

Next, mammalian 2-hybrid assays were conducted to determine if enhanced transactivation by RXR is due to direct protein-protein interactions (i.e heterodimerization with VDR) or if RXR facilitates VDR transactivation through other indirect mechanisms. As indicated in figure 4B, pM-RXR_{WT} and pVP16-VDR demonstrated a strong and significant association in all species, indicating that each VDR is likely forming heterodimers with RXR_{WT} in response to 1, $25D_3$. The presence of pSG5-SRC1 significantly increased VDR-RXR association for all VDRs except for bichir. The use of the pM-RXR_{AF2} mutant significantly attenuated the association between pVP16-VDR and pM-RXR, although a weak but significant association was still demonstrated with skate and human VDR, and bichir VDR in the presence of SRC-1.

Coregulator interaction: SRC family of nuclear receptor coactivators

Given that nuclear receptor coactivators are critical to VDR function, we next sought to investigate if co-transfection of VDR with members of the SRC family of nuclear receptor co-activators could facilitate VDR transactivation. Transient transactivation assays were conducted to determine if members of the SRC family of nuclear receptor co-activators could facilitate VDR transactivation. Transactivation assays were done in the presence and absence of supplemented RXR_{WT}.

In the absence of RXR_{WT}, the addition of SRC-1, GRIP1, or ACTR did not affect VDR transactivation for any VDR tested (Fig. 5A-D). Conversely, the combination of RXR_{WT} and SRC-1 resulted in a significant increase in VDR transactivation for lamprey and skate that was greater then the transactivation increase observed with either coregulator used individually (Fig. 5A, B, noted by the $ sign above the bars). A similar increase was observed with the cotransfection of RXR_{WT} and GRIP1 with skate VDR, but not lamprey. A significant increase was observed with human VDR co-transfected with RXR_{WT} and SRC-1, GRIP1, and ACTR, but these increases were not significant when compared to VDR + RXR_{WT} in the absence of SRC coactivators (Fig. 5D). Cotransfection with the SRC coactivators both in the presence and absence of RXR_{WT} did not affect bichir VDR transactivation with any of the coactivator combinations tested (Fig. 5C).

As with RXR, mammalian 2-hybrid assays were conducted to test the ability of the VDRs to recruit the SRC coactivators in response to 1, $25D_3$. Studies were conducted both in the presence and absence of supplemented RXR_{WT}. Results from this study demonstrate that all VDRs are capable of forming direct interactions between each respective VDR and pM-

SRC-1 (Fig. 6A-D). Further, interactions with lamprey, skate, and human were significantly enhanced in the presence of RXR_{WT}. Human was the only VDR tested that demonstrated an interaction with pM-GRIP1, although cotransfection with RXR resulted in a significant association between GRIP1 and skate VDR. None of the VDRs demonstrated an interaction with pM-ACTR whether in the presence of absence of RXR_{WT}.

Summary functional analysis

Figure 7 provides a global, multispecies context for VDR functional assays. The data resulted in three empirical clusters of [Lamprey, Bichir], [Skate, Zebrafish β, and Medaka β] and [Zebrafish α, Medaka α, and Human]. The first cluster (*C1*) included Lamprey and Bichir, which shared similar response across most of the 1, $25D_3$ mammalian 2-hybrid assays (M2H). However, the two species differ in their activity in the transient transfection (TT) assays. The next cluster (*C2*) included Skate and the beta variants of Zebrafish and Medaka. The last cluster (*C3*) grouped Humans with the alpha variants of Zebrafish and Medaka.

Permutation stability results were used to infer factors underlying the empirical clustering results. Activity associated with the coregulators GRIP1, SRC1, and ACTR drove assignment of the two Medaka variants (VDRα and VDRβ) to separate clusters. When assays involving these factors were permuted, only ~ 20% of resulting clusters maintained intact *C3* membership. Cluster *C2* was less sensitive to permutation, although SRC1 and GRIP1 cofactors disrupted the inclusion of Zebrafish VDRβ in this cluster. In this analysis, Lamprey and Bichir clustered together in 99% of permutations, regardless of functional assay(s) involved.

DISCUSSION

While significant information is available regarding functionality of mammalian nuclear receptors, there is a paucity of data regarding NR functions of basal vertebrates. This data gap limits our ability to infer derived and ancestral properties of more recent receptor functions. We have previously reported evidence of functional divergence between vitamin D receptor (VDR) paralogs isolated from teleost fish that evolved after the 3R WGD event (Chapter 1). In order to elucidate the evolutionary history and ancestral molecular functions of VDR, we have characterized VDR function from basal vertebrates that diverged at key periods in vertebrate evolution. Our results indicate that characteristic VDR functions evolved early and have been highly conserved throughout vertebrate evolution. However VDR efficacy in response to 1, $25D_3$ and the influence of protein-protein interactions between nuclear receptor coactivators and VDR varies significantly between basal and more derived vertebrates.

We first confirmed that all three basal VDRs and human VDR are capable of 1, $25D_3$-dependent transactivation. To expand on our results, we also established an EC_{50} for each VDR by titrating the concentration of 1, $25D_3$ in our transactivation assays. Combined with our previous data on medaka and zebrafish VDRα and VDRβ (Chapter 1), EC_{50} values for all VDRs, with the exception of bichir, were in the low nanomolar range (<10 nM). These results are consistent with that observed from other VDR studies which employed Gal4-VDR-LBD chimeras to assess VDR transactivation across phylogenetically diverse taxa (23,32). The EC_{50} for bichir, a 2R bony fish, was over 10-fold greater than the EC_{50} for any other VDR tested, suggesting that 1, $25D_3$ is a less potent agonist for this VDR. The fact that

the EC_{50} for VDRs from species that diverged both before and after bichir are in the low nanomolar range suggests that the decreased sensitivity observed with bichir VDR might be species or lineage specific. A decrease in VDR sensitivity to 1, 25D3 has been previously reported for another aquatic vertebrate, *Xenopus laevis* (35). While 1, $25D_3$ is a highly potent VDR ligand for the vast majority species tested, the results with both bichir and *Xenopus* indicate that potency varies in some species. However, the details behind the observed differential ligand sensitivities are currently undetermined. Despite the decreased ligand potency, our results with bichir VDR and previous reports with *Xenopus* VDR indicate that both are still capably of 1, $25D_3$-mediated transactivation, RXR heterodimerization, and DNA binding (35).

Our concentration-response curves indicate that 1, $25D_3$ has been largely conserved as a highly potent ligand throughout VDR evolution, while the ability of 1, $25D_3$ to induce a highly efficacious response is potentially a more recent innovation. High transactivational efficacy was only observed in the bony vertebrates. The maximum transactivational efficacy was highest for human and bichir, which is similar to the efficacies observed for medaka and zebrafish VDRα from our previous study (see Chapter 1). The maximum transactivational efficacy was much lower for lamprey and skate, the two most basal vertebrate species. Our lamprey transactivation data is consistent with the previous findings reported by Whitfield et al (34), and Reschly et al (32), which demonstrated that lamprey VDR maintains an EC_{50} comparable to that of human and rodent VDR, however the maximum level of transactivation exhibited by lamprey VDR was attenuated compared to human.

The observed differential transactivational efficacies are potentially caused by a variety of factors at each step in VDR activation, including essential functions involving ligand binding, DNA binding, and heterodimerization and recruitment of coregulators to the transcription complex. The perturbation of any of these steps may attenuate downstream VDR transactivation. We thus ran additional assays to assess each of these fundamental NR functions in basal vertebrates.

We first conducted saturation binding assays with our basal VDRs and [^{3}H]-1, 25D$_3$ to determine if the observed differential transactivational efficacies were a result of differential ligand affinities. Decreased ligand affinity may be indicative of a ligand's ability to stabilize a receptor in the active conformation, which may have downstream effects on subsequent steps in receptor transactivation. Our ligand binding data reveal that high ligand affinity for VDR is conserved across vertebrate evolution, even with lamprey and skate VDR. In each instance, K_D values for all VDRs tested were within the sub-nanomolar range (10^{-10} M) previously reported for mammalian high affinity VDR proteins (33). Of note, lamprey and skate had slightly lower ligand affinities compared to bichir and human. The lower affinity of lamprey VDR is consistent with previously reported ligand affinity by Whitfield et al (34). Upon closer examination of residues in the lamprey VDR LBD, Whitfield et al identified a leucine substitution for a residue known to be a ligand contact in human VDR (Val418) (36). We have identified this substitution in skate VDR as well. The interaction between Val418 (Val397Leu in lamprey, Val424Leu in skate) and 1, 25D$_3$ helps stabilize H12 of VDR in the active conformation, positioning it for optimal interaction with NR coactivators (36). The positioning of H12 is critical for NR activation, a necessity illustrated

by the fact that destabilization of H12 has been determined to be a mechanism of action for some VDR antagonists (37), and the loss of the AF2 region of H12 completely abolishes VDR transactivation (38). However, in this study we have demonstrated that both lamprey and skate VDR are both highly capable of recruiting coactivators in response to 1, $25D_3$, and thus we suspect that such a small difference in ligand affinity is not driving the transactivational variances we've observed. In addition, an in vitro study using human Val418Leu mutants found that the substitution did not affect VDR transactivation, despite the fact that the Val418Leu mutants also maintained attenuated ligand affinities (39). However, it should be noted that ligand affinity does not necessarily translate to transactivational efficacy. Accordingly, it has been previously demonstrated both by our laboratory and others that high ligand affinity and high transactivational efficacy of specific NR ligands are not proportional to each other (Chapter 1 and (22,40)). This phenomenon is likely due to the ability of ligands to induce subtle conformational differences within receptors that elicit different biological responses such as DNA binding, coactivator recruitment and heterodimerization (40).

RXR is considered the obligate heterodimer partner for VDR, and previous studies have demonstrated the necessity of this partnership in VDR mediated transcription (41,42). The cotransfection of RXR_{WT} in our VDR transactivation assays significantly increased VDR activation for all VDRs tested. This is consistent with our previous study on teleost VDR paralog transactivation with RXR, and enhanced VDR transactivation previously reported with human VDR in the presence of RXR (Chapter 1, (43)). Our mammalian 2-hybrid assays additionally demonstrate that all VDRs directly heterodimerize with RXR_{WT} in response to 1,

$25D_3$. When compared to our previous data with medaka and zebrafish VDRα and VDRβ (Chapter 1), it appears the overexpression of RXR_{WT} increases VDR activation 2.1 – 5.4-fold in our system, similar to a ~1.6 fold increase previously observed in transactivation studies with cotransfected human VDR and RXR (43). However, lamprey VDR proved to be exceptionally sensitive to RXR_{WT}. Lamprey VDR transactivation increased almost 13-fold in the presence of overexpressed RXR_{WT}. These results are in contrast to previous data from the Whitfield study that demonstrated a much smaller increase in VDR transactivation with zebrafish RXR, and a lack of heterodimer formation with human RXR in DNA binding assays (34). Our EMSA results provide additional support regarding the conservation and necessity of the VDR-RXR partnership for DNA binding. Similar to previous observations with human VDR (42,43), all basal vertebrate VDRs only formed binding complexes in the presence of RXR_{WT}, and complex binding to VDREs was enhanced with the addition of 1, $25D_3$, emphasizing the necessity of ligand binding for optimal heterodimerization. The fact all VDRs demonstrate increased transactivation in the presence of RXR, heterodimerize with RXR in response to 1, $25D_3$, and bind to both canonical and divergence VDREs with a high degree of specificity implies that VDR-RXR heterodimerization is an ancient trait that evolved early in VDR evolution, and has been highly conserved across species.

In addition to RXR, assays were run to determine the ability of the basal VDRs to recruit members of the SRC family of NR coactivators, and the effect of the coactivators on VDR activation. Leucine-rich motifs of the SRC coactivators, referred to as the NR box, interact with the AF2 region of NRs in a ligand-dependent manor (44). SRC coactivators enhance NR transactivation through chromatin remodeling and recruiting additional proteins

to the transcription complex (45). Similar to our studies with RXR, our transactivation and mammalian 2-hybrid assays with the SRC coactivators also demonstrate a strong degree of conservation: all VDRs demonstrate a strong preference for SRC-1 over GRIP1 and ACTR, a preference that has been observed previously with human VDR (46). In our system, overexpressed RXR_{WT} was necessary for the SRC coactivators to enhance transactivation. Consistent with Jurutka et al, we have hypothesized that a direct association between these proteins is necessary to drive gene expression. The SRC coactivators did not have a significant effect on bichir VDR activation, although our M2H data indicate that bichir successfully recruits SRC-1.

The ability of 1, $25D_3$ to bind the basal VDRs with high affinity yet only induce partial efficacy in transactivation assays compared to modern vertebrate VDRs suggests that 1, $25D_3$ may function as a partial agonist for the basal VDRs. Partial agonists are defined by their ability to directly bind a receptor, but are only able to induce partial efficacy compared to a full agonist. While these observations are traditionally made with a single receptor and multiple ligands, what we may be observing is a change in the pharmacodynamic relationship between VDR and 1, $25D_3$ throughout vertebrate evolution. Our lamprey and skate VDR data supports the theory that the evolution of 1, $25D_3$ as a high potency and high affinity ligand for VDR evolved early, however it appears that the ability of 1, $25D_3$ to act as a full agonist evolved later in evolution. Our bioinformatics analysis suggests that interaction with RXR and the SRC coregulators may have been influential the ability of VDR to mediate a full agonist response to D3. While VDR has maintained a high ligand affinity across species, we speculate that an increasing sensitivity to coregulators may have been an influence driving

the increased transactivational response observed in human and the teleost VDRα paralogs. The cluster analysis indicates that the coregulators have the greatest effect on the C3 cluster (human VDR, zebrafish and medaka VDRα). By examining phylogeny of our test species there appears to be a trend suggesting that full transcriptional response to 1, $25D_3$ may have appeared before the Actinopterygii/Sarcopterygii split, but after the divergence of more basal jawed vertebrates such as Chondricthyes, however additional studies are necessary to support this theory.

Overall, our results demonstrate that VDR function is highly conserved across species. Similar to previous reports on human VDR, all VDRs from basal vertebrates maintain high ligand affinities, heterodimerize with RXR, recruit members of the SRC family of NR coactivators, and mediate transactivation in response to 1, 25D3. However, the two most basal vertebrates were incapable of mediating the maximum transactivation efficacy observed with human VDR and the teleost VDRα paralogs. Our bioinformatics analysis indicates that VDR may have evolved an increasing sensitivity to coregulators later in evolution, which may have been a major influence driving the increased efficacy observed in later vertebrates compared to the basal vertebrates.

REFERENCES

1. Nelson JS. *Fishes of the World.* 4th Edition ed. New York: J. Wiley; 2006.

2. Dehal P, Boore J. Two rounds of whole genome duplication in the ancestral vertebrate. *Plos Biol.* 2005;3(10):1700-1708.

3. Hoegg S, Brinkmann H, Taylor J, Meyer A. Phylogenetic timing of the fish-specific genome duplication correlates with the diversification of teleost fish. *J Mol Evol.* 2004;59(2):190-203.

4. Crow K, Stadler P, Lynch V, Amemiya C, Wagner G. The "fish-specific" Hox cluster duplication is coincident with the origin of teleosts. *Mol Biol Evol.* 2006;23(1):121-136.

5. Taylor J, Raes J. Duplication and divergence: The evolution of new genes and old ideas. *Annu Rev Genet.* 2004;38:615-643.

6. Crow K, Wagner G. What is the role of genome duplication in the evolution of complexity and diversity? *Mol Biol Evol.* 2006;23(5):887-892.

7. Van de Peer Y, Maere S, Meyer A. OPINION The evolutionary significance of ancient genome duplications. *Nat Rev Genet.* 2009;10(10):725-732.

8. Ohno S. *Evolution by gene duplication.* New York: Springer-Verlag; 1970.

9. Force A, Lynch M, Pickett F, Amores A, Yan Y, Postlethwait J. Preservation of duplicate genes by complementary, degenerative mutations. *Genetics.* 1999;151(4):1531-1545.

10. Brunet FG, Roest Crollius H, Paris M, Aury JM, Gibert P, Jaillon O, Laudet V, Robinson-Rechavi M. Gene loss and evolutionary rates following whole-genome duplication in teleost fishes. *Molecular biology and evolution.* 2006;23(9):1808-1816.

11. Kassahn KS, Dang VT, Wilkins SJ, Perkins AC, Ragan MA. Evolution of gene function and regulatory control after whole-genome duplication: comparative analyses in vertebrates. *Genome research.* 2009;19(8):1404-1418.

12. Edger PP, Pires JC. Gene and genome duplications: the impact of dosage-sensitivity on the fate of nuclear genes. *Chromosome Res.* 2009;17(5):699-717.

13. Freeling M, Thomas BC. Gene-balanced duplications, like tetraploidy, provide predictable drive to increase morphological complexity. *Genome research.* 2006;16(7):805-814.

14. Aranda A, Pascual A. Nuclear hormone receptors and gene expression. *Physiol Rev.* 2001;81(3):1269-1304.

15. Gronemeyer H, Gustafsson J, Laudet V. Principles for modulation of the nuclear receptor superfamily. *Nat Rev Drug Discov.* 2004;3(11):950-964.

16. Maglich J, Caravella J, Lambert M, Willson T, Moore J, Ramamurthy L. The first completed genome sequence from a teleost fish (Fugu rubripes) adds significant diversity to the nuclear receptor superfamily. *Nucleic Acids Res.* 2003;31(14):4051-4058.

17. Metpally RPR, Vigneshwar R, Sowdhamini R. Genome inventory and analysis of nuclear hormone receptors in Tetraodon nigroviridis. *J Biosciences.* 2007;32(1):43-50.

18. Bertrand S, Thisse B, Tavares R, Sachs L, Chaumot A, Bardet PL, Escriva H, Duffraisse M, Marchand O, Safi R, Thisse C, Laudet V. Unexpected novel relational links uncovered by extensive developmental profiling of nuclear receptor expression. *PLoS genetics.* 2007;3(11):e188.

19. Howarth DL. *Characterization of FXR alpha in medaka and its involvement in hepatobiliary injury* [Dissertation]. Durham: Integrated Toxicology and Environmental Health Program, Duke University; 2009.

20. Robinson-Rechavi M, Carpentier AS, Duffraisse M, Laudet V. How many nuclear hormone receptors are there in the human genome? *Trends in genetics : TIG.* 2001;17(10):554-556.

21. Hawkins MB, Thomas P. The unusual binding properties of the third distinct teleost estrogen receptor subtype ERbetaa are accompanied by highly conserved amino acid changes in the ligand binding domain. *Endocrinology.* 2004;145(6):2968-2977.

22. Bury N, Sturm A, Le Rouzic P, Lethimonier C, Ducouret B, Guiguen Y, Robinson-Rechavi M, Laudet V, Rafestin-Oblin M, Prunet P. Evidence for two distinct functional glucocorticoid receptors in teleost fish. *J Mol Endocrinol.* 2003;31(1):141-156.

23. Howarth DL, Law SHW, Barnes B, Hall JM, Hinton DE, Moore L, Maglich JM, Moore JT, Kullman SW. Paralogous vitamin D receptors in teleosts: Transition of nuclear receptor function. *Endocrinology.* 2008;149(5):2411-2422.

24. Escriva H, Manzon L, Youson J, Laudet V. Analysis of lamprey and hagfish genes reveals a complex history of gene duplications during early vertebrate evolution. *Molecular biology and evolution.* 2002;19(9):1440-1450.

25. Kikugawa K, Katoh K, Kuraku S, Sakurai H, Ishida O, Iwabe N, Miyata T. Basal jawed vertebrate phylogeny inferred from multiple nuclear DNA-coded genes. *BMC Biol.* 2004;2:3.

26. Inoue JG, Miya M, Tsukamoto K, Nishida M. Basal actinopterygian relationships: a mitogenomic perspective on the phylogeny of the "ancient fish". *Mol Phylogenet Evol.* 2003;26(1):110-120.

27. Rozen SaS, HJ. *Primer3 on the WWW for general users and for biologist programmers.* Totowa, NJ: Humana Press; 2000.

28. Drocourt L, Pascussi J, Assenat E, Fabre J, Maurel P, Vilarem M. Calcium channel modulators of the dihydropyridine family are human pregnane X receptor activators and inducers of CYP3A, CYP2B, and CYP2C in human hepatocytes. *Drug Metab Dispos.* 2001;29(10):1325-1331.

29. Shaffer P, Gewirth D. Vitamin D receptor-DNA interactions. *Vitam Horm.* 2004;68:257-273.

30. Ploner A. Heatplus: Heatmaps with Row and/or Column Covariates and Colored Clusters. *R package version 260.* 2012.

31. RCoreTeam. *R: A Language and Environment for Statistical Computing.* Vienna, Austria: R Foundation for Statistical Computing; 2013.

32. Reschly EJ, Bainy ACD, Mattos JJ, Hagey LR, Bahary N, Mada SR, Ou J, Venkataramanan R, Krasowski MD. Functional evolution of the vitamin D and pregnane X receptors. *BMC Evol Biol.* 2007;7:222.

33. Dusso A, Brown A, Slatopolsky E. Vitamin D. *Am J Physiol-Renal.* 2005;289(1):F8-F28.

34. Whitfield G, Dang H, Schluter S, Bernstein R, Bunag T, Manzon L, Hsieh G, Dominguez C, Youson J, Haussler M, Marchalonis J. Cloning of a functional vitamin D receptor from the lamprey (Petromyzon marinus), an ancient vertebrate lacking a calcified skeleton and teeth. *Endocrinology.* 2003;144(6):2704-2716.

35. Li YC. Cloning and Characterization of the Vitamin D Receptor from Xenopus laevis. *Endocrinology.* 1997;138(6):2347-2353.

36. Rochel N, Wurtz J, Mitschler A, Klaholz B, Moras D. The crystal structure of the nuclear receptor for vitamin D bound to its natural ligand. *Mol Cell.* 2000;5(1):173-179.

37. Carlberg C. Ligand-mediated conformational changes of the VDR are required for gene transactivation. *The Journal of steroid biochemistry and molecular biology.* 2004;89-90(1-5):227-232.

38. Thompson PD, Remus LS, Hsieh JC, Jurutka PW, Whitfield GK, Galligan MA, Encinas Dominguez C, Haussler CA, Haussler MR. Distinct retinoid X receptor activation function-2 residues mediate transactivation in homodimeric and vitamin D receptor heterodimeric contexts. *Journal of molecular endocrinology.* 2001;27(2):211-227.

39. Bula CM, Bishop JE, Norman AW. Conservative mutageneic perturbations of amino acids connecting helix 12 in the 1alpha,25(OH)2-D3 receptor (VDR) to the ligand

cause significant transactivational effects. *The Journal of steroid biochemistry and molecular biology.* 2007;103(3-5):286-292.

40. Peleg S, Sastry M, Collins ED, Bishop JE, Norman AW. Distinct conformational changes induced by 20-epi analogues of 1 alpha,25-dihydroxyvitamin D3 are associated with enhanced activation of the vitamin D receptor. *The Journal of biological chemistry.* 1995;270(18):10551-10558.

41. Bettoun D, Burris T, Houck K, Buck D, Stayrook K, Khalifa B, Lu J, Chin W, Nagpal S. Retinoid X receptor is a nonsilent major contributor to vitamin D receptor-mediated transcriptional activation. *Mol Endocrinol.* 2003;17(11):2320-2328.

42. Thompson PD, Jurutka PW, Haussler CA, Whitfield GK, Haussler MR. Heterodimeric DNA binding by the vitamin D receptor and retinoid X receptors is enhanced by 1,25-dihydroxyvitamin D3 and inhibited by 9-cis-retinoic acid. Evidence for allosteric receptor interactions. *The Journal of biological chemistry.* 1998;273(14):8483-8491.

43. MacDonald PN, Dowd DR, Nakajima S, Galligan MA, Reeder MC, Haussler CA, Ozato K, Haussler MR. Retinoid X receptors stimulate and 9-cis retinoic acid inhibits 1,25-dihydroxyvitamin D3-activated expression of the rat osteocalcin gene. *Molecular and cellular biology.* 1993;13(9):5907-5917.

44. Heery DM, Kalkhoven E, Hoare S, Parker MG. A signature motif in transcriptional co-activators mediates binding to nuclear receptors. *Nature.* 1997;387(6634):733-736.

45. Leo C, Chen J. The SRC family of nuclear receptor coactivators. *Gene.* 2000;245(1):1-11.

46. Jurutka PW, Thompson PD, Whitfield GK, Eichhorst KR, Hall N, Dominguez CE, Hsieh J-C, Haussler CA, Haussler MR. Molecular and functional comparison of 1,25-dihydroxyvitamin D(3) and the novel vitamin D receptor ligand, lithocholic acid, in activating transcription of cytochrome P450 3A4. *J Cell Biochem.* 2005;94(5):917-943.

FIGURES

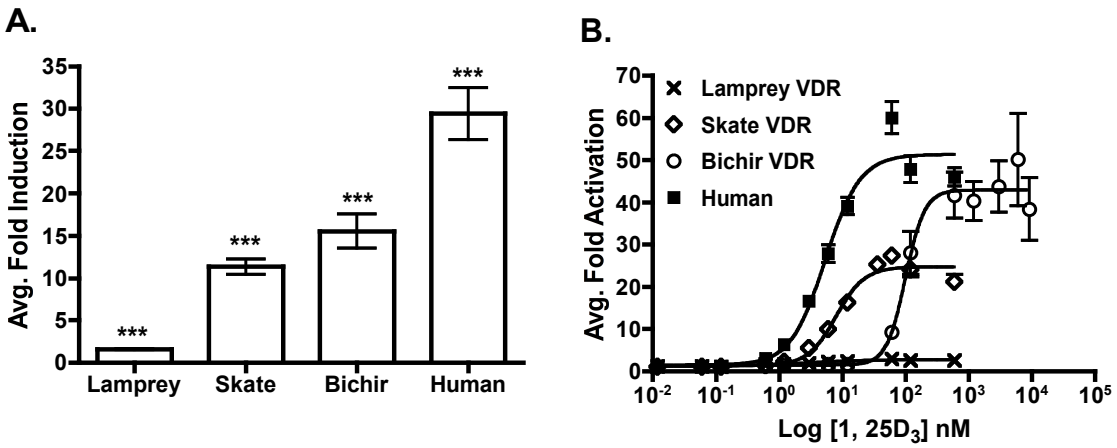

C.

	EC_{50}	95% C.I.	E_{MAX}
Lamprey VDR	2.6 nM	1.4 – 4.8 nM	2.7
Skate VDR	7.9 nM	6.5 – 9.6 nM	24.7
Bichir VDR	98.9 nM	71.4 – 137.1 nM	42.9
Human VDR	5.4 nM	4.3 – 6.7 nM	51.3

Figure 1. VDR transactivation in response to 1, $25D_3$. HepG2 cells were transiently transfected with full length pSG5-VDR, XREM-Luc, and *Renilla* as described previously in *Materials and Methods*. Cells were treated with either (**A**) 120 nM 1, 25_2D_3 or (**B**) 0 - 1200 nM 1, $25D_3$ in media for 24 hours. VDR response was measured via dual-luciferase assays. Data are represented as the mean fold activation normalized to the ethanol control ± SEM (n = 4). For (**A**), unpaired t-tests were run for each species to compare VDR transactivation to the empty vector control (*** = $p < 0.0001$ for skate, bichir and human, $p = 0.0003$ for

lamprey). For (**B**), the half-maximal effective concentration (EC_{50}), 95% confidence interval (95% CI), and maximum efficacy (E_{MAX}) values for each VDR was determined using nonlinear regression analysis using a sigmoidal dose-response calculation with variable slope in Prism 4. **(C)** is a table listing the EC_{50} concentrations, 95% confidence intervals (C.I.), and maximum efficacy (E_{MAX}) for each VDR.

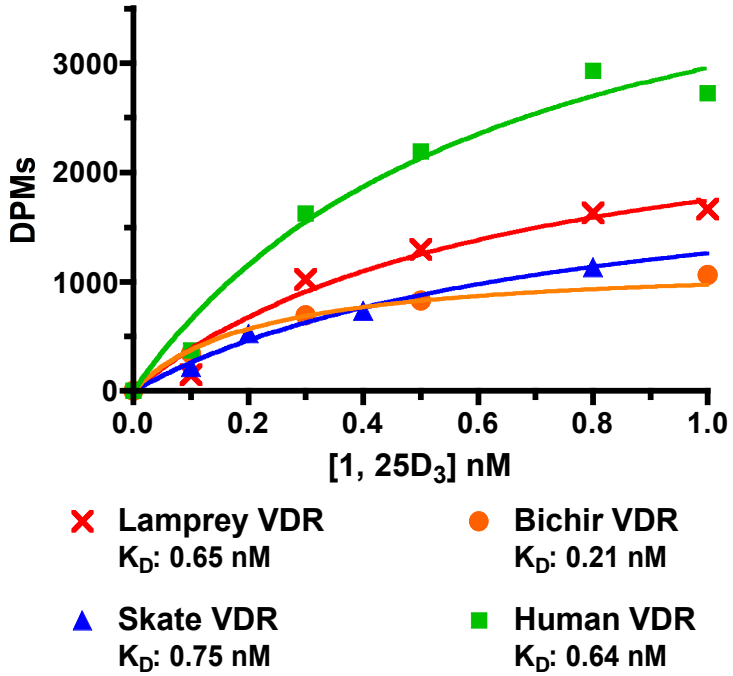

Figure 2. Saturation binding analysis of [^{3}H]-1, 25D$_3$ to lamprey VDR (*red X*), skate VDR (*blue triangle*), bichir VDR (*orange circle*), and human VDR (*green square*). Lysates were prepared from transfected Cos7 cells as described in *Materials and Methods*. Lysates were incubated with 0 – 1.6 nM [^{3}H]-1, 25$_2$D$_3$ for 18 hours at 4˚C. Unbound ligand was removed as described. Specific binding values were calculated by subtracting the average non-specific binding counts from the total binding counts. Hyperbolic one-site binding curves were fit using Prism 4. The reported dissociation constant (K_D) in the manuscript for each VDR is the average of three separate experiments ± SEM. Shown here are specific binding data from a representative experiment.

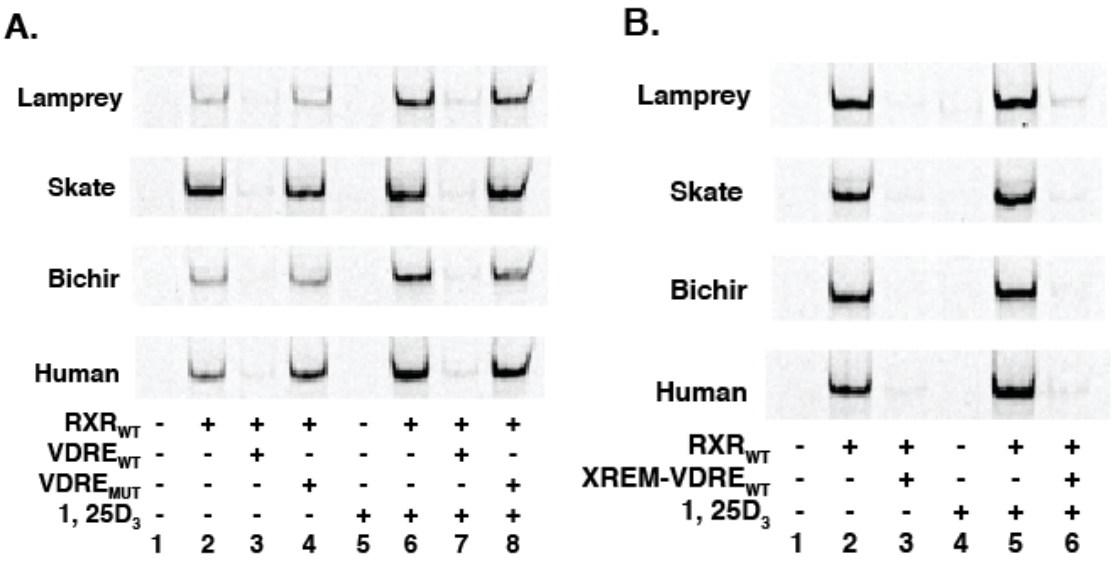

C. Canonical VDRE: AGGTCAxxxAGGTCA

D. Canonical VDR mutant: AG*AA*CAxxxAG*AA*CA

E. XREM VDRE: TGAACTxxxTGACCC

Figure 3. Electrophoretic mobility shift analysis of recombinant lamprey, skate, bichir, and human VDR binding to **(A)** the canonical VDRE, and **(B)** the VDRE from the XREM region of CYP3A4. **(C), (D),** and **(E)** depict DR3 binding site sequences within the canonical and XREM VDREs. **(A)** With the canonical VDRE, DNA binding complexes were only observed in the presence of RXR_{WT} (*lanes 2, 4, 6, 8 vs lanes 1, 3, 5, 7*). The addition of 100 nM 1, $25D_3$ (*lanes 5 – 8*) enhanced binding complex formation compared to the ethanol control (*lanes 1 – 4*). In competition assays, the addition of 100-fold molar excess of the unlabeled wild type competitor ($VDRE_{WT}$) successfully outcompeted binding to the labeled VDRE (*lanes 3 and 7 vs. lanes 2 and 6*). The use of the mutant competitor ($VDRE_{MUT}$) did not

inhibit complex formation with any VDR tested (*lanes 4 and 8 vs lanes 2 and 6*). **(B)** A similar pattern was observed with the XREM VDRE. Complex formation was only observed in the presence of recombinant RXR_{WT} (*lanes 1, 4 vs lanes 2, 5*). The addition of 100 nM 1, $25D_3$ significantly enhanced complex formation (*lane 2 vs lane 5*). In competition assays, the addition of 100-fold molar excess of the unlabeled XREM $VDRE_{WT}$ successfully outcompeted complex formation on the labeled XREM VDRE.

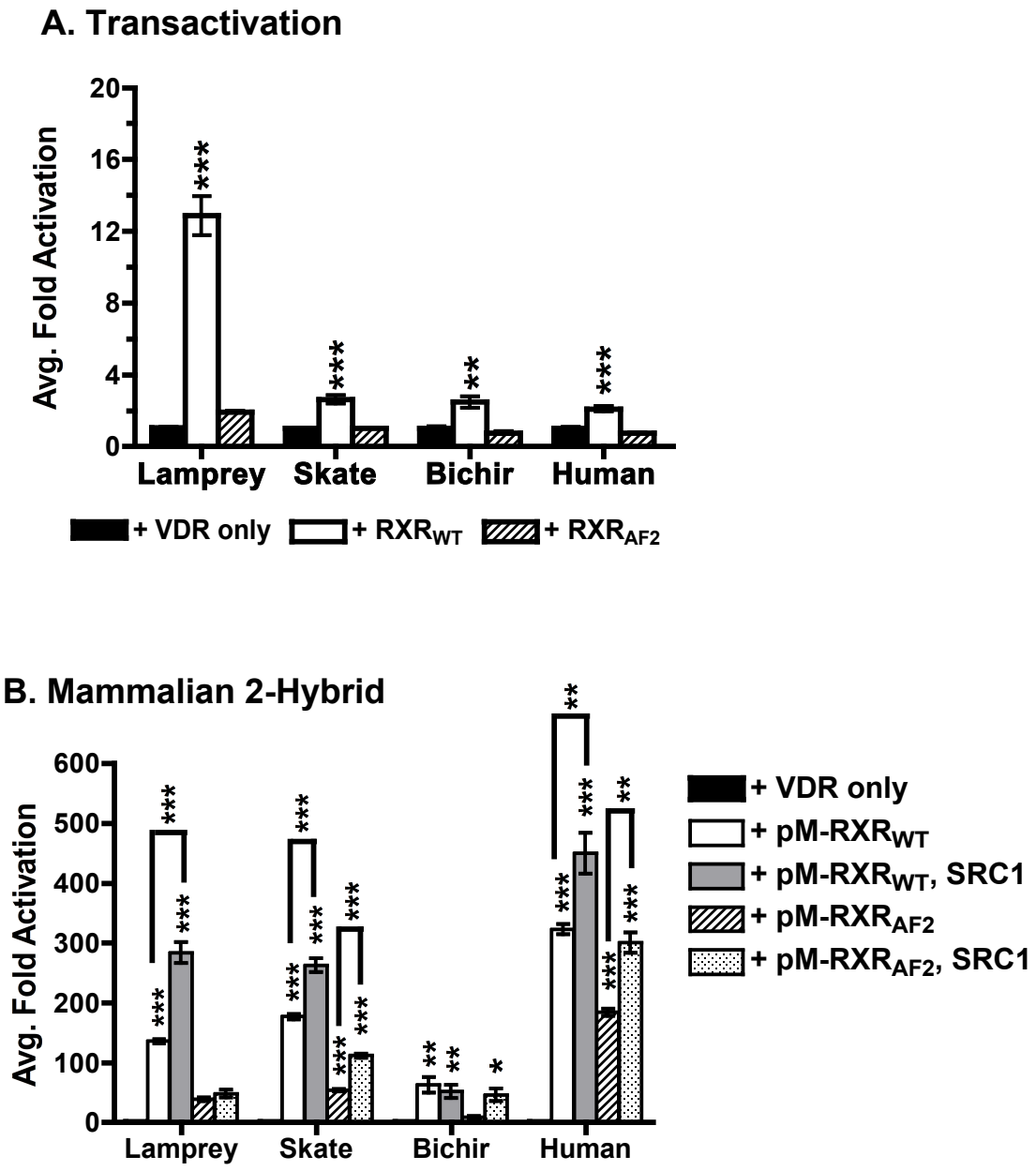

Figure 4. (A) Analysis of overexpressed RXR on VDR transactivation and **(B)** VDR-RXR heterodimerization in response to 1, 25D$_3$. **(A)** HepG2 cells were transiently transfected with pSG5-VDR, XREM-Luc, and *Renilla* as described previously in *Materials and Methods*.

Select assays were cotransfected with pCDNA-RXR_{WT} or pCDNA-RXR_{AF2} where indicated. Cells were treated with 120 nM 1, 25_2D_3 for 24 hours. VDR response was measured via dual-luciferase assays. Data are represented as the average fold activation normalized to VDR alone (no RXR) ± SEM (n=4). Asterisks represent a significant increase in transactivation compared to the VDR control: *** = $p < 0.001$, ** = $p < 0.01$, * = $p < 0.05$. **(B)** Mammalian two-hybrid assays were conducted to study VDR-RXR heterodimerization in response to 1, $25D_3$. HepG2 cells were transiently transfected with pVP16-VDR as prey and pM-RXR_{WT} or pM-RXR_{AF2} as bait, along with the Gal4 luciferase reporter 5XGal4-TATA-Luc and the *Renilla* internal luciferase control. Select experiments were also cotransfected with pSG5-SRC1 where indicated. Cells were exposed to 120 nM 1, $25D_3$ in media for 24 hours. Protein-protein interaction was measured via dual-luciferase assays as described in the Materials and Methods. Data are represented as the mean fold interaction ± SEM (n = 4). Data are normalized to VDR + empty pM vector (no RXR). Asterisks indicate significance: *** = $p < 0.001$, ** = $p < 0.01$, * = $p < 0.05$.

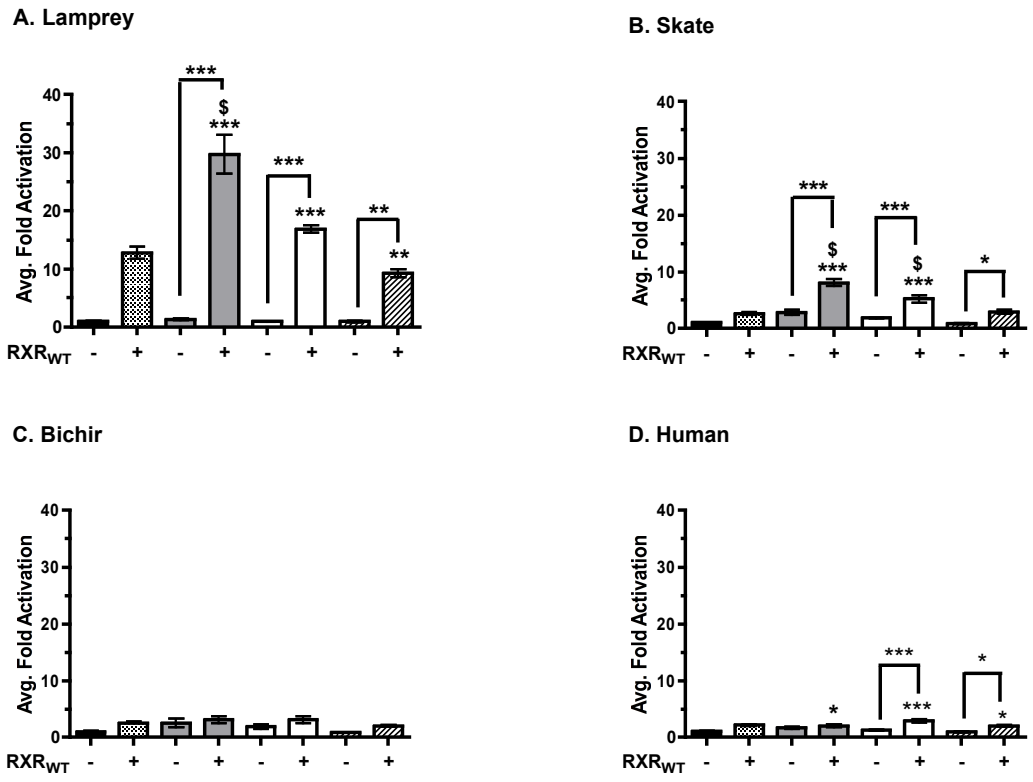

Figure 5. Influence of overexpressed SRC coactivators on VDR transactivation in response to 1, 25D_3 for **(A)** lamprey VDR, **(B)** skate VDR, **(C)** bichir VDR, and **(D)** human VDR. HepG2 cells were transiently transfected with pSG5-VDR, XREM-Luc, and *Renilla* as described previously in *Materials and Methods*. Select assays were cotransfected with pSG5-SRC-1 (*grey bars*), pSG5-GRIP1 (*white bars*), pSG5-ACTR (*striped bars*), or no coactivators (VDR only, *black bars*) where indicated. Assays were conducted both with and without pCDNA-RXR_{WT}, and a set of wells was additionally cotransfected with pCDNA-RXR_{WT} without SRC coactivators as a reference (*dotted bars*). Cells were treated with 120 nM 1, 25_2D_3 for 24 hours. VDR response was measured via dual-luciferase assays. Data are

represented as the average fold activation normalized to VDR alone ± SEM (n=4). Asterisks indicate significance: *** = $p < 0.001$, ** = $p < 0.01$, * = $p < 0.05$. A "$" sign above the bar indicates VDR+SRC+RXR_{WT} is significantly greater than VDR+RXR_{WT} ($p < 0.05$).

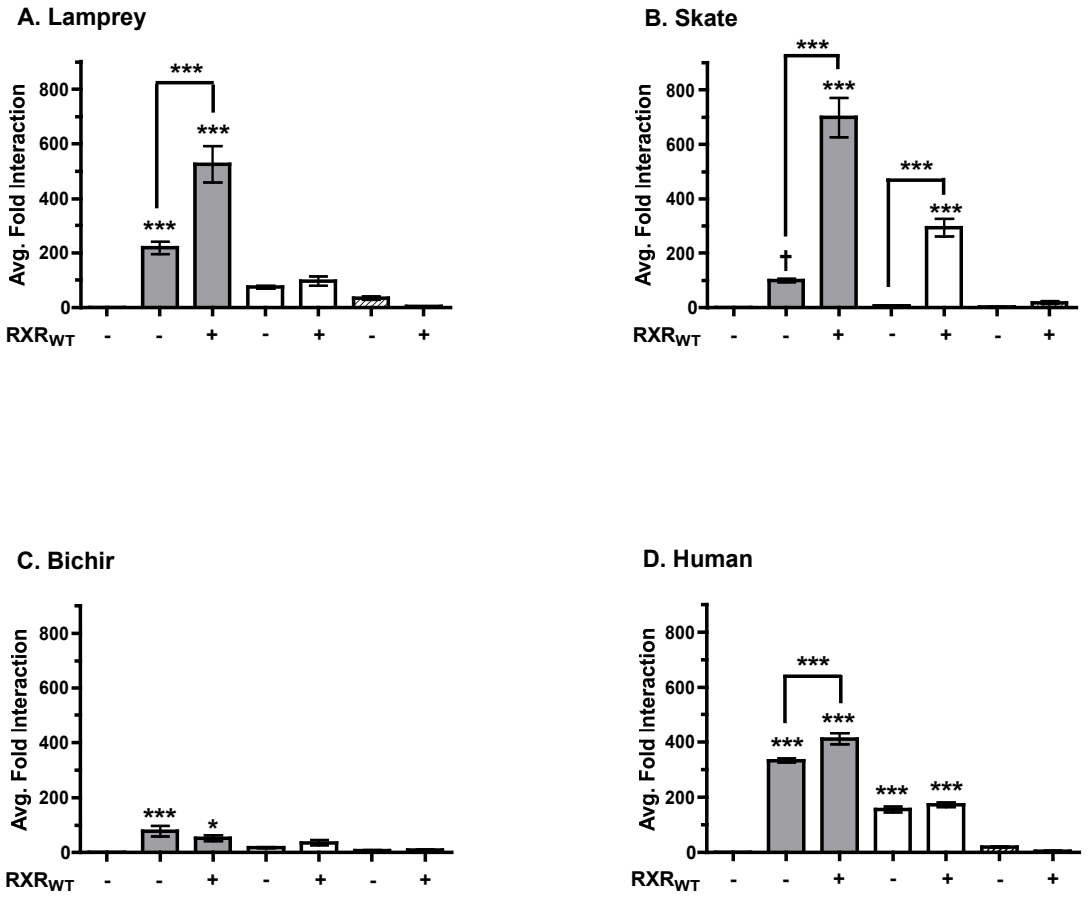

Figure 6. Mammalian 2-Hybrid analysis of VDR recruitment of SRC coactivators in response to 120 nM 1, 25D_3 for **(A)** lamprey VDR, **(B)** skate VDR, **(C)** bichir VDR, and **(D)** human VDR. Assays were conducted both in the presence and absence of pCDNA-RXR_{WT}. HepG2 cells were transiently transfected with pVP16-VDR as prey and pM-SRC-1 (*grey bars*), pM-GRIP1 (*white bars*), or pM-ACTR (*striped bars*) as bait, along with 5XGal4-TATA-Luc and *Renilla*. Cells were exposed to 120 nM 1, 25D_3 in media for 24 hours. Protein-protein interaction was measured via dual-luciferase assays as described in the *Materials and Methods*. Data are represented as the mean fold activation ± SEM (n = 4).

Data are normalized to VDR + empty pM vector (no coactivators). Asterisks above bars represent a significant interaction: *** = $p < 0.001$, ** = $p < 0.01$, * = $p < 0.05$. Asterisks above brackets indicate the addition of RXR_{WT} significantly enhanced VDR-SRC interaction.

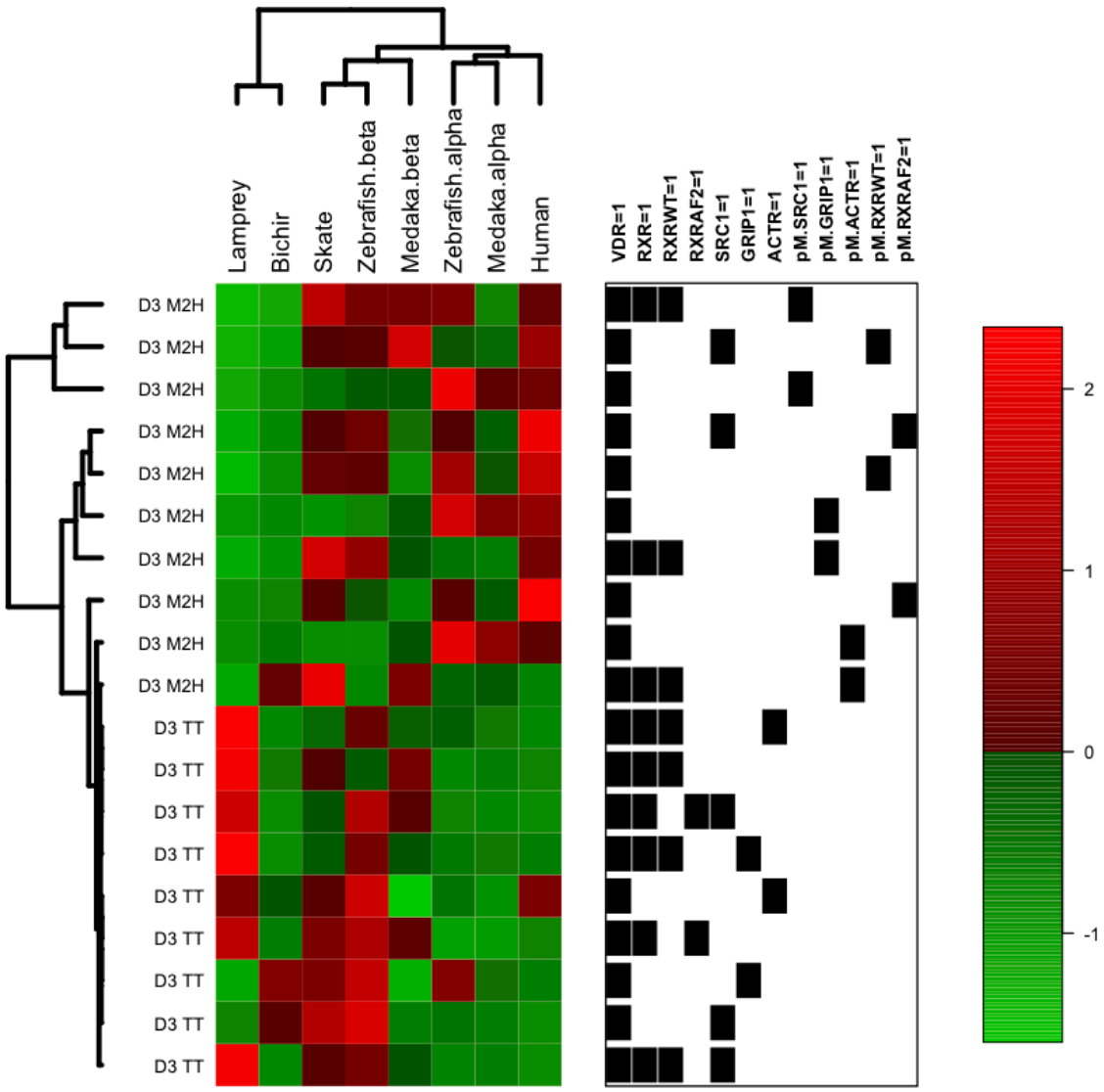

Figure 7. Hierarchical clustering transient transactivation (TT) and mammalian 2-hybrid (M2H) assays and eight VDR orthologs with Manhattan distance and complete linkage. Data for each assay (rows) was normalized across all eight VDR species (columns) to account for interspecies differences in absolute assay readout. The Pickett Plot to the right of the heatmap indicates the presence/absence of coregulators within each assay.

CHAPTER THREE

Evolution of Lithocholic Acid as a Functional Ligand for the Vitamin D Receptor in Non-Mammalian Vertebrates

Erin M. Kollitz[1], Guozhu Zhang[2], G. Kerr Whitfield[3], Mary Beth Hawkins[4], David Reif[5]

Seth W. Kullman[1]

[1] Environmental and Molecular Toxicology, Department of Biology, North Carolina State University, Raleigh, NC

[2] Bioinformatics Research Center, North Carolina State University

[3] Department of Basic Medical Sciences, The University of Arizona College of Medicine, Phoenix, AZ

[4] Department of Biology, North Carolina State University, Raleigh, NC

[5] Bioinformatics Research Center, Department of Biological Sciences, North Carolina State University

ABSTRACT

It has been speculated that the adoption of lithocholic acid (LCA) as a functional ligand for the vitamin D receptor (VDR) was an adaptation to facilitate the detoxification of the bile acid. However, the evolutionary history of this partnership is not well understood due to the lack of data from non-mammalian vertebrates. Here, using VDRs cloned from species representing key nodes in vertebrate evolution, and our previous work with 1, $25D_3$ as a comparison, we assess how the critical molecular functions of VDR have evolved over time in response to LCA. Competitive binding assays demonstrate that the VDR ligand affinities across species were comparable to that of human VDR. However, VDR transactivation in response to LCA was limited to select species. Subsequent assays were conducted to examine downstream events following ligand binding in order to characterize the functional evolution of the LCA-VDR partnership. We demonstrate that LCA and 3-keto LCA both function as full agonists only human VDR and the teleost VDRα paralogs. Interaction between the bile acids and VDRβ paralogs did not facilitate transactivation or RXR heterodimerization, and display attenuated coactivator recruitment. Similarly, VDR from basal vertebrates were not able to mediate any response to LCA or 3-keto LCA beyond ligand binding. Bioinformatics analysis suggests that functional differences between VDRs are driven though differential interactions between VDRs and essential coactivators. Taken together, our results suggest that the ability of LCA to function as a VDR ligand evolved before the bile acid itself, most likely though a process of exaptation followed by co-option once the need to detoxify LCA arose.

INTRODUCTION

Bile alcohols and bile acids (collectively referred to as bile salts) are water-soluble amphipathic end products of cholesterol metabolism that facilitate the digestion and absorption of lipids and lipid-soluble vitamins in vertebrates (1). Surveys of biliary bile salt composition revealed substantial structural variation between species. This variation is due to an evolutionary shift from C_{27} bile alcohols to C_{24} bile acids within vertebrate evolution (Fig. 1) (2,3). For example, the majority of basal vertebrates synthesize C_{27} bile alcohols, which are considered to be the most primitive bile salt (3). A transition to bile acids can be observed in basal ray-finned fish and some teleosts. The Senegal bichir (*Polypterus senegalus*) synthesizes both C_{27} bile alcohols and C_{24} bile acids, while the Japanese medaka (*Oryzias latipes*) synthesizes C_{27} and C_{24} bile acids (2). The C_{24} bile acids are the dominant bile salt in more derived teleosts such as the green-spotted pufferfish (*Tetraodon nigroviridis*). These bile acids are also the dominant bile salts in higher vertebrates such as birds and mammals.

Bile acids and alcohols are synthesized in liver and undergo enterohepatic circulation, where they are continually reabsorbed at the terminal end of the small intestine and returned to the liver for recirculation. The reabsorption process for bile acids is highly efficient, with over 95% of bile acids reabsorbed (1,4). Bile acids and alcohols that escape reabsorption enter the colon and excreted. However in higher vertebrates with a cecum (reptiles, birds, and mammals), these bile acids are subject to metabolism by anaerobic bacteria (Fig. 1) (5). These bacterially synthesized metabolites are termed secondary bile acids to differentiate them from their primary counterparts that are synthesized in hepatocytes. Bacterial

modification of bile acids is not believed to occur in lower vertebrates such as fish, as these animals lack the intestinal anatomy for the growth of the necessary anaerobes.

Lithocholic acid (LCA) is a toxic secondary bile acid formed by the bacterial 7-dehydroxylation of the primary C_{24} bile acid chenodeoxycholic acid (CDCA), which is found primarily in mammals, birds, as well as some species of teleost fish (2,3,5). LCA is a known carcinogen, inducing DNA damage through the production of reactive oxygen species and the formation of DNA adducts (6-8). LCA has also been implicated as a tumor promoter by inhibiting apoptosis and DNA repair enzymes (9,10). Additionally, increased LCA concentrations as a result of a high fat diet is associated with an increased risk of colon cancer in mammals (7). Fortunately, vertebrates have evolved detoxification mechanisms to protect against the harmful effects of LCA and LCA metabolites. This detoxification process is mediated through the action of several nuclear receptors (NRs) that modulate transcription of CYP3A4 and other detoxification genes that are associated with the metabolism and transport of LCA from the cell.

Three specific NRs have been identified as low affinity LCA "sensors" including the farnesoid X receptor (FXR, NR1H4) (11), the pregnane X receptor (PXR, NR1I2) (12), and the vitamin D receptor (VDR, NR1I1) (13). Of these three receptors, FXR and PXR display a high degree of cross-species variability in the ligand binding domains and are activated by a structurally diverse array of ligands including primary and secondary bile acids and alcohols. Studies of both FXR and PXR have found evidence of co-evolution between the increasingly complex bile salt synthesis pathways and the ligand binding domain structure of both receptors (11). For example, the ligand-binding pocket (LBP) within the LBD of zebrafish

and lamprey FXR is narrower compared to human, permitting the binding of the planar 5α-bile alcohols produced by these species. Comparatively, the LBP of human FXR and medaka FXRα2 is able to accommodate the more recent "bent" 5β-bile acid structure (11,14). The earliest PXRs that are found in bony fish have a narrow ligand selectively, and are only activated by the "ancestral" primary bile salts produced in these species. Conversely, mammalian PXRs have a larger ligand-binding pocket, and are activated by a diverse array of primary bile salts and other xenobiotic compounds (12).

In contrast, the vitamin D receptor (VDR) has been highly conserved throughout vertebrate evolution both in sequence identity and ligand specificity (see Appendix F) (12,15). However, LCA and its metabolites have recently been identified as VDR agonists in humans and rodents (13). In fact, LCA is a more potent VDR agonist in these species than it is for FXR or PXR (13). Unlike FXR and PXR, VDR does not demonstrate the large degree of sequence divergence and variation over the course of vertebrate evolution (12,16), and thus there is limited evidence for VDR coevolution with bile salts. Further evidence of VDR conservation is illustrated by crystal structures of both human and zebrafish VDRs bound to 1α, 25-dihydroxyvitamin D_3 (1, $25D_3$). These structures were nearly identical, with only minor differences noted within the loop regions (17). All of the ligand-protein contacts between 1, $25D_3$ and VDR have been conserved, and VDR ligand-binding pockets of zebrafish and human are identical in structure.

Recent studies have demonstrated that both LCA and 1, $25D_3$ occupy overlapping binding sites on VDR, but in opposite orientations, and even share select residue contacts within the LBD (18) (Table 1). This suggests that modifications to the VDR LBD to

accommodate LCA as a low-affinity ligand may have been minor, but currently there is no evidence of structural modifications in VDRs from higher vertebrates to enable the accommodation of additional ligands. Given that LCA is a byproduct of evolutionarily more recent bile acid synthesis pathways, it has been proposed that LCA was "adopted" as a VDR ligand in order to facilitate the detoxification of the bile acid (3,13,19,20). Under this model, the ability of LCA to act as a functional VDR ligand is hypothesized to be limited to higher vertebrates, as lower vertebrates lack a cecum, which is necessary for the growth of the anaerobic bacteria that metabolize LCA. In support of this theory, LCA has been demonstrated to activate mammalian VDRS in transient transactivation assays, but is unable to elicit a response from sea lamprey, zebrafish and *Xenopus* VDR (12,21).

In this study, we present evidence that the ligand-receptor partnership of LCA and VDR did not evolve through a process of adaptation and natural selection, but rather exaptation followed by co-option. We have previously characterized canonical NR functions of VDRs from species representing key nodes in vertebrate evolution in response to 1, $25D_3$. Functions include assessing receptor-ligand affinities, heterodimerization with RXR, DNA binding, coactivator recruitment, and transactivation in response to 1, $25D_3$ both in the presence and absence of coregulators. Here, using VDRs from this suite of species, and with our previous work with 1, $25D_3$ as a comparison, we assess how the critical molecular functions of VDR have evolved over time in response to LCA. Our results indicate that VDR has maintained its affinity for LCA since the origin of the receptor, despite the fact that LCA itself did not appear until millions of years later. We speculate that the consistent affinity of

the VDRs for LCA has been maintained as a result of selective pressures on a separate and unrelated trait.

MATERIALS AND METHODS

DNA constructs

All pSG5, pVP16, and pET32a – VDR constructs were obtained as previously described ((22), Chapter 1, Chapter 2). All RXR, SRC-1, GRIP1, and ACTR for transactivation and mammalian 2-hybrid studies were a gift from Dr. Donald McDonnell (Duke University, Durham, NC). All luciferase reporters were obtained as described previously ((22), Chapter 1, Chapter 2).

Competitive binding analysis

Radiolabeled 1α, 25-dihydroxyvitamin D_3 (1, 25-$(OH)_2$-26, 27 [^{3}H]dimethyl-vitamin D_3, referred to as [^{3}H]-1, 25D_3) was purchased from Perkin Elmer (Waltham, MA). Protease inhibitor cocktail was purchased from EMD Millipore (Billerica, MA). All cell culture media and other reagents were purchased from Mediatech (Manassas, VA). Cos7 cells (ATCC #CRL-1651) were maintained in complete DMEM medium supplemented with 10% FBS, and passaged every 4-5 days according to established protocols. Lysate for total binding analysis was obtained from Cos7 cells (3.0 x 10^6 cells/150 mm dish) transfected with 4 μg pSG5-VDR and 4 μg pSG5-RXR_{WT}, along with 16 μg pBSII as carrier DNA, as described previously using Lipofectamine 2000 (paper 1, paper 2). Lysate for non-specific binding was obtained from Cos7 cells transfected with 4 μg of the empty pSG5 vector, 4 μg pSG5-RXR_{WT}, and 16 μg pBSII. Hormone-free complete DMEM medium was replaced after twenty-four hours post-transfection. At forty-eight hours post-transfection, cells were harvested by trypsinization, centrifuged at 1,000 x g, and resuspended twice in 2 mL cold

Dulbecco's PBS. After the second wash, cells were resuspended in 1 mL KETZD + 5 buffer (0.15 M KCl, 1 mM EDTA, 10 mM Tris HCl, 0.3 mM $ZnCl_2$, 200x dilution protease inhibitor cocktail, 5 mM DTT, pH 7.6). Cells were lysed by sonication (12 1-second bursts at 25% power) and centrifuged at 100,000 *x g* for 30 minutes at 4˚C. The supernatant containing the lysate was divided into 300 μL aliquots and stored at -80˚C until needed. The pellet was discarded.

Total and non-specific binding was determined as follows: lysate was diluted 1/10 in cold KETZD+5 buffer. [^{3}H]-1,25D_3 (original specific activity 168 Ci/mmol) was diluted to 10 Ci/mmol with unlabeled 1 μM 1, 25D_3 to a final concentration of 4 nM. 10 μL [^{3}H]-1,25D_3 and 10 μL of 0 – 100 μM LCA in EtOH was added to each test tube, followed by 200 μL diluted lysate. Reactions were shaken to mix, and allowed to equilibrate overnight at 4˚C. Eighteen hours later unbound [^{3}H]-1,25D_3 was removed by incubation with 80 μL of a 0.5% dextran-2.5% charcoal solution in GP Buffer (0.15 M NaCl, 0.015 M NaN_3, 0.1 M anhydrous Na_2HPO_4, 0.039 M $NaH_2PO_4 \bullet H_2O$, 10% gelatin, pH 7.0) at 4˚C for 15 minutes, with shaking every 5 minutes. Samples were then centrifuged at 5,000 *x g* for 5 minutes at 4˚C, and 200 μL of supernantant was added to a scintillation vial along with 4 mL of scintillation cocktail (ScintiSafe, Fisher Scientific) for counting. All assays were repeated at least once, and duplicate tubes for each competitor concentration were run in each assay. Specific binding was determined by subtracting non-specific binding values from the total binding values. Data was analyzed using linear regression analysis with a once site binding calculation on GraphPad Prism 4 (Graphpad Software, San Diego, CA). The IC_{50} was determined from each competition curve. The receptor inhibition constant (K_i) was obtained using the calculated

IC_{50} and the previously calculated K_D (Chapter 1, Chapter 2) using the Cheng-Prusoff equation (23). The data is represented as the percent specific binding vs the log LCA concentration.

Electrophoretic mobility shift assays

Recombinant VDR and RXR proteins were expressed and purified as follows. pET32a-VDR protein expression constructs for each species and a pET32a-RXR_{WT} protein expression construct for human RXR_{WT} were transformed into the BL21(DE3)pLysS strain of *E.coli* (Genesee Scientific, San Diego, CA). Positive colonies were identified using a PCR screen and restriction digest. A starter culture consisting of 10 mL LB/amp inoculated with a single positive colony was grown overnight at 37˚C with shaking at 200 rpm. Overnight starter cultures were used to inoculate 250 mL of LB/amp and grown at 37˚C with shaking until OD_{600} = 0.6. Protein expression was induced by the addition of 1 mM IPTG and 20 μM $ZnCl_2$, and cultures were incubated at 25˚C for three hours with shaking at 200 rpm. Following incubation, cultures were centrifuged at 4,000 x g for 20 minutes at 4ºC. The supernatant was discarded, and the pellets were frozen at -20˚C overnight. The QIAexpress Ni-NTA Fast Start kit (QIAGEN, Valencia, CA) was used to lyse bacteria under native kit conditions and to purify 6xHis-tagged VDR and RXR proteins from the soluble fraction according to the manufacturer's instructions. Purified protein concentrations were determined using the average of three A280 measurements using a NanoDrop® ND-1000 spectrophotometer (Thermo Fisher Scientific, Waltham, MA). Proteins were visualized via Western Blot using antibodies to the 6xHis tags (QIAGEN, Valencia, CA).

Electrophoretic mobility shift assays (EMSAs) were carried out in a total volume of 20 μl containing 100 ng of recombinant VDR protein and 100 ng recombinant RXR where indicated. DNA–protein binding reactions were carried out using either a canonical VDRE (24) (5' – AGC TTC AGG TCA AGG AGG TCA GAG AGC – 3'), a mutant form of the canonical sequence (5' – AGC TTC AG*A A*CA AGG AG*A A*CA GAG AGC – 3'), or a VDRE found within the distal promoter region of the CYP3A4-XREM reporter used in transient transfection studies (5' – GCT GAA TGA ACT TGC TGA CCC TCT GCT – 3') (25). Single stranded Cy5-labeled and unlabeled oligos were purchased from Integrated DNA Technologies (Coralville, IA). Oligos were resuspended to a final concentration of 250 μM, and annealed by heating equal concentrations of the sense and antisense strands in annealing buffer (10 mM Tris, 50 mM NaCl, 1 mM EDTA). Annealing reactions were incubated at 95˚C for two minutes, and allowed to cool to room temperature. The annealed oligos were further diluted to a final concentration of 1 pmol/μL. For the DNA-binding reactions, receptors were incubated at 25˚ C in EMSA binding buffer (100 mM KCl, 10 mM HEPES, 1 mM EDTA, 1.0 mg/ml BSA, 4 μg/mL sonicated salmon sperm, 1.0 mM DTT, 1% glycerol, 20 mM $MgCl_2$) and 100 μM LCA or 100 μM LCA 3-Keto. 1, $25D_3$ was used as a positive control and ethanol was used as a vehicle control. After a 45-minute incubation, 1 pmol Cy5-labeled double-stranded oligo was added and the reaction was incubated for an additional 30 minutes. Competition experiments were performed in the presence of a 100-fold molar excess of unlabeled wild type or mutant oligos. Negative controls include affinity tags expressed and isolated from empty pET32a vector stocks, and reactions run in the absence of either dimer partner. Protein–DNA complexes were resolved on a 6% non-denaturing

acrylamide gel in ice-cold 0.5X TBE buffer (45 mM Tris base, 45 mM boric acid, 1 mM EDTA, pH 8.0) at 100 V for 90 minutes. Gels were visualized on a Storm 865 using the red fluorescence mode (GE Healthcare Life Sciences, Pittsburgh, PA). Densitometry was measured using ImageQuaint TL 7.0 (GE Healthcare Life Sciences, Pittsburgh, PA) for quantitative analysis.

VDR transient transactivation assays

The secondary bile acid lithocholic acid (LCA, 5β – cholanic acid-3α – ol) and the LCA metabolite, 3-keto lithocholic acid (3-Keto LCA, 5β – cholanic acid – 3 – one), were purchased from Steraloids, Inc (Newport, RI). 1α, 25-dihydroxyvitamin D_3 (1, $25D_3$) was purchased from EMD Millipore (Billerica, MA). Cell culture media and other necessary reagents were obtained from Mediatech (Manassas, VA). HepG2 cells (ATCC #HB-8065) were cultured in T75 flasks with vented caps (BD Biosciences, San Jose, CA) using Minimum Essential Medium (MEM) containing 10% heat-inactivated fetal bovine serum, 1 mM sodium pyruvate, and 1X MEM non-essential amino acids. Cells were maintained following standard protocols in a 37°C-5% CO_2 incubator and split when ~80-90% confluent (every 3-4 days).

To compare the transactivational activity of VDR from lamprey, skate, bichir, medaka and zebrafish VDRa and VDRb, and human VDR, we tested full-length pSG5-VDR constructs in transient transactivation assays with 100 μM LCA or 100 μM 3-Keto LCA as the primary ligand. Experiments were conducted using pSG5 expression vectors containing complete open reading frames of each VDR in the presence of a luciferase reporter construct

for human CYP3A4 (XREM-Luc) that contains two imperfect DR3/ER6 vitamin D response elements (VDREs) (25). HepG2 cells were seeded in 96-well plates with $2.5x10^4$ cells per well 24 hours prior to transfection. Cells were transfected at 90-95% confluency using Lipofectamine 2000 (Life Technologies, Grand Island, NY) with DNA diluted in Opti-MEM I Reduced Serum Medium as per the manufacture's recommendations. For functional comparisons, 89.7 ng of each pSG5-VDR construct was transiently transfected into HepG2 cells with 19.2 ng human XREM-Luc reporter and 4.5 ng of *Renilla* luciferase, which serves as an internal luciferase control (Promega Corporation, Madison, WI). Twenty-four hours post-transfection the medium was replaced with complete MEM containing either, 100 μM LCA or 3-Keto LCA in ethanol. Controls include 120 nM $1,25D_3$ as a positive control, and ethanol alone as a vehicle control. Twenty-four hours post-exposure cells were passively lysed and lysate tested for luciferase activity using the Dual-Glo Luciferase Assay System (Promega Corporation, Madison, WI) according to the manufacturer's protocols. Co-regulator studies included the addition of 18.3 ng human coregulators: pCDNA-RXR_{WT}, pCDNA-RXR_{AF2}, pSG5-SRC-1, pSG5-GRIP-1or pSG5-ACTR where indicated. Luciferase activities were measured using a Wallac MicroBet TriLuc Luminometer (Perkin Elmer Life Sciences, Waltham, MA). VDR response was first normalized the Renilla internal control, then normalized to the empty vector control. VDR + co-regulator response was normalized to VDR in the absence of co-regulators. All experiments were replicated at least twice, and all experiments were conducted as groups of 4 replicate wells. Significant VDR activation in the presence and absence of coregulators was determined using a one-way ANOVA followed by a Tukey's HSD post hoc test in Prism 4 (GraphPad Inc, San Diego, CA).

Protein interaction: mammalian 2-hybrid assays

To analyze protein-protein interactions between VDR and essential nuclear receptor coregulators, mammalian 2-hybrid assays were conducted with chimeric VDRs containing the herpes simplex VP16 activation domain fused to full-length VDRs as "prey" (pVP16-VDR). NR co-regulators were used as bait for each reaction and consisted of fusion proteins containing full-length wild type or the truncated RXR mutant (pM-RXR_{WT}, pM-RXR_{AF2}), or the defined NR box of each member of the SRC/p160 family fused to the yeast Gal4 DNA-binding domain (pM-$SRC1_{241-386}$, pM-$GRIP1_{479-767}$, or pM-$ACTR_{392-1005}$). Assays were conducted in HepG2 cells seeded into 96-well plates twenty-four hours pre-transfection as described above. Cells were transfected with 33.6 ng pVP16-VDR, 33.6 ng pM-coregulator, 126.6 ng 5XGal4-TATA-Luc reporter, 3 ng *Renilla*. Controls consisted of transfections containing empty pM, pVP16 or both empty pM and pVP16 vectors. Cells were treated with 100 μM LCA or 3-keto LCA twenty-four hours post-transfection. Positive controls were treated with 1, $25D_3$ and vehicle controls were treated with ethanol. Twenty-four hours post-dosing, Luciferase activity was measured using the Dual-Glo Luciferase Assay System described above. VDR response first was normalized to *Renilla,* and than normalized to the empty pVP16-VDR in the absence of bait constructs. Significant protein-protein interaction was determined using a one-way ANOVA followed by a Tukey's HSD post hoc test in Prism (GraphPad Inc, San Diego, CA).

Bioinformatic summary analysis.

In order to see these functional data in a global context, the mammalian 2-hybrid (M2H) and transient transactivation (TT) data for lamprey, bichir, skate, medaka (VDRα and VDRβ), zebrafish (VDRα and VDRβ), and human VDR were visualized as a heatmap using custom R code (26) as well as the R package Heatplus (27). The Pickett Plot to the right of the heatmap indicates the presence/absence of co-regulators within each assay. The data were then normalized for each assay (row) across all eight species to account for magnitudinal response differences. The resulting matrix was subjected to unsupervised, hierarchical clustering using Manhattan distance and complete linkage. Next, we performed bootstrap resampling over the assays according to presence/absence of each of the co-regulators to identify drivers of the overall cluster pattern as well as subclusters. For each of 10,000 bootstrap samples of assays, the accuracy was measured by counting the number of times the overall cluster pattern and species subclusters [Lamprey, Bichir, Skate, Medaka β and Zebrafish β] and [Medaka α, Zebrafish α, Human] were identical compared to the raw data. The lower the agreement with the original pattern, the higher the inferred importance of the assays to VDR functional similarity.

RESULTS

Competitive Binding Analysis

Competition binding assays were performed to determine if LCA functions as a ligand by assessing receptor binding across each species. As a control for these studies, we conducted competition assays with human VDR, which exhibits an average K_i of 6.3 μM. This result is consistent with prior studies examining LCA-VDR interaction (13). Further analysis with lamprey, skate, bichir, zebrafish VDRα and VDRβ, medaka VDRα and VDRβ demonstrate that LCA is capable of displacing radiolabeled [^{3}H]-1, 25D_3 from recombinant VDR protein in the presence of RXR_{WT} (Fig. 2). Inhibition constants (K_i) for each VDR examined was highly similar across species, ranging between 4 – 10 μM. No difference was observed in binding affinity between individual VDRs. Although lamprey and skate VDR exhibited the highest K_i values (9.5 μM and 8.0 μM respectively) these values were not statistically different from the others ($p > 0.05$).

DNA binding analysis

Electrophoretic mobility shift assays demonstrated that DNA binding with LCA-bound VDR demonstrated identical requirements for DNA binding as VDR bound to 1, 25D_3 (Chapter 1, Chapter 2) (Fig. 3). With each species examined, VDR binding was accessed with both the canonical VDRE containing a DR3 motif, and the VDRE found within the XREM region of CYP3A4 also containing a DR3 motif. Binding to either VDRE was only observed in the presence of supplemented RXR. Binding was not observed when VDR or RXR was used singularly (Fig. 3C, D), indicating the necessity for obligate VDR:RXR

heterodimerization and likely lack of functional VDR or RXR homodimers. Competition assays using wild-type unlabeled VDRE probes were effectively able to outcompete the VDR-RXR binding (Fig. 3: Canonical – lanes 2, 5, 8; XREM – lanes 2, 4, 6). Competition assays using an unlabeled mutant VDRE probe had no effect on VDR binding to the labeled canonical VDRE (Fig. 3: Canonical – lanes 3, 6, 9. No mutant probe for XREM).

While the DNA binding characteristics of the heterodimer were similar with LCA and 1, $25D_3$, LCA did not enhance DNA binding compared to the vehicle control (Fig. 3: Canonical - lanes 1 vs. 4; XREM - lanes 1 vs. 3). This is in contrast to 1, $25D_3$, which significantly enhances DNA binding with all VDRs on both response elements (Fig. 3: Canonical - lanes 1 vs. 7; XREM – lanes 1 vs. 5). The lack of LCA-enhanced DNA binding suggests that LCA is a less effective ligand compared to 1, $25D_3$.

VDR transactivation in response to LCA and 3-keto LCA

To determine if LCA and 3-keto LCA were able to induce transactivation of all VDRs tested, transient transactivation assays were conducted using full-length VDR constructs in cell-based reporter assays (Fig. 4). Of all VDRs tested, only human VDR demonstrated a significant transactivational response to both LCA and 3-keto LCA, increasing 3.5-fold and 5.4-fold, respectively. Of the non-mammalian VDRs, zebrafish VDRα demonstrated a 3.0-fold response to LCA, while skate VDR demonstrated a 3.2-fold response to 3-keto LCA. LCA and 3-keto LCA did not induce VDR transactivation in lamprey, bichir, zebrafish VDRβ, medaka VDRα and VDRβ. Of note, all of these VDRs were significantly activated by 1, $25D_3$ (Chapter 1, Chapter 2).

Coregulator interaction: RXR heterodimerization

RXR is the obligate heterodimer of VDR, and plays a critical role in VDR-mediated transcription. To determine the effect of RXR on VDR transactivation in the presence of LCA or 3-keto LCA, full-length wild type RXR (pCDNA-RXR_{WT}) or a truncated RXR mutant lacking the AF2 region (pCDNA-RXR_{AF2}) was cotransfected with VDR in transient transactivation studies. Co-transfection of RXR_{WT} with human VDR results in significant increase in VDR activation in response to both LCA and 3-keto LCA (Fig. 5A). With 3-keto LCA, the addition of RXR_{WT} produced a significant increase in VDR transactivation with both medaka and zebrafish VDRα compared to their respective VDRβ paralogs. With LCA, the addition of RXR_{WT} only significantly increased the medaka and zebrafish VDRα paralogs, but not the VDRβ paralogs. Of the basal vertebrates, skate VDR transactivation increased with RXR_{WT} and LCA, but not with 3-keto LCA. The presence of RXR_{WT} had no effect on lamprey and bichir VDR transactivation with either bile acid. The substitution of RXR_{WT} for RXR_{AF2} attenuated all VDR transactivation to background levels for each VDRs tested, emphasizing the necessity of the RXR AF2 region in VDR activation.

Our transactivation results with RXR_{WT} suggest that RXR overexpression has a positive effect on VDR-mediated transactivation, but these studies do not reveal if heterodimerization is occurring in response to LCA and 3-keto LCA. To determine if all VDRs bound to LCA or 3-keto LCA recruit and heterodimerize with RXR_{WT}, we next ran mammalian 2-hybrid assays. In these studies we only observed interaction between RXR_{WT} and human VDR, medaka VDRα, and zebrafish VDRα in response to both LCA and 3-keto LCA (Fig. 5B). By comparison, no VDR-RXR_{WT} protein-protein interaction was observed

with the medaka and zebrafish VDRβ paralogs, or any of the three basal vertebrates. The inability of these VDRs to form effective heterodimers with RXR may contribute to the low levels of transactivation. As a control, M2H experiments conducted with the pM-RXR_{AF2} mutant, and did not result in any significant protein-protein interactions. This result was expected given the lack of AF2 domain results in an unstable heterodimer incapable of transactivation even though the AF2 region is not directly involved in heterodimerization (28).

Coregulator interaction: SRC family of nuclear receptor coactivators

We next sought to determine the ability of LCA-bound VDR to recruit co-activator proteins. Our previous studies demonstrated that 1, $25D_3$ promoted the recruitment of members of the SRC family of nuclear receptor coactivators by VDR. Cells transfected with VDR and either SRC1, GRIP1, or ACTR were treated with either LCA or 3-keto LCA, both in the presence and absence of RXR_{WT}. Transactivation results were normalized to VDR response in the absence of coactivators. Human VDR was the only species that demonstrated a significant increase in transactivation with both SRC-1 and GRIP1 in the absence of RXR_{WT} (Fig. 6A, B). This increase was observed with both LCA and 3-keto LCA. The addition of RXR_{WT} only increased human VDR transactivation with GRIP1 and 3-keto LCA. With the 3R teleost VDR paralogs, transactivation reactions supplemented with both SRC-1 and RXR_{WT} resulted in differential transactivation between the VDRα and VDRβ paralogs of zebrafish with both LCA (Fig. 6A) and 3-keto LCA (Fig. 6B). Transactivation of zebrafish VDRα significantly increased with SRC-1 and RXR_{WT}, while the transactivation of VDRβ

did not increase above background. Transactivation of medaka VDRα also significantly increased with SRC-1 and RXR_{WT} with both bile acids, but VDRβ increased only with LCA and not 3-keto LCA. With the combination of GRIP1 and RXR_{WT}, a significant increase in transactivation was observed for both medaka VDRα and VDRβ with LCA, but only medaka VDRα for 3-keto LCA. Transactivation of zebrafish VDRα increased with the combination of GRIP1 and RXR_{WT} with both bile acids, however GRIP1 and RXR_{WT} did not have an effect on zebrafish VDRβ transactivation with either bile acid. Of the basal vertebrates, a significant increase in activity was only observed with skate VDR cotranfected with SRC1 and RXR_{WT} or GRIP1 and RXR_{WT} in the presence of LCA, but not 3-keto LCA. No increase in VDR transactivation was observed for lamprey and bichir with any of the SRC coactivators and either bile acid. While human appears to have a weaker response compared to the teleost VDRα paralogs, it should be noted that this data is normalized to VDR alone, and human VDR was highly activated by both LCA and 3-keto LCA compared to the teleosts in the absence of coregulators. With the exception of human and medaka VDRα, the cotransfection of RXR_{WT} with each coactivator was necessary to induce a significant increase in VDR transactivation with all coactivators.

As with RXR, we conducted mammalian 2-hybrid assays in HepG2 cells to assess the ability of the VDRs to recruit the SRC coactivator proteins in response to LCA and 3-keto LCA both in the presence and absence of RXR_{WT} (Fig. 7A, B). A significant interaction was observed with human VDR and SRC1 was observed with both 3-keto LCA and LCA. Cotransfection with RXR_{WT} was necessary for human VDR to interact with GRIP1 with both bile acids. In the presence of RXR_{WT}, both LCA and 3-keto LCA were able to induce a

strong interaction between SRC-1 and the four 3R teleost VDR paralogs and human. Both bile acids induced interaction between GRIP1 and human, medaka VDRα, and zebrafish VDRα in the presence of RXR_{WT}, but only LCA inducted VDR-GRIP1 interaction with the two VDRβ paralogs. 3-keto LCA induced interaction between zebrafish VDRβ and GRIP1, but not medaka VDRβ. For the basal vertebrates, a weak but significant interaction was observed with skate VDR and SRC-1 and LCA and RXR_{WT}, (16-fold) but not 3-keto LCA. Neither bile acid was able to induce significant interaction with lamprey and bichir VDR and any SRC coactivator. No interaction was observed between ACTR and VDR for any species tested with either bile acid.

Bioinformatics summary analysis

Figure 8 provides a global, multispecies context for VDR functional assays. The data resulted in two empirical clusters of *C1* = [lamprey, bichir, skate, medaka β and zebrafish β] and *C2* = [zebrafish α, medaka α, and human]. These clusters were defined by responses across the entire assay set (rows), as annotated by the presence/absence of coregulators (indicated by presence or absence of black boxes in the Pickett Plot to the right of the heatmap in Fig. 8). The first cluster (*C1*) contained a tight subcluster of lamprey, bichir, and skate VDR, defined by low activity across the majority of assays. The zebrafish and medaka VDRα and VDRβ variants segregated with each other (VDRβ in *C1*, and VDRα in *C2*), rather than by species. Human VDR clustered with the VDRα variants.

The bootstrap permutation results showed *C1* to be considerably more stable than *C2*, with greater than 99% recapitulation rate across all assay permutations. For *C2*, this analysis

highlighted the importance of co-regulators in driving the observed cluster pattern, especially RXR and SRC1. Beyond specific cofactors, these results suggest that the functional-assay based clustering of the two alpha variants with human in *C2* depends on responses across two-hybrid 3-keto LCA assays.

DISCUSSION

In this study we present evidence suggesting that the ligand-receptor partnership between LCA and VDR may not have evolved through a process of adaptation and natural selection, but rather exaptation followed by co-option. We have previously characterized canonical NR functions of VDR activation by 1, $25D_3$ from vertebrates that represent key nodes in evolution (Chapter 1, Chapter 2). Functions include assessing receptor-ligand affinities, heterodimerization with RXR, receptor binding to well defined DNA response elements, coactivator recruitment, and transactivation in response to 1, $25D_3$ both in the presence and absence of coregulators. Here, using the same VDRs and using our previous work with 1, $25D_3$ as a comparison, we assessed how critical molecular functions of VDR have evolved over time in response to LCA as an agonist.

The VDR-LCA partnership has been previously speculated to be a recent innovation that evolved in higher vertebrates as an adaptive response to the need to detoxify LCA (3,13,15,20). Subsequent transient transactivation studies demonstrated that LCA-induced transactivation is limited to mammalian VDRs, as no observable response was detected with VDRs from lower vertebrates such as lamprey and zebrafish (21). Based on these studies and the fact that basal vertebrates do not synthesize the parent compound of LCA, we hypothesized that LCA would not function as a VDR ligand in the majority of the species examined in this study. However, contrary to our hypothesis we observed that LCA was capable of competitively displacing the biologically active form of vitamin D with each VDR tested. Binding affinities for 3R teleosts as well as basal vertebrates were all comparable to that observed with human VDR, the only species tested that produces endogenous LCA.

These initial results support the notion that ancestral VDR exhibits an affinity for LCA that is equal to human, despite the fact that VDR evolved millions of years before the bile acid (3,29). In other words, our results suggest that the receptor's affinity for LCA is more ancient then LCA itself. However, while all VDRs across evolution maintain the ability to activate gene expression in response to 1, $25D_3$, the ability to respond to LCA as an agonist likely did not evolve until later in time. We speculate that the consistent affinity for LCA evolved through exaptation, possibly as a by-product of selection on a different trait such as affinity for 1, $25D_3$. It is possible that the receptor's affinity for LCA may be a by-product of selection for 1, $25D_3$, as LCA and 1, $25D_3$ utilize the same ligand binding pocket and similar ligand-protein contact residues. Of note, our previous studies have demonstrated that VDR maintains a consistent affinity for 1, $25D_3$ across evolution (Chapter 1, Chapter 2).

However, ligand affinities only describe ligand-receptor interaction. They do not describe structural changes induced by ligand binding, and the subsequent downstream steps in transactivation. This is illustrated by the transient transactivation results in this study: in the absence of overexpressed coregulators, significant VDR transactivation was only observed with human VDR and zebrafish VDRα in response to LCA, despite the fact that all VDRs maintained equal affinity for the bile acid. Thus our subsequent assays were conducted in order to characterize the functional evolution of the LCA-VDR partnership by examining downstream events subsequent to ligand binding.

We next examined the ability of VDR to heterodimerize with the retinoid X receptor (RXR) in the presence of LCA and the 3-keto LCA metabolite of LCA. RXR is a member of the NR2B subfamily of nuclear receptors and is the obligate heterodimer partner of VDR

(28,30). The conformation change induced by ligand binding repositions Helix 9 (H9) and Helix 10 (H10) of VDR for high affinity interaction with the identical helices in RXR (31). Heterodimerization plays a multifunctional role in VDR transactivation, including coactivator recruitment, increasing DNA binding affinity and specificity, and enhancement of transactivational efficacy. The c-terminal AF2 region of RXR is essential for coactivator recruitment, as the loss of the AF2 abolishes VDR-mediated transactivation (28,32). In our previous studies we reported that VDR binding with 1, $25D_3$ both enhanced VDR transactivation and induced heterodimerization for 3R teleost as well as basal vertebrate VDRs (Chapter 1, Chapter 2). By comparison, in this study we demonstrate that LCA and 3-keto LCA only facilitate heterodimerization with human VDR and the VDRα paralogs of the 3R teleosts medaka and zebrafish. This observation is in contrast to the fact that RXR heterodimerization is not detected with the basal vertebrates and VDRβ paralogs, despite the fact that cotransfection with RXR_{WT} in the transactivation assays resulted in a significant increase in transactivation for the VDRβ paralogs and skate VDR with both bile acids. We do not believe the observed lack of heterodimerization is a result of an incompatibility with human RXR, as all VDRs examined in this study previously exhibit successful heterodimerization with human RXR in the presence of 1, $25D_3$ as the primary ligand (Chapter 1, Chapter 2). As RXR heterodimerization is an essential step in VDR activation, the lack of heterodimerization may explain the lack of transactivation in these species.

In contrast to our mammalian two hybrid studies, EMSA data for basal, 3R teleost and human VDRs demonstrated RXR-VDR interactions for all species tested, and are required to facilitate binding to canonical and non-canonical VDREs. In the absence of RXR

protein we do not observed VDR-DNA binding even with the addition of LCA. We also demonstrate that the presence of LCA did not significantly enhance DNA binding over the vehicle control with any VDR tested. This is in contrast to previous data with 1, $25D_3$ where basal and 3R teleost VDRs exhibit a significant increase in DNA binding to both canonical and non-canonical VDREs (Chapter 1, Chapter 2). While mammalian 2-hybrid and EMSA data are seemingly contradictory, previous studies have demonstrated that the use of high concentrations of recombinant VDR and RXR protein in EMSA studies results in ligand independent heterodimerization and weak background binding with VDREs (30).

In addition to heterodimerization, we also investigated the impact of overexpressed SRC coactivators on VDR transactivation, and the ability of the VDRs to recruit coactivators in response to LCA and 3-keto LCA. Overall, the human and the VDRα paralogs of medaka and zebrafish exhibited the greatest enhancement in transactivation with cotransfected SRC-1 and GRIP1 with RXR_{WT} compared to their respective VDRβ paralogs. This enhancement was particularly evident with 3-keto LCA as the primary ligand. Mammalian 2-hybrid assays additionally confirmed a direct interaction between VDRα and VDRβ paralogs and SRC coactivators in response to both bile acids, although these interactions were dependent upon coexpression of RXR. In contrast, the more ancient VDRs of the basal vertebrates did not exhibit significant enhancement in transactivation with cotransfected SRC members and were unable to directly recruit any of the coactivators in the presence of either bile acid, with the exception of skate VDR and LCA as a ligand. It appears that transactivational response and ability of this set of VDRs to recruit SRC co-regulators may be ligand specific. This notion is supported by our previous work with 1, $25D_3$ where we observed enhanced transactivation

and direct VDR-coregulator interactions with both 3R teleost and basal vertebrate VDRs. Additionally we previously demonstrated that 1, $25D_3$ exhibited the greatest transactivational effect with SRC-1 and VDRβ paralogs. Comparatively, with bile salts used in this study SRC-1 exhibited the greatest effect with the VDRα paralogs, not VDRβ. Ligand-specific protein recruitment has previously been demonstrated with human VDR (33). Specifically significant differences were observed with RXR heterodimerization, recruitment of SCR-1 and VDR interaction with NCoA-62 or TRIP1/SUG1 between 1, $25D_3$ and LCA as ligands. These combined data suggest putative differences in ligand-VDR coregulator associations. Further supporting this theory are recently determined crystal structures for mammalian VDR bound to LCA. These structures have revealed clues regarding differential ligand affinities, heterodimerization, and coactivator recruitment between the two ligands (18). Specifically, it appears that LCA is less able to stabilize H12 and the AF2 region for optimal interaction with the SRC coactivators compared to 1, $25D_3$. The decreased ability of LCA to stabilize H12 may be what is driving the attenuated VDR-SRC interaction we observe in this study.

The role of RXR and the SRC family as important drivers of LCA response is further supported by a bioinformatics that clusters species according to functional similarities. The three basal vertebrates, the three species that were unable to respond to either bile acid, form a subcluster in C1. This cluster additionally includes both VDRβ paralogs, although they form a separate subcluster from the basal vertebrates due to their ability to interact with coregulators. However, the VDRα paralogs cluster with human VDR in a completely separate cluster from the VDRβ paralogs and basal VDRs. This is likely due to the fact that the VDRα paralogs were able to heterodimerize with RXR and recruit coregulators similar to

human VDR. The bioinformatics analysis suggests that coactivator interaction had a major role in the evolution of LCA as a functional VDR ligand. Although VDR has maintained a consistent affinity for LCA, the ability of VDR to interact with coregulators in order to mediate a functional response did not evolve until later in time. Further supporting this notion is the observation that species clustering is similar to phylogeny. Of note, the bile acid pathway that synthesizes the parent compound of LCA first appeared in early Actinopterygians and Sarcopterygians, which is where a functional response to LCA is first observed.

Taken together, our results indicate that the affinity of VDR for LCA evolved prior to the bile acid itself. Basal vertebrates bind LCA with equal affinity to human, even though these species diverged before the evolution of the C24 bile acid pathway, and both utilize evolutionarily simpler bile alcohols. Thus we are presented with a bit of a puzzle: if the ligand did not exist, how did VDR maintain an affinity for it maintained over millions of years?

We hypothesize that the evolution of the VDR-LCA partnership evolved through a process of exaptation, rather then adaptation. Adaptation is defined as a trait that has been shaped by natural selection for its current use. On the other hand, exaptation defines a trait whose current function was not created by natural selection (34). This trait may have previously been shaped by natural selection for its ancestral function, but was later co-opted for its current role. Alternatively, the trait may be a non-adaptive "accident" of selection on another, unrelated trait, and this fortuitous effect was later co-opted for the function it currently serves (34). Evolution by exaptation has been previously demonstrated in NRs. The

glucocorticoid receptor (GR) and mineralocorticoid receptor (MR) both descended from an ancestral gene that was duplicated in the 2R event, and currently maintain distinct signaling functions (35). GR is activated by cortisol, while MR is activated by aldosterone, a hormone that is specific to tetrapods. To date, aldosterone has not been identified in lower vertebrates such as jawless fish, sharks, and teleosts. However, functional assays using basal MRs and an ancestral MR/GR created through gene resurrection, found that these MRs were activated by aldosterone, despite the fact that the hormone is only present in higher vertebrates (36). The authors argue that the ability to bind aldosterone is an exaptive trait that was later co-opted by tetrapods once they evolved the ability to synthesize aldosterone.

Given that VDR is under strong selective pressures to be conserved, and both $1,25D_3$ and LCA utilize identical ligand binding pockets and share amino acid residues, it is conceivable that selection for $1,25D_3$ as a high affinity ligand may have influenced the consist affinity of VDR for LCA. VDR is highly expressed in the large intestine in many species (22,37-39), and the VDR signaling pathway, including target detoxification genes, was well established early in VDR evolution (29). Thus it appears that the inherent affinity of VDR for LCA and the already established VDR signaling pathway may have been co-opted by vertebrates as a means to detoxify LCA. Unlike other NRs that have evolved in a similar fashion (36), VDR has maintained it's ancestral relationship with vitamin D, and thus serves a dual purpose as a high affinity endocrine receptor and a low affinity detoxification sensor.

REFERENCES

1. Hofmann AF, Hagey LR. Bile acids: Chemistry, pathochemistry, biology, pathobiology, and therapeutics. *Cell Mol Life Sci.* 2008;65(16):2461-2483.

2. Hagey LR, Moller PR, Hofmann AF, Krasowski MD. Diversity of Bile Salts in Fish and Amphibians: Evolution of a Complex Biochemical Pathway. *Physiol Biochem Zool.* 2010;83(2):308-321.

3. Hofmann AF, Hagey LR, Krasowski MD. Bile salts of vertebrates: structural variation and possible evolutionary significance. *J Lipid Res.* 2010;51(2):226-246.

4. Mukhopadhyay S, Maitra U. Chemistry and biology of bile acids. *Curr Sci India.* 2004;87(12):1666-1683.

5. Hofmann AF. Detoxification of lithocholic acid, a toxic bile acid: relevance to drug hepatotoxicity. *Drug Metab Rev.* 2004;36(3-4):703-722.

6. Hamada K, Umemoto A, Kajikawa A, Seraj MJ, Monden Y. In vitro formation of DNA adducts with bile acids. *Carcinogenesis.* 1994;15(9):1911-1915.

7. Nagengast FM, Grubben MJ, van Munster IP. Role of bile acids in colorectal carcinogenesis. *Eur J Cancer.* 1995;31A(7-8):1067-1070.

8. Bernstein H, Bernstein C, Payne CM, Dvorakova K, Garewal H. Bile acids as carcinogens in human gastrointestinal cancers. *Mutat Res-Rev Mutat.* 2005;589(1):47-65.

9. Kozoni V, Tsioulias G, Shiff S, Rigas B. The effect of lithocholic acid on proliferation and apoptosis during the early stages of colon carcinogenesis: differential effect on apoptosis in the presence of a colon carcinogen. *Carcinogenesis.* 2000;21(5):999-1005.

10. Ogawa A, Murate T, Suzuki M, Nimura Y, Yoshida S. Lithocholic acid, a putative tumor promoter, inhibits mammalian DNA polymerase beta. *Jpn J Cancer Res.* 1998;89(11):1154-1159.

11. Reschly EJ, Ai N, Ekins S, Welsh WJ, Hagey LR, Hofmann AF, Krasowski MD. Evolution of the bile salt nuclear receptor FXR in vertebrates. *Journal of lipid research.* 2008;49(7):1577-1587.

12. Krasowski MD, Yasuda K, Hagey LR, Schuetz EG. Evolution of the pregnane x receptor: adaptation to cross-species differences in biliary bile salts. *Molecular endocrinology.* 2005;19(7):1720-1739.

13. Makishima M, Lu T, Xie W, Whitfield G, Domoto H, Evans R, Haussler M, Mangelsdorf D. Vitamin D receptor as an intestinal bile acid sensor. *Science.* 2002;296(5571):1313-1316.

14. Howarth DL, Hagey LR, Law SH, Ai N, Krasowski MD, Ekins S, Moore JT, Kollitz EM, Hinton DE, Kullman SW. Two farnesoid X receptor alpha isoforms in Japanese medaka (Oryzias latipes) are differentially activated in vitro. *Aquat Toxicol.* 2010;98(3):245-255.

15. Reschly EJ, Krasowski MD. Evolution and function of the NR1I nuclear hormone receptor subfamily (VDR, PXR, and CAR) with respect to metabolism of xenobiotics and endogenous compounds. *Curr Drug Metab.* 2006;7(4):349-365.

16. Krasowski MD, Ai N, Hagey LR, Kollitz EM, Kullman SW, Reschly EJ, Ekins S. The evolution of farnesoid X, vitamin D, and pregnane X receptors: insights from the green-spotted pufferfish (Tetraodon nigriviridis) and other non-mammalian species. *BMC Biochem.* 2011;12:5.

17. Ciesielski F, Rochel N, Mitschler A, Kouzmenko A, Moras D. Structural investigation of the ligand binding domain of the zebrafish VDR in complexes with 1 alpha,25(OH)(2)D-3 and Gemini: purification, crystallization and preliminary X-ray diffraction analysis. *J Steroid Biochem.* 2004;89-90(1-5):55-59.

18. Masuno H, Ikura T, Morizono D, Orita I, Yamada S, Shimizu M, Ito N. Crystal structures of complexes of vitamin D receptor ligand-binding domain with lithocholic acid derivatives. *Journal of lipid research.* 2013;54(8):2206-2213.

19. Krasowski MD, Ni A, Hagey LR, Ekins S. Evolution of promiscuous nuclear hormone receptors: LXR, FXR, VDR, PXR, and CAR. *Molecular and cellular endocrinology.* 2010.

20. Krasowski MD, Yasuda K, Hagey LR, Schuetz EG. Evolutionary selection across the nuclear hormone receptor superfamily with a focus on the NR1I subfamily (vitamin D, pregnane X, and constitutive androstane receptors). *Nucl Recept.* 2005;3:2.

21. Reschly EJ, Bainy ACD, Mattos JJ, Hagey LR, Bahary N, Mada SR, Ou J, Venkataramanan R, Krasowski MD. Functional evolution of the vitamin D and pregnane X receptors. *BMC Evol Biol.* 2007;7:222.

22. Howarth DL, Law SHW, Barnes B, Hall JM, Hinton DE, Moore L, Maglich JM, Moore JT, Kullman SW. Paralogous vitamin D receptors in teleosts: Transition of nuclear receptor function. *Endocrinology.* 2008;149(5):2411-2422.

23. Motulsky H, Christopoulos A. *Fitting Models to Biological Data using Linear and Nonlinear Regression.* San Diego, CA: GraphPad Software, Inc; 2005.

24. Shaffer P, Gewirth D. Vitamin D receptor-DNA interactions. *Vitam Horm.* 2004;68:257-273.

25. Drocourt L, Pascussi J, Assenat E, Fabre J, Maurel P, Vilarem M. Calcium channel modulators of the dihydropyridine family are human pregnane X receptor activators and inducers of CYP3A, CYP2B, and CYP2C in human hepatocytes. *Drug Metab Dispos.* 2001;29(10):1325-1331.

26. RCoreTeam. *R: A Language and Environment for Statistical Computing.* Vienna, Austria: R Foundation for Statistical Computing; 2013.

27. Ploner A. Heatplus: Heatmaps with Row and/or Column Covariates and Colored Clusters. *R package version 260.* 2012.

28. Thompson PD, Remus LS, Hsieh JC, Jurutka PW, Whitfield GK, Galligan MA, Encinas Dominguez C, Haussler CA, Haussler MR. Distinct retinoid X receptor activation function-2 residues mediate transactivation in homodimeric and vitamin D

receptor heterodimeric contexts. *Journal of molecular endocrinology.* 2001;27(2):211-227.

29. Whitfield G, Dang H, Schluter S, Bernstein R, Bunag T, Manzon L, Hsieh G, Dominguez C, Youson J, Haussler M, Marchalonis J. Cloning of a functional vitamin D receptor from the lamprey (Petromyzon marinus), an ancient vertebrate lacking a calcified skeleton and teeth. *Endocrinology.* 2003;144(6):2704-2716.

30. Thompson PD, Jurutka PW, Haussler CA, Whitfield GK, Haussler MR. Heterodimeric DNA binding by the vitamin D receptor and retinoid X receptors is enhanced by 1,25-dihydroxyvitamin D3 and inhibited by 9-cis-retinoic acid. Evidence for allosteric receptor interactions. *The Journal of biological chemistry.* 1998;273(14):8483-8491.

31. Zhang J, Chalmers MJ, Stayrook KR, Burris LL, Wang Y, Busby SA, Pascal BD, Garcia-Ordonez RD, Bruning JB, Istrate MA, Kojetin DJ, Dodge JA, Burris TP, Griffin PR. DNA binding alters coactivator interaction surfaces of the intact VDR-RXR complex. *Nat Struct Mol Biol.* 2011;18(5):556-563.

32. Bettoun D, Burris T, Houck K, Buck D, Stayrook K, Khalifa B, Lu J, Chin W, Nagpal S. Retinoid X receptor is a nonsilent major contributor to vitamin D receptor-mediated transcriptional activation. *Mol Endocrinol.* 2003;17(11):2320-2328.

33. Jurutka PW, Thompson PD, Whitfield GK, Eichhorst KR, Hall N, Dominguez CE, Hsieh J-C, Haussler CA, Haussler MR. Molecular and functional comparison of 1,25-dihydroxyvitamin D(3) and the novel vitamin D receptor ligand, lithocholic acid, in activating transcription of cytochrome P450 3A4. *J Cell Biochem.* 2005;94(5):917-943.

34. Gould SJ, Vrba ES. Exaptation - a Missing Term in the Science of Form. *Paleobiology.* 1982;8(1):4-15.

35. Thornton JW. Evolution of vertebrate steroid receptors from an ancestral estrogen receptor by ligand exploitation and serial genome expansions. *Proceedings of the National Academy of Sciences of the United States of America.* 2001;98(10):5671-5676.

36. Bridgham JT, Carroll SM, Thornton JW. Evolution of hormone-receptor complexity by molecular exploitation. *Science.* 2006;312(5770):97-101.

37. Craig TA, Sommer S, Sussman CR, Grande JP, Kumar R. Expression and regulation of the vitamin D receptor in the zebrafish, Danio rerio. *J Bone Miner Res.* 2008;23(9):1486-1496.

38. Burmester JK, Wiese RJ, Maeda N, DeLuca HF. Structure and regulation of the rat 1,25-dihydroxyvitamin D3 receptor. *Proceedings of the National Academy of Sciences of the United States of America.* 1988;85(24):9499-9502.

39. Meyer J, Fullmer CS, Wasserman RH, Komm BS, Haussler MR. Dietary restriction of calcium, phosphorus, and vitamin D elicits differential regulation of the mRNAs for avian intestinal calbindin-D28k and the 1,25-dihydroxyvitamin D3 receptor. *Journal of bone and mineral research : the official journal of the American Society for Bone and Mineral Research.* 1992;7(4):441-448.

TABLES

Table 1. Residues within the LBD of human VDR that directly contact 1, $25D_3$ and/or LCA. Shared residues that contact both ligands are highlighted in yellow.

Residue	1, $25D_3$	LCA
Tyr 143	√	√
Leu 230		√
Leu 233	√	√
Val 234	√	√
Ser 237	√	√
Ile 268	√	√
Ile 271		√
Met 272		√
Arg 274	√	√
Ser 275	√	
Ser 278	√	√
Trp 286	√	√
Val 300		√
Ala 303		√
His 305	√	
Leu 309		√
Ile 310		√
Leu 313		√
His 397	√	√
Tyr 401	√	
Val 418	√	
Phe 422	√	

FIGURES

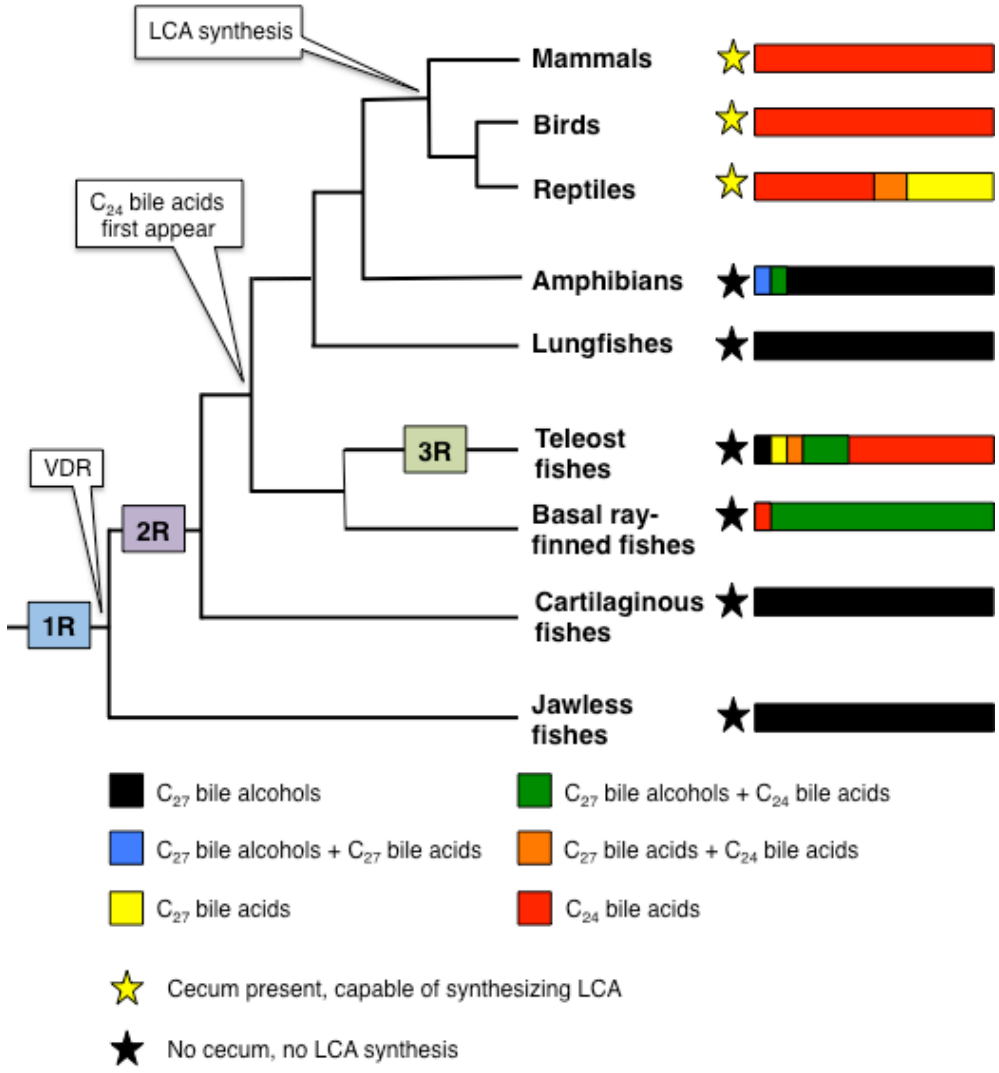

Figure 1. Bile salt profiles and vertebrate phylogeny. The colored bars on the right indicate the types of bile salts synthesized. The start to the left of the bar indicates the presence (yellow), or absence (black) of a cecum, which is necessary for the growth of anaerobic bacteria responsible for LCA synthesis. (See following page for references).

Tree adapted and modified from:

Ravi V, Venkatesh B. Rapidly evolving fish genomes and teleost diversity. *Curr Opin Genet Dev.* 2008;18(6):544-550.

Bile salt profile overlay from:

Hofmann AF, Hagey LR, Krasowski MD. Bile salts of vertebrates: structural variation and possible evolutionary significance. *J Lipid Res.* 2010;51(2):226-246

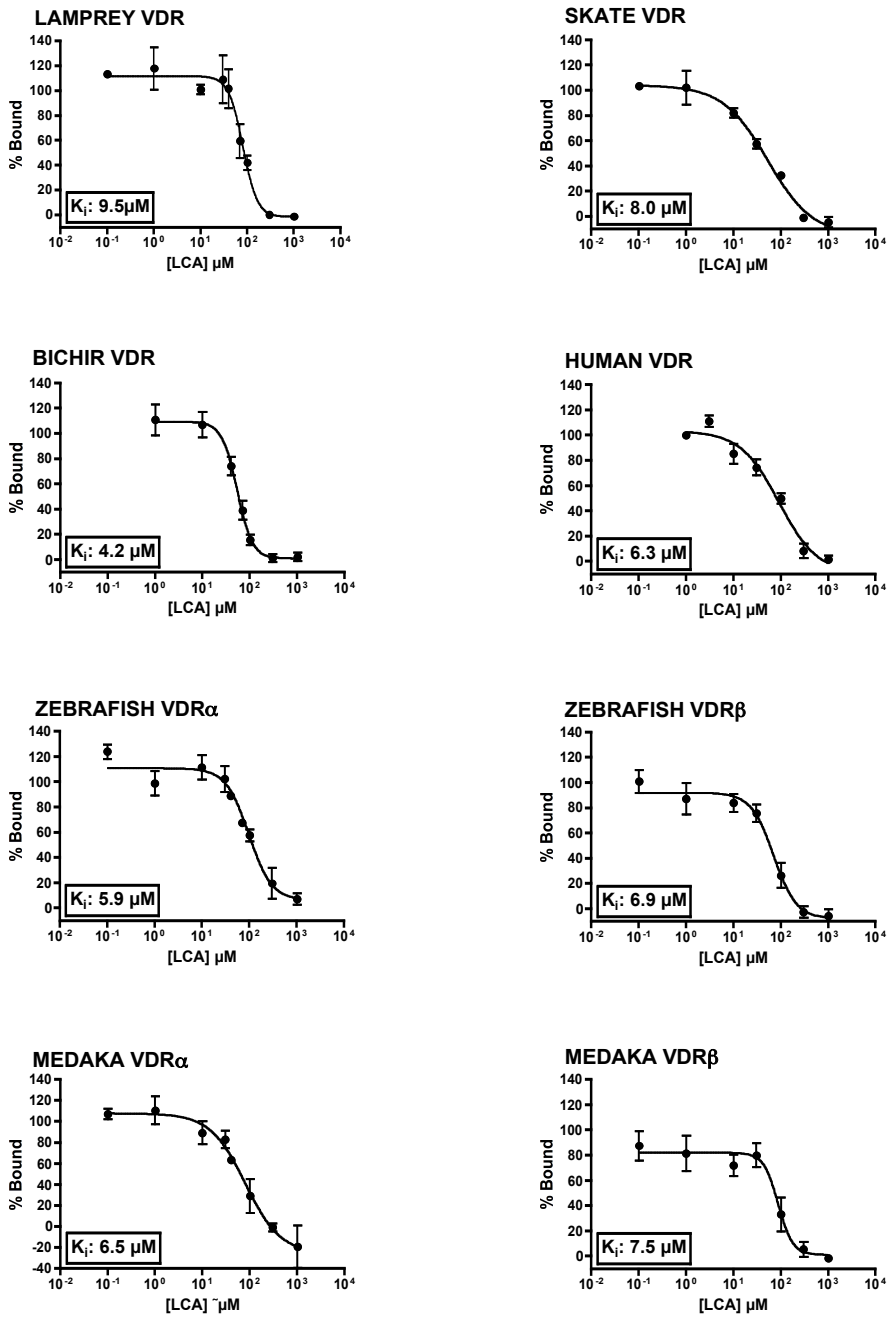

Figure 2. Competitive binding assays with saturating concentrations of [^{3}H]-1, 25D$_3$ and increasing concentrations of LCA (0 – 300 μM). Lysates were prepared from transfected

Cos7 cells as described in *Materials and Methods*. Lysates containing expressed VDR and RXR were incubated ligand for 18 hours at 4˚C. Unbound ligand was removed as described. Specific binding values were determined by subtracting the average non-specific binding counts from the total binding counts. The K_i for each curve was determined by a nonlinear regression analysis in Prism 4. The reported K_i for each VDR is the average of three separate experiments.

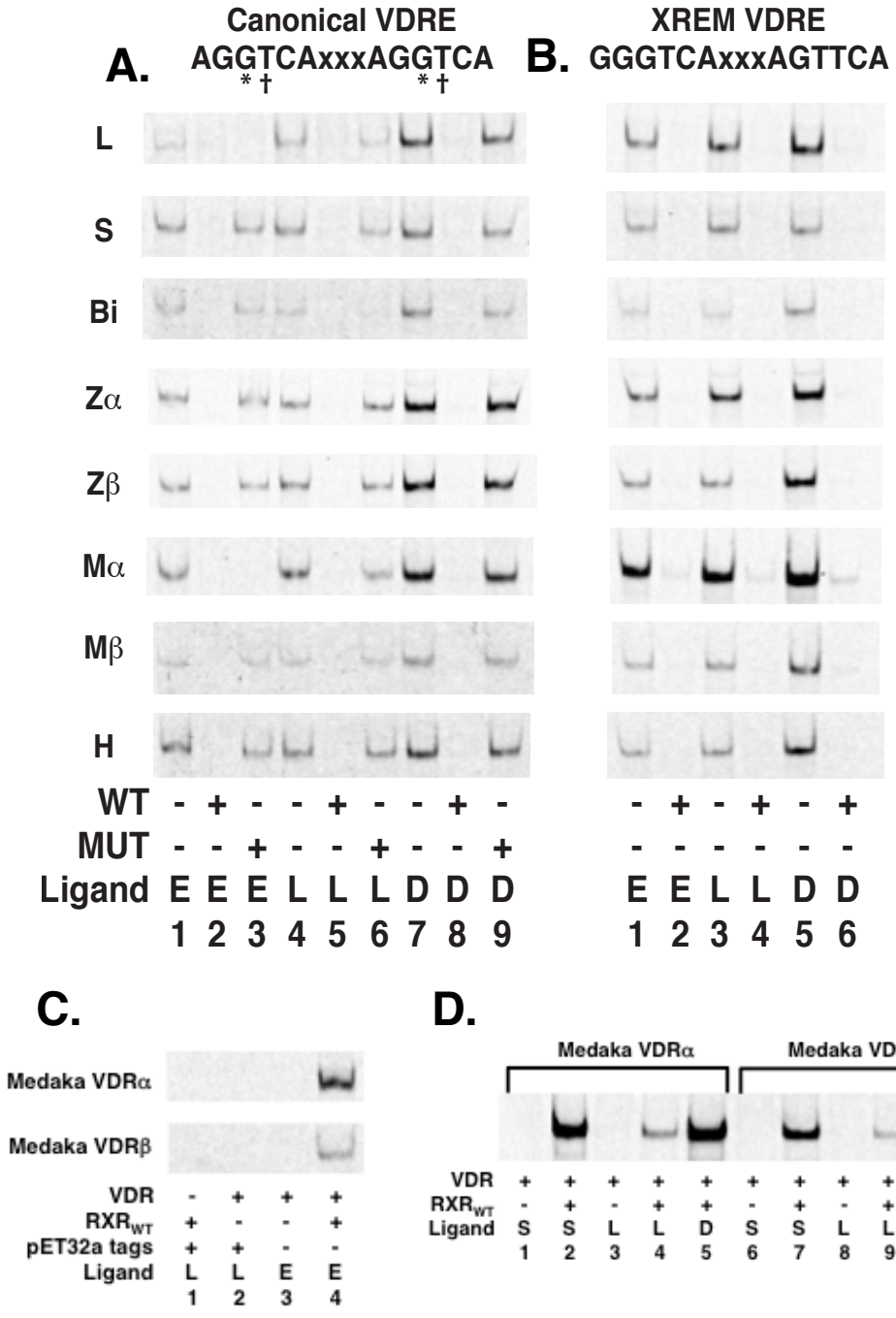

Figure 3. Electrophoretic mobility shift analysis of recombinant VDRs and RXR binding to both a canonical VDRE and a divergent VDRE from the XREM region of CYP3A4 in

response to 100 μM LCA (L), 100 nM 1, 25D_3 (D), or the ethanol control (E). Letters designate species: Lamprey (L), Skate (S), Bichir (Bi), Zebrafish alpha (Zα), Zebrafish beta (Zβ), Medaka alpha (Mα), Medaka beta (Mβ), and Human (H). * = G to A in mutant VDRE. † = T to A in mutant VDRE. **(A)** With the canonical VDRE, receptors were analyzed for their ability to form protein-DNA complexes in the absence of a ligand (*lanes 1 – 3*), presence of 100 μM LCA (*lanes 4 – 6*), and presence of 100 nM 1, 25D_3 (*lanes 7 – 9*). The addition of 100x unlabeled canonical probe outcompeted binding to the labeled probe (*lanes 2, 5, 8*). The addition of 100x unlabeled mutant probe did not affect DNA binding (*lanes 3, 6, 9*), indicating VDR binding to the canonical VDRE is specific. 100 μM LCA significantly attenuated heterodimer binding to the canonical VDRE compared to 100 nM 1, 25D_3 (*lane 4 vs. lane 7*), and did not visibly enhance heterodimer binding to the canonical VDRE over the vehicle control (*lane 1 vs. lane 4*). **(B)** Similar patterns were observed with the XREM VDRE. The addition of 100x unlabeled XREM VDRE outcompeted binding (*lanes 2, 4, 6*). 100 μM LCA visibly attenuated heterodimer binding to the XREM VDRE compared to 100 nM 1, 25D_3 (*lane 3 vs. lane 5*). 100 μM LCA did not significantly enhance heterodimer binding to the XREM VDRE over the vehicle control (*lane 1 vs. lane 3*). **(C)** and **(D)** illustrate the absence of complex formation using VDR or RXR singularly. "S" stands for DMSO.

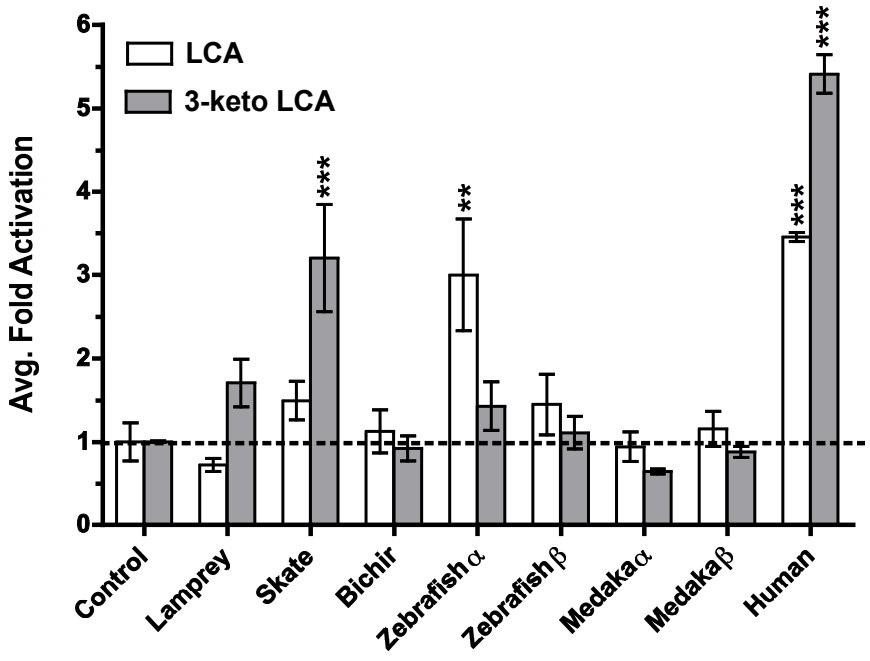

Figure 4. VDR transactivation in response to LCA and 3-keto LCA for all species. HepG2 cells were transiently transfected with pSG5-VDR, XREM-Luc, and *Renilla* as described previously in *Materials and Methods*. Cells were treated with either 100 μM LCA (*white bars*) or 100 μM 3-keto LCA (*grey bars*) in medium for 24 hours (V represents the ethanol control). VDR response was measured via dual-luciferase assays. Data are represented as the mean fold activation normalized to the ethanol control ± SEM (n = 4). Significant activation was determined via one-way ANOVA followed but Tukey's HSD post hoc test. Asterisks indicate significant VDR activation over the ethanol control: *** = $p < 0.001$, ** = $p < 0.01$, * = $p < 0.05$.

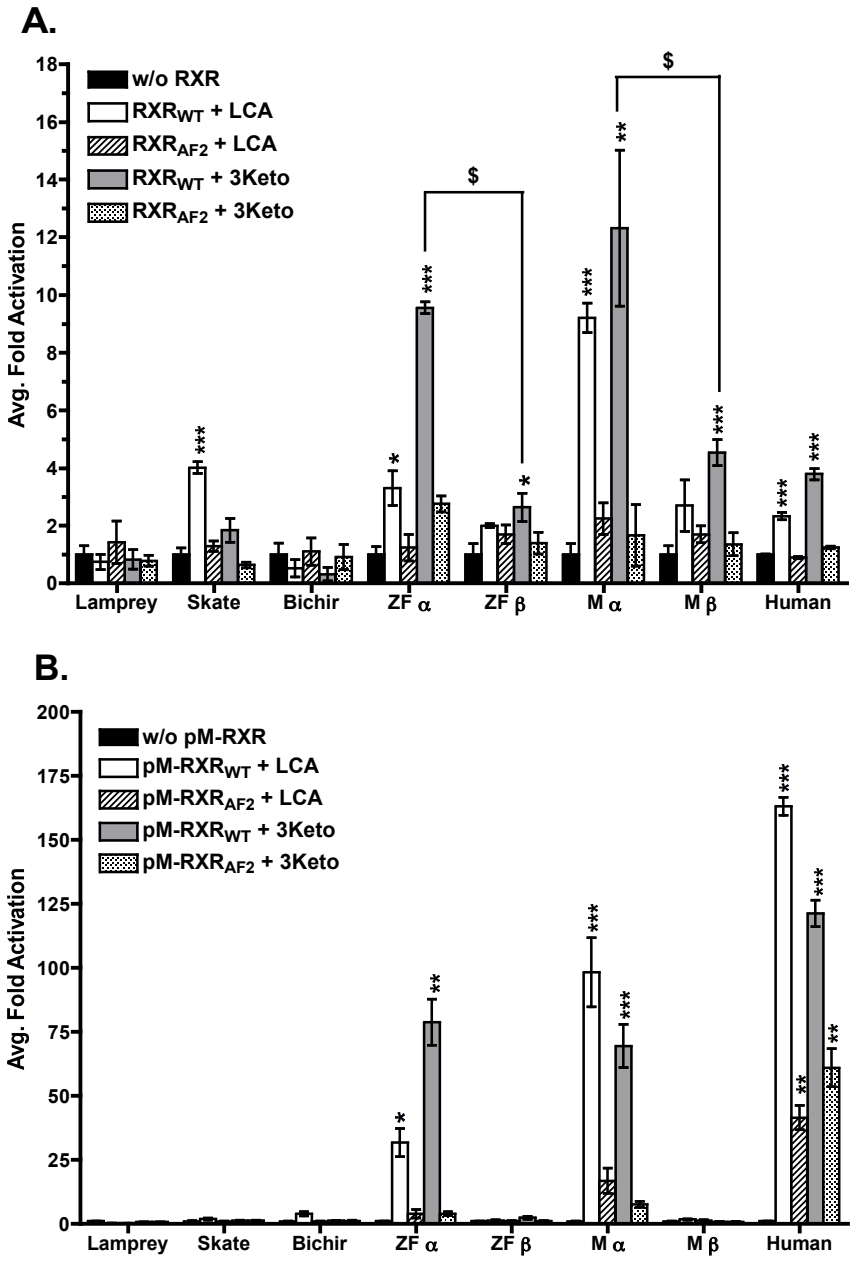

Figure 5. **(A)** Analysis of overexpressed RXR on VDR transactivation in response to 100 μM LCA and 3-keto LCA. HepG2 cells were transiently transfected with pSG5-VDR, XREM-Luc, and *Renilla* as described previously in *Materials and Methods*. Select assays

were cotransfected with pCDNA-RXR_{WT} or pCDNA-RXR_{AF2} where indicated. Cells were treated with 100 μM LCA or 3-keto LCA for 24 hours. VDR response was measured via dual-luciferase assays. Data are represented as the average fold activation normalized to VDR alone (no RXR) ± SEM (n=4). Asterisks represent a significant increase in transactivation compared to the VDR control: *** = $p < 0.001$, ** = $p < 0.01$, * = $p < 0.05$. The "$" sign over a bracket indicates a significant difference between the VDRα and VDRβ paralogs of the indicated species. **(B)** VDR-RXR heterodimerization in response to 100 μM LCA or 3-keto LCA. HepG2 cells were transiently transfected with pVP16-VDR as prey and pM-RXR_{WT} or pM-RXR_{AF2} as bait, along with 5XGal4-TATA-Luc and *Renilla*. Cells were exposed to 100 μM LCA or 3-keto LCA in medium for 24 hours. Protein-protein interaction was measured via dual-luciferase assays as described in the *Materials and Methods*. Data are represented as the mean fold interaction ± SEM (n = 4). Data are normalized to VDR + empty pM vector (no RXR). Asterisks represent a significant interaction compared to the control: *** = $p < 0.001$, ** = $p < 0.01$, * = $p < 0.05$.

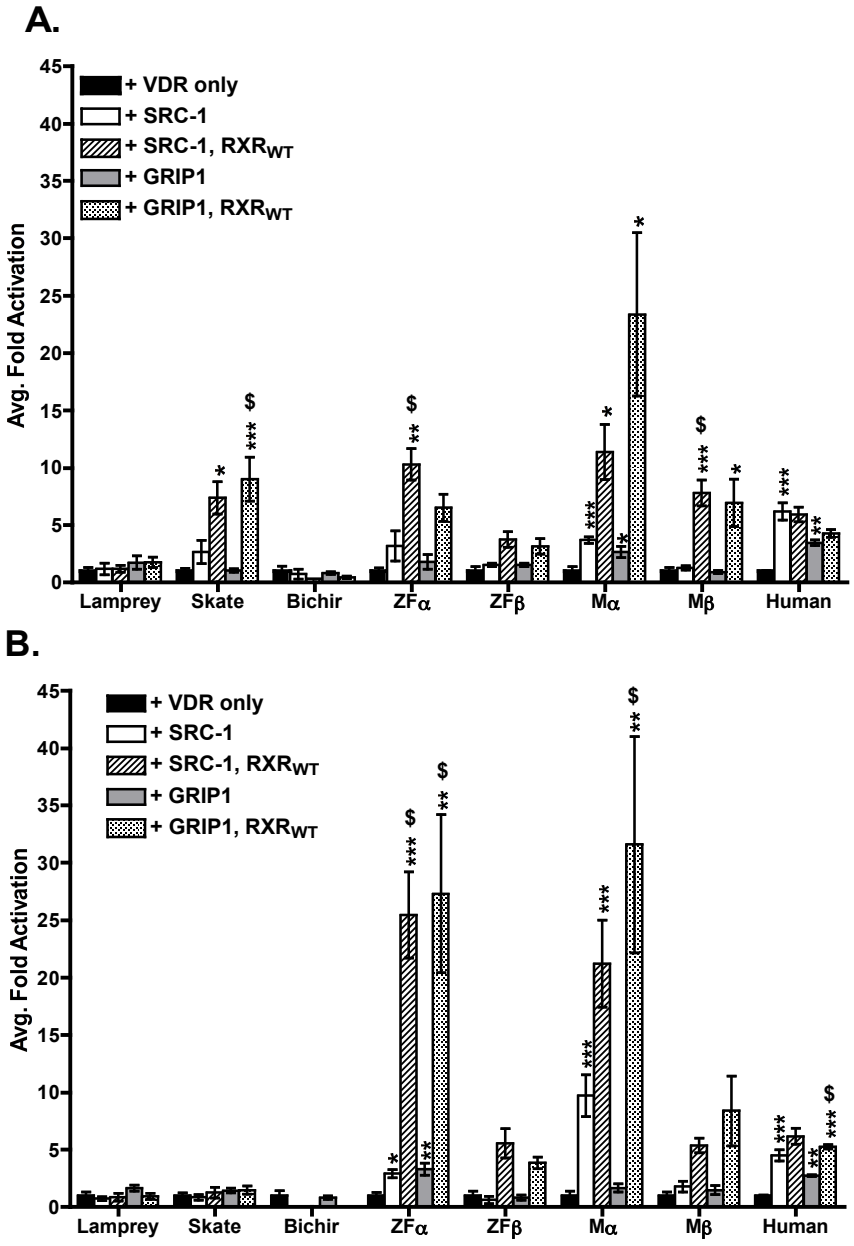

Figure 6. VDR transactivation in the presence of SRC-1 and GRIP1 (ACTR not shown) with and without RXR_{WT}, in response to (A) 100 μM LCA, and (B) 100 μM 3-keto LCA. HepG2 cells were transiently transfected with pSG5-VDR, XREM-Luc, and Renilla as described

previously in *Materials and Methods*. Select assays were cotransfection with pSG5-SRC-1, pSG5-GRIP1, pSG5-ACTR where indicated. Assays were conducted both in the presence and absence of pCDNA-RXR_{WT}. Cells were treated with 100 μM LCA or 3-keto LCA in medium for 24 hours. VDR response was measured via dual-luciferase assays. Data are represented as the average fold activation normalized to VDR alone ± SEM (n=4). One-way ANOVAs followed by a Tukey's HSD post hoc tests were utilized to compare the effect of the SRC-1, GRIP1, and ACTR on VDR transactivation for each paralog, and to compare the effects of the presence and absence of RXR_{WT}. Asterisks represent a significant difference in transactivation compared to the control: *** = $p < 0.001$, ** = $p < 0.01$, * = $p < 0.05$. $ = the combination of RXR_{WT} and SRC-1 on VDR transactivation was significantly greater than either coregular used singularly.

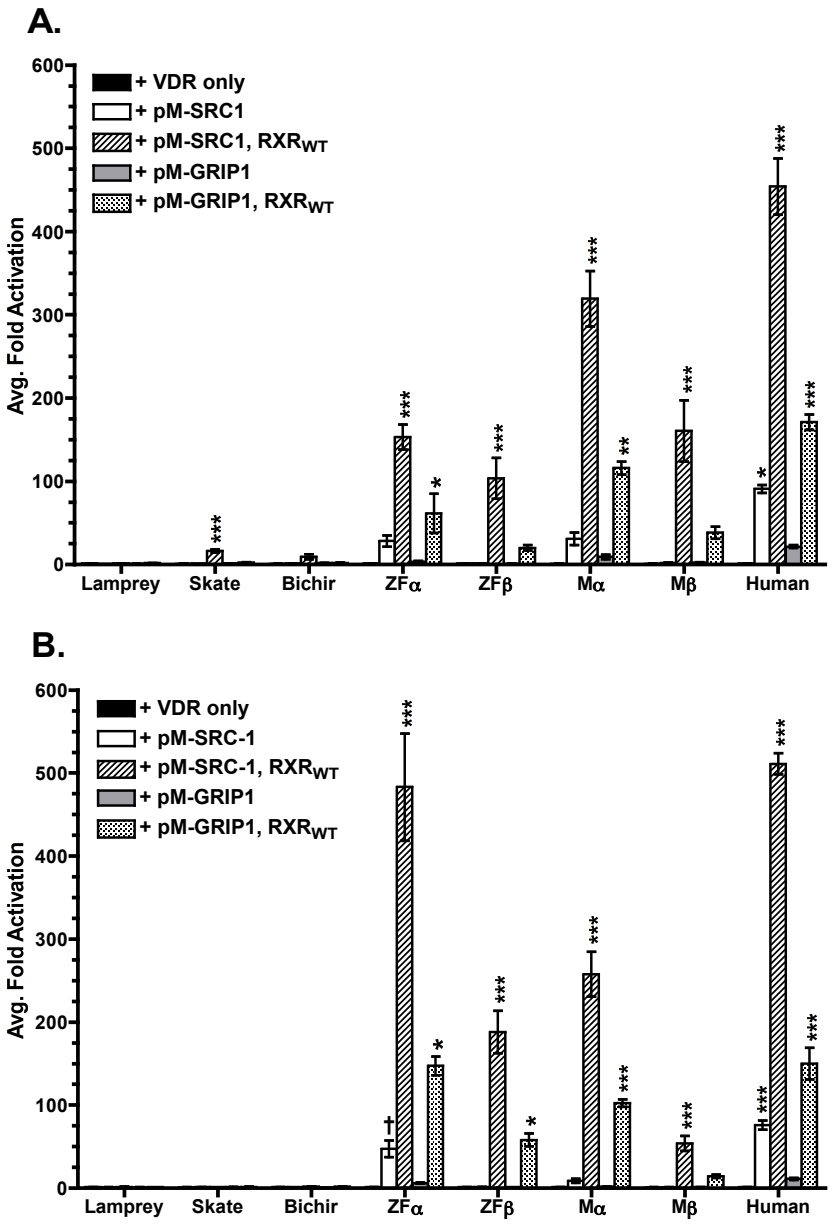

Figure 7. Mammalian 2-hybrid analysis of protein-protein interactions between VDR and pM-SRC-1 and pM-GRIP1 (pM-ACTR not shown) with and without RXR_{WT} in response to **(A)** 100 μM LCA and **(B)** 100 μM 3-keto LCA. HepG2 cells were transiently transfected

with pVP16-VDR as prey and pM-SRC-1, pM-GRIP1, or pM-ACTR as bait, along with 5XGal4-TATA-Luc and *Renilla*. Select assays were cotransfected with pCDNA-RXR_{WT} where indicated. Cells were exposed to 100 μM LCA or 3-keto LCA in medium for 24 hours. Protein-protein interaction was measured via dual-luciferase assays as described in the *Materials and Methods*. Data are represented as the mean fold activation ± SEM (n = 4). Data are normalized to VDR + empty pM vector (no coactivators). One-way ANOVAs followed by Tukey's HSD post doc test were conducted to test for significant interaction between VDR and the SRC coactivators both in the presence and absence of RXR_{WT}. Asterisks represent a significant interaction: *** = $p < 0.001$, ** = $p < 0.01$, * = $p < 0.05$.

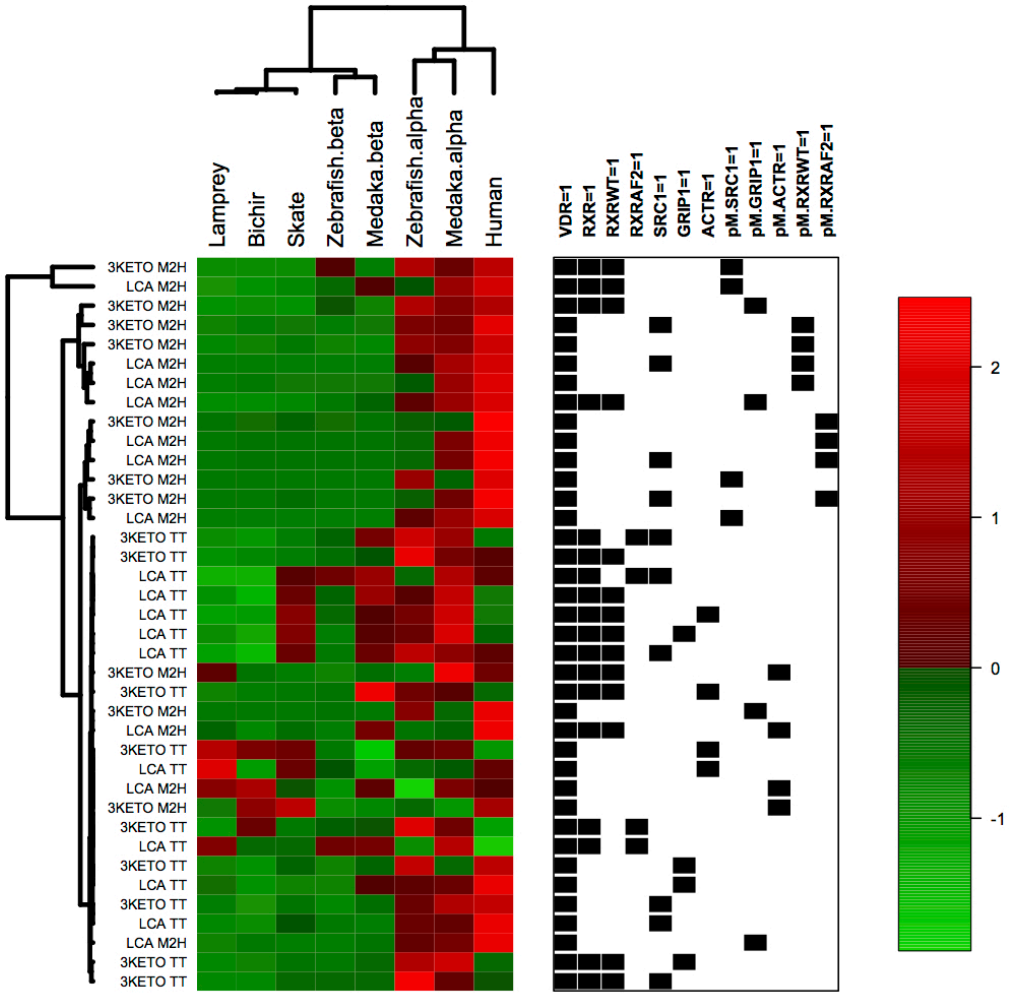

Figure 8. Heatmap depicting the results of the bioinformatics summary analysis. Analysis included mammalian 2-hybrid (M2H) and transient transactivation (TT) data for all eight species in response to both LCA and 3-Keto. The Picket Plot to the right of the heat map indicates the presence (black box) or absence (no box) of coregulators in each assay. Data were normalized for each assay (rows) across all species (columns) to account for magnitudinal response differences. The resulting matrix was subjected to unsupervised, hierarchical clustering using Manhattan distance and complete linkage. Bootstrap resampling

was performed over the assays according to presence/absence of each of the co-regulators to identify drivers of the overall cluster pattern as well as subclusters. For each of 10,000 bootstrap samples of assays, the accuracy was measured by counting the number of times the overall cluster pattern and species subclusters [Lamprey, Bichir, Skate, Medaka β and Zebrafish β] and [Medaka α, Zebrafish α, Human] were identical compared to the raw data.

GENERAL DISCUSSION AND FUTURE DIRECTIONS

The vitamin D receptor was one of the first nuclear receptors identified in humans and rodent models. While the molecular biology and physiological roles of mammalian VDR have been extensively studied, large data gaps exist in our knowledge regarding the molecular function and physiological roles of non-mammalian VDRs. Thus the major objective of this dissertation was to study the functional diversification of the vitamin D receptor (VDR) with increasing genome complexity within teleost and vertebrate evolution. In order to address this objective, this dissertation was split into three aims: In Chapter 1 studied the hypothesis that VDR duplicates are derived from 3R event and that retention of duplicate VDRs is likely due to the Duplication-Degeneration-Complementation (DCC) model (1), resulting in sub- and/or neofunctionalization of VDR function. In Chapter 2 I studied the hypothesis that the receptor-ligand partnership between VDR and 1, $25D_3$ is ancient and traceable to basal extant vertebrate species. Lastly, Chapter 3 examines the hypothesis that the VDR - LCA partnership evolved as a result of exaptation, rather than adaptation specific to higher vertebrates.

The first study (Chapter 1) focused on dissecting the critical nuclear receptor functions of the VDRα and VDRβ paralogs from teleost fish. The results demonstrate differential functional activities between the VDR paralogs. Here we demonstrate that maximal transactivation (efficacy) is significantly attenuated in VDRβ paralogs compared to the VDRα paralogs, and propose a likely mechanism of differential protein-protein interaction between the VDR paralogs and essential co-regulators, including RXR and the SRC family of nuclear receptor co-activators. Differential protein-protein interactions are

evidence of a functional divergence between the VDRα and VDRβ paralogs. Due to the high degree of conservation of other receptor functions such as ligand binding affinities, our results are more suggestive of subfunctionalization rather then neofunctionalization. Our studies support the notion that the differential functions of the paralogous VDRs is likely a result of the DDC model, which lead to subfunctionalization between the VDRα and VDRβ paralogs function following the 3R event.

While these studies aid in increasing our understanding of the molecular activities of the VDRα and VDRβ paralogs, additional studies are necessary to fully understand the specific physiological roles of the VDR paralogs. This dissertation has only focused on the protein-coding region of the VDR gene, however, it is important to recognize that subfunctionalization can be induced by subtle sequence mutations in non-coding regulatory regions of a gene. Changes in regulatory regions (such as the promoter, enhancer, or silencer elements) may result in paralog-specific tissue- or temporal-specific expression patterns (1). Neofunctionalization may also result from mutations within regulatory region by promoting expression in a novel tissue or developmental stage. Furthermore, these functional changes may make significant contribution(s) to evolutionary novelty as they can be highly localized, and thus are more tolerated as pleiotropic effects are reduced (2). Thus it is entirely possibly for two paralogs to maintain highly similar protein functions, yet to have undergone subfunctionalization due to divergent tissue expression patterns. The focus of future studies should be expanded to include the regulatory regions of each VDR paralog in order to further explore this possibility.

The inclusion of in vivo studies would facilitate our understanding of the physiological significance of each paralog. For example, previous studies using loss of function morpholinos in zebrafish have demonstrated that VDRα is solely responsible for regulating calcium absorption in this species. The loss of VDRβ did not have any effect on calcium mobilization (3). As VDR is thought to maintain many diverse roles that extend beyond calcium homeostasis, knock-down and overexpression studies will aid in our understanding of the physiological functions and significance of each paralog in additional physiological systems, such as neurodevelopment and immune system function. Furthermore, assessment of VDRα and VDRβ physiological functions across multiple teleost models will enable cross species comparisons and further facilitate our understanding of conservation or divergence in VDR endocrinology at the molecular and physiological levels.

After identifying functional differences between teleost VDRα and VDRβ, the next objective was to determine if the observed differences represented either ancestral or derived VDR traits. Thus, the purpose of Chapter 2 was to examine the ancestral molecular function of VDRs from basal vertebrates that diverged at key points in vertebrate evolution, with the hypothesis that the 1, $25D_3$ – VDR partnership is ancient and traceable to basal species. Species include the sea lamprey (*Petromyzon marinus*), a jawless fish that diverged after the 1R event and is considered to be one of the most basal extant vertebrates (4). The little skate (*Leucoraja erinacea*), is a cartilaginous fish of the class Chondrichthyes, the sister group to all other jawed vertebrates and the first lineage to diverge after the 2R duplication (5). The study also included the Senegal bichir (*Polypterus senegalus*), a ray-finned fish that diverged before the 3R event, and thus maintains a single VDR ortholog (6). Lastly, human VDR was

included as a tetrapod and mammalian comparison. We found that many functions were highly conserved between basal vertebrates, teleosts, and mammals, including: high affinity binding to 1, $25D_3$, the necessity of RXR heterodimerization, 1, $25D_3$-enhanced DNA binding, and transactivation in response to 1, $25D_3$. However, transactivational efficacy and protein-protein interaction varied greatly between species. In order to gain a global perspective on our collective functional data we conducted a cluster analysis to identify key drivers of the observed functional differences across species. This analysis included results from the medaka and zebrafish VDRα and VDRβ paralogs in addition to the three basal VDRs and human. The VDRα and VDRβ paralogs separated into two separate subclusters, providing further evidence of a functional divergence between the two paralogs. Our results indicate that while 1, $25D_3$ has been maintained as a high affinity and potent ligand with teleost VDRα and mammalian VDR, it only serves as a partial/weak agonist in basal species tested. We thus conclude that the full agonist activity of 1, $25D_3$ may be a derived trait that did not evolved until bony vertebrates.

We speculate that receptor-ligand interactions of VDR and 1, $25D_3$ may result in defined differences between *apo* and *holo* receptor conformations that impact essential protein-protein interactions between VDRs and co-regulators examined in this study. The fact that differential ligand sensitivities are driven by differential protein interactions suggests that the active receptor conformation induced by 1, $25D_3$ may not be optimal for all VDRs. Unfortunately, structural data for non-mammalian VDRs is lacking, and thus this assumption remains speculative. Future research should include structure modeling and mutational analysis of the VDRs to determine if differential protein interactions between

receptors are related to differences in VDR conformation. Structural modeling may help identify defined mechanisms driving observed functional differences. Homology modeling may also aid in identifying key residues that vary between VDRs, and mutational analysis of these residues will aid in determining their impact on VDR function.

In addition to 1, $25D_3$, it was recently demonstrated that mammalian VDR exhibits low affinity interactions with lithocholic acid (LCA), a toxic secondary bile acid (7). Studies with mammalian VDR have demonstrated that LCA-bound VDR activates feed-forward catabolic pathways, resulting in the detoxification of LCA. Studies examining the VDR-LCA receptor-ligand evolution suggest that the partnership between VDR and LCA is an adaptation limited to higher vertebrates, as lower vertebrates do not possess the intestinal anatomy necessary for LCA production, and many do not synthesize the parent compound (CDCA). However, VDR has been highly conserved throughout vertebrate evolution, and to date there is no evidence of receptor-ligand coevolution between VDR and LCA. Thus, in the third study of this dissertation (Chapter 3) I examine the hypothesis that the VDR-LCA partnership is a result of exaptation, rather than an adaptation specific to higher vertebrates. Adaptation is defined as a trait that has been shaped by natural selection for its current use. On the other hand, exaptation defines a trait whose current function was not created by natural selection (33). This trait may have previously been shaped by natural selection for its ancestral function, but was later co-opted for its current role. Alternatively, the trait may be a non-adaptive "accident" of selection on another, unrelated trait, and this fortuitous effect was later co-opted for the function it currently serves (33). To gain insight into the functional evolution of LCA-VDR partnership, VDRs from Chapter 1 and Chapter 2 were utilized in

assays designed to study essential molecular functions in VDR activation in response to LCA and its metabolite, 3-keto LCA. We demonstrate that LCA and 3-keto LCA both function as full agonists only with human VDR and the teleost VDRα paralogs. Interaction between the bile acids and the VDRβ paralogs did not facilitate transactivation or RXR heterodimerization, while none of the three basal VDRs were able to mediate any response to LCA or 3-keto LCA beyond ligand binding. As in Chapter 2, we conducted a cluster analysis with the functional data to identify key VDR parameters across species. Similar to our analysis with 1, $25D_3$, the cluster analysis indicated that functional differences between the vertebrate VDRs are likely driven through differential interactions between VDR and essential coregulators. These results suggest that the ability of LCA to function as a VDR ligand likely evolved before the bile acid itself due to the ability of LCA to function as a VDR agonist with teleost VDRα, despite the fact that fish do not have a cecum, and thus do not synthesize LCA. We speculate that the VDR – LCA partnership most likely occurred through a process of exaptation, rather than adaptation. The consistent affinity of VDR for LCA has most likely been maintained as a result of selective pressure on a separate, unrelated trait, such as high affinity binding with 1, $25D_3$, due to both ligands utilizing the same ligand binding pocket and maintaining similar ligand-protein contacts. The VDR pathway was later co-opted by higher vertebrates once the need to detoxify LCA arose. As mentioned previously, structural modeling and docking studies would aid in identifying conformational differences in VDR bound to LCA compared to 1, $25D_3$. In addition, further assessment of the ancestral NR1I identified in *Ciona intestinalis* may facilitate a greater understanding of

ancestral NR function, and further support the hypothesis of the VDR-LCA partnership evolved through exaptation.

To gain a global perspective on VDR function across species and with different ligands, we combined data derived from each chapter of this dissertation and conducted a cluster analysis. This includes data with all three ligands: 1, $25D_3$, LCA, and 3-keto LCA. This analysis also included VDRα and VDRβ paralogs from medaka and zebrafish in addition to VDR orthologs from basal species and human (Fig. 1). These results further support our hypothesis that interactions with coregulator proteins exhibit a significant influence on VDR functional evolution. Furthermore, the fact that both VDRα paralogs are in a separate cluster from the VDRβ paralogs is additional evidence of a divergence in function between the two paralogs. Our results indicate that the VDRβ paralogs function more similar to the basal vertebrates, while the VDRα paralogs function more similar to human VDR. Furthermore, the species cluster organization based on our functional data is quite similar to a phylogenetic tree created from sequence data (Fig. 2A, B). For both trees, the VDRα and VDRβ paralogs cluster separately from one another. Similar to the bioinformatics data, the VDRβ paralogs form a separate subcluster within the basal vertebrates. However human VDR clusters with other tetrapod VDR sequences as a subcluster that branch off from the basal species rather than with the VDRα paralogs. This may be due to the inclusion of additional mammalian and tetrapod sequences. Further analysis is necessary, but the idea of VDR function mirroring phylogeny is intriguing.

In summary, these studies provide an initial deconstruction of the molecular mechanisms driving VDR function in non-mammalian vertebrates. This dissertation has laid

the groundwork for identifying both conserved and divergent molecular functions critical to VDR activation. Specifically, the results from each chapter suggest that differential protein-protein interactions between VDR and essential coregulator proteins are driving the observed differences in transactivation between VDRα and VDRβ, as well as between the basal VDRs and mammalian VDR. Further studies are necessary to gain a better understanding of the physiological significant of VDR both at the tissue and organism level for both basal vertebrates and 3R teleosts. Teleosts are of particular interest, as their popularity as model organisms continues to grow (8). Further understanding of the functional similarities and differences will aid in the development of an advantageous teleost model for VDR research.

REFERENCES

1. Force A, Lynch M, Pickett F, Amores A, Yan Y, Postlethwait J. Preservation of duplicate genes by complementary, degenerative mutations. *Genetics.* 1999;151(4):1531-1545.

2. Kassahn KS, Dang VT, Wilkins SJ, Perkins AC, Ragan MA. Evolution of gene function and regulatory control after whole-genome duplication: comparative analyses in vertebrates. *Genome research.* 2009;19(8):1404-1418.

3. Lin CH, Su CH, Tseng DY, Ding FC, Hwang PP. Action of vitamin D and the receptor, VDRa, in calcium handling in zebrafish (Danio rerio). *Plos One.* 2012;7(9):e45650.

4. Escriva H, Manzon L, Youson J, Laudet V. Analysis of lamprey and hagfish genes reveals a complex history of gene duplications during early vertebrate evolution. *Molecular biology and evolution.* 2002;19(9):1440-1450.

5. Kikugawa K, Katoh K, Kuraku S, Sakurai H, Ishida O, Iwabe N, Miyata T. Basal jawed vertebrate phylogeny inferred from multiple nuclear DNA-coded genes. *BMC Biol.* 2004;2:3.

6. Inoue JG, Miya M, Tsukamoto K, Nishida M. Basal actinopterygian relationships: a mitogenomic perspective on the phylogeny of the "ancient fish". *Mol Phylogenet Evol.* 2003;26(1):110-120.

7. Makishima M, Lu T, Xie W, Whitfield G, Domoto H, Evans R, Haussler M, Mangelsdorf D. Vitamin D receptor as an intestinal bile acid sensor. *Science.* 2002;296(5571):1313-1316.

8. Schartl M. Beyond the zebrafish: diverse fish species for modeling human disease. *Disease Models and Mechanisms.* 2014;7(2):181-192.

FIGURES

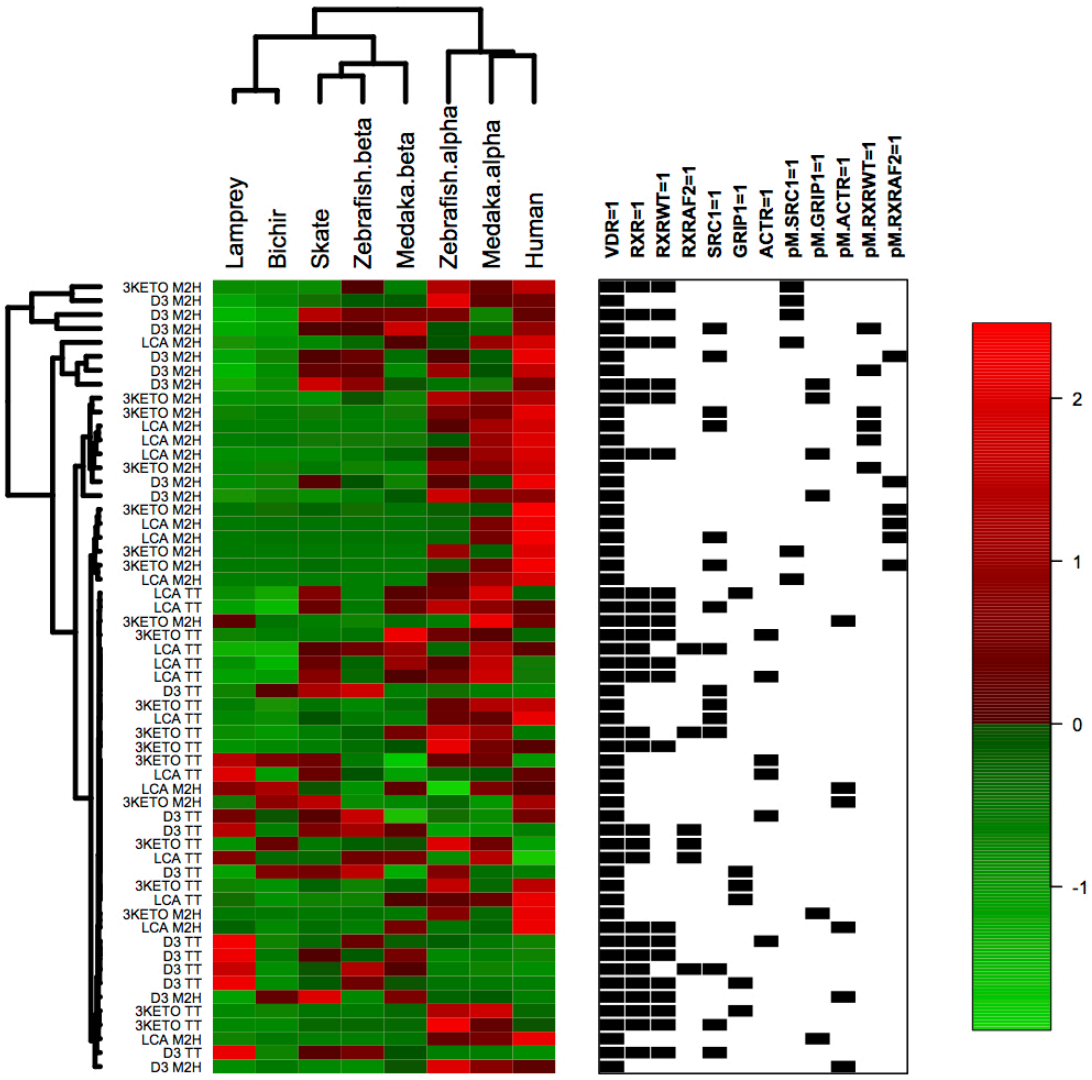

Figure 1. Heatmap depicting the results of the bioinformatics summary analysis. Analysis included mammalian 2-hybrid (M2H) and transient transactivation (TT) data for all eight species in response to 1α, 25-dihydroxyvitamin D_3 (D3), lithocholic acid (LCA), and 3-keto lithocholic acid (3KETO). The Picket Plot to the right of the heat map indicates the presence (black box) or absence (no box) of coregulators in each assay. Data were normalized for each assay (rows) across all species (columns) to account for magnitudinal response differences.

The resulting matrix was subjected to unsupervised, hierarchical clustering using Manhattan distance and complete linkage. Bootstrap resampling was performed over the assays according to presence/absence of each of the co-regulators to identify drivers of the overall cluster pattern as well as subclusters.

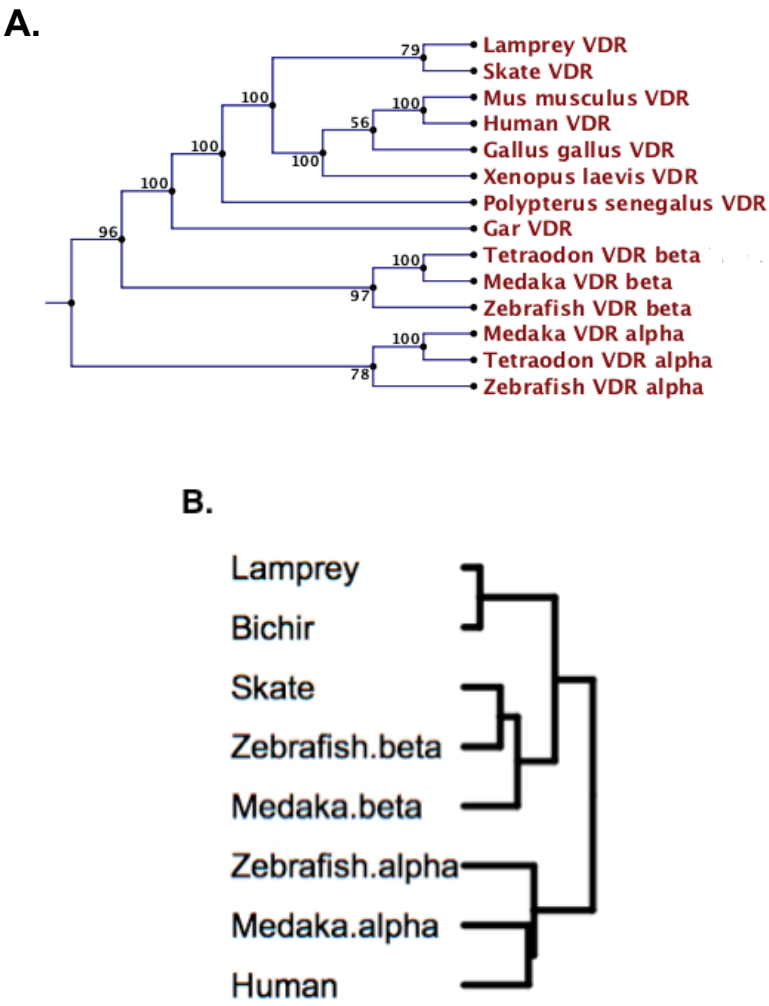

Figure 2. Comparison of **(A)** phylogenetic analysis of VDR sequences, and **(B)** species clustering based on bioinformatics analysis. Phylogenetic analysis for **(A)** was conducted in CLC Sequence Viewer 6 (CLC Bio) using neighbor-joining trees and was bootstrapped to access robustness. The species clustering in **(B)** was taken from the bioinformatics results from figure 1.

APPENDICES

Appendix A

Table 1.0: List of primers. [1,2] pSG5 and [1]pVP16 constructs were a gift from Dr. Kerr Whitfield[1] and Dr. John Moore[2] (See Chapter 2)

Name	Vector	App.	R.S.	F/R	Sequence (5' → 3')
Lamprey VDR[1]	pET32a	Cloning	SalI	F	5' – GAT A**GT CGA C**TG ATG ATG GCC ACT CAG ACC – 3'
			NotI	R	5' – GAT T**GC GGC CGC** TGC GGT TGG GTT GCC AAA – 3'
Skate VDR	N/A	PCR Amp	N/A	F	5' – GCA GGA AGC TGA TTT CCA AG – 3'
			N/A	R	5' – CCA AGC CTG TTT ACC CTG TG – 3'
	pSG5	Transactivation	BamHI	F	5' – AGC TA**G GAT CC**A TGG AAC AGA TGG CAG TG – 3'
			BglII	R	5' – ACG TA**A GAT CT**T CAT TTC GCA TCA TCA TT – 3'
	pVP16	M2H	BamHI	F	5' – AGC TA**G GAT CC**T TAT GGA ACA GAT GGC AGT – 3
			HindIII	R	5' – ACG TA**A AGC TT**T CAT TTC GCA TCA TCA TT – 3'
	pET32a	Protein Expression	SalI	F	5' – GAT A**GT CGA C**TG ATG GAA CAG ATG GCA GTG – 3'
			NotI	R	5' – GAT T**GC GGC CGC** TTT CGC ATC ATC ATT ACT – 3'
Bichir VDR	pSG5/ pVP16	Transactivation/ M2H	EcoR1	F	5' – AGC T**GA ATT C**AT GGC AGC CAT ATC AGT G – 3'
			BamHI	R	5' – AGC T**GG ATC C**CT AAG ACA CTT CAT TGC C – 3'
	pET32a	Protein Expression	SalI	F	5' – GAT A**GT CGA C**TG ATG GCA GCC ATA TCA GTG – 3'
			NotI	R	5' – TAT C**GC GGC CGC** AGA CAC TTC ATT GCC AAA – 3'
Human VDR[2]	pVP16	M2H	EcoRI	F	5' – GAT A**GA ATT C**AT GGA GGC AAT GGC GGC CAG – 3'
			BamHI	R	5' – TAT C**GG ATC C**TC AGG AGA TCT CAT TGC CAA – 3'
	pET32a	Protein Expression	SalI	F	5' – CAT A**GT CGA C**TG ATG GAG GCA ATG GCG GCC AG – 3'
			NotI	R	5' – TAT **GCG GCC GC**G GAG ATC TCA TTG CCA AAC AC – 3'
Zebrafish VDRα	pSG5/ pVP16	Transactivation/ M2H	EcoRI	F	5' - GC**G AAT TC**G CCA TGC TTA CGG AAA ATA GTG CC - 3'
			BamHI	R	5' - AT**G GAT CC**A AAC TAG GAC ACC TCA CTC C - 3'
	pET32a	Protein Expression	SalI	F	5' – GAT A**GT CGA C**TG ATG GAT CTG ATG GCC GTG – 3'
			NotI	R	5' – GAT T**GC GGC CGC** ACT GGA CAC CTC ACT CC – 3'
Zebrafish VDRβ	pSG5/ pVP16	Transactivation/ M2H	EcoRI	F	5' - GC**G AAT TC**A TGG AGT CAG CTG TCA GTA C - 3'
			BamHI	R	5' – AT**G GAT CC**A GAA AAC TAG GTG ACC TGC C - 3'
	pET32a	Protein Expression	SalI	F	5' – GAT A**GT CGA C**TG ATG GAG TCA GCT GTC AGT – 3'
			NotI	R	5' – GAT T**GC GGC CGC** ACT GGT GAC CTG CCC GCC – 3'
Medaka VDRα	pSG5	Transactivation	BglII	F	5'- GA**A GAT CT**A TGG AGT CCA TTA CCG TGA C - 3'
			BglII	R	5' - CG**A GAT CT**C TAT GAC ACC TCG CTG CCG A - 3'
	pVP16	M2H	SalI	F	5' – CTC **GTC GAC** TTA TGG AGT CCA TTA CG TG – 3'
			HindIII	R	5' – GCT **AAG CTT** CTC TAT GAC ACC TCG CTG CC – 3'
	pET32a	Protein Expression	SalI	F	5' – GAT A**GT CGA C**TG ATG GAG TCC ATT ACC GTG – 3'
			NotI	R	5' – GAT T**GC GGC CGC** ACT TGA CAC CTC GCT GCC – 3'
Medaka VDRβ	pSG5	Transactivation	EcoRI	F	5'- GC**G AAT TC**A TGG AGG CCA CTG TTG TGA G - 3'
			BglII	R	5' - CG**A GAT C**TC TAG GAG ACC TCG CTG CCA A - 3'
	pVP16	M2H	EcoRI	F	5' – CCA **GAA TTC** ATG GAG GCC ACT GTT GTG – 3'
			HindIII	R	5' – ATT **AAG CTT** CTC TAG GAG ACC TCG CTG CC – 3'
	pET32a	Protein Expression	SalI	F	5' – GAT A**GT CGA C**TG ATG GAG GCC ACT GTT GTG – 3'
			NotI	R	5' – GAT T**GC GGC CGC** ACT GGA GAC CTC GCT GCC – 3'

Appendix B

Kollitz EM and Kullman SW. Chapter 7: The Vitamin D Signaling Pathway. In: State of the Science on Novel In Vitro and In Vivo Screening and Testing Methods and Endpoints for Evaluating Endocrine Disruptors. A Detailed Review Paper submitted to RTI International, June 2011.

The Vitamin D Signaling Pathway

7.1 Overview

Vitamin D is a steroid hormone. Like other members of this family, the biological effects of vitamin D are mediated through the binding of 1α, 25-dihydroxyvitamin D_3 to its hormone receptor, vitamin D receptor (VDR). VDR is a member of the nuclear receptor superfamily, which makes up a large group of ligand-activated transcription factors. The mechanism of VDR-mediated gene transcription closely resembles that of other steroid hormones. 1α, 25-dihydroxyvitamin D_3 binds to the ligand-binding pocket of VDR with high affinity ($K_D = 10^{-10}$ to 10^{-11} M).(1) The binding of VDR to its ligand causes a conformational change in the receptor to its active form. VDR heterodimerizes with RXR, and the heterodimer binds to target genes containing a canonical vitamin D response element (VDRE) within the promoter region.(2) Co-regulatory proteins are recruited, followed by the recruitment of RNA polymerase II and the initiation of gene transcription.

Vitamin D is an ancient molecule that is found in animals, plants, and zooplankton. While vitamin D is ubiquitous among organisms, VDR is only found in vertebrates.(3) VDR

and vitamin D signaling likely originated with stem vertebrates, as a functional VDR has been identified in the sea lamprey (*Petromyzon marinus*), a basal vertebrate lacking a calcified skeleton.(4,5) Comparisons of vertebrate VDR protein sequences demonstrate a high degree of conservation across species, suggesting that the vitamin D endocrine axis may be highly conserved throughout vertebrate evolution.(6) In humans and rodents, 36 tissues express VDR, including tissues that are not associated with the classic vitamin D effects of calcium mobilization and ion homeostasis.(2) In fact, recent investigation of VDR function suggests that VDR signaling has additional non-calcemic roles, including roles in immune system function, cell proliferation, and neurodevelopment (**Figure 7-1**).

7.1.1 Synthesis

All vertebrates possess the vitamin D endocrine axis.(7) Aquatic vertebrates obtain vitamin D solely from the diet, while terrestrial vertebrates can obtain vitamin D from both the diet and from the photolytic conversion of 7-dehydrocholesterol to pre-vitamin D_3 in the skin. 7-dehydrocholesterol is present in large quantities in the skin of higher vertebrates and is a precursor molecule in the cholesterol biosynthesis pathway.(2,8) 7-dehydrocholesterol absorbs UVB light in the 290–315 nm wavelength, which breaks the bond between carbons 9 and 10, creating pre-vitamin D_3. Pre-vitamin D_3 is thermodynamically unstable and rapidly isomerizes to vitamin D_3. (1,9) This photochemical reaction does not involve any enzymes and is related to the amount of UVB exposure an individual receives. Factors such as latitude, sunscreen use, ethnicity, age, and nutritional status can affect vitamin D_3 production

in the skin.(10) Vitamin D_3 is not biologically active and must be metabolized to its active form through two hydroxylation reactions.

The first hydroxylation reaction takes place in the liver. Vitamin D_3 is transported from the skin bound to transport proteins in the bloodstream. Most vitamin D_3 is bound to vitamin D binding protein (VDBP), but some is also bound to albumin.(1,11) Once in the liver, the P450 enzyme 25-hydroxylase (CYP2R1) adds a hydroxyl group to carbon 25, creating 25-hydroxyvitamin D_3. Several P450 enzymes have been shown to hydroxylate vitamin D on carbon 25, but only CYP2R1 is highly expressed in the liver, and mutations in CYP2R1 are linked to low vitamin D levels and rickets. (1) (12-14) Mutations in other candidate P450s do not alter 25-hydroxyvitamin D_3 levels. This hydroxylation step is not well regulated and is dependent on vitamin D_3 substrate availability. Because this reaction reflects the vitamin D_3 status of an individual, measuring serum levels of 25-hydroxyvitamin D_3 is a common method of determining the vitamin D status of patients.(1)

After the initial hydroxylation, 25-hydroxyvitamin D_3 is once again bound to transport proteins and transported in the blood from the liver to the kidney for the second hydroxylation reaction. The 25-hydroxyvitamin D_3-DBP complex is filtered out of the blood by the glomerulus and is absorbed at the proximal tubules of the kidney by endocytosis mediated by a surface receptor protein called megalin.(15) Megalin-deficient mice are unable to reabsorb 25-hydroxyvitamin D_3 at the proximal tubules and instead excrete the vitamin D_3 metabolite in their urine. These mice suffer from vitamin D deficiency and rickets.(15) Once inside the cells of the proximal tubules, DBP is degraded while 25-hydroxyvitamin D_3 is transported to the mitochondria for the second hydroxylation. The P450 enzyme 1α-

hydroxylase (CYP27B1) adds a hydroxyl group to carbon 1 of 25-hydroxyvitamin D_3, creating 1α, 25-dihydroxyvitamin D_3, which is the active metabolite of vitamin D_3.(1)

Unlike the first hydroxylation, the second hydroxylation is tightly regulated. This regulation is necessary in order to maintain proper 1α, 25-dihydroxyvitamin D_3 levels. One of the major roles for vitamin D in vertebrates is calcium homeostasis through the control of calcium absorption in the intestine, and releasing calcium from skeletal stores. Calcium-sensing receptors in the parathyroid gland detect when serum calcium levels are low and trigger the release of parathyroid hormone (PTH). PTH induces the expression of 1α-hydroxylase, which increases the concentration of 1α, 25-dihydroxyvitamin D_3, which, in turn, causes an increase in serum calcium concentration.(13,16) 1α, 25-dihydroxyvitamin D_3 does not directly bind calcium, but binds to its nuclear receptor, the vitamin D receptor, activating it and initiating the transcription genes involved in calcium uptake and transport.

7.1.2 Catabolism

1α, 25-dihydroxyvitamin D_3 regulates its levels by suppressing the expression of CYP27B1 and by inducing the expression of its major catabolism enzyme: 24-hydroxylase (CYP24A1). This P450 enzyme initiates the breakdown of 1α, 25-dihydroxyvitamin D_3 to calcitroic acid through a series of hydroxylations and side chain oxidations.(14) The breakdown products are eliminated from the body. Nearly all cells in the body express 24-hydroxylase, but the highest activity is seen in the kidney.(16) Mice lacking CYP24A1 cannot clear 1α, 25-dihydroxyvitamin D_3 from their bloodstream, and the active form of vitamin D remains in their bloodstream for days.(17) Many other compounds and receptors

are capable of inducing CYP24A1 expression, suggesting that these compounds could have an effect on the vitamin D status of the animal. 24-hydroxylase is regulated by many of the same compounds as 1α-hydroxylase, but in an opposite fashion.

7.1.3 Calcium and Skeletal Maintenance

Classically, vitamin D is necessary for normal bone development and remodeling. Vitamin D-VDR signaling controls the differentiation of bone-forming osteoblasts and bone-resorbing osteoclasts. The vitamin D controlled balance between these two cell types is necessary for proper bone growth and function.(18) Vitamin D regulates many actions of osteoblasts, including cell proliferation, bone matrix synthesis, mineralization, and the initiation of osteoclastogenesis.(19,20)

Vitamin D and VDR are both necessary for the expression of transport channels and proteins necessary for proper calcium absorption from the small intestine.(1) Vitamin D and VDR are also necessary for proper skeletal growth in the young and skeletal maintenance in adults. Vitamin D deficiencies result in the bone-softening disease, rickets, in the young and in osteomalacia in adults.

7.1.4 Immune System Function

VDR is widely expressed in multiple immune cell types, including testosterone lymphocytes, macrophages, and dendritic cells.(21,22) Immune cells are capable of producing and maintaining local concentrations of 1α, 25-dihydroxyvitamin D_3 through the expression of both 1α-hydroxylase and 24-hydroxylase (reviewed in Bouillon et al., 2008(8)). 1α, 25-dihydroxyvitamin D_3 is thought to play a role in the differentiation and

function of immune cells. The lack of vitamin D contributes to the etiology of multiple autoimmune diseases, such as multiple sclerosis, rheumatoid arthritis, inflammatory bowel disease, and type 1 diabetes.(19,23-25) Vitamin D prevents or suppresses autoimmune diseases by preventing the immune system from attacking body tissues, and proper vitamin D supplementation during infancy and childhood has been shown to decrease the incidence of autoimmune disease in adult life.(22)

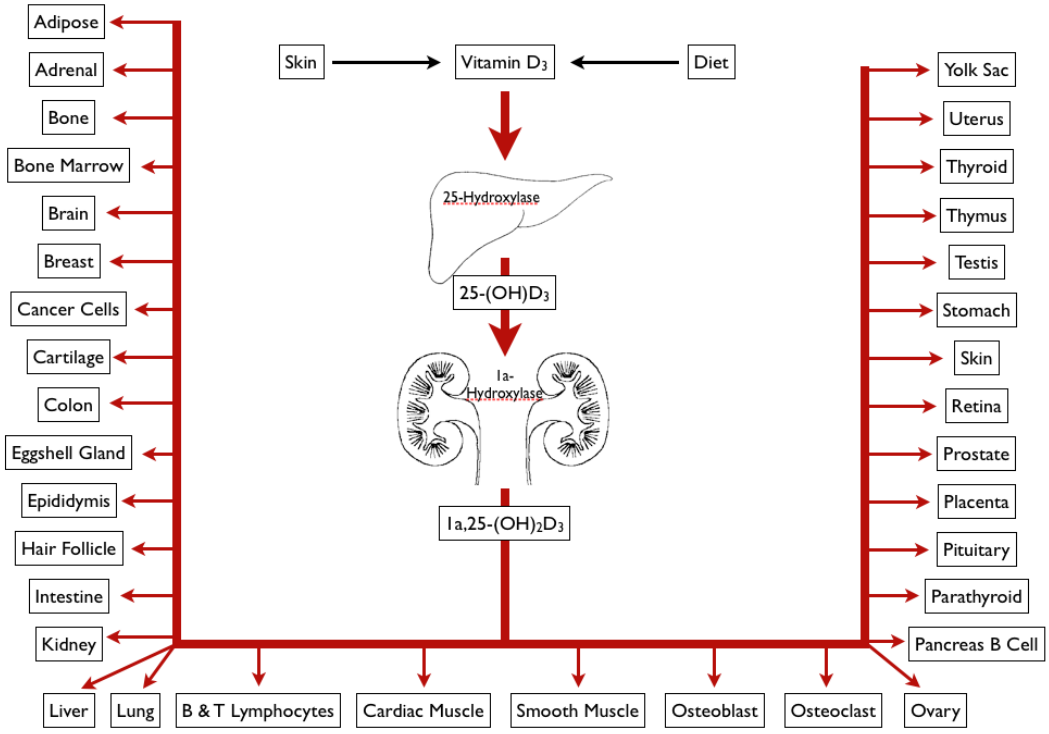

Figure 7-1. Vitamin D synthesis and sites of action.

Vitamin D is either synthesized in the skin or obtained through the diet. Vitamin D_3 is transported to the liver and undergoes the first hydroxylation reaction by 25-hydroxylase, creating 25-hydroxyvitamin D_3. This compound is transported to the kidneys for the second

hydroxylation by 1α-hydroxylase to create the active metabolite: 1α, 25-hydroxyvitamin D_3. The active form is carried in the blood to multiple tissues in the body, where its biological functions are mediated though binding to and activating the VDR. The list of tissues for this diagram was taken from Table 1 in Norman.(2)

7.1.5 Cancer

VDR and vitamin D status have an inverse relationship with the incidence of multiple cancers, including breast, colon, and prostate cancers. Additionally, there is an inverse relationship between many cancers and UVB exposure.(19) The activation of VDR by vitamin D in cancer cells has been shown to inhibit cancer cell proliferation, induce apoptosis, inhibit angiogenesis, and decrease the metastatic potential of cancer cells. Vitamin D analogs are currently being studied as potential therapeutic agents in cancer treatment.(1,19)

7.1.6 Neurodevelopment

The vitamin D receptor and P450 enzymes involved in vitamin D synthesis and catabolism are expressed in the brain, CNS, and PNS.(1,19) Vitamin D is an important neurosteroid, with critical roles in vertebrate brain development.(26,27) Numerous studies have shown that gestational vitamin D deficiency results in offspring with abnormal brain development. Developmental alterations in mouse models include abnormal brain size, increased cell proliferation, decreased cortical brain thickness, and altered neurotransmitter production.(26,27) The effects of developmental vitamin D deficiency are often permanent in adulthood.

Vitamin D activates both tyrosine hydroxylase and choline acetyltransferase, which are important for the production of dopamine, noradrenaline, adrenaline, and acetylcholine. These neurotransmitters are known to have roles in neurobehavioral disorders such as autism, schizophrenia, and ADHD. Vitamin D deficiency has been linked to an increased risk for these disorders. Many risk factors for vitamin D deficiency, such as living in areas with little UV light exposure, are also linked to increased risk for schizophrenia, autism, and other mental health disorders.(26,27)

Although vitamin D deficiencies can result in neurodevelopmental disorders, adequate levels of vitamin D may have neuroprotective effects. For example, vitamin D increases levels of nerve growth factor (NGF), which is believed to counteract neural degeneration in Alzheimer's disease.(28) Vitamin D also helps defend the brain against oxidative degeneration by increasing the expression of γ-glutamyltranspeptidase. This enzyme is involved in the production of the antioxidant glutathione.(26) Vitamin D has also been shown to protect against the neurotoxic effects of the street drug methamphetamine.(29)

7.1.7 Cardiac Function

Cardiac disease is the most common cause of mortality and morbidity in the United States. Many cardiovascular cells express VDR and respond to 1α, 25-dihydroxyvitamin D_3. One such system is the renin-angiotensin system directly regulates blood pressure and electrolyte homeostasis. Renin is a protease that cleaves angiotensin I from angiotensinogen. Angiotensin I is converted to angiotensin II, which exerts its effects on multiple organs to regulate blood pressure and electrolyte balance. The production of angiotensin II is tightly

regulated, and the overproduction of angiotensin II has been linked to hypertension, heart attack, and stroke.(30) 1α, 25-dihydroxyvitamin D_3-bound VDR directly inhibits renin expression by binding to the VDRE in the promoter of the renin gene. In VDR-null mice, renin expression was increased, leading to hypertension, cardiac hypertrophy, and increased water intake. Vitamin D supplementation was shown to significantly decrease blood pressure in multiple human studies.(31) There is a strong correlation between vitamin D deficiency and many cardiovascular diseases, including hypertension, coronary artery disease, and heart failure.(31)

7.1.8 Metabolism of Secondary Bile Acids

Bile acids are end products of cholesterol metabolism that play an important role in the intestinal absorption of lipids.(32) Bile acids aid in lipid digestion by breaking up large lipids into smaller droplets, and aid lipid absorption by forming water-soluble micelles around the droplets. Bile acids are produced in the liver and secreted into the duodenum. Bile acids are stored in the gallbladder between meals. After lipids are digested and absorbed, bile acids are returned to the liver through enterohepatic circulation.

Not all bile acids are recycled. In the large intestine, bile acids may undergo bacterial dehydroxylation, forming a new compound. These end products are called “secondary” bile acids, in reference to the role of the bacterial modification in their creation. “Primary” bile acids refer to bile acids that are synthesized from cholesterol in the hepatocyte of the liver.(33) The most common secondary bile acid in humans is lithocholic acid (LCA). LCA is formed from the primary bile acid chenodeoxycholic acid (CDCA). Unlike CDCA, LCA is

a highly toxic and carcinogenic compound and has been shown to cause DNA strand breaks, form DNA adducts,and inhibit DNA repair enzymes, and has been linked to colon cancer.(34) There is a positive correlation among high-fat diets, increased LCA concentrations, and colon cancer.

LCA is broken down in the intestine by the P450 enzyme CYP3A4, which is also under the regulatory control of vitamin D, suggesting that vitamin D has an important role in LCA detoxification. LCA and its major metabolites have been shown to be VDR ligands, binding to and activating VDR and inducing the expression of CYP3A4.(35,36) Other bile acid receptors such as FXR and PXR can be activated by LCA, but VDR is activated at much lower concentrations. Vitamin D increases CYP3A4 expression, thus decreasing the levels of LCA. Indeed, vitamin D and calcium levels are related to reduced incidence of colon cancer, and vitamin D supplementation reduces colon cancer risk.(34) VDR-mediated protection against colon cancer is decreased in situations, resulting in vitamin D deficiency or in high-fat diets. The highest death rates from colon cancer occur in areas with a high prevalence of rickets.(34)

It should be noted that vertebrate bile acid and alcohol evolution is extremely complex, with many vertebrates having bile acids or alcohols that are unique to that species. For a detailed, in-depth review of vertebrate bile acids and alcohols, see Hagey et al.(32) and Hofmann et al.(37)

7.2 Consequences of Disruption

Most of the current knowledge of the consequences of vitamin D signaling pathway disruption has been gained through the use of knock-out mouse models and, to a lesser extent, studying vitamin D-related diseases in humans. Few studies have addressed vitamin D signaling disruption in wildlife. VDR knock-out mice are born phenotypically normal, but show decreased levels of calcium absorption after weaning. The decreased serum calcium levels lead to hypocalcemia, hyperparathyroidism, and elevated serum 1α, 25-dihydroxyvitamin D_3 levels. These animals develop severe growth retardation, rickets, and osteomalacia. Bones of VDR knock-out mice are more fragile compared to their wild type counterparts due to decreased bone mineralization and the uncoupling of bone remodeling. VDR is necessary for proper calcium absorption, and the lack of calcium absorption in the VDR knock-out is thought to be responsible for the skeletal phenotype seen. This phenotype can be "rescued" with a high calcium diet, supporting the hypothesis of decreased calcium absorption as the cause for the skeletal phenotype. 1α-hydroxylase knock-out mice show a similar skeletal phenotype, although these mice have undetectable levels of 1α, 25-dihydroxyvitamin D_3 and elevated levels of 25-hydroxyvitamin D_3. The skeletal phenotype of the 1α-hydroxylase knock-out can be rescued with the administration of 1α, 25-dihyroxyvitamin D_3 and a high calcium diet.(1,8,38) In humans, vitamin D–dependent rickets type I (VDDR-I) is associated with the loss of 1α-hydroxylase, and vitamin D–dependent rickets type II (VDDR-II) is associated with the loss of VDR. The knock-out mouse models for 1α-hydroxylase and VDR are both used as animal models of human disease.

The role of vitamin D extends beyond the skeleton. Knock-out mouse models have shown that the disruption of the vitamin D endocrine pathway can have detrimental impacts on additional vitamin D target systems. As described above in Section 7.1.6, *Neurodevelopment*, vitamin D is important for vertebrate neural development. VDR knock-out mice display abnormal muscle and motor behavior and abnormal cognition.(8) Numerous studies have shown that gestational vitamin D deficiency results in offspring with abnormal brain development. Developmental alterations in mouse models include abnormal brain size, increased cell proliferation, decreased cortical brain thickness, and altered neurotransmitter production.(26,27) The effects of developmental vitamin D deficiency on the nervous system are often permanent in adulthood.

VDR is widely expressed in the immune system and is necessary for proper immune system function. Impaired immune defense has been linked to vitamin D deficiency.(1) The loss of vitamin D is also linked to an increased risk for multiple autoimmune diseases. The loss of vitamin D and VDR also have been linked to increased risk for heart disease and many types of cancer.(8)

7.3 Precedent Chemicals

7.3.1 2,3,7,8-tetrachlorodibenzo-p-dioxin (TCDD)

The VDR maintains high substrate fidelity; thus, few EDCs are likely to interact with this receptor directly.(4) However, studies in laboratory animals and wildlife exposed to dioxins (such as TCDD) and dioxin-like compounds have shown altered vitamin D_3 serum levels and associated bone malformations.(39-43) Although this evidence suggests that

dioxins may be disrupting the vitamin D endocrine system, it is fairly clear that dioxins are not VDR ligands.(6) Dioxins are ubiquitous and persistent environmental contaminants and potent endocrine disruptors in multiple biological systems. The effects of dioxin exposure include reduced reproductive success, decreased survival of early life stages, and perturbations in growth and development.(44) Classic signs of TCDD toxicity in teleosts include alterations in cardiovascular development and function, craniofacial malformations, delayed growth, and death.(44,45) Effects of TCDD are mediated by the AhR in vertebrates. Although the endogenous ligand and role for AhR are unknown, AhR has an important role in the metabolism of many xenobiotics.(46) Xenobiotic detoxification is the classic role of AhR. It is also thought to be associated with organogenesis and development.(46,47) Like VDR, AhR is expressed in both osteoblasts and osteoclasts.(48,49) TCDD has been shown to inhibit osteoblast differentiation and osteoclastogenesis, but the mechanism(s) of action remain unknown.(48,50) Vitamin D 1-hydroxylase and 24-hydroxylase, the two most important P450 enzymes for maintaining vitamin D homeostasis, have recently been shown to be AhR targets.(41,51)

The current understanding of putative association(s) between TCDD, vitamin D, and the resulting effects on bone development and remodeling is poor. Few studies have evaluated the effects of TCDD on bone formation, and even fewer studies have included the assessment of a putative vitamin D mechanism. One study found that mouse pups that were lactationally exposed to TCDD had increased expression levels of 1-hydroxylase and increased levels of serum vitamin D.(42) Lake Ontario is highly contaminated with dioxins, and minks consuming fish from the lake have a specific jaw lesion that is considered a

biomarker for TCDD exposure.(40) While there are likely several mechanistic links between AhR activation and bone/cartilage modifications, few studies have examined AhR modifications within the vitamin D endocrine axis.

7.3.2 Polychlorinated Biphenyls (PCBs)

Polychlorinated biphenyls (PCBs) are persistent organic pollutants that were commonly used as coolants and insulators in capacitors and transformers. Exposure to PCBs has been shown to alter bone homeostasis, strength, and composition. Few studies exist that assess PCB effects on vitamin D_3. Alvarez-Lloret et al.(43) found decreased serum vitamin D_3 levels and decreased bone mineralization and composition in rats exposed to PCB126. Lilienthal et al.(42) also noted decreased serum vitamin D_3 levels in rats exposed to a PCB mixture. Wild seals exposed to high PCB and DDT levels exhibited bone lesions that may have been related to a disruption of the vitamin D and thyroid hormone pathways.(39) The exact mechanism of action of PCB disruption of the vitamin D endocrine pathway is unknown, but may involve AhR activation.

7.3.3 Ethanol

Chronic alcohol consumption can alter bone growth and remodeling, resulting in decreased bone density and an increased risk of bone fractures.(52) Studies in rats have shown that chronic alcohol consumption results in reduced serum 1α, 25-dihydroxyvitamin D_3 levels as a result of both decreased CYP27B1 and increased CYP24A1 expression.(53) Other studies have shown similar results in rats and chickens.(54,55)

7.3.4 Lead

Many VDR polymorphisms exist in the human population. Some are associated with decreased bone density, hyperparathyroidism, resistance to vitamin D, and increased susceptibility to infections, autoimmune diseases, and cancers.(1) Three VDR polymorphisms— *BsmI, ApaI, FokI* (named for their identifying restriction sites)—have been shown to affect lead concentrations in whole blood and plasma.(56) Lead accumulates in bone tissue during bone growth and remodeling and has been shown to compete with calcium for common transport mechanisms.(57) During normal bone remodeling, stored lead is released into the bloodstream. Individuals who are homozygous for these polymorphisms have lower concentrations of lead in their whole blood and plasma.(56) It is thought that these polymorphisms produce a less-functional VDR, which could potentially reduce lead accumulation in the bone, leading to lower blood and plasma concentrations from bone remodeling. More studies are needed to better understand the functionality of these polymorphisms. Lead is teratogenic to the developing fetus, and one study has suggested that the presence of all three of these polymorphisms may have a protective effect on the fetus against lead exposure.(58) Although these VDR polymorphisms may have a protective effect against lead toxicity, it is important to remember that these VDR polymorphisms may be less functional and could cause other health consequences related to the vitamin D endocrine system.

7.4 In Vitro Assays

There are very few studies that have evaluated the effects of contaminants on the vitamin D signaling pathway. Of those conducted, specific endpoints incorporated include assessment of contaminants on serum vitamin D levels, vitamin D receptor binding, transcriptional activation of vitamin D target genes, and assessment of apical endpoints within the vitamin D endocrine axis, including alterations in skeletal morphology. Common methods used in these studies are summarized below.

7.4.1 Transactivation VDR Reporter Assays

Transactivation reporter assays, as described in previous sections, have been used to assess the responsiveness of VDRs from different species or different isoforms from the same species to vitamin D.(6,59,60) However, we are aware of no reports of the use of a VDR reporter assay to evaluate responsiveness to potential EDCs. The high fidelity of the VDR may severely limit the promiscuity of the receptor. Transactivation reporter assays would be a viable means of assessing chemical interactions with the VDR when structure-activity analysis or apical toxicity suggests such a molecular interaction.

7.4.2 AhR Transactivation Reporter Assays

Considering that AhR agonists can modulate modulate vitamin D levels by inducing enzymes involved in vitamin D metabolism (see Section 7.3.1, *2,3,7,8-tetrachlorodibenzo-p-dioxin*), AhR transactivation assays would facilitate the identification of putative disruptors of vitamin D signaling. AhR transactivation reporter assays are described in Section 5.4.1, *AhR Transactivation Reporter Assay*.

7.5 In Vivo Assays

7.5.1 Serum Vitamin D Levels

Analyses of circulating vitamin D_3 and vitamin D_3 metabolite levels in exposed and non-exposed populations, or in the same animal both before and after exposure to a chemical, are commonly used to assess the vitamin D endocrine axis. As described above, levels of the active metabolite of vitamin D are maintained through tightly regulated feedback mechanisms governing both its synthesis and catabolism. Other vitamin D metabolites, such as 25-hydroxyvitamin D_3, are less regulated. The conversion of pre-vitamin D_3 to 25-hydroxyvitamin D_3 relies on substrate availability and thus reflects the vitamin D status of an animal. Because serum levels of 1α, 25-dihydroxyvitamin D_3 change depending on the vitamin D needs of the animal, clinicians often measure 25-hydroxyvitamin D_3 to determine vitamin D status. A similar assay to the radioimmunoassay is the enzyme immunoassay (EIA). The EIA offers the advantage of not requiring the use of radioactive material.(61) HPLC and LC-MS/MS also are used to measure serum vitamin D levels; however, these approaches have typically not been used in evaluations of chemical-induced endocrine disruption. RIA is by far the most common method used to assess chemical effects on vitamin D levels. See Wallace et al.(61) for a thorough review of methods and commercial assays.

RIA and EIA assays have been successfully used to determine serum vitamin D levels in both laboratory animals and wildlife. Routti et al.(39) used radioimmunoassay to determine circulating levels of 1α, 25-dihydroxyvitamin D_3 in seals exposed to DDT and

PCBs and found decreased levels of 1α, 25-dihydroxyvitamin D_3 in exposed populations. Shankar et al.(53) used this approach to measure both serum 25-hydroxyvitamin D_3 and 1α, 25-dihydroxyvitamin D_3 levels in rats after long term ethanol exposure. They observed that ethanol decreased 1α-hydroxylase expression and increased 24-hydroxylase expression, resulting in reduced levels of 1α, 25-dihydroxyvitamin D_3. Levels of 25-hydroxyvitamin D_3 remained unchanged. Nishimura et al.(41) employed an enzyme immunoassay to determine serum 1α, 25-dihydroxyvitamin D_3 levels in neonatal mice that were lactationally exposed to TCDD. They found that exposure to TCDD caused an increase in serum 1α, 25-dihydroxyvitamin D_3 levels as a result of increased 1α-hydroxylase expression.

7.5.2 Microarrays

Microarrays have been used previously to unravel the molecular pathway involved in vitamin D signaling, as well as the effects of vitamin D on various target tissue and cancers.(8) To date, microarrays have not been used to study toxicant-induced gene expression changes within the vitamin D endocrine pathway. Microarrays could be a very useful tool to study the effects of a toxicant on the genes involved in vitamin D signaling. Microarrays could also be used to discover previously unknown vitamin D–related genes that are targets of toxicants of concern.

7.5.3 Skeletal Morphology and Bone Densitometry

Mineral ion homeostasis within bone is a classical VDR responsive target, and while vitamin D endocrine system has an effect on numerous tissue types, most studies have

focused upon the development of skeletal abnormalities in response to chemical disruption. Skeletal abnormalities accompanied by changes in vitamin D status are typically evaluated by measuring changes in various bone characteristics, such as bone mineral density, bone mineral content, bone thickness, mechanical strength, changes in cell content, and gross changes in skeletal structure. Although these measurements are quite useful when looking at changes in bone morphology, they require specialized equipment that is not available in most laboratories.

Nishimura et al.(41) and Finnilä et al.(62) examined the tibias of mice exposed to TCDD for changes in bone characteristics, while Alvarez-Lloret et al.(43) used lumbar vertebra in PCB126 exposed Sprague-Dawley rats. All three groups measured bone mineral density, bone mineral content, and bone thickness, but Finnilä's group also measured the cross-sectional area. Nishimura's group made their measurements using dual energy X-ray absorptiometric analysis, while the Finnilä group and Alvarez-Lloret used peripheral quantitative computed tomography (pQCT). All three groups found that exposure to TCDD or PCB126 caused a significant decrease in bone mineral density, bone thickness, and bone mineral content. Nishimura et al. and Alvarez-Lloret et al. reported decreased vitamin D levels in the treated mice. Finnilä et al.(62) did not measure vitamin D levels.

7.5.4 Histology

Histological approaches have been employed to assess both cellular and gross morphological changes following exposure to compounds that may target the vitamin D axis. In general, target tissues are fixed, dehydrated, embedded, and sectioned onto slides. After

the tissues are mounted, a wide variety of stains can be used to help visualize the cells or tissues of interest. For example, many contaminants, such as TCDD and PCBs, have been shown to alter bone development. A number of stains can be used to visualize these alterations: Alizarin red S and alcian blue to differentiate between calcified structures and cartilage, alkaline phosphatase to stain bone-forming osteoblasts, tartrate-resistant acid phosphatase (TRAP) to stain bone-resorbing osteoclasts, and Villanueva's Goldner stain to differentiate between mineralized and unmineralized bone.

Histology is a common method used in many studies that have examined the effects of contaminants on bone. Nishimura et al.(41) stained tibia sections from 21-day-old TCDD-exposed mice with Villanueva's Goldner stain to distinguish between mineralized and unmineralized bone. These slides were used in morphometric bone analysis. They also used a TRAP staining method to stain for osteoclasts to determine if TCDD induced osteoclastic bone formation. Immunohistochemical approaches can also been used to infer modification of protein expression of target genes following disruption within the vitamin D signaling axis. For example, Nishimura et al.(41) examined calbindin-D28K and 1α-hydroxylase proteins in the kidneys of mice exposed to TCDD and visualized calbindin-D28K in the small intestine and PTH in the parathyroid gland.

7.6 Current Challenges and Limitations

7.6.1 Limited Knowledge Regarding Non-mammalian Vertebrates

Most of our knowledge regarding the vitamin D endocrine system has come from mammalian studies. Studies performed with non-mammalian vertebrates suggest that the

vitamin D signaling pathway may have important differences among taxa. For example, teleost fish have two copies of the VDR as a result of a whole-genome duplication event specific to the teleost lineage. Mammals and other vertebrates only have one copy.(60,63) The fact that VDR has been cloned from the sea lamprey (*Petromyzon marinus*) and the little skate (*Leucoraja erinacea*)—two vertebrates lacking a calcified skeleton—suggests that early VDR may have additional functions other than calcium mobilization.(64) Studies in *Xenopus* have shown that VDR is expressed before bone formation takes place.(59) Howarth et al.(60) has shown that teleost VDR paralogs have different sensitivities to vitamin D. Additional studies are needed to fully elucidate the functions of early vertebrate VDR and its role in the vitamin D endocrine system.

7.6.2 Broaden Focus beyond Skeletal Effects

While it is well known that vitamin D plays a role in numerous systems, tissues, and disease processes, the majority of studies addressing chemical-induced disruption of vitamin D signaling have focused exclusively on bone. Changes in vitamin D levels have been shown to affect many other biological processes, such as development, immune function, nervous system development and function, and disease status (see above); however, apical consequences to these processes resulting from chemical disruption of vitamin D signaling remains largely unknown. The evaluation of additional vitamin D target tissues and systems could broaden our understanding of both the importance of vitamin D signaling and the multi-faceted effects of contaminant exposure (**Table 7-1**).

Table B.1(Table 7-1). Integration of the adverse outcome pathway and OECD conceptual framework with most promising assays to detect and characterize chemical effects on the vitamin D signaling pathway.

Adverse Outcome Pathway	OECD Conceptual Framework	New Assays/ Modified OECD Test Guidelines
	Level 1 Collation of existing data	
Initiating event: 1. Activation/inhibition of VDR 2. Activation of AhR	**Level 2** *In vitro* mechanistic assays	1. VDR transactivation reporter assay 2. AhR transactivation reporter assay
Tissue-level responses 2. Induction of vitamin D metabolizing enzymes	**Level 3** *In vivo* single mechanism effects assays	2. Vitamin D.hydroxylase assay, EROD activity assay (biomarker) (could potentially be applied to any *in vivo* exposure assays)
Organ-level responses 2. Reduced serum vitamin D levels	**Level 4** *In vivo* multiple endocrine mechanism effects assays	2. RIA/EIA for serum vitamin D levels (could potentially be applied to any *in vivo* exposure assays)
Whole organism responses Neuro-developmental abnormalities; reduced skeletal growth	**Level 5** *In vivo* multiple mechanism effects assays	Brain size measurements in rodent offspring; reduced bone length in juvenile rodent (assays have been performed in mice, could potentially be applied to rat 2-generation assays) (TG416)

REFERENCES

1. Dusso A, Brown A, Slatopolsky E. Vitamin D. *Am J Physiol-Renal.* 2005;289(1):F8–F28.

2. Norman AW. From vitamin D to hormone D: Fundamentals of the vitamin D endocrine system essential for good health. *Am J Clin Nutr.* 2008;88(2):491S–499S.

3. Owen G, Zelent A. Origins and evolutionary diversification of the nuclear receptor superfamily. *Cell Mol Life Sci.* 2000;57(5):809–827.

4. Reschly EJ, Krasowski MD. Evolution and function of the NR1I nuclear hormone receptor subfamily (VDR, PXR, and CAR) with respect to metabolism of xenobiotics and endogenous compounds. *Curr Drug Metab.* 2006;7(4):349–365.

5. Whitfield GK, Dang HT, Schluter SF, Bernstein RM, Bunag T, Manzon LA, Hsieh G, Dominguez CE, Youson JH, Haussler MR, Marchalonis JJ. Cloning of a functional vitamin D receptor from the lamprey (Petromyzon marinus), an ancient vertebrate lacking a calcified skeleton and teeth. *Endocrinology.* 2003;144(6):2704-2716.

6. Reschly EJ, Bainy ACD, Mattos JJ, Hagey LR, Bahary N, Mada SR, Ou J, Venkataramanan R, Krasowski MD. Functional evolution of the vitamin D and pregnane X receptors. *BMC Evol Biol.* 2007;7:222.

7. Lock E-J, Waagbo R, Bonga SW, Flik G. The significance of vitamin D for fish: A review. *Aquacult Nutr.* 2010;16(1):100–116.

8. Bouillon R, Carmeliet G, Verlinden L, Van Etten E, Verstuyf A, Luderer HF, Lieben L, Mathieu C, Demay M. Vitamin D and human health: Lessons from vitamin D receptor null mice. *Endocr Rev.* 2008;29(6):726–776.

9. Holick MF, Frommer JE, McNeill SC, Richtand NM, Henley JW, Potts JT. Photometabolism of 7-dehydrocholesterol to previtamin D3 in skin. *Biochem Bioph Res Co.* 1977;76(1):107–114.

10. Holick MF, Chen TC. Vitamin D deficiency: a worldwide problem with health consequences. *Am J Clin Nutr.* 2008;87(4):1080S-1086S.

11. Christakos S, Dhawan P, Liu Y, Peng X, Porta A. New insights into the mechanisms of vitamin D action. *J Cell Biochem.* 2003;88(4):695-705.

12. Cheng JB, Levine MA, Bell NH, Mangelsdorf DJ, Russell DW. Genetic evidence that the human CYP2R1 enzyme is a key vitamin D 25-hydroxylase. *Proc Natl Acad Sci U S A.* 2004;101(20):7711–7715.

13. Schuster I. Cytochromes P450 are essential players in the vitamin D signaling system. *BBA - Proteins and Proteomics.* 2010;1814(1):186-199.

14. Prosser D, Jones G. Enzymes involved in the activation and inactivation of vitamin D. *Trends Biochem Sci.* 2004;29(12):664-673.

15. Nykjaer A, Dragun D, Walther D, Vorum H, Jacobsen C, Herz J, Melsen F, Christensen E, Willnow T. An endocytic pathway essential for renal uptake and activation of the steroid 25-(OH) vitamin D-3. *Cell.* 1999;96(4):507-515.

16. Omdahl JL, Morris HA, May BK. Hydroxylase enzymes of the vitamin D pathway: Expression, function, and regulation. *Annu Rev Nutr.* 2002;22(1):139–166.

17. St-Arnaud R, Arabian A, Travers R, Barletta F, Raval-Pandya M, Chapin K, Depovere J, Mathieu C, Christakos S, Demay MB, Glorieux FH. Deficient mineralization of intramembranous bone in vitamin D-24-hydroxylase-ablated mice is due to elevated 1,25-dihydroxyvitamin D and not to the absence of 24,25-dihydroxyvitamin D. *Endocrinology.* 2000;141(7):2658-2666.

18. Clarke B. Normal bone anatomy and physiology. *Clin J Am Soc Nephrol.* 2008;3 Suppl 3:S131–139.

19. Nagpal S, Na S, Rathnachalam R. Noncalcemic actions of vitamin D receptor ligands. *Endocr Rev.* 2005;26(5):662–687.

20. van Driel M, Pols HAP, van Leeuwen JPTM. Osteoblast differentiation and control by vitamin D and vitamin D metabolites. *Current Pharmaceutical Design.* 2004;10(21):2535-2555.

21. Veldman C. Expression of 1,25-dihydroxyvitamin D3 receptor in the immune system. *Arch Biochem Biophys.* 2000;374(2):334–338.

22. Mathieu C, Van Etten E, Decallonne B, Guilietti A, Gysemans C, Bouillon R, Overbergh L. Vitamin D and 1,25-dihydroxyvitamin D-3 as modulators in the immune system. *J Steroid Biochem.* 2004;89-90(1-5):449-452.

23. Compston A, Coles A. Multiple sclerosis. *The Lancet.* 2008;372(9648):1502-1517.

24. Hanwell HEC, Banwell B. Assessment of evidence for a protective role of vitamin D in multiple sclerosis. *BBA - Molecular Basis of Disease.* 2010;1812(2):202-212.

25. Danescu LG, Levy S, Levy J. Vitamin D and diabetes mellitus. *Endocrinology.* 2009;35(1):11–17.

26. Humble MB. Vitamin D, light and mental health. *Journal of Photochemistry & Photobiology, B: Biology.* 2010;101(2):142-149.

27. Cannell JJ. Autism and vitamin D. *Med Hypotheses.* 2008;70(4):750-759.

28. Cattaneo A, Capsoni S, Paoletti F. Towards non invasive nerve growth factor therapies for Alzheimer's disease. *J Alzheimers Dis.* 2008;15(2):255–283.

29. Cass WA, Smith MP, Peters LE. Calcitriol protects against the dopamine- and serotonin-depleting effects of neurotoxic doses of methamphetamine. *Ann N Y Acad Sci.* 2006;1074:261–271.

30. Li A, Zhu X, Brown B, Craft CM. Gene expression networks underlying retinoic acid-induced differentiation of human retinoblastoma cells. *Invest Ophthalmol Vis Sci.* 2003;44:996–1007.

31. Vanga SR, Good M, Howard PA, Vacek JL. Role of Vitamin D in Cardiovascular Health. *AJC.* 2010;106(6):798-805.

32. Hagey LR, Moller PR, Hofmann AF, Krasowski MD. Diversity of bile salts in fish and amphibians: Evolution of a complex biochemical pathway. *Physiol Biochem Zool.* 2010;83(2):308–321.

33. Hofmann AF, Hagey LR. Bile acids: Chemistry, pathochemistry, biology, pathobiology, and therapeutics. *Cell Mol Life Sci.* 2008;65(16):2461–2483.

34. Makishima M, Lu T, Xie W, Whitfield G, Domoto H, Evans R, Haussler M, Mangelsdorf D. Vitamin D receptor as an intestinal bile acid sensor. *Science.* 2002;296(5571):1313–1316.

35. Matsubara T, Yoshinari K, Aoyama K, Sugawara M, Sekiya Y, Nagata K, Yamazoe Y. Role of vitamin D receptor in the lithocholic acid- mediated CYP3A induction in vitro and in vivo. *Drug Metab Dispos.* 2008;36(10):2058–2063.

36. Jurutka PW, Thompson PD, Whitfield GK, Eichhorst KR, Hall N, Dominguez CE, Hsieh J-C, Haussler CA, Haussler MR. Molecular and functional comparison of 1,25-dihydroxyvitamin D(3) and the novel vitamin D receptor ligand, lithocholic acid, in activating transcription of cytochrome P450 3A4. *J Cell Biochem.* 2005;94(5):917–943.

37. Hofmann AF, Hagey LR, Krasowski MD. Bile salts of vertebrates: structural variation and possible evolutionary significance. *J Lipid Res.* 2010;51(2):226–246.

38. Panda DK, Miao D, Tremblay ML, Sirois J, Farookhi R, Hendy GN, Goltzman D. Targeted ablation of the 25-hydroxyvitamin D 1alpha -hydroxylase enzyme: evidence for skeletal, reproductive, and immune dysfunction. *Proc Natl Acad Sci U S A.* 2001;98(13):7498–7503.

39. Routti H, Nyman M, Jenssen BM, Backman C, Koistinen J, Gabrielsen GW. Bone-related effects of contaminants in seals may be associated with vitamin D and thyroid hormones. *Environ Toxicol Chem.* 2008;27(4):873–880.

40. Haynes JM, Wellman ST, Beckett KJ, Pagano JJ, Fitzgerald SD, Bursian SJ. Histological Lesions in Mink Jaws Are a Highly Sensitive Biomarker of Effect After Exposure to TCDD-Like Chemicals: Field and Literature-Based Confirmations. *Arch Environ Con Tox.* 2009;57(4):803-807.

41. Nishimura N, Nishimura H, Ito T, Miyata C, Izumi K, Fujimaki H, Matsumura F. Dioxin-induced up-regulation of the active form of vitamin D is the main cause for its inhibitory action on osteoblast activities, leading to developmental bone toxicity. *Toxicology and Applied Pharmacology.* 2009;236(3):301–309.

42. Lilienthal H, Fastabend A, Hany J, Kaya H, Roth-Harer A, Dunemann L, Winneke G. Reduced levels of 1,25-dihydroxyvitamin D-3 in rat dams and offspring after exposure to a reconstituted PCB mixture. *Toxicol Sci.* 2000;57(2):292–301.

43. Alvarez-Lloret P, Lind PM, Nyberg I, Orberg J, Rodriguez-Navarro AB. Effects of 3,3 ',4,4 ',5-pentachlorobiphenyl (PCB126) on vertebral bone mineralization and on thyroxin and vitamin D levels in Sprague-Dawley rats. *Toxicol Lett.* 2009;187(2):63-68.

44. Jobling S, Tyler C. Endocrine disruption in wild freshwater fish. *Pure Appl Chem.* 2003;75(11-12):2219–2234.

45. Dong W, Matsumura F, Kullman SW. TCDD Induced Pericardial Edema and Relative COX-2 Expression in Medaka (Oryzias Latipes) Embryos. *Toxicol Sci.* 2010;118(1):213-223.

46. Gu Y, Hogenesch J, Bradfield C. The PAS superfamily: Sensors of environmental and developmental signals. *Annu Rev Pharmacol.* 2000;40:519-561.

47. Bock KW, Koehle C. Ah receptor: Dioxin-mediated toxic responses as hints to deregulated physiologic functions. *Biochem Pharmacol.* 2006;72(4):393-404.

48. Ryan EP, Holz JD, Mulcahey M, Sheu T-j, Gasiewicz TA, Puzas JE. Environmental toxicants may modulate osteoblast differentiation by a mechanism involving the aryl hydrocarbon receptor. *J Bone Miner Res.* 2007;22(10):1571–1580.

49. Ilvesaro J, Pohjanvirta R, Tuomisto J, Viluksela M, Tuukkanen J. Bone resorption by aryl hydrocarbon receptor-expressing osteoclasts is not disturbed by TCDD in short-term cultures. *Life Sci.* 2005;77(12):1351-1366.

50. Korkalainen M, Kallio E, Olkku A, Nelo K, Ilvesaro J, Tuukkanen J, Mahonen A, Viluksela M. Dioxins interfere with differentiation of osteoblasts and osteoclasts. *Bone.* 2009;44(6):1134–1142.

51. Matsunawa M, Amano Y, Endo K, Uno S, Sakaki T, Yamada S, Makishima M. The aryl hydrocarbon receptor activator benzo[a]pyrene enhances vitamin D3 catabolism in macrophages. *Toxicol Sci.* 2009;109(1):50–58.

52. Sampson HW. Alcohol's harmful effects on bone. *Alcohol Health Res World.* 1998;22(3):190-194.

53. Shankar K, Liu X, Singhal R, Chen J-R, Nagarajan S, Badger TM, Ronis MJJ. Chronic ethanol consumption leads to disruption of vitamin D3 homeostasis associated with induction of renal 1,25 dihydroxyvitamin D3-24-hydroxylase (CYP24A1). *Endocrinology.* 2008;149(4):1748–1756.

54. Peng T, Lobough B, Lester G, Hirsch P. Ethanol inhibits renal 25-hydroxyvitamin D-1-a-hydroxylase in rats. *Journal of Bone Mineral Research.* 1990;5(245).

55. Kent JC, Devlin RD, Gutteridge DH, Retallack RW. Effect of alcohol on renal vitamin D metabolism in chickens. *Biochemical and Biophysical Research Communications.* 1979;89(1):155–161.

56. Rezende VB, Barbosa F, Jr., Montenegro MF, Sandrim VC, Gerlach RF, Tanus-Santos JE. Haplotypes of vitamin D receptor modulate the circulating levels of lead in exposed subjects. *Arch Toxicol.* 2008;82(1):29–36.

57. Fullmer CS. Lead-calcium interactions: involvement of 1,25-dihydroxyvitamin D. *Environmental research.* 1997;72(1):45-55.

58. Rezende VB, Amaral JH, Quintana SM, Gerlach RF, Barbosa F, Jr., Tanus-Santos JE. Vitamin D receptor haplotypes affect lead levels during pregnancy. *The Science of the total environment.* 2010;408(21):4955-4960.

59. Li YC. Cloning and Characterization of the Vitamin D Receptor from Xenopus laevis. *Endocrinology.* 1997;138(6):2347-2353.

60. Howarth DL, Law SHW, Barnes B, Hall JM, Hinton DE, Moore L, Maglich JM, Moore JT, Kullman SW. Paralogous vitamin D receptors in teleosts: Transition of nuclear receptor function. *Endocrinology.* 2008;149(5):2411–2422.

61. Wallace AM, Gibson S, de la Hunty A, Lamberg-Allardt C, Ashwell M. Measurement of 25-hydroxyvitamin D in the clinical laboratory: current procedures, performance characteristics and limitations. *Steroids.* 2010;75(7):477-488.

62. Finnilä MAJ, Zioupos P, Herlin M, Miettinen HM, Simanainen U, Håkansson H, Tuukkanen J, Viluksela M, Jämsä T. Effects of 2,3,7,8-tetrachlorodibenzo-p-dioxin exposure on bone material properties. *Journal of Biomechanics.* 2010;43(6):1097-1103.

63. Meyer A, Van de Peer Y. From 2R to 3R: evidence for a fish-specific genome duplication (FSGD). *Bioessays.* 2005;27(9):937-945.

64. Whitfield G, Dang H, Schluter S, Bernstein R, Bunag T, Manzon L, Hsieh G, Dominguez C, Youson J, Haussler M, Marchalonis J. Cloning of a functional vitamin D receptor from the lamprey (Petromyzon marinus), an ancient vertebrate lacking a calcified skeleton and teeth. *Endocrinology.* 2003;144(6):2704-2716.

Appendix C

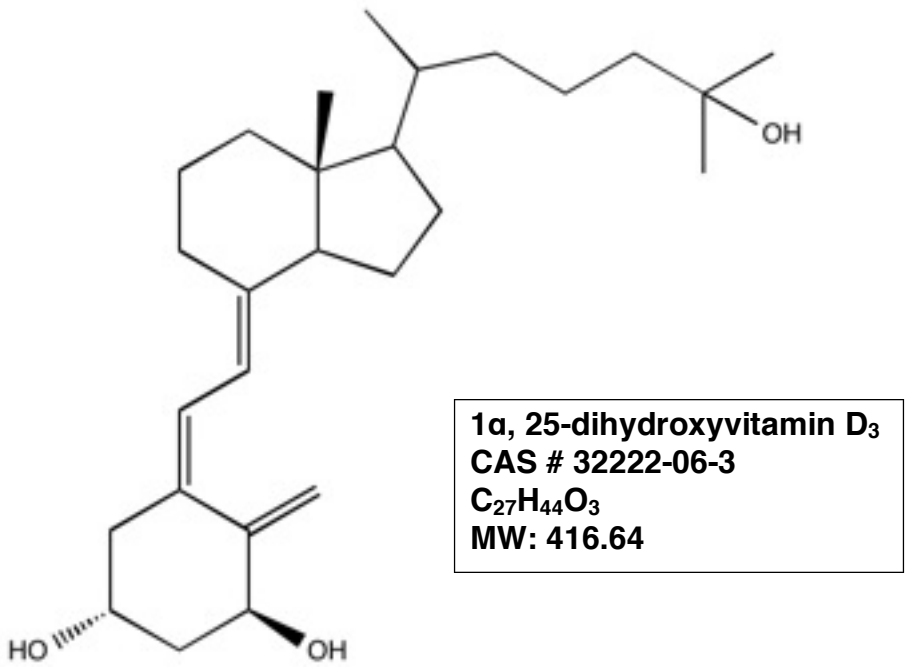

Figure C.1. Chemical structure of 1α, 25-dihydroxyvitamin D_3 (1, $25D_3$), the hormonally active form of vitamin D_3. Structures were created in ChemBioDraw version 13 (Perkin Elmer).

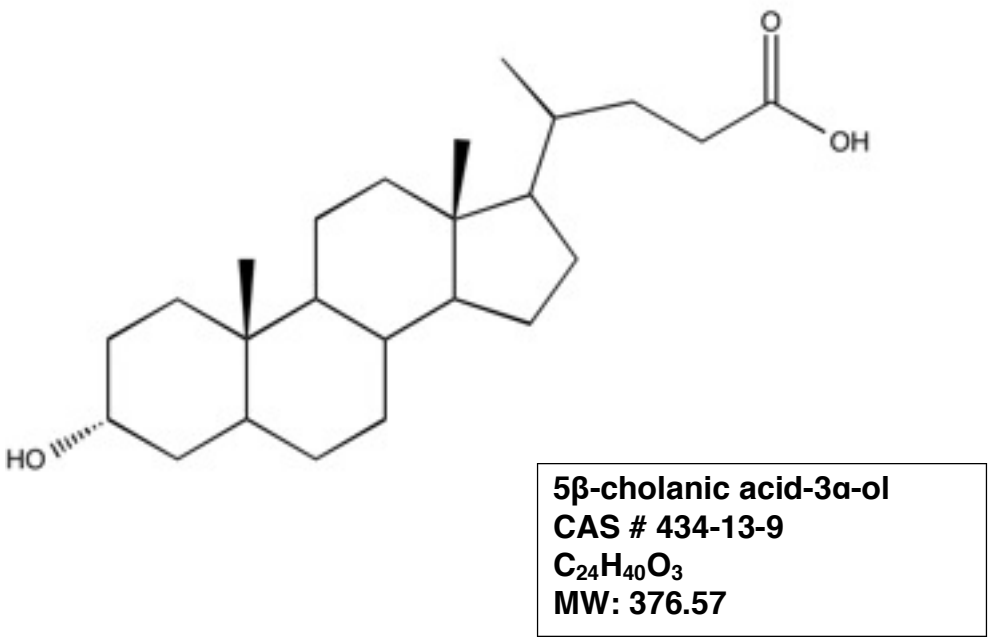

Figure. C.2. Chemical structure of lithocholic acid (LCA), a secondary bile acid. LCA is produced from the bacterial modification of chenodeoxycholic acid (CDCA), a primary bile acid. LCA synthesis takes place in the large intestine.

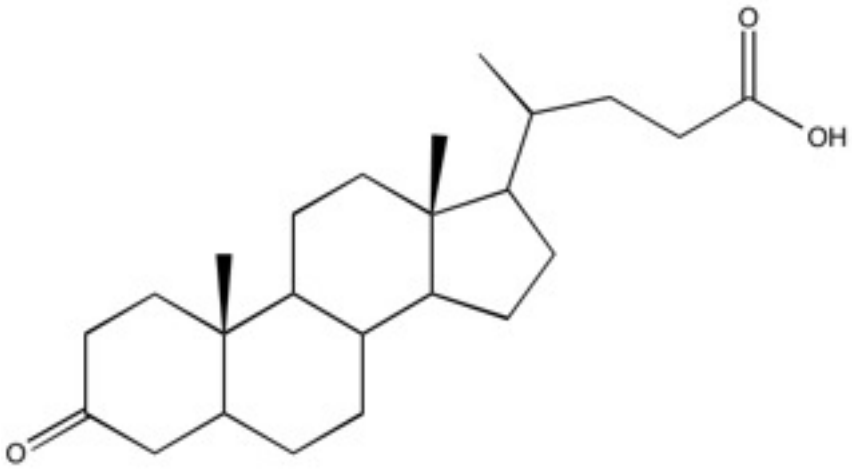

5β-cholanic acid-3-one
CAS # 1553-56-6
$C_{24}H_{38}O_3$
MW: 374.56

Figure C.3. Chemical structure of 3-keto lithocholic acid (3Keto). 3Keto is produced through the oxidation of LCA by CYP3A4.

Appendix D

(Color key located after figure in Appendix E)

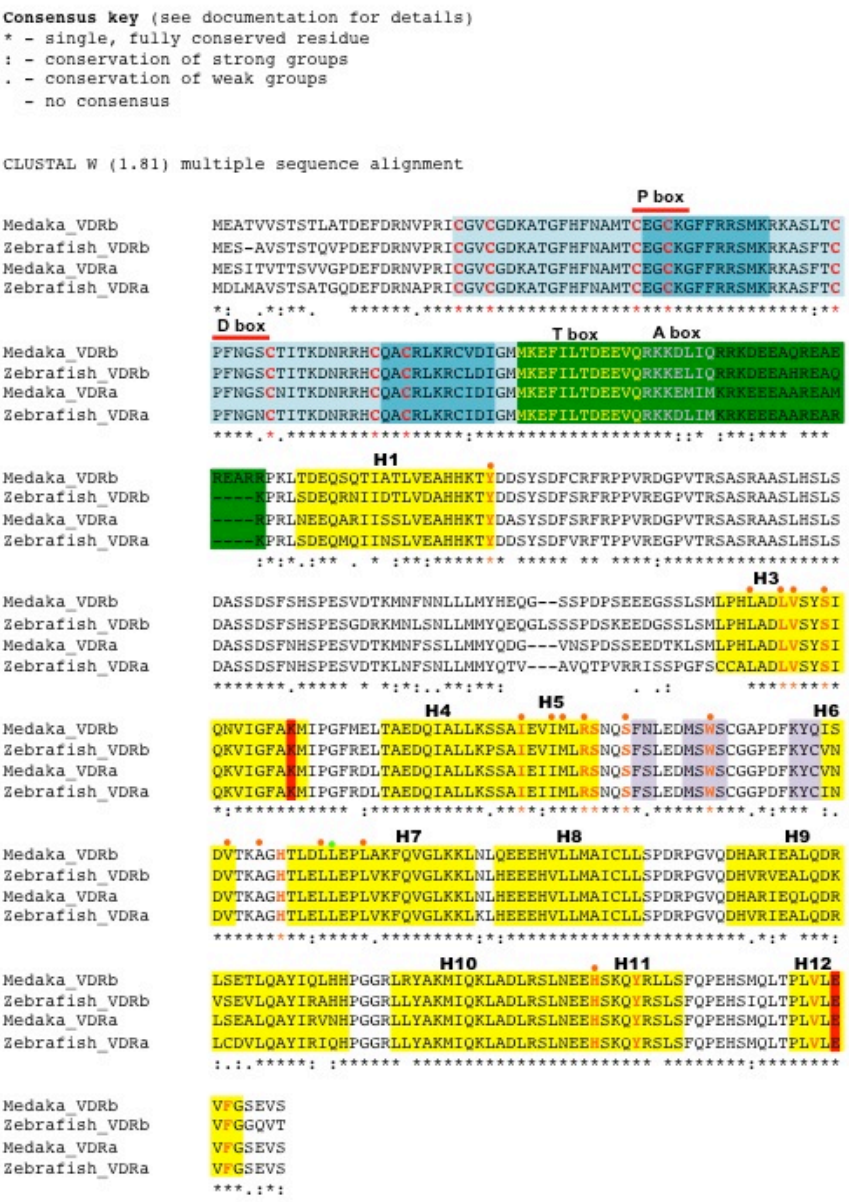

Figure D.1. Alignment of amino acid sequences of medaka and zebrafish VDRα and VDRβ.

Appendix E

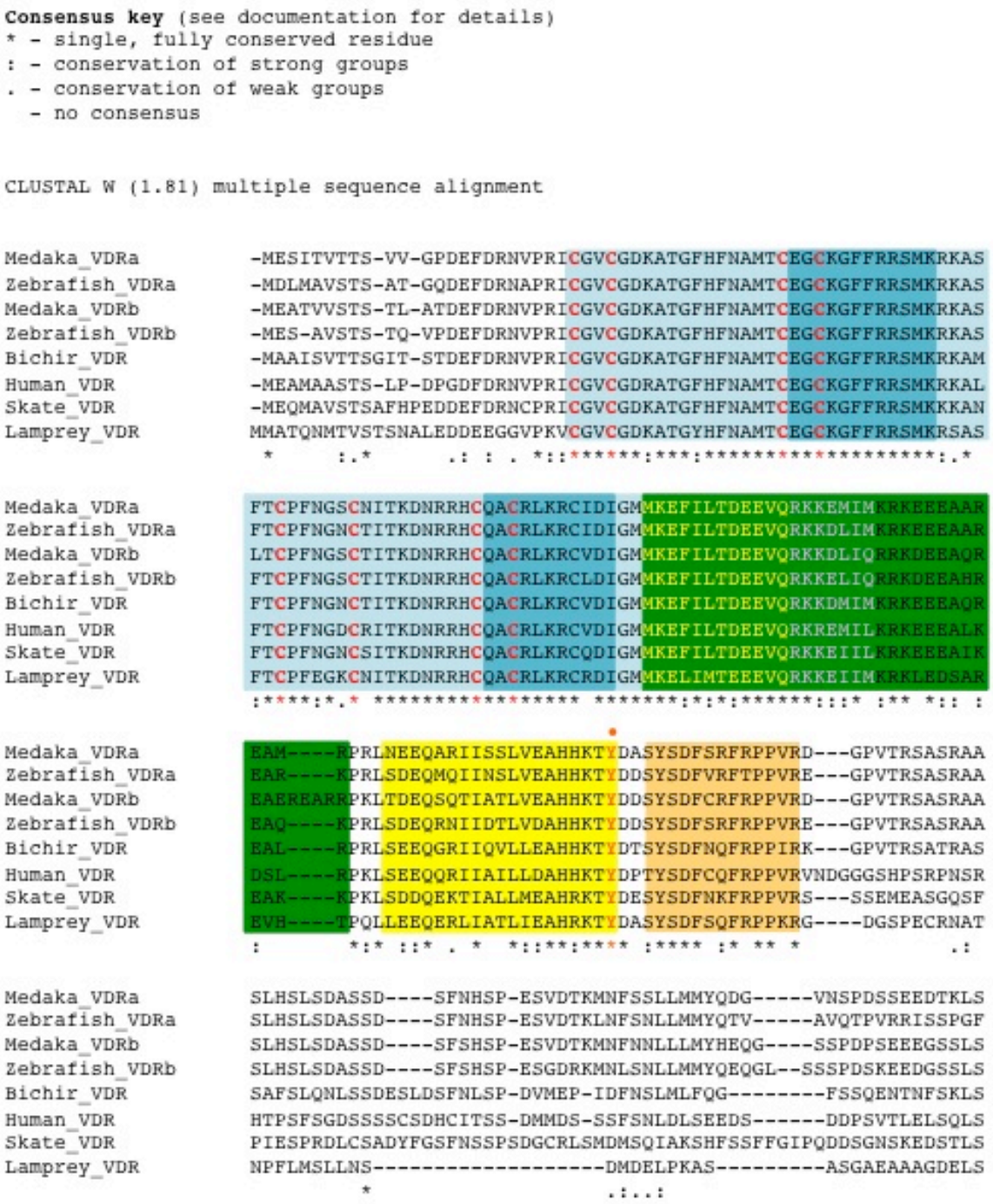
Consensus key (see documentation for details)
* - single, fully conserved residue
: - conservation of strong groups
. - conservation of weak groups
- no consensus
CLUSTAL W (1.81) multiple sequence alignment
Medaka_VDRa -MESITVTTS-VV-GPDEFDRNVPRICGVCGDKATGFHFNAMTCEGCKGFFRRSMKRKAS
Zebrafish_VDRa -MDLMAVSTS-AT-GQDEFDRNAPRICGVCGDKATGFHFNAMTCEGCKGFFRRSMKRKAS
Medaka_VDRb -MEATVVSTS-TL-ATDEFDRNVPRICGVCGDKATGFHFNAMTCEGCKGFFRRSMKRKAS
Zebrafish_VDRb -MES-AVSTS-TQ-VPDEFDRNVPRICGVCGDKATGFHFNAMTCEGCKGFFRRSMKRKAS
Bichir_VDR -MAAISVTTSGIT-STDEFDRNVPRICGVCGDKATGFHFNAMTCEGCKGFFRRSMKRKAM
Human_VDR -MEAMAASTS-LP-DPGDFDRNVPRICGVCGDRATGFHFNAMTCEGCKGFFRRSMKRKAL
Skate_VDR -MEQMAVSTSAFHPEDDEFDRNCPRICGVCGDKATGFHFNAMTCEGCKGFFRRSMKKKAN
Lamprey_VDR MMATQNMTVSTSNALEDDEEGGVPKVCGVCGDKATGYHFNAMTCEGCKGFFRRSMKRSAS
Medaka_VDRa FTCPFNGSCNITKDNRRHCQACRLKRCIDIGMMKEFILTDEEVQRKKEMIMKRKEEEAAR
Zebrafish_VDRa FTCPFNGNCTITKDNRRHCQACRLKRCIDIGMMKEFILTDEEVQRKKDLIMKRKEEEAAR
Medaka_VDRb LTCPFNGSCTITKDNRRHCQACRLKRCVDIGMMKEFILTDEEVQRKKDLIQRRKDEEAQR
Zebrafish_VDRb FTCPFNGSCTITKDNRRHCQACRLKRCLDIGMMKEFILTDEEVQRKKELIQRRKDEEAHR
Bichir_VDR FTCPFNGNCTITKDNRRHCQACRLKRCVDIGMMKEFILTDEEVQRKKDMIMKRKEEEAQR
Human_VDR FTCPFNGDCRITKDNRRHCQACRLKRCVDIGMMKEFILTDEEVQRKREMILKRKEEEALK
Skate_VDR FTCPFNGNCSITKDNRRHCQACRLKRCQDIGMMKEFILTDEEVQRKKEIILKRKEEEAIK
Lamprey_VDR FTCPFEGKCNITKDNRRHCQACRLKRCRDIGMMKELIMTEEEVQRKKEIIMKRKLEDSAR
Medaka_VDRa EAM----RPRLNEEQARIISSLVEAHHKTYDASYSDFSRFRPPVRD---GPVTRSASRAA
Zebrafish_VDRa EAR----KPRLSDEQMQIINSLVEAHHKTYDDSYSDFVRFTPPVRE---GPVTRSASRAA
Medaka_VDRb EAEREARRPKLTDEQSQTIATLVEAHHKTYDDSYSDFCRFRPPVRD---GPVTRSASRAA
Zebrafish_VDRb EAQ----KPRLSDEQRNIIDTLVDAHHKTYDDSYSDFSRFRPPVRE---GPVTRSASRAA
Bichir_VDR EAL----RPRLSEEQGRIIQVLLEAHHKTYDTSYSDFNQFRPPIRK---GPVTRSATRAS
Human_VDR DSL----RPKLSEEQQRIIAILLDAHHKTYDPTYSDFCQFRPPVRVNDGGGSHPSRPNSR
Skate_VDR EAK----KPKLSDDQEKTIALLMEAHRKTYDESYSDFNKFRPPVRS---SSEMEASGQSF
Lamprey_VDR EVH----TPQLLEEQERLIATLIEAHRKTYDASYSDFSQFRPPKRG----DGSPECRNAT
Medaka_VDRa SLHSLSDASSD----SFNHSP-ESVDTKMNFSSLLMMYQDG-----VNSPDSSEEDTKLS
Zebrafish_VDRa SLHSLSDASSD----SFNHSP-ESVDTKLNFSNLLMMYQTV-----AVQTPVRRISSPGF
Medaka_VDRb SLHSLSDASSD----SFSHSP-ESVDTKMNFNNLLLMYHEQG----SSPDPSEEEGSSLS
Zebrafish_VDRb SLHSLSDASSD----SFSHSP-ESGDRKMNLSNLLMMYQEQGL--SSSPDSKEEDGSSLS
Bichir_VDR SAFSLQNLSSDESLDSFNLSP-DVMEP-IDFNSLMLFQG--------FSSQENTNFSKLS
Human_VDR HTPSFSGDSSSSCSDHCITSS-DMMDS-SSFSNLDLSEEDS------DDPSVTLELSQLS
Skate_VDR PIESPRDLCSADYFGSFNSSPSDGCRLSMDMSQIAKSHFSSFFGIPQDDSGNSKEDSTLS
Lamprey_VDR NPFLMSLLNS-------------------DMDELPKAS---------ASGAEAAAGDELS

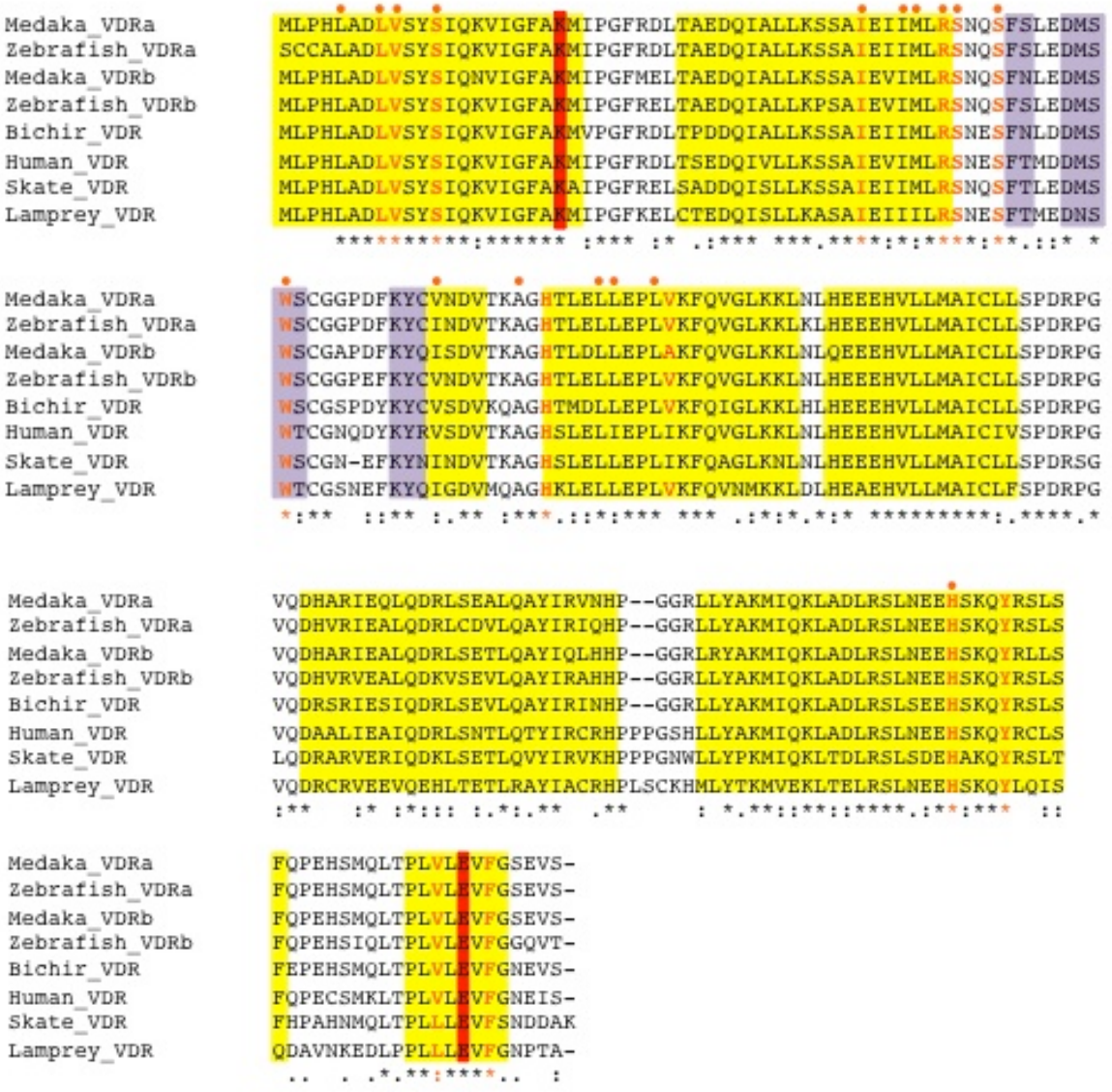

Figure E.1. Alignment of VDR amino acid sequences from all eight species.

COLOR KEY

Red "C".....zinc finger cysteine residue

Light blue box.....DNA binding domain (DBD)

Medium blue boxes.....Helices 1 and 2 in DBD

Green box.....C-terminal extension

Yellow font.....T Box

Purple font.....A box

Yellow boxes.....Helices 1-12 of ligand binding domain (LBD)

Orange box.....Possibly helix 2?

Orange font.....1, 25D_3 residue contacts

• Orange dots.....LCA residue contacts

Purple boxes.....beta sheets in LBD

Red boxes.....charge clamp residues

Appendix F

VDR amino acid sequence homology. Numbers in the table correspond to percent amino acid sequence identity as determined through ClustalW analysis (SDSC Biology workbench, URL http://workbench.sdsc.edu).

Table F.1. Homology of VDR DNA binding domains (DBD).

	L	S	B	ZFα	ZFβ	Mα	Mβ	H
Lamprey	100	87	89	90	90	92	89	87
Skate		100	93	93	92	92	90	90
Bichir			100	96	95	93	95	93
Zebrafishα				100	96	96	96	92
Zebrafishβ					100	96	96	92
Medakaα						100	95	92
Medakaβ							100	92
Human								100

Table F.2. Homology of VDR ligand binding domains (LBD).

	L	S	Bi	ZFα	ZFβ	Mα	Mβ	H
Lamprey	100	59	59	57	61	61	60	60
Skate		100	62	60	63	64	62	62
Bichir			100	74	72	75	73	68
Zebrafish α				100	84	86	82	63
Zebrafish β					100	85	85	66
Medaka α						100	86	68
Medaka β							100	67
Human								100

Table F.3. Homology of full VDR sequences

	L	S	Bi	ZFα	ZFβ	Mα	Mβ	H
Lamprey	100	61	61	61	63	64	62	62
Skate		100	67	66	68	70	65	66
Bichir			100	76	74	77	76	71
Zebrafish α				100	84	86	83	68
Zebrafish β					100	85	86	69
Medaka α						100	85	71
Medaka β							100	70
Human								100

Appendix G

Gar VDR (*Lepisosteus oculatus*)

The spotted far (*Lepisosteus oculatus*) is a member of the order Lepisosteiformes, one of four orders of ray-finned fishes (class: Actinopterygii) that diverged before the teleost 3R duplication event. As a result, gar maintains a single VDR ortholog. While the Polypteryiformes (which includes bichir), was the first lineage to diverge within Actinopterygii and therefore is the most basal order, the Lepisosteiformes were the last lineage to diverge before the teleosts. Because of their unique position within Actinopterygii, both bichir and gar were originally included in the basal VDR accessment in Chapter 2. However, gar VDR proved to be almost nonfunctional. A small increase in transactivation was observed with extremely high doses of 1, $25D_3$ or overexpressed coregulators. Furthermore, recombinant gar VDR protein demonstrated very poor binding to the canonical VDRE. This is in stark contrast to every other VDR, including other basal VDRs such as lamprey and bichir. Despite extensive scrutiny of the nucleotide sequence and multiple recloning efforts, the specific reason driving the lack of function could not be identified. As we could not be sure that the functional response was truly representative of gar VDR function, or if the response was due to a currently unidentified mutation within the sequence, we decided to remove gar from our analysis.

To aid future research, I have included here the methods for cloning gar VDR, as well

as a representative set of results. The methods for each assay can be found in Chapter 2.

CLONING

Total RNA was isolated from whole embryos (stage 28). Embryos were homogenized in 1 mL of RNA Bee (TelTest, Friendswood, RX) using a stainless steel Polytron homogenizer (Kinematica, Newark, NJ) cleaned with RNaseZAP (Sigma), DEPC-treated water, and sterile deionized water. Following homogenization, total RNA was isolated as described by Volz et al. 2005. RNA quantity and 260/280 ratios were determined using a NanoDrop ND-1000 spectrophotometer (NanoDrop, Wilmington, DE).

First-strand cDNA was made from total RNA and diluted with RNase-free water to a final volume of 10 μL, and 1 μL oligo $(dT)_{15}$ (500 μg/mL, Promega, Madison, WI) and 1 μL 10 mM deoxynucleotide triphosphates were mixed with diluted RNA to yield a final volume of 20 μL. The mix was heated to 65ºC for 5 minutes and chilled on ice for 2 minutes. After centrifugation, 4 μL 5X first-strand buffer (Invitrogen, Carlsbad, CA), 2 μL of 0.1 M dithiothreitol and 1 μL RNase OUT inhibitor (40 U/μL; Invitrogen) were added to each reaction and heated to 37ºC. After a 2-minute incubation, 1 μL SuperScript reverse transcriptase (200 U/μL; Invitrogen) was added to each reaction and mRNA reverse transcribed at 37ºC for 1 hour. All reverse transcriptase reactions were then inactivated by incubating at 70ºC for 15 minutes.

Degenerate PCR primers were designed for the based on a conserved central region of the VDR amino acid sequence between amino acid #s 40-384 using known teleost VDR sequences. Forward Primer 1 was 5' – TGY GTN GAY ATH GGN ATG ATG – 3; Forward Primer 2 5' – GGN TTY CAY TTY AAY GCN ATG – 3'; reverse primer 1 5' – RTC NGC NTR VTT VTG DAT CAT – 3'; reverse primer 2 5' – KTT KTG DAT CAT TTY NGC RTA – 3'. Degeneracy code: D = A, G, T; H = A, C, T; N = any base; R = A or G; V = C, A, G; Y = C or T (IDT DNA). For each 25 μL PCR, VDR was amplified using 1 μL cDNA, 1 μL forward primer, 1 μL reverse primer, 12.5 μL GoTaq PCR Master Mix (Promega) and 9.5 μL nuclease free water. A touchdown PCR protocol was used with the following conditions: 95ºC for 4 minutes to start, followed a denaturing step of 95ºC for thirty seconds, 62ºC for thirty seconds for the primers to anneal, and an elongation step at 72ºC for 1.5 minutes. These three steps were repeated thirty four times with a 0.5ºC decrease in annealing temperature with each cycle. After the final cycle was completed, a second cycle began: 95ºC for 30 seconds, 45ºC for 30 seconds, and 72ºC for 1.5 minutes. These three cycles were repeated 29 times. The thermocycle was held at 72ºC for 7 minutes after the final cycle was completed. PCR products were run on a 1.5% agarose gel, and 1.3 kB bands were isolated and cloned into the TA cloning vector pCR2.1 (Invitrogen) as per manufacturer's suggestions. Positive clones were isolated and sequenced.

3' and 5' Rapid amplification of cDNA ends (RACE) was conducted using a cDNA library from gar embryos (from Postlewaithe lab) to identify both 3' and 5' ends of gar VDR using the SMART™ RACE cDNA amplification system (Clontech). Inner and outer RACE

primers were designed using Primer3. 3'RACE outer 5' – ACA AGG GCT GGA CAC ACA ATG – 3'; 3'RACE inner 5' – GAG GAG CAT GTG CTG CTG ATG – 3'; 5'RACE outer 5' – CTC CTT CAT CAT GCC GAT CT – 3'; 5'RACE inner 5' – CGG TTG TCC TTG GTT ATG GT – 3'. [what is primer #7968?]

Once the 5' and 3' regions were sequenced, primers were designed to amplify the entire gar VDR sequence. Restriction sites were incorporated into each primer to aid in vector ligation. Forward primer 5' – CGC GAA TTC ATG GAA TCA ATG GCA GTG AGC – 3'; Reverse primer 5' – TAT GGA TCC CTA GGA CAC CTC GCT GCC AAA – 3'. Full length gar VDR was amplified, digested using incorporated EcoR1 and BglII sites, gel purified, ligated into the pSG5 vector, and transformed into TOP10 cells (Invitrogen). Colonies were isolated and sequenced. Positive colonies were grown overnight in 250 mL LB/amp and isolated using the HiSpeed MaxiPrep kit (QIAGEN).

FIGURES

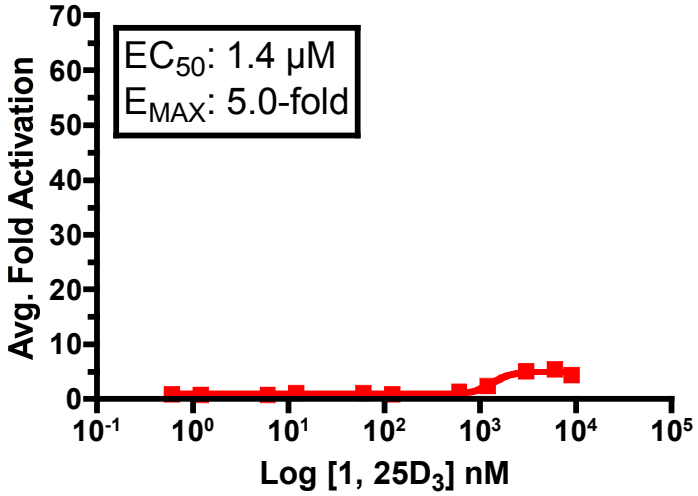

Figure G.1. Concentration-response curve of Gar VDR transactivation in response to 0 – 9 µM 1, 25D_3. HepG2 cells were transiently transfected with pSG5-Gar VDR, XREM-Luc, and *Renilla* as described in Materials and Methods of Chapter 2. Cells were treated with 0 – 9 µM 1, 25D_3 in medium for 24 hours. VDR response was measured via dual-luciferase assays. Luciferase response to normalized to the *Renilla* control, and VDR response was normalized to the ethanol control (0 µM). The EC_{50} and the E_{MAX} were determined using nonlinear regression analysis using a sigmoidal dose-response calculation with variable slope in GraphPad Prism 4.

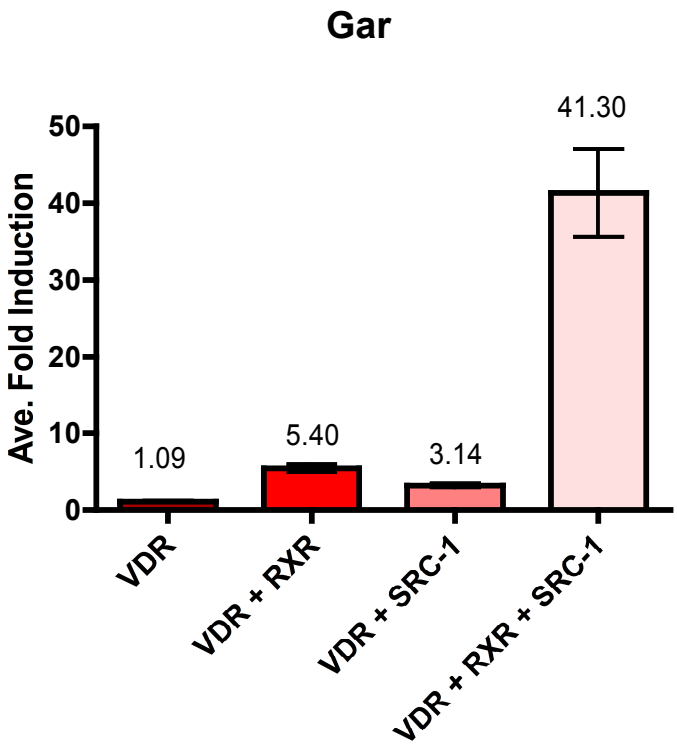

Figure G.2. Gar VDR transactivation in response to 1, 25D_3, in the presence and absence of cotransfected RXR and/or SRC-1. HepG2 cells were transiently transfected with pSG5-Gar VDR, XREM-Luc, and *Renilla* as described in Materials and Methods of Chapter 2. Cells were treated with 120 nM 1, 25D_3 in medium for 24 hours. VDR response was measured via dual luciferase assays. Luciferase response was first normalized to *Renilla*, followed by VDR response normalized to the empty pSG5 control. NOTE: previous coregulator studies normalized VDR+coreg response to VDR in the absence of coregulators, not the empty pSG5 vector. Data are represented as the average fold activation ± SEM.

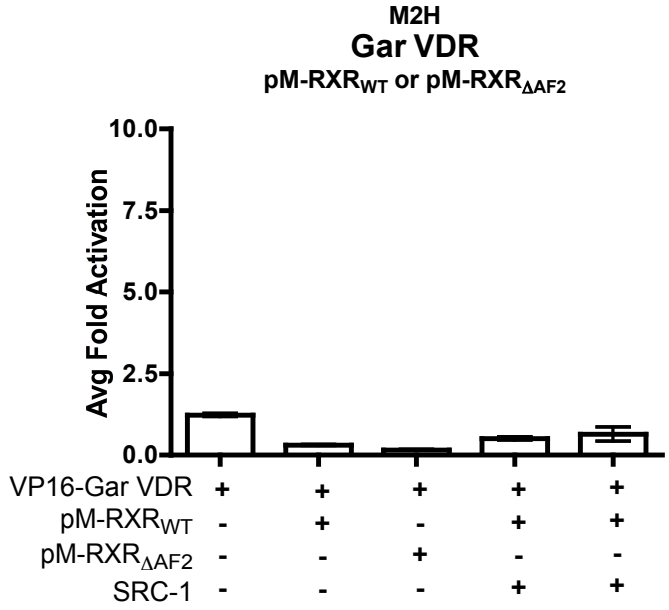

Figure G.3. Mammalian 2-hybrid analysis of VDR heterodimerization with RXR in response to 120 nM 1, 25D3. RXR interaction was accessed with both a wild type construct, and a truncated RXR mutant lacking the c-terminal AF2 region. Assays were conducted in the presence or absence of cotransfected SRC-1. HepG2 cells were transiently transfected with pVP16-Gar VDR, 5XGal4-TATA-Luc, and *Renilla,* as well as pM-RXR$_{WT}$, pM-RXR$_{AF2}$, and SRC-1 where indicated, as described in Materials and Methods of Chapter 2. Cells were treated with 120 nM 1, 25D$_3$ in medium for 24 hours. VDR response was measured via dual luciferase assays. Luciferase response was normalized to *Renilla*, and VDR-RXR interaction was normalized to VDR in absence of coregulators. No VDR-RXR interaction was detected with any assay condition tested.

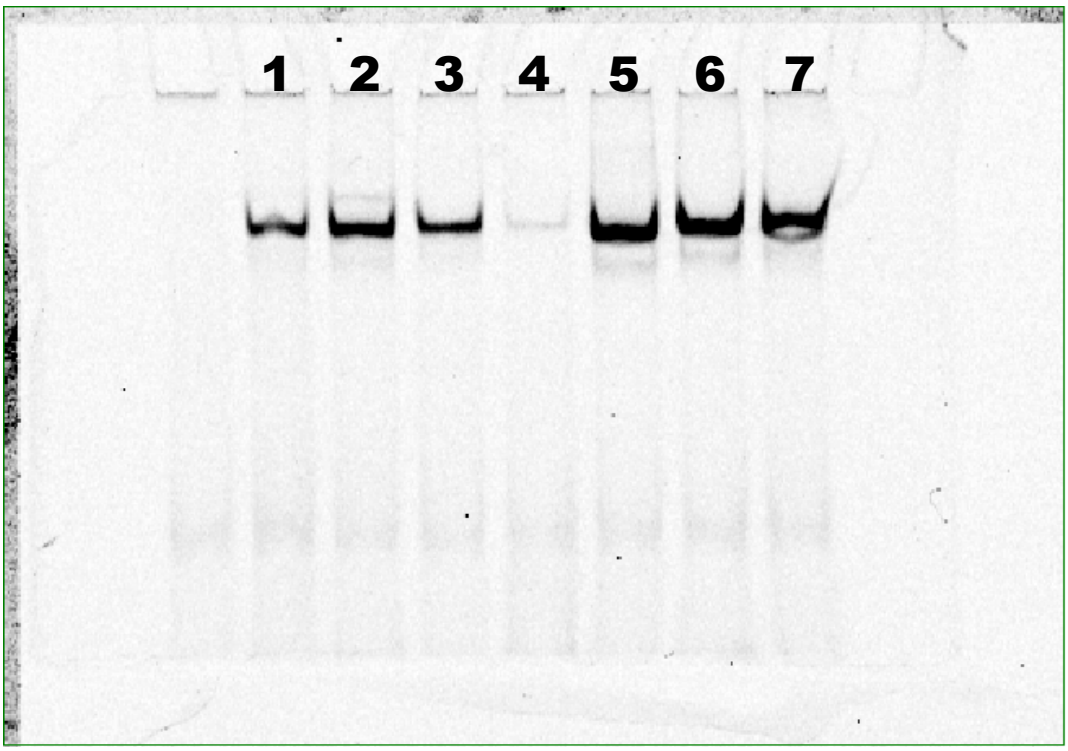

Figure G.4. Electrophoretic mobility shift analysis of VDR-RXR forming a binding complex with the canonical VDRE in response to 1, 25D_3. See Chapter 2 for materials and methods. Lanes are identified as follows: 1 – lamprey, 2 – skate, 3 – bichir, 4 – gar, 5 – human, 6 – medaka VDRα, 6 – medaka VDRβ. This figure illustrates the attenuated degree of binding of Gar VDR in comparison to the other VDRs tested.

Gar full sequence homology:

Lamprey 60
Skate 66
Bichir 78
Zebrafish a 80
Zebrafish b 80
Medaka a 85
Medaka b 80
Human 69

Consensus key (see documentation for details)
* - single, fully conserved residue
: - conservation of strong groups
. - conservation of weak groups
  - no consensus

CLUSTAL W (1.81) multiple sequence alignment

```
Medaka_VDRb          -MEATVVSTSTLA--TDEFDRNVPRICGVCGDKATGFHFNAMTCEGCKGFFRRSMKRKAS
Zebrafish_VDRb       -MES-AVSTSTQV--PDEFDRNVPRICGVCGDKATGFHFNAMTCEGCKGFFRRSMKRKAS
Zebrafish_VDRa       -MDLMAVSTSATG--QDEFDRNAPRICGVCGDKATGFHFNAMTCEGCKGFFRRSMKRKAS
Medaka_VDRa          -MESITVTTSVVG--PDEFDRNVPRICGVCGDKATGFHFNAMTCEGCKGFFRRSMKRKAS
Gar_VDR              -MESMAVSTSVMGS-ADEFDRNVPRICGVCGDKATGFHFNAMTCEGCKGFFRRSMKRKAT
Bichir_VDR           -MAAISVTTSGITS-TDEFDRNVPRICGVCGDKATGFHFNAMTCEGCKGFFRRSMKRKAM
Human_VDR            -MEAMAASTSLPD--PGDFDRNVPRICGVCGDRATGFHFNAMTCEGCKGFFRRSMKRKAL
Skate_VDR            -MEQMAVSTSAFHPEDDEFDRNCPRICGVCGDKATGFHFNAMTCEGCKGFFRRSMKKKAN
Lamprey_VDR          MMATQNMTVSTSNALEDDEEGGVPKVCGVCGDKATGYHFNAMTCEGCKGFFRRSMKRSAS
                      *     :.*      .: : . *::******:***:********************:.*

Medaka_VDRb          LTCPFNGSCTITKDNRRHCQACRLKRCVDIGMMKEFILTDEEVQRKKDLIQRRKDEEAQR
Zebrafish_VDRb       FTCPFNGSCTITKDNRRHCQACRLKRCLDIGMMKEFILTDEEVQRKKELIQRRKDEEAHR
Zebrafish_VDRa       FTCPFNGNCTITKDNRRHCQACRLKRCIDIGMMKEFILTDEEVQRKKDLIMKRKEEEAAR
Medaka_VDRa          FTCPFNGSCNITKDNRRHCQACRLKRCIDIGMMKEFILTDEEVQRKKEMIMKRKEEEAAR
Gar_VDR              FTCPFNGSCTITKDNRRHCQACRLKRCVEIGMMKEFILTDEEVQRKKDLIMKRKEEEALR
Bichir_VDR           FTCPFNGNCTITKDNRRHCQACRLKRCVDIGMMKEFILTDEEVQRKKDMIMKRKEEEAQR
Human_VDR            FTCPFNGDCRITKDNRRHCQACRLKRCVDIGMMKEFILTDEEVQRKREMILKRKEEEALK
Skate_VDR            FTCPFNGNCSITKDNRRHCQACRLKRCQDIGMMKEFILTDEEVQRKKEIILKRKEEEAIK
Lamprey_VDR          FTCPFEGKCNITKDNRRHCQACRLKRCRDIGMMKELIMTEEEVQRKKEIIMKRKLEDSAR
                     :****:*.* ***************** :******:*:*:*******:::* :** *:: :

Medaka_VDRb          EAEREARRPKLTDEQSQTIATLVEAHHKTYDDSYSDFCRFRPPVRDGPVTRS-ASRAASL
Zebrafish_VDRb       EAQ----KPRLSDEQRNIIDTLVDAHHKTYDDSYSDFSRFRPPVREGPVTRS-ASRAASL
Zebrafish_VDRa       EAR----KPRLSDEQMQIINSLVEAHHKTYDDSYSDFVRFTPPVREGPVTRS-ASRAASL
Medaka_VDRa          EAM----RPRLNEEQARIISSLVEAHHKTYDASYSDFSRFRPPVRDGPVTRS-ASRAASL
Gar_VDR              EAS----RPRLSEEQSRVISMLVEAHRKTYDDSYSDFKQFRPPVREGPVTRS-ASRAASL
Bichir_VDR           EAL----RPRLSEEQGRIIQVLLEAHHKTYDTSYSDFNQFRPPIRKGPVTRS-ATRASSA
Human_VDR            DSL----RPKLSEEQQRIIAILLDAHHKTYDPTYSDFCQFRPPVRVNDGGGSHPSRPNSR
Skate_VDR            EAK----KPKLSDDQEKTIALLMEAHRKTYDESYSDFNKFRPPVRSSSEMEA-SGQSFPI
Lamprey_VDR          EVH----TPQLLEEQERLIATLIEAHRKTYDASYSDFSQFRPPKRGDGSPECRNATNPFL
                     :       *:* ::* . *  *::**:**** :**** :* ** * .    .
```

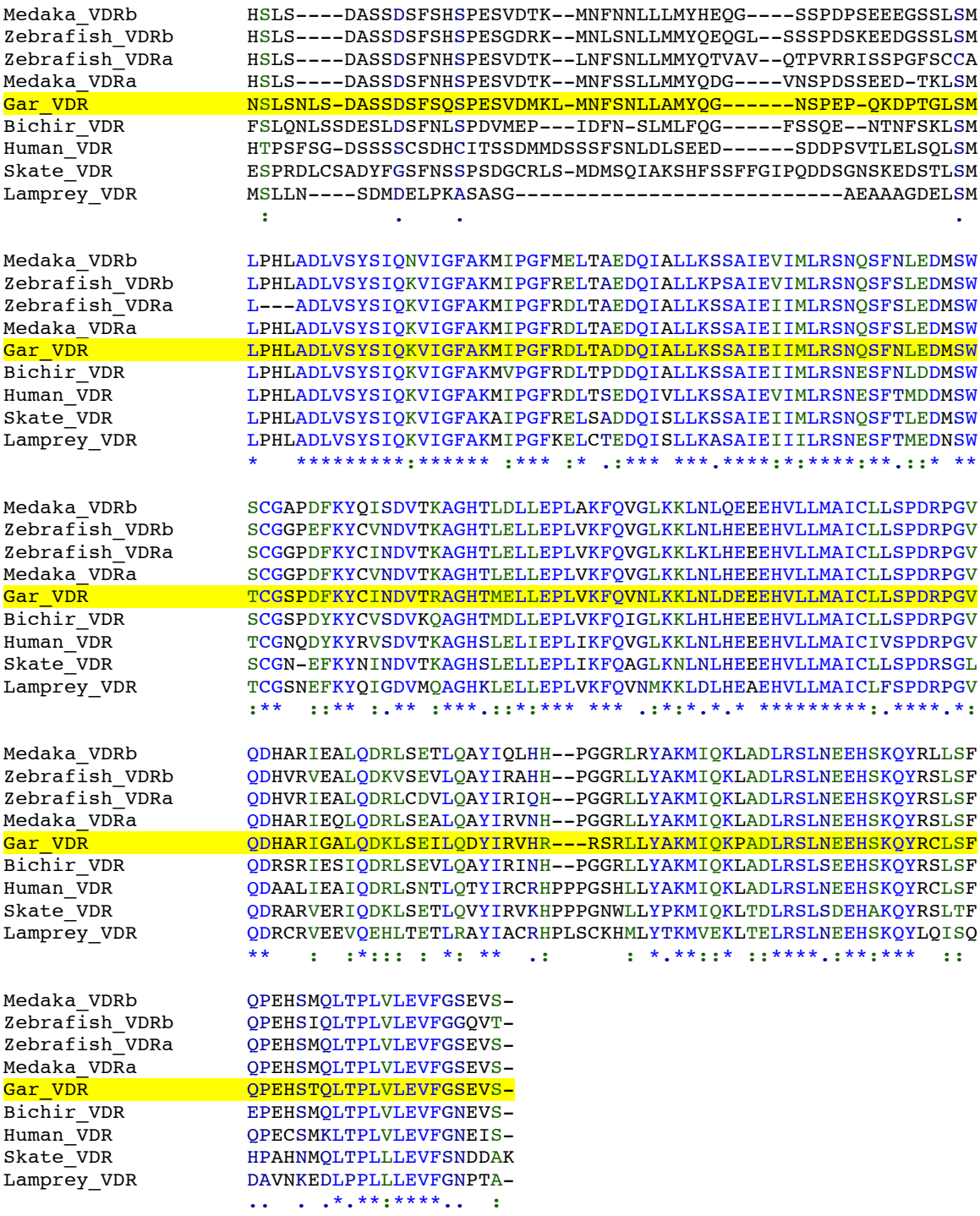

Figure G.5. Sequence alignment of gar VDR with other eight VDR amino acid sequences.

Alignment done in ClustalW (SDSC Biology Worbench. URL: workbench.sdsc.edu).

Appendix H

VDR-RXR permissive studies

Receptors that heterodimerize with RXR have been demonstrated to form both permissive and non-permissives heterodimers. In a permissive heterodimer, such as those formed with the liver X receptor (LXR), the farnesoid X receptor (FXR), and the peroxisome proliferator-activated receptor (PPAR), both RXR and the NR may bind their cognate ligands and initiate transcription (1,2). In contrast, a nonpermissive heterodimer is one where only the NR partner may bind a ligand and induce transactivation. The transcriptional activities of RXR are suppressed (1,2). Nuclear receptors such as the vitamin D receptor (VDR) and the thyroid receptor (TR) form nonpermissive heterodimers with RXR (3).

The goal of this study was to determine if the non-permissive characteristic of the VDR-RXR heterodimer has been conserved across evolution. HepG2 cells were transfected with pSG5-VDR, pCDNA-RXR_{WT}, along with XREM-Luc and Renilla as described in materials and methods. Cells were treated with either 1) 100 nM 1, $25D_3$, 2) 100 nM LG208, a synthetic RXR agonist, or 3) the combination of 100 nM 1, 25D3 and LG268, a synthetic RXR antagonist. Luciferase response was determined with a dual luciferase assay as described previously.

Our results indicate that the VDR-RXR heterodimer for lamprey, human, and the medaka and zebrafish VDR paralogs is nonpermissive. The use of the RXR agonist did not induce VDR transactivation for any species. The use of the RXR antagonist with 1, $25D_3$ did

not have any effect on 1, 25D_3-mediated VDR transactivation. These results suggest that the non-permissive characteristic of this heterodimer has been conserved since first true VDR appeared in Agnathans.

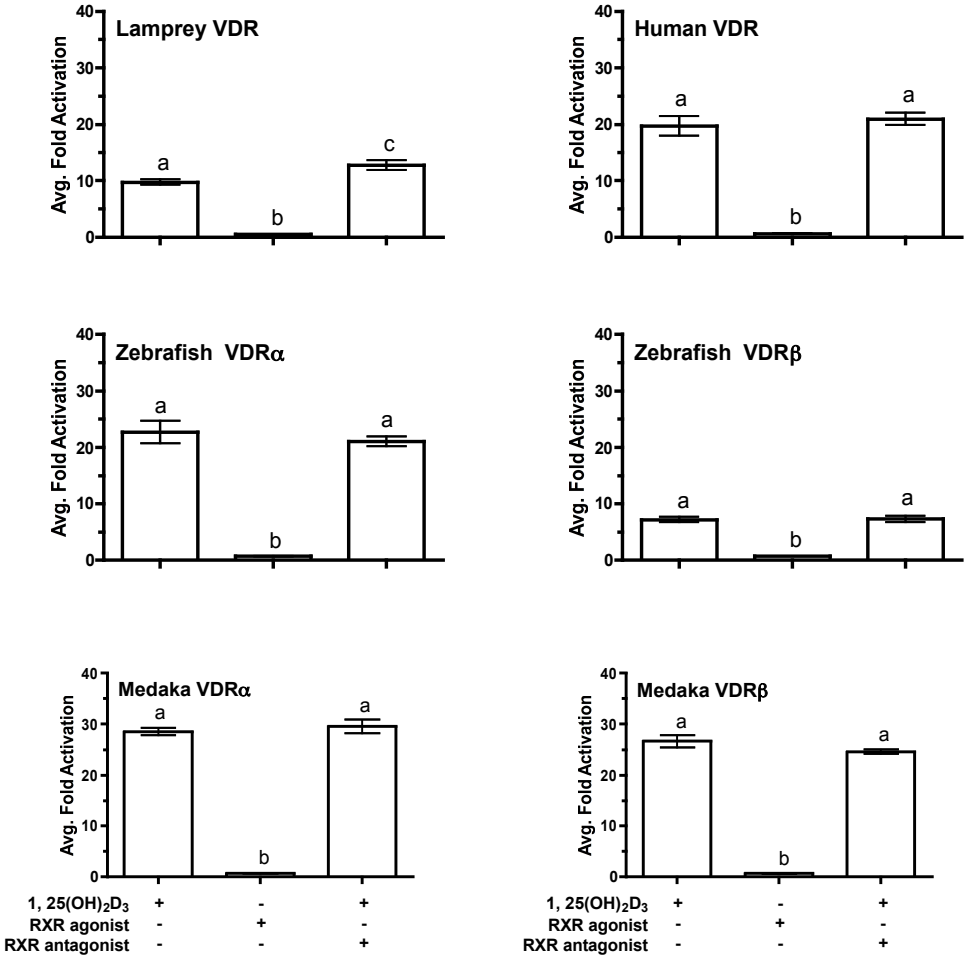

Figure H.1. Results from the permissive studies. HepG2 cells were transiently transfected with pSG5-VDR, pCDNA-RXR_{WT}, along with XREM-Luc and Renilla as described previously in Materials and Methods of the dissertation chapters. Cells were treated with 100 nM 1, $25D_3$, 100 nM RXR agonist (LG268), or the combination of 100 nM 1, $25D_3$ and 100 nM RXR antagonist (LG208). Cells were treated in media for 24 hours. VDR transactivation was measured via dual-luciferase assays. Data are represented as the mean fold activation

normalized to the empty pSG5 vector control ± SEM. Significance difference between assays was determined by a one-way ANOVA followed by Tukey's HSD post hoc test. No significant difference in VDR transactivation was detected in response to 1, $25D_3$ in the presence or absence of the RXR antagonist. The use of the RXR agonist did not induce VDR transactivation beyond background levels.

REFERENCES

1. Aranda A, Pascual A. Nuclear hormone receptors and gene expression. *Physiol Rev.* 2001;81(3):1269-1304.

2. Gronemeyer H, Gustafsson J, Laudet V. Principles for modulation of the nuclear receptor superfamily. *Nat Rev Drug Discov.* 2004;3(11):950-964.

3. Bettoun D, Burris T, Houck K, Buck D, Stayrook K, Khalifa B, Lu J, Chin W, Nagpal S. Retinoid X receptor is a nonsilent major contributor to vitamin D receptor-mediated transcriptional activation. *Mol Endocrinol.* 2003;17(11):2320-2328.

Appendix I

Domain Swaps

The purpose of this study was to explore the hypothesis that transactivational differences between the VDRα and VDRβ paralogs were attributed to specific functional domains. The DNA binding domain (DBD) and ligand binding domain (LBD) of medaka VDRα and VDRβ were switched as described below (Fig. I.1). Transactivation assays were conducted with full length medaka VDRα, medaka VDRβ, and the two domain swamp constructs medaka $VDR\alpha_{DBD}$-β_{LBD}, and $VDR\beta_{DBD}$-α_{LBD}. If transactivational differences were ascribed to a specific domain, we expected the swap mutant containing the responsible domain to mediate transactivation in a similar manner to the full length construct. As illustrated in the graphs of figure I.2, the transactivational response of the domain swap constructs did not recapitulate the response observed with either full length VDR paralog. These results indicate that both the DBD and the LBD contribute to the observed transactivational differences between VDRα and VDRβ. This is an important point, considering a major take-home point of each chapter emphasized the importance of coregulator interaction as an important driver of VDR functional evolution. The majority of coregulator-receptor interact occurs within the LBD. These results suggest that differences within the DBD may also be responsible. Further studies are necessary to rule out possible structure problems within the domain swaps.

MATERIALS AND METHODS

Medaka VDRα and VDRβ were excised from the pSG5 expression construct described in Chapter 1. Excised ~1200 base pair products were gel purified using the Wizard SV PCR cleanup system (Promega). The 1200 bp product was cut with StyI, yielding a 200 bp fragment containing the DBD, and a 1000 bp fragment containing the LBD of each VDR paralog. The DBD fragment from VDRα was ligated to the LBD fragment from VDRβ, and the DBD fragment from VDRβ was ligated to the LBD fragment from VDRα using T4 DNA ligase following the manufacturers protocol. Following ligation, each domain swap was PCR amplified using the previously described PCR protocol from chapter 1. The medaka VDRαDBD-βLBD product was amplified using the pSG5-medaka VDRα forward primer, and the pSG5-medaka VDRβ reverse primer (see Appendix A for primer sequences). The medaka VDRβDBD-αLBD was amplified using the pSG5-medaka VDRβ forward primer and the pSG5-medaka VDRα reverse primer. PCR products were run on a 1.5% agarose gel, and 1.2 kB bands were isolated and cloned into the pGEM-T easy vector (Promega) as per manufacturer's suggestions. Positive clones were selected based on a blue/white screen, and were isolated and sequenced. Following screening, cDNAs for each domain swap were subcloned into the pSG5 expression vector (Agilent Technologies) for transient transactivation studies. All constructs were restriction mapped and sequenced to ensure integrity and orientation of each VDR within defined vectors.

Transient transactivation assays were conducted as described in Chapter 1. Transactivation assays were conducted in the presence and absence of RXR_{WT} and SRC-1.

All assays were conducted with 120 nM 1, $25D_3$ as the primary ligand. Assays were additionally conducted with full length medaka VDRα and VDRβ for comparative purposes.

FIGURES

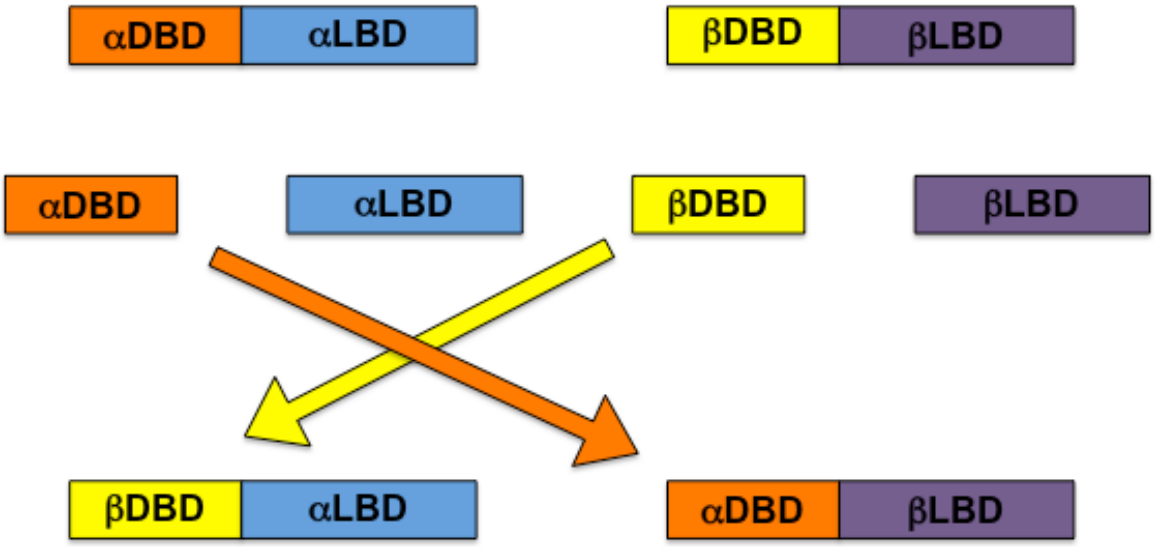

Figure I.1. Diagram depicting the domain swaps. The DBD and LBD of medaka VDRα and VDRβ were separated via restriction digest. The DBD of VDRα was ligated to the LBD of VDRβ, and the DBD of VDRβ was ligated to the LBD of VDRα.

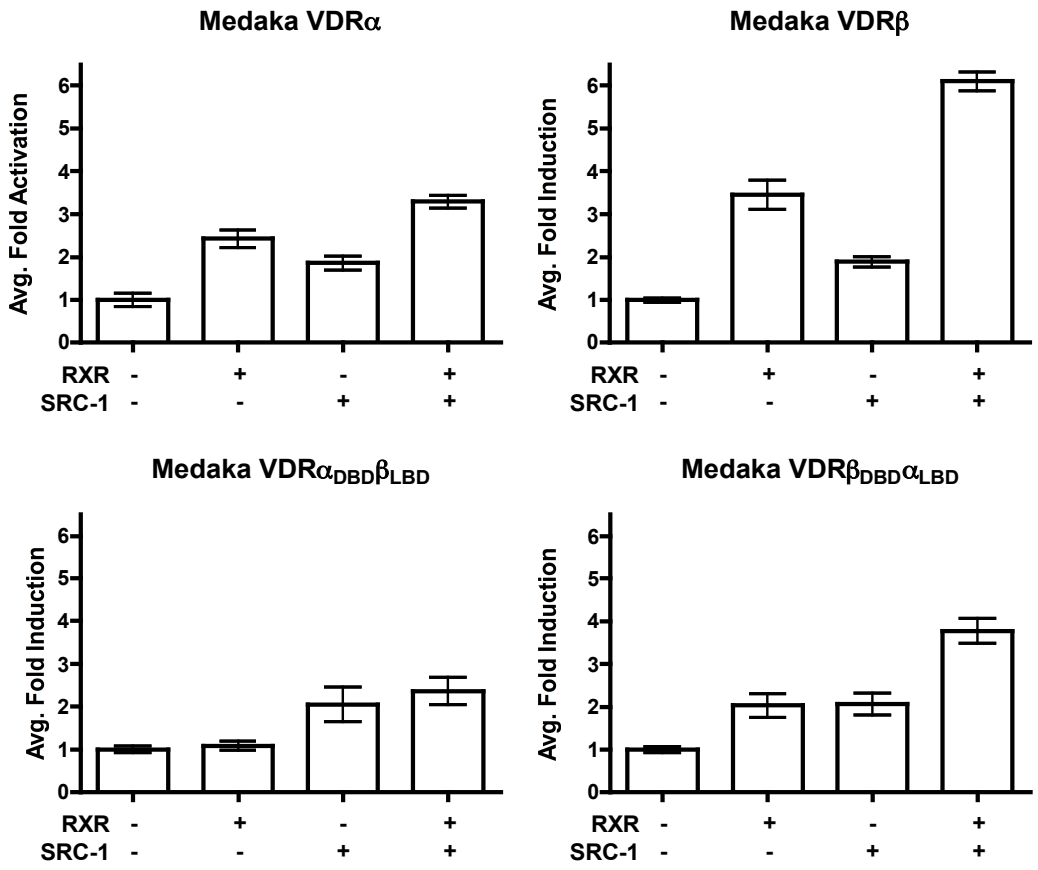

Figure I.2. Transactivation in response to 1, 25 D3 in the presence and absence of RXRWT and SRC-1, in response to 1, 25D_3. HepG2 cells were transiently transfected with pSG5-VDR, XREM-Luc, and *Renilla* as described previously in *Materials and Methods* in Chapter 1. Select assays were cotransfected with RXR_{WT} and/or SRC-1 where indicated. Cells were treated with 120 nM 1, 25_2D_3 in media for 24 hours. VDR response was measured via dual-luciferase assays. Data are represented as the mean fold activation normalized to the ethanol control ± SEM (n = 4).